Laboratori per a la Innovació Tecnològica d'Estructures i Materials
UNIVERSITAT POLITÈCNICA DE CATALUNYA

Ph.D. Thesis

Analysis of unreinforced and TRM-strengthened brick masonry walls subjected to eccentric axial load

by

Ernest Bernat-Maso

Directed by:

Lluís Gil Espert
Pere Roca Fabregat

Tesi presentada per obtenir el títol de Doctor per la Universitat Politècnica de Catalunya

Programa de doctorat d'Anàlisis Estructural, Departament de Resistència de Materials i Estructures a l'Enginyeria

Escola Tècnica Superior d'Enginyeria Industrial i Aeronàutica de Terrassa. Universitat Politècnica de Catalunya, *BarcelonaTECH*

Terrassa, octubre de 2013

A1

Experimental data annex

A1.1 Introduction

Hundreds of tests on component materials and composites materials have been carried out in order to provide the necessary data to analyse, model, understand and extract feasible conclusions from the 29 tests on full scale brickwork walls under eccentric compression load whether they were unreinforced or TRM strengthened ones. Both tests, on materials and on structures, have been summarised and their main results are shown in Chapter 3.

This annex gathers all relevant data obtained along the experimental campaign that took place at LITEM-RMEE-UPC lab installations between April 2009 and February 2012. Detailed information on every sample fabrication, test set up, testing procedure, data post processing and results is presented and it is the basis on which Chapter 3 is founded on.

Firstly, data corresponding to those tests oriented to characterise the materials is exposed to progressively reach the data of the most complex tests which are the TRM strengthened brickwork walls. Along this chapter, data of small unreinforced and strengthened prisms is also gathered together with the information about the full scale unreinforced brickwork walls.

It is a data annex so neither extensive conclusions nor data applications are included.

A1.2 Mortars characterization tests

Five different mortars have been tested to obtain their flexural tensile strength and compressive strength. Firstly, a description of each mortar is provided. Secondly, a full explanation about each test procedure including sample fabrication is presented and finally, the results of each single sample are summarised in tables.

A1.2.1. Mortars description

All mortars considered in this campaign are described summarising the main mechanical properties from their commercial data sheets. Some mixing advice from their official labourers has been also included.

A1.2.1.1 Propamsa M7,5

It is a dry Portland cement mortar that contains cement, selected siliceous aggregates and chemical admixes to improve its workability. It is suitable for general bricklaying purposes but not for projecting.

Figure A1. 1 Propamsa M7,5 25kg bag

It could be manually or mechanically mixed with approximately 14% of water content. For $1m^3$ of mixed mortar 2400kg of dry mortar is required.

Table A1. 1 summarises producer's technical data for Propamsa M7,5 mortar. Figure A1. 1 shows the aspect of the 25kg paper bags in which this mortar was presented. It was produced by Ciments Molins Group.

Parameter	***Value***
UNE-EN 998-2 classification	G-M7.5
Reaction to fire	Euroclass A1
Application data	
Mixing water	14 ± 1%
Application temperature range	+5ºC to +35ºC
Pot life of mix	20 minutes
Final performance	
Compressive strength (MPa)	≥ 7.5
Bond strength (MPa)	≥ 0.15
Chloride contents	≤ 0.1%
Thermal conductivity	0.8 ± 0.1 W/m·K

Table A1. 1 Propamsa M7,5 technical data

A1.2.1.2 Durland M7,5

As the previous one, it is a dry Portland cement mortar that contains cement, selected aggregates and chemical admixes to improve its workability and its adherence. It is suitable for general bricklaying purposes or rendering.

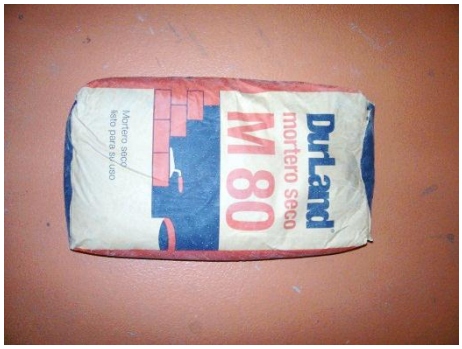

Figure A1. 2 Durland M7,5 25kg bag

It could be manually or mechanically mixed with approximately 13% of water content. Although this amount of water is slightly less than the required by Propamsa M7,5, the material consumption is the same because 2400kg of dry mortar is required for $1m^3$ of mixed mortar.

Table A1. 2 summarises producer's technical data for Durland M7,5 mortar. Figure A1. 2 shows the aspect of the 25kg paper bags in which this mortar was presented. It was produced by Durland Cementos S.L.

Parameter	***Value***
Dry mortar density (kg/m^3)	1700
Application data	
Mixing water	13%
Density of mix (kg/m^3)	2100
Pot life of mix	60 minutes
Final performance	
Compressive strength (MPa)	9
Flexural strength (MPa)	3

Table A1. 2 Durland M7,5 technical data

A1.2.1.3 Planitop HDM Maxi

According to manufacturer's data sheet it is a "two-component, high-ductility, fibre-reinforced cementitious mortar with a pozzolanic-reaction binder base". It may be used as a repairing mortar, as filler or as in the case of the present investigation, as a part of a strengthening system together with a fibre grid.

The powder component is a "fibre-reinforced, high-strength-cement-based mortar with fine-grained selected aggregates" and the liquid component contains special admixes and synthetic polymers (resin) dispersed in water. It could be applied at a thickness of up to 25mm.

Once hardened this mortar offers high bonding strength and it is impermeable to liquid water and aggressive gases while it allows a high water vapour permeability which is necessary to a suitable hygrometric compatibility with brickwork.

Planitop HDM Maxi accomplishes the requirements of EN 1504-9 and it could be classified as R2 class by EN 1504-3. Mixing should be done with a low-speed mechanical mixer and manual mixing is forbidden. According with Mapei technicians once the mixing was complete, the mix was let rest for two minutes before remixing it again to get the final product ready to be applied.

It is recommended to protect the mortar surface from water evaporation in dry, hot or windy conditions for a better curing process. However, none of the mortar specimens, the reinforced wallets or walls where cured with this kind of protection.

Planitop HDM Maxi is distributed in kits that contain one 25kg plastic bag of component A (powder) for each drum of 6.75kg of component B (liquid). See Figure A1. 3. Table A1. 3 summarises the main technical data extracted from the corresponding commercial data sheet. It is produced by Mapei S.p.A.

Parameter	***Value***
Component A characteristics	
Appearance	Grey powder
Maximum aggregate size (mm)	1
Density (kg/m^3)	1200
Chloride ions content (%)	≤0.05
Component B characteristics	
Appearance	White fluid liquid
Density (kg/m^3)	1070
Dry solids content (%)	13
Chloride ions content (%)	≤0.05
Application data	
Mixing ratio	25kg component A with 6.75kg component B
Consistency	Plastic-thixotropic
Density of mix (kg/m^3)	1850
Application temperature range	+5ºC to +35ºC
Maximum thickness (mm)	25
Pot life of mix	60 minutes
Final performance	
Compressive strength (MPa)	>25
Flexural strength (MPa)	>8
Compressive modulus of elasticity (GPa)	11
Bond strength on masonry (MPa)	>2
Reaction to fire	Euroclass E

Table A1. 3 Planitop HDM Maxi technical data

A1.2.1.4 Planitop HDM Restauro

According to manufacturer's data sheet it is a "two-component, high-ductility, fibre-reinforced, hydraulic lime mortar with Eco-Pozzolana". It is thought as a levelling mortar for stone structures and it is also indicated for its application as part of strengthening systems like TRM.

Figure A1. 3 Planitop HD Maxi components

The powder component (A) is a hydraulic-lime-based-mortar with eco-pozzolana that also contains natural sand as main aggregate, glass fibres and special admixtures. The liquid component (B) contains both special admixtures and synthetic polymers (resin) dispersed in water. It could be applied at a thickness of up to 10mm.

Once hardened this mortar, as the previous one, offers high bonding strength and is impermeable to liquid water and aggressive gases while it gives a high water vapour permeability which is essential to be applied in most of the historical masonry structures because of the need of hygrometric compatibility.

Planitop HDM Restauro accomplishes the requirements of M15 classification according with EN 998-2. Under EN 998-1 code it is classified as GP mortar, class CS IV. As in Planitop HDM Maxi, Restauro should be mixed with a low-speed mechanical mixer and the mix should have reposed for two minutes before remixing it again to get the final product ready to be applied.

Although it is highly recommended to cover the mortar during its curing in dry environments, any precaution was taken in this direction neither in the mortar nor in the walls.

Planitop HDM Restauro is distributed in kits that contain one 25kg plastic bag of component A (powder) for each drum of 5kg of component B (liquid). See Figure A1. 4. Table A1. 4 summarises the main technical data extracted from the corresponding commercial data sheet. It is produced by Mapei S.p.A.

Figure A1. 4 Planitop HDM Restauro components

Parameter	***Value***
Component A characteristics	
Appearance	White powder
Maximum aggregate size (mm)	1,5
Density (kg/m^3)	1400
Chloride ions content (%)	≤0.05
Component B characteristics	
Appearance	White fluid liquid
Density (kg/m^3)	1020
Dry solids content (%)	1
Chloride ions content (%)	≤0.05
Application data	
Mixing ratio	25kg component A with 5kg component B
Consistency	Fluid-spatulable
Density of mix (kg/m^3)	1900
Application temperature range	+5ºC to +35ºC
Maximum thickness (mm)	10
Pot life of mix	60 minutes
Final performance	
Compressive strength (MPa)	>15
Compressive modulus of elasticity (GPa)	8
Bond strength on masonry (MPa)	>0.8
Reaction to fire	Euroclass E

Table A1. 4 Planitop HDM Restauro technical data

A1.2.1.5 XMesh M25

According to the commercial sheet provided by Ruredil S.p.A. it is a "mono-component mortar made specifically to be used on masonry". Its main characteristics are its applicability on damp substrates, the vapour transpiration because of the hydraulic binder constituting the matrix, its high adhesion with masonry and fire resistance.

Actually, it is a "stabilized inorganic matrix consisting of special pozzolanic binder, selected aggregates, sand and special additives". Each paper bag of XMesh M25 contains 25kg of the dry product (See Figure A1. 5).

Figure A1. 5 Ruredil XMesh M25

According with highly experienced company's workers, there is no need of smoothing the surface before applying XMesh M25 and 90% of the recommended amount of water should have to be used to mix the mortar instead of the quantity from Table A1. 5 . If more water is needed, it is added up to 100% of the data in Table A1. 5. Then, the mortar has to be mixed for 1-2 minutes more than the initial 3 minutes. After that, the mortar should rest before it is remixed for acquiring its suitable consistency.

Parameter	***Value***
Application data	
Mixing water	26% weight
Density of mix (kg/m^3)	1750
Temperature applicability	5ºC-35ºC
Consistency (EN 1015-3)	Plastic. Fluidity = 75%
Final performance	
Compressive strength (MPa)	38
Compressive modulus of elasticity (GPa)	15
Bond strength on masonry (MPa)	>0.8
Flexural strength (MPa)	7.5

Table A1. 5 Ruredil XMesh M25 technical data

A1.2.2. Samples preparation and test procedures for mortars

Same samples were used, first to obtain information about the flexural strength with three-points-bending tests and after this, to obtain the compressive strength with a direct compression test over each one of the halves resulting from the flexural test.

All samples were 40mm x 40mm x 160mm prisms which were fabricated in a standardized steel mould for 3 specimens, unmould between three and ten days and cured at environmental indoor conditions for at least 28 days. General purpose mechanical oil was used as unmoulding and the mortar was manually vibrated after been poured into the mould.

Figure A1. 6 Standardized mould for mortar samples fabrication. Propamsa samples

Two different tests were carried out on mortar samples:

A1.2.2.1 Flexural strength test procedure

Tests were executed according with the standard EN 1015-11:2000 [113] which defines a three-points-bending test on a simple supported prismatic sample (40mm x 40 mm x 160mm) which is punctually loaded at half its span (distance between supports, which was 100mm). See Figure A1. 7. To assure the test set up a standardized tool specifically designed for these tests was used (see Figure A1. 8). A Suzpecar electromechanical test machine with a maximum load of 50000N was used. The test procedure was:

- Positioning the sample into the standardized flexural testing tool making sure the specimen contacted the physical back limits in order to have a correct alignment of the mortar sample. After this, a longitudinal centring of the sample was done. This first step was oriented to meet the requirements of the boundary conditions of the test

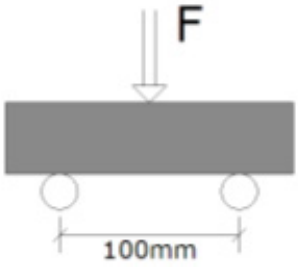

Figure A1. 7 Sketch of the flexural strength test set up.

Figure A1. 8 Standardized flexural testing tool.

- Descending the loading tool of the test machine until the application element was closer than 1mm to the sample (see Figure A1. 9).

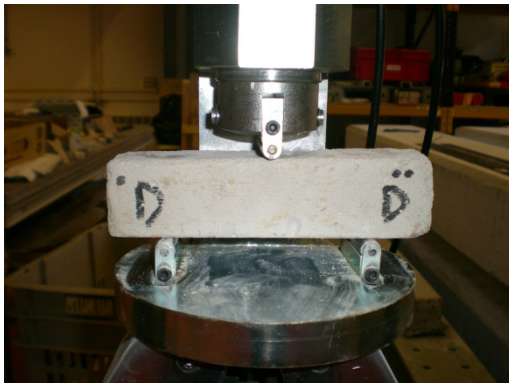

Figure A1. 9 Initial position of the test set up.

- Begin the data acquisition together with the test which was controlled by a constant force increasing ratio of 10N/s. Applied force and descending displacement of the loading element were recorded at 5Hz although the most significant result was the maximum load.
- Together with the previous step a slow-cam video was recorded in order to capture the crack opening in a few tests (see Figure A1. 10).

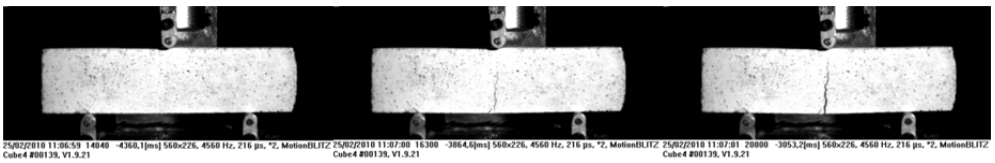

Figure A1. 10 Crack growing pattern in a flexural test

- As there was always a brittle failure, the test finished breaking the specimen.
- From the maximum load and assuming a linear stress distribution in the most loaded cross-section, the flexural strength (f_{xm}) was calculated.

Tensile strength (f_{tm}) can be calculated from the flexural tensile strength (f_{xm}) using the following formula from EHE-08 [114], which has been previously used with the same aim by other investigators [115]. The value h (40mm) is the height of the sample:

$$f_{tm} = f_{xm} \frac{1.5\left(\frac{h}{100}\right)^{0.7}}{1 + 1.5\left(\frac{h}{100}\right)^{0.7}} \quad \text{(Eq A1. 1)}$$

Two halves resulted from each flexural test. After, these were tested under uniform compression.

A1.2.2.2 Compressive strength test procedure

Compressive strength tests were based on the standard EN 1015-11:2000 [113]. Direct uniform compression test is defined to be applied on each one of the halves resulting from a flexural test so no new samples were needed. The procedure is aimed at testing 40mm x 40mm x 40mm mortar cubes under uniform compression. Two 40mm x 40mm x 10mm steel plates are required to define a uniform surface of 40mm x 40mm where the load should be distributed. A sketch of the test set up is shown in Figure A1. 11, and Figure A1. 12 is a picture of a typical test.

A Suzpecar electromechanical test machine with a maximum load of 50kN was used. The test procedure was:

- Positioning a 40mm X 40mm X 10mm steel plate centred under the loading tool of the test machine.
- Placing the sample (half specimen from the flexural strength test) centred over the steel plate so that one of the two opposite moulded faces was in contact with the plate.
- Positioning the second steel plate lined up with the first one and checking up that all pieces were centred under the loading tool.

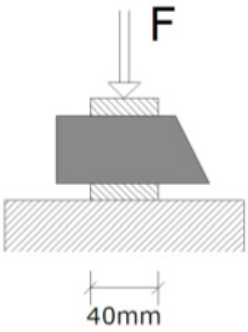

Figure A1. 11 Sketch of the compressive strength test set up

Figure A1. 12 Initial state of the test

- Descending the loading tool until contact with the plate on the sample (see Figure A1. 12).
- Starting data acquisition together with the test execution which was a constant force increasing with ratio of 100N/s. Applied force and descending displacement of the loading tool were recorded at 5Hz. The main result was the maximum load.
- Together with the previous step a slow-cam video was recorded in order to capture crushing failure (see Figure A1. 13).

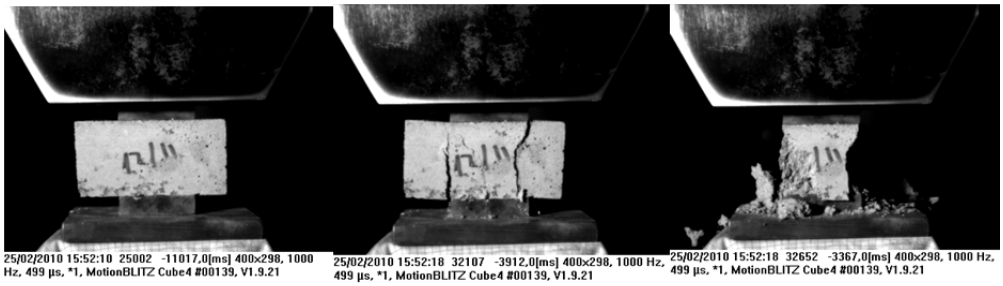

Figure A1. 13 Crushing failure in mortar compressive strength test

- With the maximum applied load (P) and assuming a uniform stress distribution, the compressive strength (f_{cm}) was calculated. See (Eq A1. 2) where b is the edge length, 40mm, of the loaded square surface.

$$f_{cm} = \frac{P}{b^2} \qquad \text{(Eq A1. 2)}$$

A1.2.3. Experimental results of the tests on mortar

The five tables below detailed each test result including the age of the sample at testing time and the calculated tensile strength, whereas the sixth (Table A1. 11) summarised these results with the corresponding average values and coefficients of variation.

Sample	*Age (days)*	*Flexural strength, f_{xm} (MPa)*	*Tensile strength, f_{tm} (MPa)*	*Compressive strength, f_{cm} (MPa)*	
P1	277	0.61	0.27	5.22	4.82
P2	277	1.64	0.72	4.50	
P3	277	1.22	0.54	5.36	
P4	277	1.31	0.58	3.73	
P5	277	1.89	0.83	5.16	
P6	277	1.68	0.74	4.49	
P7	239	0.66	0.29	1.34	
P8	239	0.75	0.33	1.35	
P9	239	0.95	0.42	2.72	
P10	239	0.90	0.40	1.59	
P11	239	0.94	0.41	3.52	
P12	239	0.68	0.30	1.20	
P13	350	1.76	0.78	3.39	2.99
P14	350	1.35	0.60	3.12	3.40
P15	350	1.32	0.58	3.08	3.32
P16	350	1.54	0.68	3.63	2.88
P17	350	1.35	0.60	3.63	3.45
P18	350	1.46	0.64	3.82	3.46
P19	334	1.35	0.59	3.45	3.26
P20	334	1.56	0.69	2.76	3.14
P21	334	1.43	0.63	3.34	2.53
P22	334	1.48	0.65	3.60	2.81
P23	334	1.68	0.74	3.44	3.94
P24	334	1.62	0.71	3.45	3.08
P25	225	0.77	0.34	1.20	1.37
P26	225	0.59	0.26	1.13	1.10
P27	225	0.69	0.31	1.37	1.37
P28	49	1.03	0.45	1.86	
P29	49	1.29	0.57	2.56	
P30	49	1.05	0.46	2.61	
P31	34	0.93	0.41	2.15	
P32	34	1.09	0.48	3.41	
P33	34	0.95	0.42	3.15	
P34	67	2.10	0.93	4.11	5.26
P35	67	1.89	0.83	4.27	4.76
P36	67	1.72	0.76	4.07	4.40
P37	67	1.42	0.63	4.62	4.54
P38	67	1.48	0.65	4.12	3.94
P39	67	1.44	0.64	4.16	4.29
P40	55	1.23	0.54	3.18	3.00
P41	55	1.13	0.50	2.45	3.10
P42	55	1.07	0.47	2.50	2.79
P43	53	1.18	0.52	2.50	2.83
P44	53	1.12	0.49	3.16	3.10
P45	53	1.27	0.56	2.81	3.28
P46	172	0.72	0.32	2.84	2.80
P47	172	0.98	0.43	1.96	2.57

Table A1. 6 Results of the tests on Propamsa M7,5 mortar

Sample	*Age (days)*	*Flexural strength, f_{xm} (MPa)*	*Tensile strength, f_{tm} (MPa)*	*Compressive strength, f_{cm} (MPa)*	
D1	77	1.39	0.61	5.90	4.65
D2	77	1.37	0.60	5.44	4.57
D3	77	1.67	0.74	4.92	4.61
D4	77	1.51	0.67	5.61	4.71
D5	77	1.32	0.58	4.16	5.02
D6	77	1.25	0.55	3.99	4.96
D7	34	0.75	0.33	5.52	2.39
D8	34	0.69	0.31	2.63	2.11
D9	34	0.59	0.26	1.71	2.33
D10	34	0.64	0.28	2.13	2.26
D11	34	0.61	0.27	2.07	2.03
D12	34	0.60	0.26	2.32	2.31
D13	157	0.54	0.24	2.03	1.72
D14	157	0.54	0.24	2.04	2.17
D15	157	0.62	0.27	2.08	2.17
D16	157	0.32	0.14	1.62	1.76
D17	157	0.09	0.04	1.85	1.66
D18	157	0.52	0.23	2.15	2.01
D19	154	0.68	0.30	2.57	4.20
D20	154	1.13	0.50	4.05	3.82
D21	154	0.66	0.29	2.60	2.39
D22	154	0.87	0.38	2.70	2.60
D23	154	0.70	0.31	1.80	3.84
D24	143	0.75	0.33	2.83	1.94
D25	143	0.58	0.26	1.92	2.72
D26	143	0.56	0.25	2.42	2.35
D27	128	1.67	0.74	2.44	1.82
D28	128	0.71	0.31	2.42	1.99
D29	128	1.39	0.62	1.90	1.87
D30	127	0.71	0.31	1.48	2.31
D31	127	0.71	0.31	1.40	2.50
D32	127	0.58	0.25	1.78	1.65
D33	82	1.95	0.86	6.23	6.02
D34	82	2.18	0.96	4.92	3.55
D35	82	2.23	0.98	4.15	5.37
D36	82	1.89	0.83	4.40	6.27
D37	82	2.13	0.94	3.64	5.74
D38	82	1.75	0.77	4.21	6.25
D39	43	1.38	0.61	2.99	2.81
D40	43	1.65	0.73	3.23	3.97
D41	43	1.20	0.53	2.88	2.28
D42	43	0.92	0.40	3.68	5.65
D43	43	1.12	0.49	3.29	5.67
D44	43	0.91	0.40	5.27	3.73
D45	43	0.91	0.40	5.30	4.99
D46	43	0.88	0.39	4.56	4.01
D47	43	0.99	0.44	4.75	4.17
D48	34	0.55	0.24	2.23	2.03
D49	34	0.37	0.16	1.77	1.93
D50	34	0.37	0.16	2.19	1.75
D51	34	0.34	0.15	2.56	2.45
D52	34	0.35	0.16	1.64	2.08

Sample	*Age (days)*	*Flexural strength, f_{xm} (MPa)*	*Tensile strength, f_{tm} (MPa)*	*Compressive strength, f_{cm} (MPa)*	
D53	34	0.37	0.16	2.49	1.86
D54	30	0.58	0.26	2.86	2.58
D55	52	0.76	0.33	2.41	2.76
D56	52	1.16	0.51	2.85	2.57
D57	52	0.93	0.41	2.11	1.78
D58	52	1.13	0.50	2.35	2.09
D59	39	1.20	0.53	2.20	1.64
D60	39	1.27	0.56	1.43	2.14
D61	39	0.99	0.44	2.24	2.07
D62	31	2.24	0.99	4.86	3.46
D63	31	2.49	1.10	4.72	4.43
D64	31	2.36	1.04	4.82	4.35
D65	31	0.27	0.12	4.57	3.74
D66	31	1.88	0.83	4.11	4.17
D67	31	2.11	0.93	3.94	2.14
D68	49	2.22	0.98	8.36	8.16
D69	49	2.24	0.99	5.49	7.41
D70	45	2.11	0.93	4.47	4.41
D71	45	2.50	1.10	5.75	5.26
D72	45	2.25	0.99	6.19	5.07
D73	45	2.13	0.94	5.17	4.52
D74	126	1.29	0.57	2.79	3.19
D75	126	1.19	0.53	3.66	4.05
D76	126	1.50	0.66	3.40	3.61
D77	126	1.27	0.56	3.06	3.04
D78	126	1.46	0.64	3.62	3.93
D79	55	1.08	0.48	2.17	1.87
D80	55	1.07	0.47	2.72	1.88
D81	55	1.06	0.47	3.20	2.75
D82	55	3.79	1.67	14.45	12.48
D83	62	4.10	1.81	13.08	12.11
D84	62	3.60	1.59	14.24	12.07

Table A1. 7 Results of the tests on Durland M7,5 mortar

Sample	*Age (days)*	*Flexural strength, f_{xm} (MPa)*	*Tensile strength, f_{tm} (MPa)*	*Compressive strength, f_{cm} (MPa)*	
M1	48	9.82	4.33	37.98	36.55
M2	48	6.27	2.77	67.10	35.44
M3	48	8.09	3.57	39.11	36.99

Table A1. 8 Results of the tests on Planitop HDM Maxi mortar

Sample	*Age (days)*	*Flexural strength, f_{xm} (MPa)*	*Tensile strength, f_{tm} (MPa)*	*Compressive strength, f_{cm} (MPa)*	
R1	48	6.83	3.01	13.10	14.33
R2	48	6.28	2.77	13.64	14.79
R3	48	6.59	2.91	14.67	16.64

Table A1. 9 Results of the tests on Planitop HDM Restauro mortar

Sample	Age (days)	Flexural strength, f_{xm} (MPa)	Tensile strength, f_{tm} (MPa)	Compressive strength, f_{cm} (MPa)	
X1	52	9.18	4.05	36.80	36.65
X2	52	9.68	4.27	33.57	36.76
X3	52	8.65	3.82	31.55	34.32
X4	52	10.84	4.79	32.68	34.53
X5	52	8.07	3.56	28.05	38.02
X6	52	9.92	4.38	34.44	36.23

Table A1. 10 Results of the tests on XMesh M25 mortar

Mortar	Flexural strength, fxm (MPa)	Tensile strength, f_{tm} (MPa)	Compressive strength, f_{cm} (MPa)
Propamsa M7,5	1.24 (0.30)	0.55	3.18 (0.33)
Durland M7,5	1.25 (0.89)	0.55	3.70 (0.63)
Planitop HDM Maxi	8.06 (0.18)	3.56	42.20 (0.27)
Planitop HDM Restauro	6.57 (0.03)	2.90	14.53 (0.08)
XMesh M25	9.39 (0.10)	4.15	34.47 (0.08)

Table A1. 11Results summary of the tests on mortar. CV in brackets.

Both flexural and compressive tests showed a linear behaviour up to a brittle failure for all mortars as can be observed in the typical force-displacement graphs (Figure A1. 14 to Figure A1. 23) presented below for each combination of type of mortar and test.

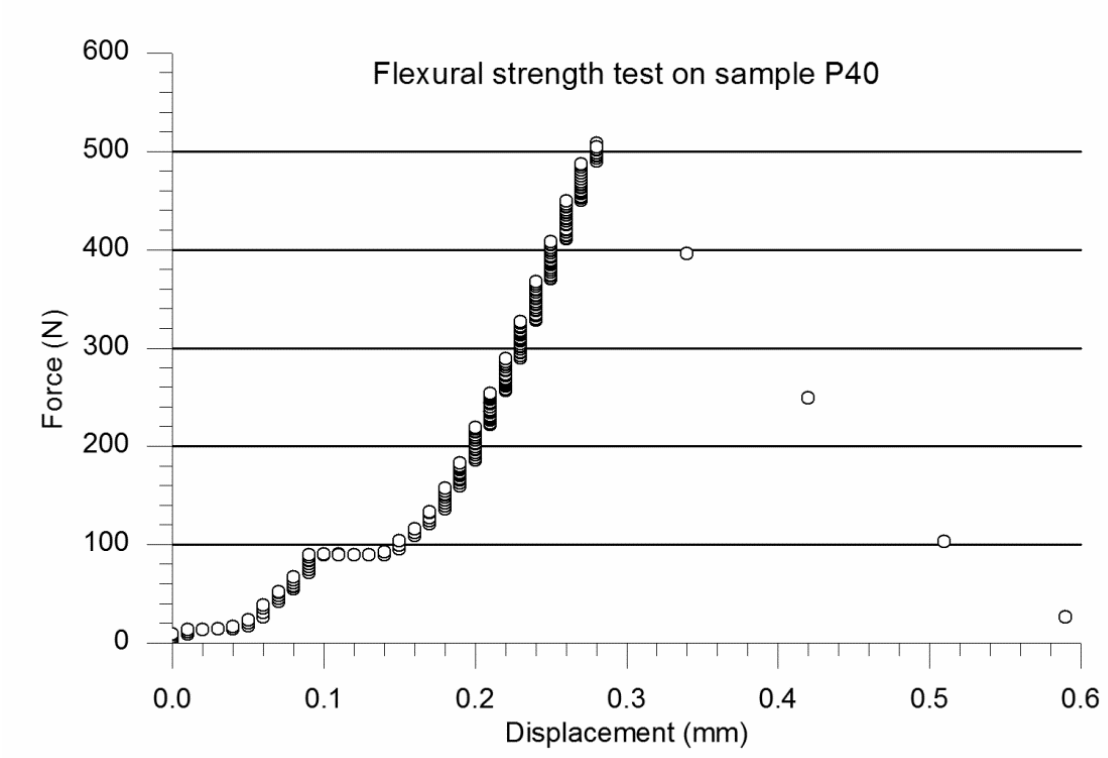

Figure A1. 14 Result of the flexural strength test on a typical Popamsa M7,5 mortar sample

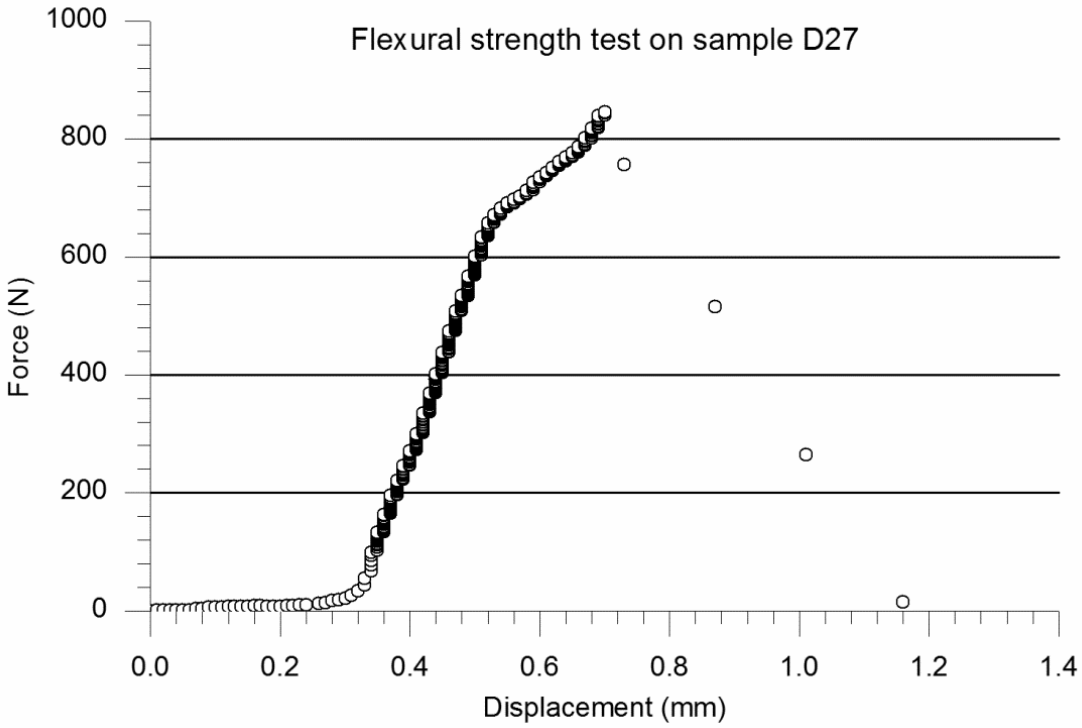

Figure A1. 15 Result of the flexural strength test on a typical Durland M7,5 mortar sample

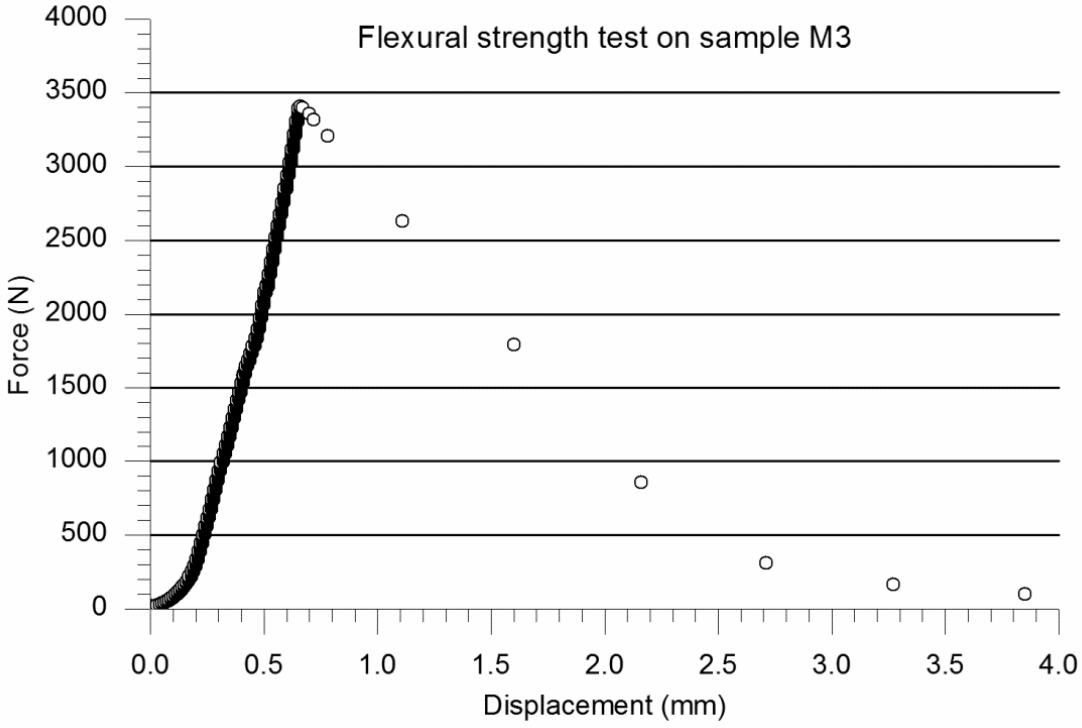

Figure A1. 16 Result of the flexural strength test on a typical Planitop HDM Maxi mortar sample

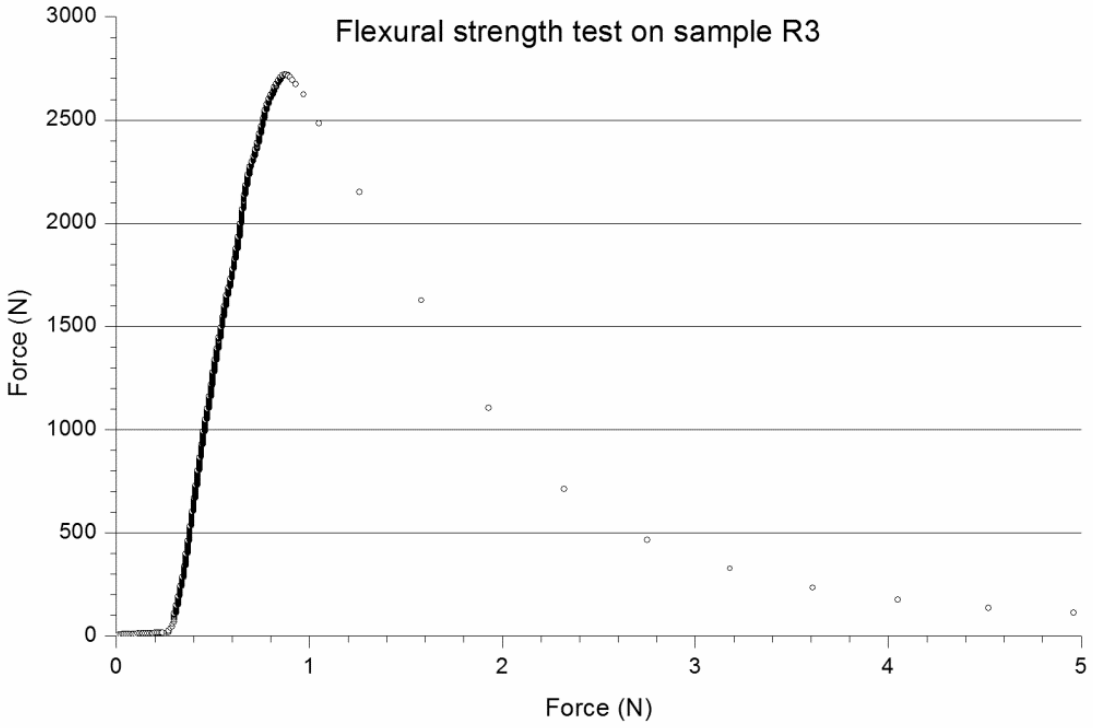

Figure A1. 17 Result of the flexural strength test on a typical Planitop HDM Restauro mortar sample

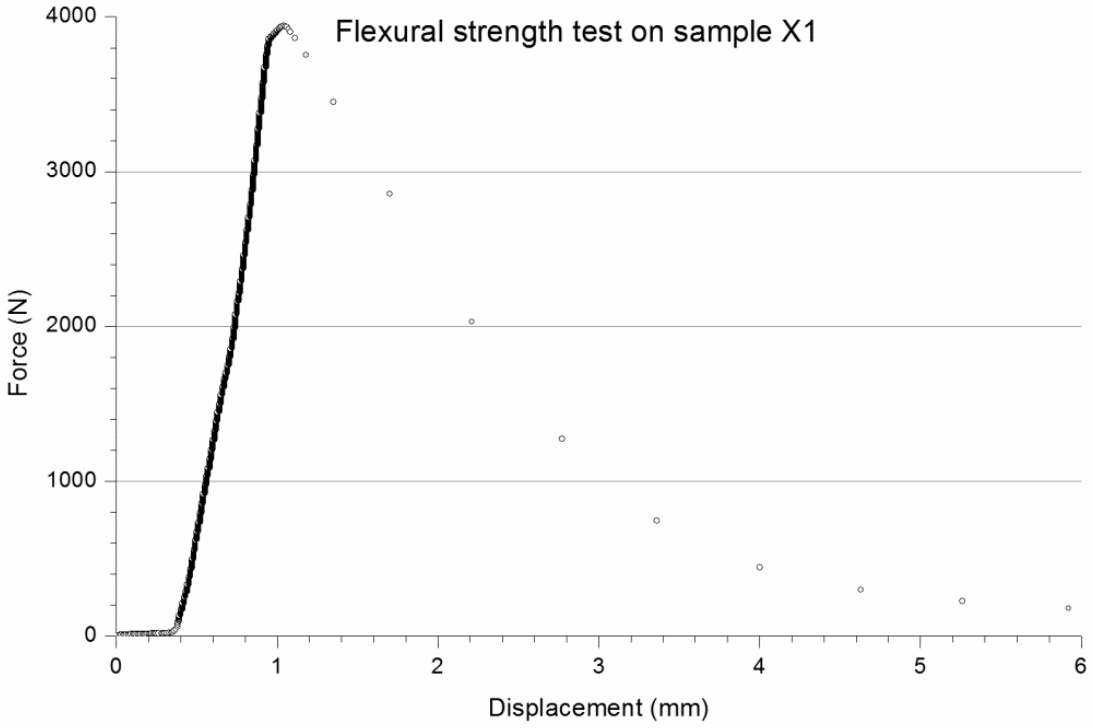

Figure A1. 18 Result of the flexural strength test on a typical XMesh M25 mortar sample

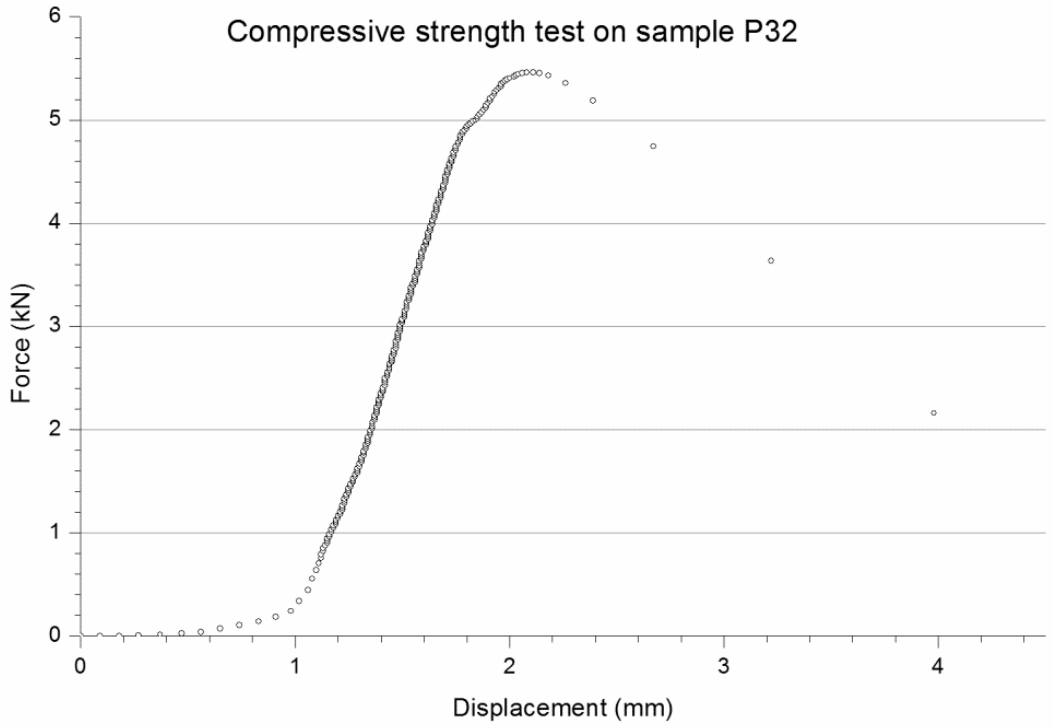

Figure A1. 19 Result of the compressive strength test on a typical Propamsa M7,5 mortar sample

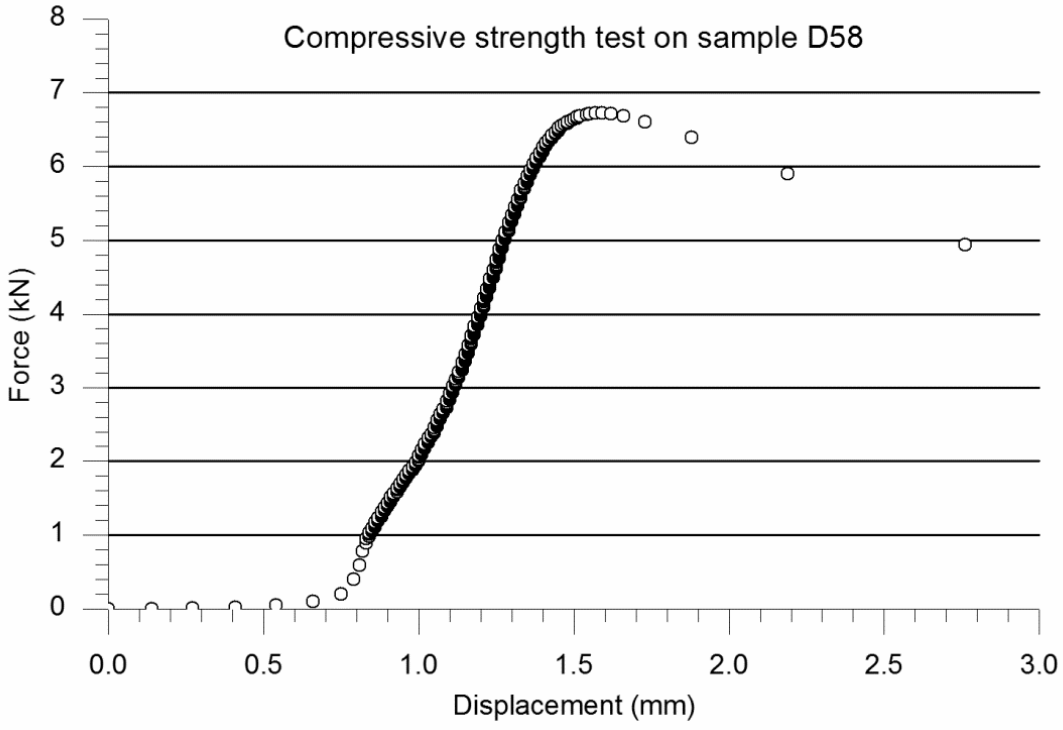

Figure A1. 20 Result of the compressive strength test on a typical Durland M7,5 mortar sample

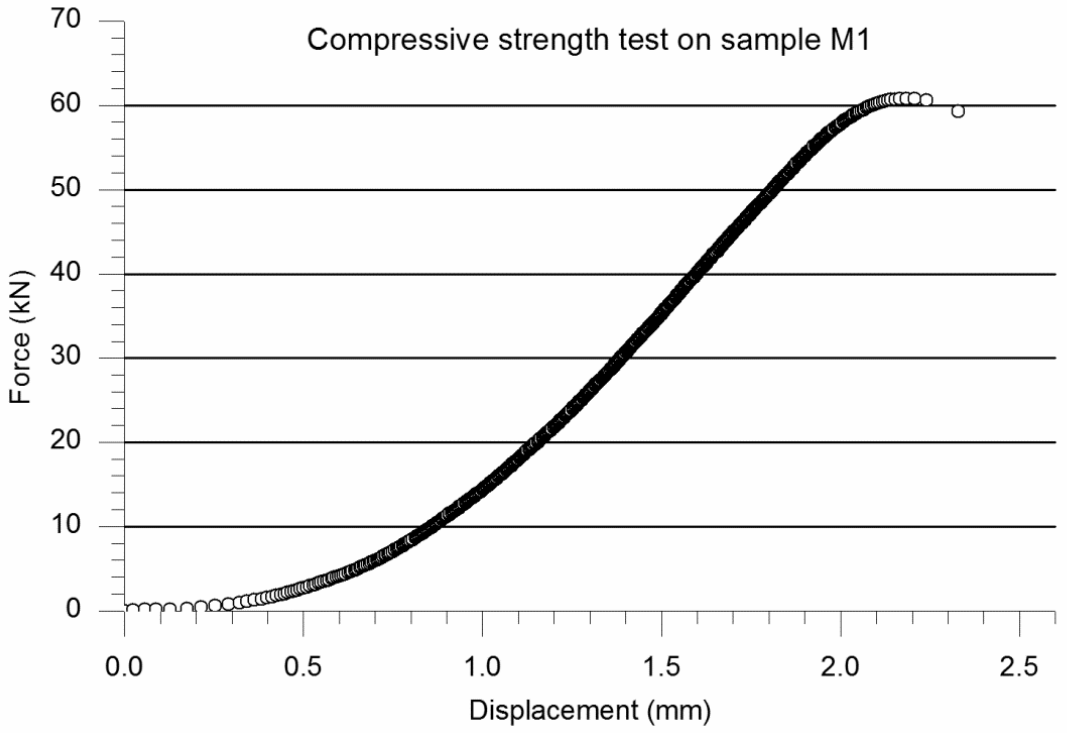

Figure A1. 21 Result of the compressive strength test on a typical Planitop HDM Maxi mortar sample

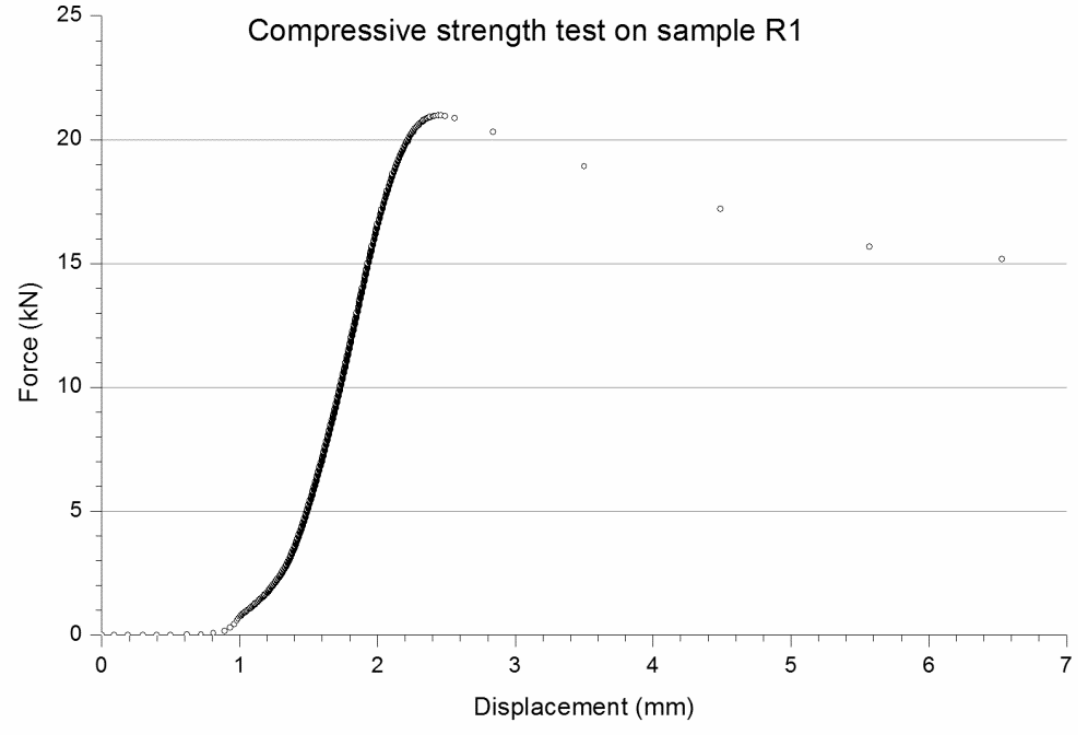

Figure A1. 22 Result of the compressive strength test on a typical Planitop HDM Restauro mortar sample

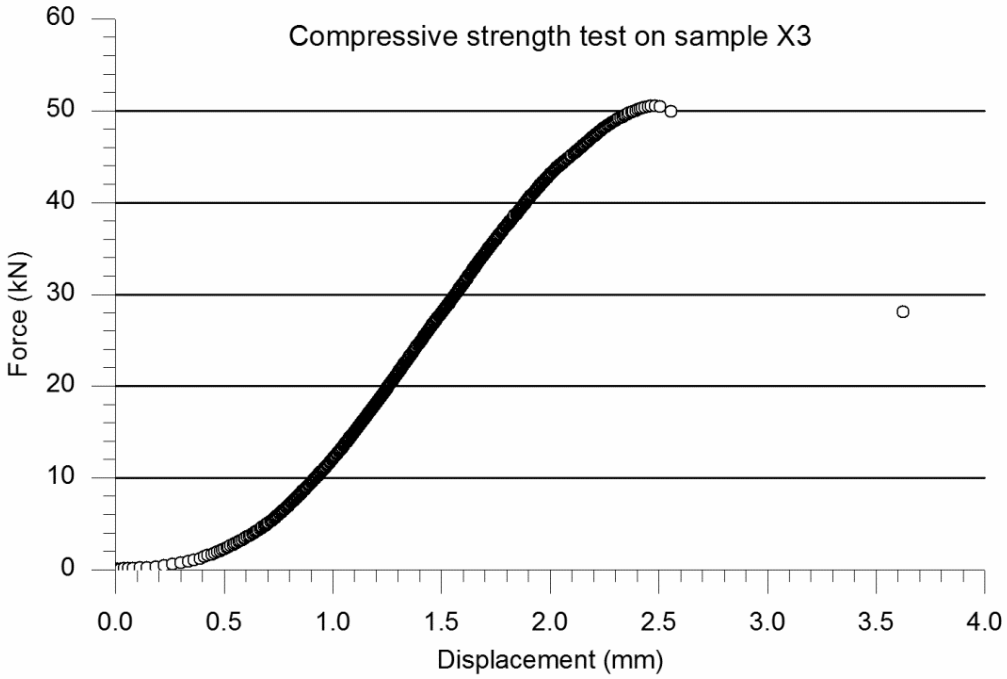

Figure A1. 23 Result of the compressive strength test on a typical XMesh M25 mortar sample

Flexural tests on specimens P1, P2, P5 and P6 was carried out at 20N/s whereas P3 and P4 were tested at 10mm/min. Compressive tests on P1 samples were done at 200 N/s. All remaining tests were carried out at the previously specified velocity.

A1.3 Brick characterization tests

One single type of brick has been used in the experimental campaign. It is a solid commercial locally-produced clay brick distributed by Calvente Hermanos S.L. which is called *"Tocho macizo máquina"*. Its dimensions are shown in Figure A1. 24.

Three different characterization tests have been performed on bricks in order to determine their flexural strength, compressive strength and water absorption. Furthermore, density and real average dimensions were also determined. Each test procedure is fully explained below as well as the results are presented in subsection A1.3.2.

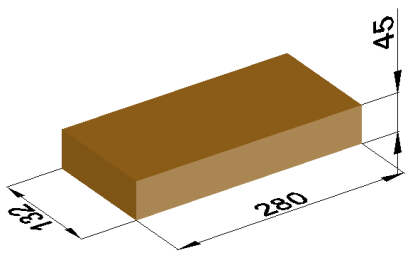

Figure A1. 24 Dimensions of the bricks

A1.3.1. Samples preparation and test procedures for bricks

Different samples were used to characterize each one of the studied properties of bricks. For flexural strength and water absorption full bricks were considered whereas half bricks mechanically cut were prepared to obtain the compressive strength. Together with each testing procedure the main description of the sample conditioning is provided.

A1.3.1.1 Flexural strength test procedure

The aim of flexural strength tests on bricks was to indirectly obtain the tensile strength whose value could determine the resistance of the strengthening system if a debonding failure occurs and it pulls out the brick's surface.

As it was previously proposed for the mortar, the same expression from (EHE-08 [114]), (Eq A1. 1), is used to obtain the tensile strength (f_{tb}) from the values of the flexural strength (f_{xb}) which were obtained with a three-points bending test according with the sketch in Figure A1. 25. The resulting formula to relate tensile and flexural strength once adapted to the notation referring bricks is (Eq A1. 3) where h is the height (45mm) of the brick.

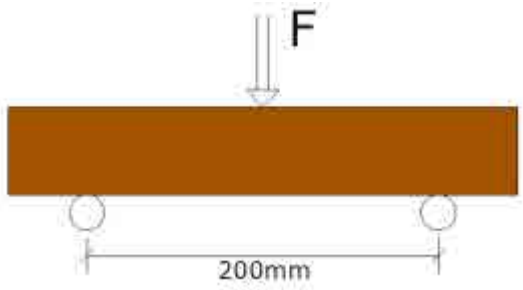

Figure A1. 25 Sketch of the flexural strength test set up for bricks

$$f_{tb} = f_{xb} \frac{1.5\left(\frac{h}{100}\right)^{0.7}}{1 + 1.5\left(\frac{h}{100}\right)^{0.7}} \qquad \text{(Eq A1. 3)}$$

These tests were carried out in a Suzpecar electromechanical test machine with 50kN of load capacity. The only preparation of the bricks was a basic surface cleaning to assure a good contact between the brick, the supports and the loading tool. 19 bricks were tested to obtain the flexural strength. The test procedure was:

- Cleaning the surface of the brick and measuring its main dimensions.
- Placing the brick in the testing position so it was centred under the loading tool and with a clear span (l) of 200mm between cylindrical rolling supports. The contact with the supports was through a

rubber plate to avoid local damages of the brick during the test and to uniformly distribute the force reaction in the supports.

- Descending the loading tool until it got near (less than 1mm) the sample. The test set up before starting the experiment is shown in Figure A1. 26.

Figure A1. 26 Brick flexural strength test set up

- Starting the data acquisition of the applied force and the loading tool's displacement at 5Hz together with the execution of the test at 100N/s (force-controlled test).
- Tests ended with a brittle bending failure of the brick that resulted broken in two parts. The maximum load (*P*) was used to calculate the flexural strength (f_{xb}) under the hypothesis of linear strain distribution (see (Eq A1. 4) where b and h are the width of the brick respectively).

$$f_{xb} = \frac{3Pl}{2bh^2} \qquad \text{(Eq A1. 4)}$$

A1.3.1.2 Compressive strength test procedure

Compressive strength of bricks was evaluated following the guidelines of standard EN 772-1:2002 [116]. Tests were carried out on mechanically cut halves of bricks because of a loading capacity limitation of the Veritest testing machine (1MN) whereas in the referred code the possibility of executing the test on cut samples is not contemplated.

Before placing the sample in the press to test it, it was necessary to prepare the contact surface in order to assure a uniform load distribution which avoided any problem related with local damages due to punctual contacts. Three preparation procedures where tested to compare their influence in the results although only mortar layering is contemplated in the standard. The other two were mechanical polish and sulphur mortar layering which did not require waiting 28 days for curing. In the results, Table A1. 13, it could be observed that the average values obtained with a cement mortar layering are almost the same than the ones obtained with a thin sulphur mortar regularisation layer. For this reason this last surface

preparation procedure was the one used in most of the cases. Polishing preparation procedure was discarded because of the difficulty to execute it in LITEM installations and the quality of the result.

The test set up consisted on applying a compressive uniformly distributed load on a brick sample in the same direction it would actuate in a brickwork element. A sketch of the test set up is shown in Figure A1. 27 . The testing procedure is detailed below:

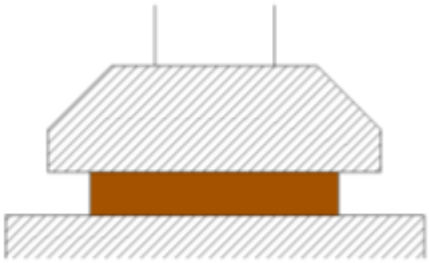

Figure A1. 27 Sketch of the compressive strength test set up for bricks

- Cutting the brick in two halves.
- Cleaning the sample and measuring its main dimensions (this step was done after the next one if a polish preparation procedure was chosen).
- Regularisation of the surface with a cement mortar layering, a sulphur mortar layering or polishing it.

Figure A1. 28 Brick compressive strength test set up

- Placing the prepared sample in the testing position (see Figure A1. 28), centred in the press. Some metallic pieces were placed below the specimen to meet the range requirements of the press.

- Starting the data acquisition (just the applied force registered at 5Hz) together with the test that was carried out with a force-controlled procedure. In order to reach the initial contact position a ratio of 1N/s was used up to this contact stage. After that, the loading rate was incremented to 10kN/s which was constant during all the loading phase up to the brick crushing failure (See Figure A1. 29).

Figure A1. 29 Typical crushing failure of a uniformly compressed brick

- Calculating, see (Eq A1. 5), the compressive strength (f_{cb}) from the value of the maximum applied load (P), the loaded area (A) and a shape correction factor (δ) included in the standard EN 772-1:2002 [116]. In some cases, the value of δ had to be extrapolated from the tabulated values of the code.

$$f_{cb} = \delta \frac{P}{A} \qquad \text{(Eq A1. 5)}$$

Thirty compressive tests on bricks were done. 3 of them with a cement mortar layering as a surface preparation. 3 polished to superficial regularisation and the other 24 with a sulphur mortar layering.

A1.3.1.3 Water absorption test procedure

Tensile strength of brickwork has been highlighted by some authors [73,87,89] as a defining parameter in front of out-of-plane-bending and buckling combined failure. This variable is controlled by adherence between mortar and bricks, and Knowing that this adherence strongly depends on the water absorption of bricks, it is fundamental to study this parameter.

A high water absorption ratio means that the brick will absorb the water of the mortar when placed at its position, preventing the cement mortar to correctly set and resulting in a poor adherence between bricks and joints. This is why some standards limit the water absorption. E.g. ACI-530 [43] does not allow a brick with an absorption ratio higher than 1.6mg/(min·mm^2) to be used in brickwork construction.

The aim of these tests was to define a procedure that allowed us to assure that there was enough water content in bricks to guarantee a good adherence of the resulting brickwork. With this purpose two series of tests were carried out: one to obtain the water absorption of dry bricks and the other one to obtain the same parameter once bricks had been immersed into water for one minute (wet reference).

All these tests met the requirements of standard EN 772-11:299 [117] which fully describes the test procedure. Briefly, the test consisted on measuring the weigh variation of a brick due to the water absorption through a measured area when the piece is partially immersed in water for a known time.

All tests began with bricks in the indoor storage conditions. For the dry reference (27 samples), the test procedure was:

- Dry-cleaning the surface of the brick.
- Measuring the main dimensions of the brick and weighing it.
- Partially immersing the brick into water and measuring the immersed height in order to calculate the area in contact with water.
- Taking out the brick after 1 minute partially immersed, drying its surface with a wet cloth and immediately weighing it.

For the wet reference (15 samples) the test procedure was:

- Measuring the main dimensions of the brick.
- Wet-cleaning the surface of the brick and partially immersing it for one minute.
- Taking out the brick, drying it with a wet cloth and immediately weighing it.
- Immersing the brick in water again for one minute.
- Again, taking out the brick, drying it with a wet cloth and weighing it.

Figure A1. 30 Water absorption test set up and scales used

For immersing the bricks a general purpose container with water was used and the bricks were supported over 4 little nuts (M8) in order to assure a full water contact between the lower brick face and the water, see Figure A1. 30. Bricks were never let in direct contact with the bottom of the container. Weight was measured with electronic scales with precision of 0.1g.

For each test the water absorption ratio was calculated with (Eq A1. 6). This expression considers the two weighs (m_{wet} and m_{dry}) and the area (A) in contact with the water. Immersion always lasted one minute (t=1min).

$$C_{wi,s} = \frac{m_{wet} - m_{dry}}{A \cdot t} \qquad \text{(Eq A1. 6)}$$

27 tests of water absorption from dry initial state were done and 15 on previously wetted bricks.

A1.3.1.4 Dimensions and density

Average main dimensions of bricks were determined experimentally. As the weight of every measured brick was also registered, the density of this solid ceramic bricks stored indoors was obtained.

The dimensions measurement was carried out with a digital micrometre with 0.01mm of precision for lengths under 150mm and with a graduated metallic ruler with a precision of 0.5mm for bigger dimensions.

A1.3.2. Experimental results of the tests on bricks

In this subsection all results of the tests on bricks are presented. Firstly the tests are summarised in tables, one for each kind of experiment. After this, a typical graph representing the behaviour of a brick sample for each type of test is also shown.

First of all, results of flexural strength tests on bricks are gathered in Table A1. 12. In this table are also presented the values of height (*h*) and width (*b*) of each tested brick as well as the maximum applied load (*P*) and the calculated tensile strength of the bricks (f_{tb}).

Test	***h (mm)***	***b (mm)***	***P(N)***	***f_{xb} (MPa)***	***f_{tb} (MPa)***
F1	47.55	135.78	6316	6.17	2.91
F2	47.55	135.20	6648	6.53	3.08
F3	47.21	135.78	7451	7.39	3.47
F4	46.03	134.36	8412	8.86	4.13
F5	47.41	135.71	6287	6.18	2.91
F6	45.45	135.73	4215	4.51	2.09
F7	47.54	135.74	8666	8.47	3.99
F8	47.01	135.18	8928	8.97	4.21
F9	46.76	136.00	5918	5.97	2.80
F10	47.63	136.37	3003	2.91	1.37
F11	47.47	135.53	5405	5.31	2.50
F12	47.50	136.26	5164	5.04	2.37
F13	46.82	136.25	3598	3.61	1.69
F14	46.29	135.68	6604	6.82	3.18
F15	46.86	135.86	5187	5.22	2.45
F16	46.61	136.20	4846	4.91	2.30
F17	46.43	136.43	6920	7.06	3.30
F18	47.05	136.22	5896	5.87	2.75
F19	48.19	135.55	4241	4.04	1.91

Table A1. 12 Results of flexural strength tests on bricks

Looking at the results in Table A1. 12 it is observed that there is a considerable dispersion (*CV*=0.28) in the results although bricks are industrially produced.

The behaviour of these tests was linear up to a fragile failure of the brick with one big centred crack, except for the starting stage in which the sample settlement causes a less stiff behaviour. Figure A1. 31 shows a typical flexure test on a brick.

Results of the compressive strength tests (f_{cb}) also show a considerable dispersion even between the tests carried out with the same surface preparation (*CV*= 0.19 for C_s). A grater difference is observed comparing tests of the samples prepared with a mortar layering (C_c and C_s) and those polished to regularise the surface before the test (C_p). Results are summarised in Table A1. 13 where are classified by the surface preparation (C_c for cement mortar layering, C_p for polished preparation and C_s for sulphur mortar layering) and the number of test repetition. For each experiment the maximum load (*P*) as well as the loaded area (*A*) are presented together with the shape correction factor (δ).

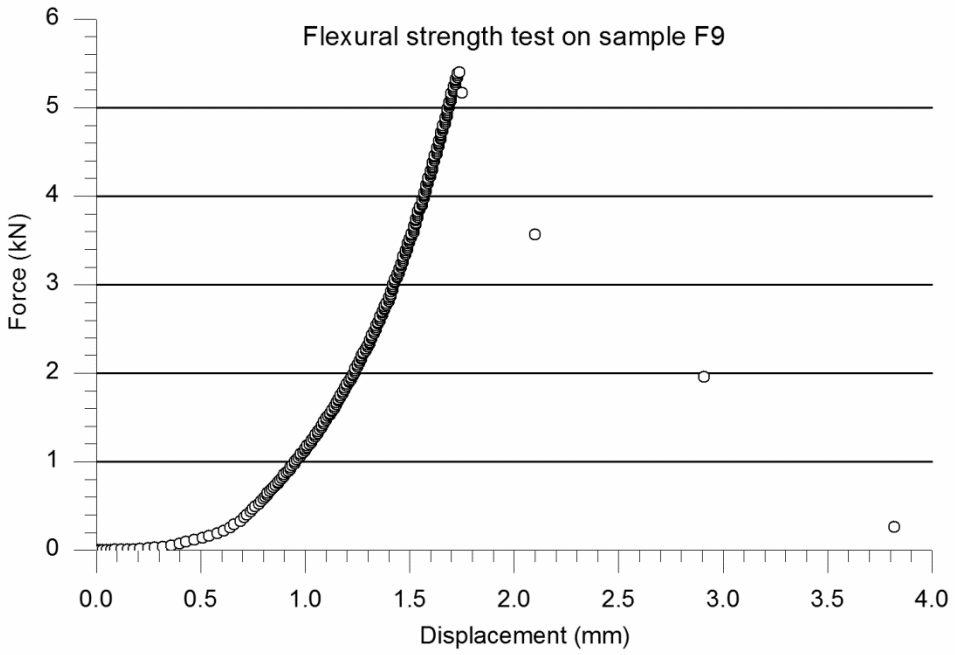

Figure A1. 31 Result of the flexural strength test on a typical brick sample

Surface preparation	***Test #***	***P (kN)***	***A (mm^2)***	***δ***	***f_{cb} (MPa)***
C_c	1	533.6	18387.20	0.757	21.97
	2	660.2	18356.25	0.754	27.12
	3	680.5	19132.02	0.748	26.61
C_p	1	1033.0	18063.27	0.689	39.40
	2	1407.7	18033.60	0.688	53.71
	3	>1880.0	18088.81	0.688	>71.50
C_s	1	910.2	18495.00	0.734	36.12
	2	503.6	18739.36	0.732	19.67
	3	639.6	18856.32	0.727	24.67
	4	846.6	18448.72	0.728	33.40
	5	772.2	18704.40	0.727	30.02

Surface preparation	*Test #*	*P (kN)*	*A (mm^2)*	*δ*	*f_{cb} (MPa)*
	6	836.8	18873.92	0.731	32.40
	7	728.2	19189.60	0.728	27.61
	8	853.1	19111.02	0.713	31.84
	9	481.9	18303.84	0.737	19.39
	10	564.0	19868.58	0.719	20.41
	11	680.2	18427.94	0.732	27.02
	12	603.7	17766.64	0.728	24.74
	13	542.7	18603.96	0.745	21.73
	14	597.6	19735.38	0.736	22.27
	15	493.6	18998.42	0.723	18.79
	16	844.8	18596.65	0.729	33.11
	17	825.0	18187.94	0.731	33.14
	18	791.8	18481.46	0.719	30.83
	19	905.2	18661.00	0.724	35.10
	20	1017.0	18866.55	0.714	38.50
	21	746.7	19139.45	0.726	28.31
	22	526.0	18425.97	0.735	20.99
	23	714.0	18980.40	0.726	27.32
	24	731.6	18762.08	0.717	27.98
	25	782.4	18557.80	0.733	30.91
	26	737.4	18874.78	0.729	28.49
	27	698.3	18002.58	0.730	28.30
	28	642.4	18326.38	0.740	25.93
	29	847.3	18877.65	0.714	32.06
	30	671.3	19209.83	0.719	25.13

Table A1. 13 Results of compressive strength tests on bricks

As the average of the results from C_c and C_s preparations are almost the same, these 3+30=33 samples were used to calculate the average compressive strength of the bricks.

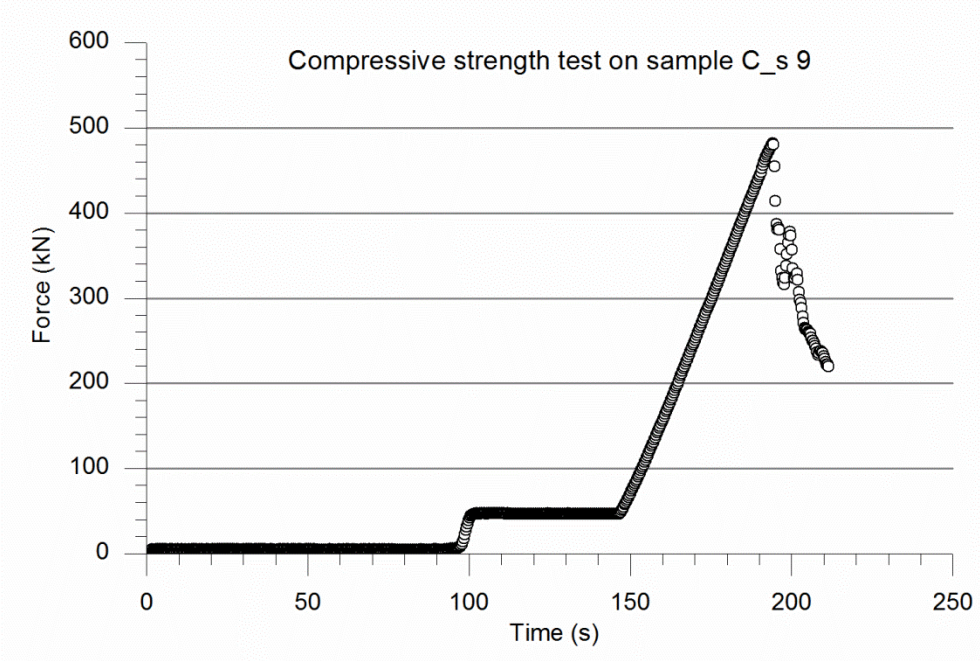

Figure A1. 32 Result of the compressive strength test on a typical brick sample

The typical behaviour of a compressive test on a brick is shown in Figure A1. 32. The fragile behaviour in failure at constant increasing force rate could be highlighted. The first horizontal stage corresponds to the free movement of the press until it reaches the contact with the specimen. Once the contact is produced, the load suddenly increases up to 45kN for a testing machine limitation in control. After the initial settlement has been assured the loading rate was changed to 10kN/s to begin the testing phase. At this rate the second and longer ramp of the graph is recorded up to failure.

In relation with the water absorption ($C_{wi,s}$) tests, Table A1. 14 summarises the results. The first and second columns refer to the initial condition of the test (dry or wet) and the test repetition number. There is also presented the contact area with the water (A) and the two weights, previous (M_0) and after (M_f) wetting are showed just before the absorption ration in the last column.

The tests have a considerable variation, with a coefficient of variation of 0.39 and 0.36 for dry and wet bricks respectively. But the most important information is that all wetted bricks had an absorption ration below 1.6mg/(mm^2·min) which was the limit proposed by ACI-530 [43]. So for all masonry specimen production, the bricks were wetted for at least 1 minute before placing them in brickwork.

Initial state	*#*	*A (mm^2)*	*M_0 (g)*	*M_f (g)*	*$C_{wi,s}$ (mg/(mm^2·min))*
Dry	1	25749.0	1412.3	1440.1	1.08
	2	25912.5	1411.6	1441.4	1.15
	3	27315.0	1520.7	1546.3	0.94
	4	27826.5	1524.1	1564.3	1.44
	5	27805.3	1505.3	1546.8	1.49
	6	26571.5	1423.7	1475.9	1.96
	7	21730.0	1420.3	1437.9	0.81
	8	21860.2	1421.8	1444.8	1.05
	9	23014.4	1523.0	1541.1	0.79
	10	23272.5	1536.5	1567.7	1.34
	11	23354.3	1522.3	1568.6	1.98
	12	22362.8	1451.3	1492.8	1.86
	13	24471.0	1499.6	1527.2	1.13
	14	23856.5	1435.6	1483.5	2.01
	15	23430.9	1407.9	1472.9	2.77
	16	23662.5	1441.8	1458.5	0.71
	17	24933.0	1530.6	1572.6	1.68
	18	24390.3	1511.1	1541.0	1.23
	19	24424.3	1453.2	1502.3	2.01
	20	22740.1	1365.7	1387.8	0.97
	21	25752.8	1606.9	1626.5	0.76
	22	24625.0	1476.6	1525.2	1.97
	23	23354.5	1400.1	1441.2	1.76
	24	23739.5	1455.1	1489.5	1.45
	25	24620.5	1479.7	1525.0	1.84
	26	24834.4	1467.1	1484.3	0.69
	27	24086.0	1510.1	1570.6	2.51

Initial state	*#*	*A (mm^2)*	*M_0 (g)*	*M_f (g)*	*$C_{wi,s}$ ($mg/(mm^2 \cdot min)$)*
Wet (1min)	1	24471.0	1555.7	1567.2	0.47
	2	23856.5	1540.9	1565.0	1.01
	3	23430.9	1540.2	1564.9	1.05
	4	23662.5	1478.8	1488.0	0.39
	5	24933.0	1617.0	1636.2	0.77
	6	24390.3	1578.4	1592.8	0.59
	7	24424.3	1565.6	1583.5	0.73
	8	22740.1	1417.7	1426.5	0.39
	9	25752.8	1650.3	1658.7	0.33
	10	24625.0	1589.8	1609.1	0.78
	11	23354.5	1497.1	1512.3	0.65
	12	23739.5	1539.8	1555.1	0.64
	13	24620.5	1586.9	1603.2	0.66
	14	24834.4	1508.2	1516.6	0.34
	15	24086.0	1645.1	1667.0	0.91

Table A1. 14 Results of the water absorption tests on bricks

Finally, real dimensions of a different series of bricks were precisely measured with a micrometre (0.1mm precision) for lengths under 150mm and with a metallic ruler (0.5mm precision) for longer lengths. Three different measures of length, three of width and three of height were taken from each one of the 20 bricks which were also weighed in storage conditions. The average values obtained were:

- Length = 281.9mm
- Width = 134.8mm
- Height = 46.6mm
- Weight = 2985.8g
- Dry density = 1679.4kg/m^3

A1.4 Masonry characterisation tests

Although there are different expressions and formulations to calculate the masonry properties from the characteristics of their components, it was preferred to experimentally determine some of the most important features in order to introduce the less possible uncertainty in the later on analysis.

This is why compressive strength tests, modulus of linear deformation tests, mortar-brick bonding tests and density characterisation tests were carried out.

A1.4.1. Samples preparation and test procedures on masonry

All masonry samples were manufactured by LITEM staff inside laboratory facilities and later air cured for at least 28 days before any test was performed on them. The atmospheric current conditions into the laboratory were a temperature between 15°C and 25°C and a relative humidity between 30% and 70%. These parameters were controlled but not registered.

The fabrication procedure was:

- Selecting bricks with an acceptable appearance discarding those ones that presented cracks, a strange coloration or major shape irregularities.
- Superficial cleaning of the bricks with water
- Totally immersion of the bricks in water for at least 1 minute before placing them in brickwork. Once taken out of the water the bricks were placed at their final position within the following 2 minutes.
- Levelling the supports on which the samples were going to be constructed in order to assure a correct alignment and initial levelled position of the sample.
- Manually mixing the mortar for brick layering (Propamsa M7,5 or Durland M7,5) according with the producer specifications (14% in weigh for Propamsa M7,5 and 13% for Durland M7,5). A maximum of 15kg were mixed at each batch.
- Placing bricks and mortar controlling the alignment and the levelling at each row, as well as the mortar thickness, usually ranged between 15mm and 20mm except for the cases explained below. Before placing the mortar under the following brick in the pile, the previous brick (already placed) was wetted to improve the mortar adherence.
- Cleaning the mortar excess and regularising the joint to get a final uniform surface at every face of the masonry pile.
- Numbering the specimen and writing down the construction date.

5 rows (piled bricks) prism samples were fabricated for testing the modulus of linear deformation (E) and the compressive strength (f_c). Some of them were used with both tests: first to obtain the modulus of linear deformation and after that they were loaded until crushing failure to study the compressive strength. For the bonding strength (f_{bw}) tests 3 row prism samples were constructed. The following (Table A1. 15) specimens were built and used in the indicated tests:

		Numeration of the samples used in each test			
Sample type	***Total samples***	***Density***	***Modulus of deformation***	***Compressive strength***	***Bonding strength***
Comp_Def	29	4-29	14-20; 22-29	1-29	---
Bond	26	---	---	---	1-26

Table A1. 15 Tested masonry samples

In addition to the samples summarised in Table A1. 15, ten more samples were built in order to qualitatively study the effect of the wetting procedure and the effect of the joint thickness on the results of compressive strength of brickwork. These samples are referred with the notation OF_X_(# of sample). Samples OF_X_1 to OF_X_3 were produced by simply piling 5 bricks with dry joint (no joint). Samples OF_X_4 to OF_X_6 had a particularly thin mortar joint (about 5mm) whereas samples OF_X_7 and OF_X_8 had an especially thick mortar joint (up to 30mm). Finally, samples OF_X_9 and OF_X_10 had the commonly used joint thickness (between 10mm and 15mm) but the bricks were not wetted before constructing the samples.

Each test procedure is detailed below.

A1.4.1.1 Modulus of linear deformation test procedure

Determining the modulus of linear deformation of masonry (*E*) is essential to face any further calculation or simulation. Although standards propose different formulations to calculate this modulus (most of them from the values of compressive strength of the material), the great disagreement observed in literature about this parameter makes having experimental values crucial.

Tests were performed on prisms of 5 bricks with their 4 corresponding joints. No standardised tests were carried out. However, tests on little masonry prisms like the ones studied have been used by some authors in order to obtain the values for compressive strength and also the modulus of linear deformation (see [118]).

The test procedure consisted in:

- Measuring the dimensions of the masonry prism and weigh it to calculate the density.
- Placing the sample in the test position: centred under the loading tool. The test set up consisted in a fixed steel beam that worked as a regular support. Over this beam the sample was directly placed. The loading tool was a rigid steel plate.
- Descending the loading tool until the steel plate was perfectly supported by the masonry prism. This rigid loading tool assured a uniform displacement imposition, so a good load distribution in all the area of the masonry.
- Putting the sensors in the correct position (See Figure A1. 33). 4 potentiometers were used to measure the displacement of the steel plate at its four vertexes. This displacement was between the loading plate (in rigid contact with the masonry prism) and the steel beam where the sample was placed. This sensor positioning allowed controlling any flexural effect due to an eventual non perfect parallelism between the supporting and loaded faces of the specimen or any accidental eccentricity of the load.

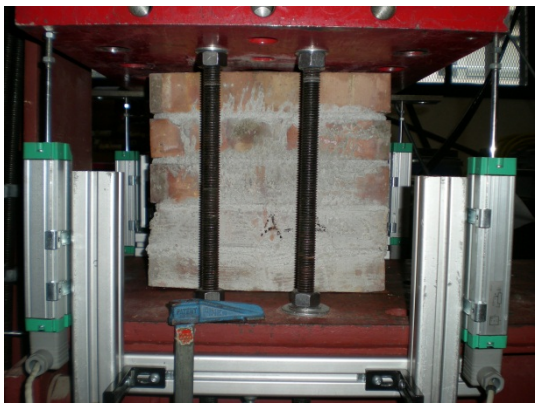

Figure A1. 33 Set up for the test to obtain the modulus of linear deformation of brickwork

- Descending the actuator (MTS 250kN dynamic actuator) until it contacted the steel plate and making sure that all the system was aligned before begin with the test.

Two different loading procedures were used. Both consisted in three loading-unloading cycles with a rising maximum load of the cycle up to approximately the half of the maximum bearable force in compression for third and last cycle. For samples Comp_Def_14 to Comp_Def_19 the maximum of each cycle was 100kN, 175kN and 250kN respectively and the loading rate was 25kN/min whereas for samples Comp_Def_20 and Comp_def_22 to Comp_Def_29 the maximums were 40kN, 80kN and 120kN with a loading rate of 15kN/min

After the test, the actuator was elevated and the loading steel plate moved away to take away the sample that was after used in compressive tests.

Data from the three loading cycles was used to obtain the modulus of linear deformation. For the first loading cycle a range of stresses was fixed (the same for all the samples subjected at the same test procedure) and the deformation at both limits of this interval was calculated. With this data a secant modulus of linear deformation was obtained. This procedure was repeated for a range over the previous one for the next loading cycle, and the third one. Finally, three different secant modulus were obtained for each sample and a weighted average (depending on the length of the stress interval used) was calculated.

Ultrasound (55kHz) inspection was tried as an alternative test procedure to obtain the modulus of linear deformation but the results were not consistent so it was discarded as an appropriate technique for the studied samples.

A1.4.1.2 Compressive strength test procedure

Compressive strength of masonry was expected to be, together with modulus of linear deformation, a defining variable of the ultimate load in full scale walls subjected to eccentric axial load but it was likely to be even more important in strengthened walls for which the capacity to increase the ultimate moment strongly depends on the possibility of developing a compression head.

Although almost every code includes at least one expression to calculate the compressive strength of masonry from the values of the compressive strength of its components (bricks and mortar), it was considered better to gather experimental information about this parameter because of the high influence it has in the behaviour of brickwork walls.

That is why 29 tests were carried out to determine the compressive strength of the used brickwork. Moreover, 8 extra tests were done just to obtain qualitative information about the effect of joint thickness or wetting procedure. No quantitative information was used from these tests in the later on calculus and simulations because these variables of influence were out of this research scope.

The masonry specimens used to carry out the compressive strength tests were not the ones recommended by internationally accepted codes (like RILEM) because of equipment limitations but the same procedure and/or geometry of the samples have been used by other authors [89,118] in similar

researches. Height to width ratio was determined to be more than 2 in order to reduce the friction effects on the load-bearing capacity due to the contact between the plates of the press and the sample. Tested prisms were 5 bricks high so the samples included 4 mortar joints.

The followed compressive strength test procedure was:

- Measuring the main dimensions of the prism if they were not previously measured for a modulus of linear deformation test. It was for samples Comp_Def-1 to Comp_Def-13 and Comp_Def-21.
- Placing the sample inside the press assuring it was centred under the loading plate and press plates were parallel. An initial levelling of the upper press' plate was done to assure the first contact being uniform.
- Beginning the test registering the force against the time at 5Hz. No displacement was measured in these tests and the main result was the maximum load supported by the sample under uniform compression. As there was no displacement control, an initially low ratio of force increment was fixed (1N/s) to limit the force applied once the contact with the upper press plate was reached. After this initial contact the loading rate was increased up to 10000N/s and the test finished within the following two minutes with a crushing failure of the masonry prism (see Figure A1. 34).

Figure A1. 34 Crushing failure of a brickwork prism under the compressive strength test

The loading machine was a Veritest hydraulic press with a maximum loading force of 1MN.

Calculating (Eq A1. 7) the compressive strength of brickwork (f_c) assuming a uniform distribution of the maximum applied load (P) on the brut area of the prism horizontal section (A).

$$f_c = \frac{P}{A} \quad \text{(Eq A1. 7)}$$

Samples were divided in four series, A to D (plus another one for the 8 extra samples already commented), according with the materials used and the date in which were fabricated to correlate with real scale walls. The relation between the compressive tests and the brickwork used in the real scale walls is presented in Table A1. 16. It is shown that the last series (D) did not directly correspond with any real scale wall because of the date it was fabricated. However, as the materials were the same as the ones used for series B and C, and average value of these three series (B, C and D) is used to characterise the walls that had no associated compressive test on their material. It is for walls from #10 up to #29.

Series	***Mortar***	***Corresponding walls***	***Samples***
A	Propamsa M7,5	1	OF_1 to OF_3
B	Durland M7,5	2 to 5	OF_4 to OF_7
C	Durland M7,5	6 to 9	OF_8 to OF_13
D	Durland M7,5	None	OF_14 to OF_29

Table A1. 16 Correspondence between compressive strength tests on masonry and real scale walls that used the same material production

These same experimental steps were followed to evaluate the compressive strength of the eight prisms with modified mortar thickness or wetting procedure.

A1.4.1.3 Mortar-bricks bonding test procedure

General guidelines of ASTM C1072 (bond wrench test, [123]) were followed to design the test set up and procedure although tests did not fully meet the requirements of this standard.

Spanish standard EN 1052-2:1999, [124] sets a procedure to determine the flexural strength of the brickwork but as far as the real scale walls were going to be subjected to eccentric compression it was decided that a test equivalent to the one presented in ASTM C1072 would be more representative of the real stress distribution and the real behaviour at failure point when masonry was part of a larger wall tested for bending-buckling failure study. This test setup was used in comparable researches like [8].

The carried out tests, as the one presented in ASTM C1072, required a test set up consisting of two clearly differentiated parts: a support to fix the lower part of the sample and an upper part used as a loading tool. The aim of the supporting part was to stiffly hold the brick that was being tested just under the mortar joint whilst the upper part of the test set up was intended to hold the brick over the tested joint and apply a bending-compression compound load (a punctual load at the end of a lever arm) that caused the failure of the mortar or the joint's adherence.

The main dimensions of the test set up as well as a sketch are showed in Figure A1. 35. The distance between the load application position and the mortar joint edge (*d*) is measured for each test.

Three-brick prisms were fabricated to carry out these adherence tests so each one provided two joints which were tested. Three tests on Propamsa M7,5 mortar joint were completed whereas 23 tests were carried out with Durland M7,5 mortar joints.

The testing procedure was:

- Measuring the main dimensions of the joint which was going to be tested.
- Measuring the weight of the loading tool and determining its gravity centre.
- Placing the sample in the testing position and fixing it to the lower part of the test setup.
- Measuring the real distance from the joint to the load application point (*d*) for each case.
- Applying the load controlling the test by imposing a descending displacement of the loading tool at a fixed rate. During the test, the applied load as well as the descending displacement of the loading tool were continuously measured acquiring data at 5Hz.

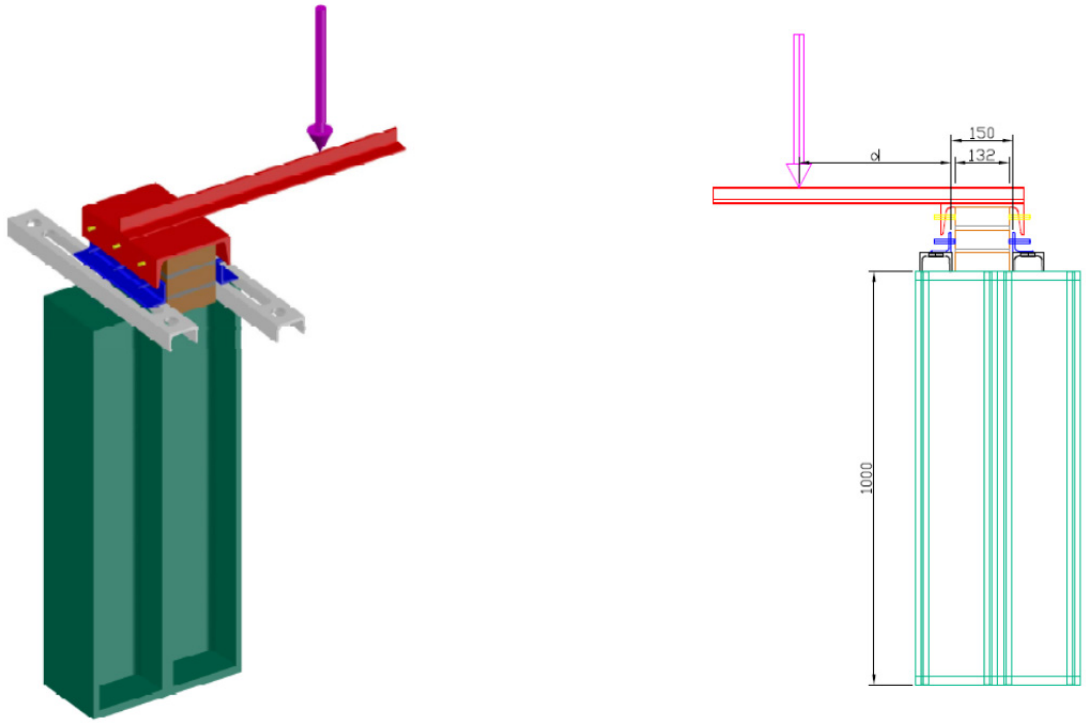

Figure A1. 35 Sketch of the test set up for mortar-brick bonding experiments

Figure A1. 36 Testing machine and setup for the mortar-brick adherence tests

The testing machine was an electromechanic press of 50kN range Suzpecar. The test finished with the sudden failure of the tested joint (see Figure A1. 37).

Figure A1. 37 Failure mode of the mortar-brick adherence tests

After the test, the weight of the debonded brick was determined to take it into account in the following calculus.

Calculating the maximum tensile stress reached in the joint assuming a linear stress distribution. For this purpose, (Eq A1. 8) was used.

$$f_t = \frac{F}{A} - \frac{6M}{lb^2} \quad \text{(Eq A1. 8)}$$

Where, *F* is the applied axial load (adding the applied load to the self-weigh of the debonded brick and the loading tool), *M* is the momentum (applied load by its distance from the joint, *d*, plus the weight of the loading tool by the distance from the joint to its gravity centre), A was the area of the joint cross section, and *l* and *b* the major and minor lengths of the joint cross section respectively.

A1.4.1.4 Dimensions and density

In order to obtain the density value of the masonry 26 samples of 5 piled bricks were weighted and measured. It also provides enough information, together with the dimensions of the bricks, to evaluate the joint thickness average.

Before each test the corresponding samples were measured with a measuring tape (1mm precision) for lengths over 300mm and with a metallic ruler (0.5mm precision) for lengths under 300mm. The mass was determined in the testing conditions with an electronic scales of 50g precision.

Density was directly calculated as the mass of the sample divide by the volume calculated from its main three dimensions, height (*h*), width (*w*) and thickness (*t*). The mortar joint thickness, tm, was calculated for each sample dividing the total mortar thickness by the number of joints (*n-1*). The total mortar thickness is obtained subtracting the total brick height (average height of one brick, h_b, by the number of bricks, *n*) from the total sample height (*H*). See (Eq A1. 9).

$$t_m = \frac{H - h_b \cdot n}{n - 1} \quad \text{(Eq A1. 9)}$$

A1.4.2. Experimental results of the tests on masonry

In this subsection the results of all tests carried out on masonry samples in order to obtain the values of the main mechanical characteristics are presented. For each test type numerical results are summarised in a table. There is also one graph to illustrate the typical mechanical response for each kind of test.

To begin with, Table A1. 17 summarises the results of the tests to obtain the modulus of linear deformation. According with the test procedure (see section A1.4.1.1), three secant modulus were obtained and a weighted average was then calculated according with the stress range of each secant modulus. The three secant modulus, the weighted average modulus and the ratio of this modulus of linear deformation out of the compressive strength are the four parameters summarised in Table A1. 17. E1 is the secant modulus of linear deformation for a stress range between 1MPa and 2.5MPa, E2 for 2.8 to 4.5

MPa and E3 for 4.8 to 5.6MPa in the case of samples 14 to 19. This ranges limits vary to 0.3-1MPa, 1.2-2.1MPa and 2.2-3.1MPa for samples 20 to 29. Modulus of linear deformation was not determined for sample 21.

Sample	***E_1 (MPa)***	***E_2 (MPa)***	***E_3 (MPa)***	***E (MPa)***	***E/f_k***
OF_14	1140	608	1714	1029	122.7
OF_15	1735	543	556	993	148.8
OF_16	192	483	662	409	69.0
OF_17	326	455	441	404	59.4
OF_18	409	818	658	632	81.2
OF_19	986	1629	1566	1375	133.4
OF_20	244	534	483	435	59.2
OF_22	120	664	817	567	81.1
OF_23	1669	518	1447	1175	129.2
OF_24	919	368	832	690	80.5
OF_25	831	1170	1455	1178	102.3
OF_26	697	782	790	761	77.2
OF_27	565	756	1225	871	83.2
OF_28	705	357	632	553	42.0
OF_29	320	560	932	627	42.5

Table A1. 17 Results of the modulus of linear deformation tests of brickwork

The typical behaviour of deformability tests is shown in Figure A1. 38 where a curve with slightly varying slope is presented. For all cases there is an initial range with increasing slope due to the initial settling of the system followed by a linear response for intermediate stresses. Closer to the failure load the sample shows relaxation effects and the slope of the stress-strain curve decrease. It is also shown that unloading and reloading the sample does not change the behaviour so in the reloading stage the curve is practically bonded to the point of the maximum load of the previous loading cycle. It is also worth noticing that large permanent strains remain when unloading. So the masonry compressive behaviour is non-linear and non-elastic. Finally it has to be highlighted that the obtained modulus of Young is far littler than the values proposed by the standards and slightly lower than the values obtained in other researches [2-4]. For numerical purposes, the Young's modulus is chosen to range from 400MPa to 1100MPa according with the previous results. The most representative value for this variable is set to 780MPa.

In relation with the compressive strength tests, Table A1. 18 summarises the results. In Table A1. 18 the main dimensions of the samples as well as the density values for 33 specimens are also presented. Furthermore, there are also summarised the compressive strength results of the specimens built up to qualitatively analyse the effect of the joint thickness or the wetting process of the bricks in the prisms production procedure. They are presented with the label OF_X_1 to OF_X_10.

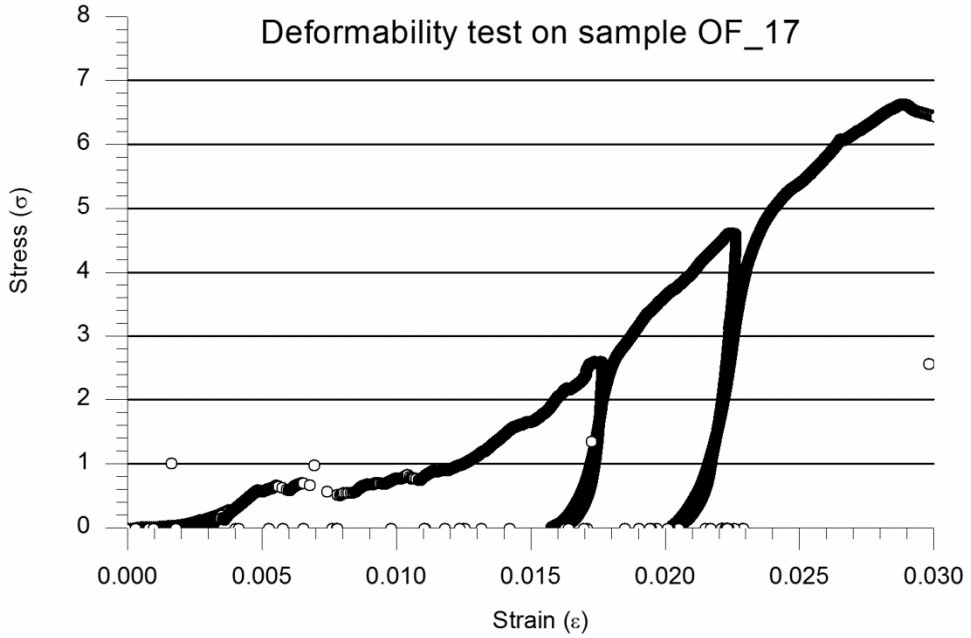

Figure A1. 38 Typical response of a masonry deformability test carried out

Sample	*h (mm)*	*w (mm)*	*t (mm)*	*Mass (kg)*	*Density (kg/m^3)*	*f_c (MPa)*
OF_1	286.7	279.9	132.0	---	---	9.42
OF_2	285.0	280.0	132.0	---	---	16.39
OF_3	297.5	280.0	132.0	---	---	20.00
OF_4	290.6	280.2	131.8	18.85	1756.4	14.86
OF_5	292.4	281.0	135.0	18.85	1699.4	12.42
OF_6	282.0	278.6	132.0	18.50	1783.9	12.36
OF_7	288.2	279.6	134.0	19.40	1796.7	12.32
OF_8	292.0	279.5	132.0	19.30	1791.5	14.83
OF_9	287.3	280.0	131.5	18.75	1772.8	17.01
OF_10	286.8	279.0	131.5	18.90	1796.5	13.63
OF_11	290.0	279.5	132.5	18.55	1727.2	11.94
OF_12	286.3	281.0	131.0	18.95	1798.4	11.76
OF_13	286.0	281.0	131.0	18.85	1790.5	13.07
OF_14	306.5	280.8	132.5	19.45	1705.9	8.38
OF_15	302.3	280.5	132.5	19.00	1691.4	6.67
OF_16	292.0	280.8	132.8	18.20	1672.4	5.93
OF_17	295.3	281.8	132.0	18.55	1689.3	6.80
OF_18	291.8	280.0	132.5	18.35	1695.3	7.79
OF_19	289.8	280.3	132.5	18.55	1724.1	10.31
OF_20	295.5	280.8	132.5	18.60	1692.1	7.35
OF_21	308.5	280.5	131.0	19.20	1693.7	7.81
OF_22	305.8	281.0	131.8	19.15	1691.8	6.99
OF_23	299.3	280.3	132.3	19.10	1722.1	9.09
OF_24	297.5	284.5	132.0	19.05	1705.1	8.56
OF_25	293.5	281.5	133.0	19.50	1774.6	11.51
OF_26	287.0	280.0	131.0	18.90	1795.4	9.86
OF_27	281.5	281.0	131.5	15.50	1490.1	10.47
OF_28	282.5	280.0	131.0	18.50	1785.4	13.16

Sample	*h (mm)*	*w (mm)*	*t (mm)*	*Mass (kg)*	*Density (kg/m^3)*	*f_c (MPa)*
OF_29	242.5	281.0	132.5	16.15	1788.7	14.76
OF_X_1	238.5	131.5	277.5	---	---	---
OF_X_2	234.5	133.5	277.5	---	---	---
OF_X_3	238	131.5	178.5	---	---	---
OF_X_4	253	132.5	278.5	16.2	1735.2	19.70
OF_X_5	252	132	279.5	16.3	1753.2	21.86
OF_X_6	260	132	279.5	16.95	1767.0	22.11
OF_X_7	366.5	131.5	277.5	24.95	1865.6	12.34
OF_X_8	305.5	131	279.5	21.3	1904.2	11.15
OF_X_9	324	131	280	21.2	1783.9	15.10
OF_X_10	331.5	132.5	278.5	21.8	1782.1	14.01

Table A1. 18 Results of the compressive strength tests of brickwork

Large dispersion is observed in masonry compressive strength with values that range from 6MPa to 20MPa for the ordinary samples (no the OF_X_ samples which are not included in the numerical analysis). The representing range of the compressive strength is chosen to be from 7MPa to 15MPa because these two limits are centred and contain most of the experimental values. It is in keeping with the scattering registered for brick and mortar compressive strength. The correspondence of each test with the later on presented full-scale tests has already been presented in Table A1. 16.

A typical force-time response of the compressive strength test is presented in Figure A1. 39. The force application rate was constant after an initial contact increase and the failure by crushing the masonry was sudden.

Regarding the qualitative analysis of the joint thickness it is observed that thinner joints mean greater compressive strength values. It is clear if comparing the fc average value of OF_X_4 to OF_X_6, with thinner joints, with the results of OF_X7 and OF_X_8 which had larger joints. However, if there is no mortar the sample cannot be tested in compression because the punctual contacts fragilely break the bricks at little load levels. This is the case of samples OF_X_1 to OF_X_3. Finally, there is no difference observed between wetting and not wetting the bricks before producing the masonry samples as the strength of OF_X_9 and OF_X_10 is similar to the average of OF_1 to OF_29.

The results of the mortar-brick adherence tests (Bond wrench) are gathered in Table A1. 19. These are divided depending on the mortar used and the loading rate is also shown.

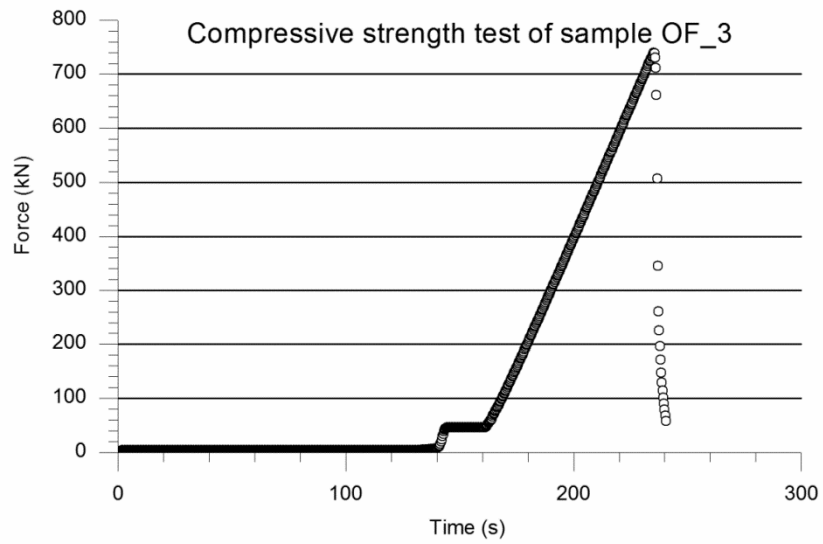

Figure A1. 39 Used loading process for a masonry compressive strength test

Sample	***Mortar type***	***Loading rate (mm/min)***	***f_t (MPa)***
B1	Propamsa M7,5	1	0.28
B2	Propamsa M7,5	1	0.10
B3	Propamsa M7,5	1	0.30
B4	Durland M7,5	2	0.95
B5	Durland M7,5	5	0.41
B6	Durland M7,5	2	0.38
B7	Durland M7,5	2	0.44
B8	Durland M7,5	2	0.54
B9	Durland M7,5	2	0.49
B10	Durland M7,5	2	0.26
B11	Durland M7,5	2	0.67
B12	Durland M7,5	2	0.18
B13	Durland M7,5	2	0.23
B14	Durland M7,5	2	0.25
B15	Durland M7,5	2	0.33
B16	Durland M7,5	2	0.17
B17	Durland M7,5	2	0.29
B18	Durland M7,5	2	0.17
B19	Durland M7,5	2	0.36
B20	Durland M7,5	2	0.33
B21	Durland M7,5	2	0.16
B22	Durland M7,5	2	0.32
B23	Durland M7,5	2	0.21
B24	Durland M7,5	2	0.43
B25	Durland M7,5	2	0.21
B26	Durland M7,5	2	0.42

Table A1. 19 Results of the mortar-brick bond strength tests

The bond wrench quantitative results show considerable scattering. However, the failure mode was the same for all cases. The weaker point was the interface between mortar and brick and the joint suddenly opened at reaching the maximum load (see Figure A1. 41). Peeling phenomena was observed in all samples but it was more evident for the first 12 tests. This peeling effect (see Figure A1. 40) indicates that the adherence between mortar and the surface of the brick was good and that it was the low tensile strength of the surface layer of the brick the limiting property.

Figure A1. 40 Peeling effect in mortar-brick adherence tests

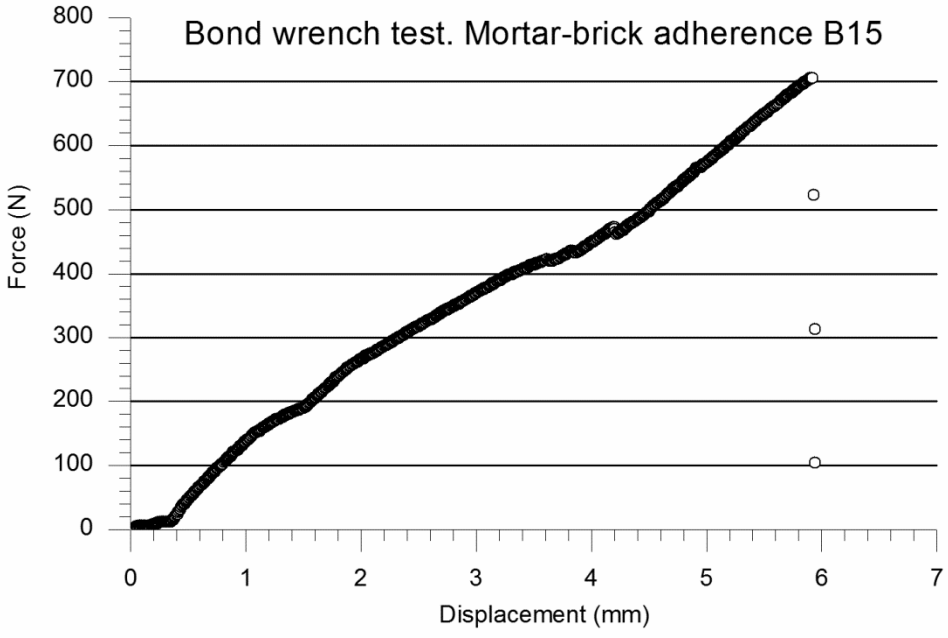

Figure A1. 41 Typical response of a bond wrench test. Mortar-brick adherence experiment B15

The typical force-displacement response measured in the load application point for the bond wrench tests is shown in Figure A1. 41. After an initial settling stage the behaviour is linear up to failure which happens suddenly. The collapse causes the total loss of strength and the total opening of the joint.

Finally, the density of the indoor conditions cured masonry tested is summarised in Table A1. 18. From the main dimensions (average height of 5-bricks piles, H=290.8mm, n=5, and average height of a brick, h_b= 46.6mm) it is obtained that the average mortar joint thickness of the testes samples is 14.4mm.

A1.5 TRM strengthened masonry bending tests

The flexural-tensile behaviour of TRM strengthened brickwork was tested in order to obtain useful information for the simulation or calculus of the TRM strengthened walls carried out later on. It was also important to analyse the possibility of debonding of the strengthening system. No tests of TRM under compressive forces were done because in all the studied cases of the present work the strengthening system was placed in the tensile side of the walls.

The strengthening procedure as well as the testing procedure (three points bending, TPB, test) are fully explained in the next subsection. Finally, results for each test are presented and analysed.

A1.5.1. Sample preparation

13 piles of 10 bricks height and 1 of 9 bricks height were fabricated and air cured in indoor conditions for at least 28 days before applying the strengthening system. The components used to produce the masonry were the bricks characterised in section A1.3 and Durland M7,5 mortar which was described in section A1.2.1.2. The construction procedure was the same than the one described in section A1.4.1 that consist in bricks cleaning and initial levelling, mortar mixing and piling the components with level control. The only difference was that the side that was going to be strengthened was scraped with a metallic brush with the mortar still fresh to ensure there was any excess of mortar that would make it more difficult to apply the TRM afterwards.

The initial geometry of the samples is summarised in Table A1. 20. h is height and b the width measured in the half span section for each sample. n_f is the number of fibre rows placed in the sample width and t_{TRM} is the thickness of the strengthening layer. e_{TRM} is the distance from the masonry side to the position of the fibre grid embedded into the mortar layer. The type of strengthening system used in each sample is also shown. Samples C1 and C2 are the control ones, so no strengthening information is provided for them.

Sample	*b (mm)*	*h (mm)*	*Strengthening mortar (*)*	*Grid(**)*	n_f	t_{TRM} *(mm)*	e_{TRM} *(mm)*
C1	280	133	---	---	---	---	---
C2	280.0	134.0	---	---	---	---	---
R1(***)	283.0	133.0	R	G	10	11.0	7.0
R2	279.5	131.5	R	G	10	13.5	7.0
R3	280.0	133.0	R	G	11	10.5	5.0
M1	277.0	125.0	M	G	10	10.5	7.0
M2	278.5	131.5	M	G	10	9.0	4.5
M3	280.0	131.5	M	G	11	11.5	9.0
X1	278.5	131.5	X	C	29	11.0	4.0
X2	281.0	129.0	X	C	29	11.0	5.0
X3	280.0	133.5	X	C	30	5.0	3.5
X4	281.0	127.0	X	C	28	12.0	6.0
X5	280.0	132.0	X	C	28	15.0	9.0
X6	279.0	133.0	X	C	28	8.0	5.0

(*) R = Planitop HDM Restauro; M = Planitop HDM Maxi; X = Ruredil X Mesh M25

(**) G = Mapegrid G220; C = Ruredil XMesh C10

(***) Nine bricks height specimen

Table A1. 20 Geometry and materials of the samples for the TRM strengthened masonry bending tests

To apply the strengthening the procedure was:

- Cleaning the masonry surface. First of all a metallic brush was used to remove any little imperfections and possible surface efflorescence. After this compressed air was projected against the masonry surface in order to remove any dust or the powder generated in the previous cleaning operation.
- Cutting the fibre grid so it was 10mm shorter in length and width than the masonry side that was going to be strengthened. It is important that the fibre grid do not exceed the dimensions of the masonry surface to be strengthened to prevent any abnormal behaviour due to the stress focusing in grid areas that were not covered with mortar. See Figure A1. 42.
- Wetting the surface pouring water on it. It took several minutes to wet the surface of each specimen. The water was directly poured from a pot to the masonry surface at different points so the whole side that was going to be strengthened got wetted. The wetting process finished when the sample could not absorb any more water. Once finished the watering process the sample was always strengthened within the next 30 min. Right before applying the first mortar layer the water excess was removed with a quick projection of compressed air. See Figure A1. 43.

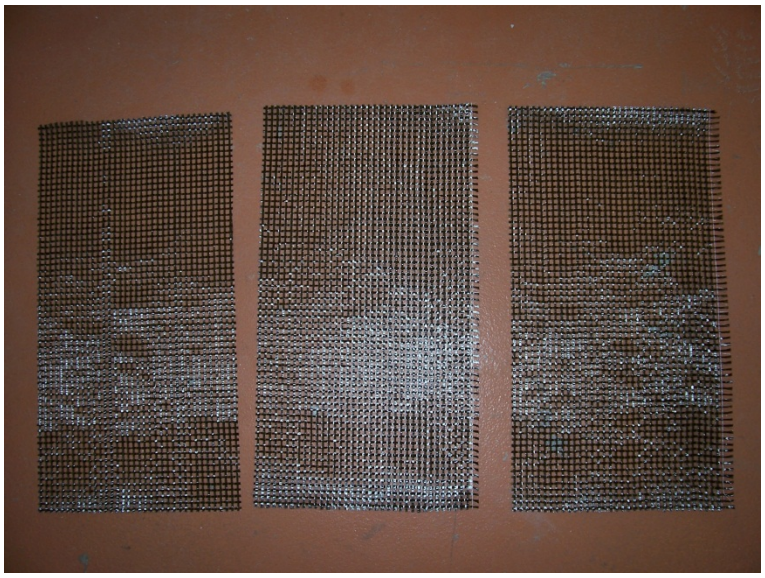

Figure A1. 42. XMesh C10 cut for the specimens X1 X2 and X3

Figure A1. 43. View of a wetted sample ready to receive the first mortar layer

- Mixing the mortar according with the guidelines of the mortar manufacturer for each type. It has been already presented in sections A1.2.1.3 to A1.2.1.5. The main considerations that have to be taken into account are that Planitop HDM Maxi and Planitop HDM Restauro are bicomponent mortars, so the powder phase has to be mixed with the latex-based liquid phase in the proportions indicated by the producer whereas XMesh M25 has to be mixed with current water. All of them have to rest for 2 minutes after mixing them and then carry out a second remix to achieve the correct consistency. If necessary and some minutes after finishing the mixing, they can be remixed to obtain a more fluid texture without

adding any liquid because of their thixotropic behaviour. All the mixing tasks of the used strengthening mortars have to be done with a low velocity mechanical mixer. See Figure A1. 44.

Figure A1. 44. Mixing procedure of mortar XMesh M25 for strengthening samples X1, X2 and X3

- Application of the first layer of the strengthening mortar. Using a trowel, the first layer of mortar was applied with a thickness that should range from 3 to 6mm depending on the mortar. Planitop HDM Maxi is the mortar that allows greater thickness whereas XMesh M25 is the one that requires a thinner layer to be applied. Nevertheless, the first layer thickness has to be uniform in the whole masonry surface. Special attention on edges and corners is required to reach this requirement. See Figure A1. 45.

Figure A1. 45. Application of the first mortar layer. Sample M1

- Presenting the fibre grid in its position, aligning it and embedding it into the first mortar layer. Firstly, the fibre grid is manually positioned on the mortar layer applying little pressure in discrete points so it was possible to adjust it and align the fibre line according with the desired direction. In this case the fibres were vertically and horizontally aligned. Once correctly placed in its position the grid was embedded into the first layer passing a trowel over it with a slight pressure. It is important to be careful in this point to prevent the grid to be moved from the desired position. See Figure A1. 46.

Figure A1. 46. Grid positioning sample M1.

Figure A1. 47. Second mortar layer spreading process for sample X1

- Applying a second mortar layer with a trowel. This layer has to be uniform and the total amount of mortar should not overpass the producer suggested thickness (25mm for Planitop HDM Maxi and 10 mm for Planitop HDM Restauro and XMesh M25). Once again, the performance at edges and corners of the sample is the most difficult point. It is recommended to apply this second mortar layer spreading the product always in the same direction to prevent the formation of voids into the mortar. See Figure A1. 47.
- After applying the second layer mortar the samples rest to air curing at indoor laboratory atmospheric conditions for at least 28 days before testing.

A1.5.2. TPB Test procedure and calculations

Three point bending (TPB) tests were carried out with the strengthened samples and the control ones. The test setup consisted in a specific tool which was used to provide two support lines. Practically these supports were two steel rods (red ones in Figure A1. 48). The sample laid over these supports and a punctual load (distributed along the width of the sample) was applied at the span centre using a steel beam, connected to an electromechanic press. In detail, the testing procedure consisted in:

Placing the sample on the supports with the strengthened side upside down. It was the most sensitive step of all because the samples were fabricated in vertical position to reproduce any possible effect of gravity on the strengthening mortar during the installation of TRM or the curing time. Thus, it was necessary to lift the samples and turn them into horizontal position. The strengthened ones were lifted with a belt straight away and with the assistance of a crane were placed horizontal on a stacking machine. Then the samples slid over the stacking machine directly to the position on the supports. Two people were always necessary to carry out this operation. In contrast, control samples were pre-compressed before following the same movement procedure:

- The supports were placed as the free span was 560mm in all cases except for sample R1. In this case the gap between supports was 460mm.
- Aligning the sample, centring it and levelling the support tool if necessary so the specimen rest perfectly horizontal on the support system and the contact with the rod supports was maximized. See Figure A1. 48.
- Approaching the loading tool (steel beam) up to the contact with the sample checking that the contact was as uniform as possible and that the loading tool was placed exactly in the span's centre. If not the support system and the sample was adjusted to achieve the desired positioning. See Figure A1. 48.
- Installing two potentiometers, one connected to each side of the loading beam to register any in-plane rotation of the loading beam. These sensors measured the vertical descending movement of the loading tool with 0.1mm precision. Connecting the press to the acquisition system so data of applied force and externally measured displacement was simultaneously recorded at 50Hz. See Figure A1. 48.
- Applying the load controlling the electromechanic press (Suzpecar with force range of 50kN) by displacement. The loading rate was 1mm/min. After reaching the maximum load tests followed until the applied load descended under 1kN.
- Measuring the real thickness of the TRM strengthening system as well as the grid position in the mid-span section (e_{TRM}) and the number of fibre rows (n_f) that were contained in the mid-span section. See Figure A1. 49. These data has been presented in Table A1. 20. Taking pictures of the failure mode.

Calculating the maximum bending moment, Mmax, applied for each sample from the data of the sample self-weight, the weight of the loading tool and the applied and registered load.

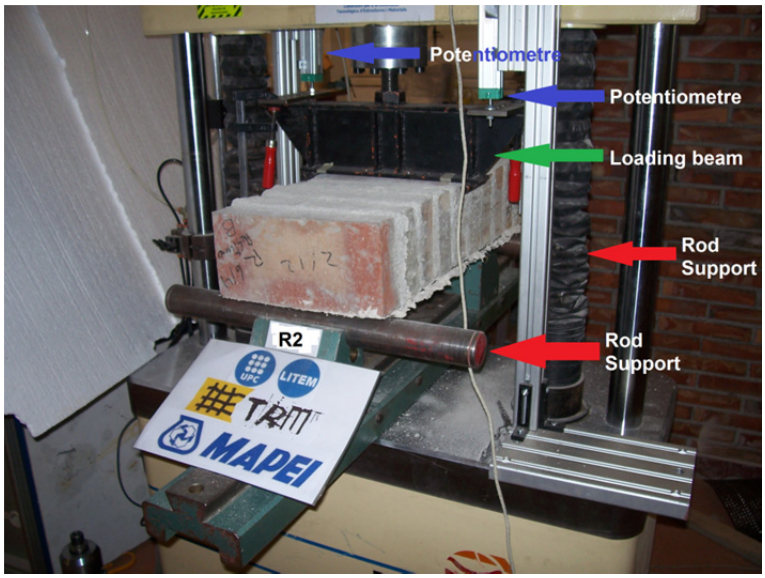

Figure A1. 48 TPB test setup. Sample R2.

Figure A1. 49 Measuring the fibre grid position, the mortar thickness and the number of fibre rows contained in the mid-span section of sample M2

Knowing the position of the fibre grid and the distance from extreme compression fibre to centroid of tension reinforcement, d (Eq A1. 10), the maximum tensile force applied in the TRM reinforcement, Fmax, was calculated according with (Eq A1. 11) which arises from equilibrium equations in the mid-span section.

$$d = h + e_{TRM} \quad \text{(Eq A1. 10)}$$

$$F_{max} = M_{max}/d \quad \text{(Eq A1. 11)}$$

Figure A1. 50. Mid-span cracking. Failure mode of the sample M3

Comparing the maximum tensile force applied on the TRM, F_{max}, with the expected maximum tensile capacity, T, from the manufacturer data, defining an effectiveness ratio, ER which will simplify the comparison between different TRM systems.

$$ER = \frac{\text{Maximum applied tensile force } [F_{max}]}{\text{Manufacturer's tensile strength } [T]} \quad \text{(Eq A1. 12)}$$

A1.5.3. TPB Tests results

Two failure modes were noticed. The first one was the bending failure mode which was associated with breaking the strengthening fibres by tension. See Figure A1. 51. The masonry compressed area was not damaged except from some local damage due to the contact of the loading tool. Any debonding process was observed in the samples that failed this way. Nevertheless, the structural response depended on the type of fibre used as commented below. This was the failure mode of samples R1 to R3, M1 to M3 and X1 to X4.

The second failure mode was associated with the fibres sliding and TRM debonding near the supports of the samples. This phenomenon allowed the masonry structure to fail by shear stresses in the mortar-brick interface. The fibres slid inside the mortar and this inorganic matrix punctually failed by shear near the support area. Finally a clear debonding process of the strengthening mortar happened. See Figure A1. 52. This was the failure mode of two samples: X5 and X6.

Samples with no strengthening (C1 and C2) broke by flexion due to self-weight (650N/m approx.) when removed the tool that made a pre-compression during the placing step. So the produced masonry could not bear its own weight in flexion for a span of 560mm or larger.

Figure A1. 51 Bending failure of the sample R2. One big crack in the mid-span breaking the TRM strengthening system

Figure A1. 52 Shear failure of the sample X6. TRM debonding near the support. Masonry joint failure.

Experimental results of the 14 samples described in Table A1. 20 are presented in Table A1. 21. The maximum applied load, the corresponding bending moment (M_{max}) and the corresponding tensile force in the strengthening (T_{max}) as well as the efficiency ratio (ER) calculated as shown in (Eq A1. 12) are summarised in Table A1. 21.

Sample	*Applied load (N)*	M_{max} *(N·m)*	F_{max} *(N)*	*T (N)*	*ER*
C1	---	< 25.5	---	---	---
C2	---	< 25.5	---	---	---
R1	13030.5	1505.4	10948.4	10975.6	0.998
R2	9372.5	1320.5	9534.6	10975.6	0.869
R3	10979.8	1545.6	11199.8	12073.2	0.928
M1	10265.1	1445.5	10144.0	10975.6	0.924
M2	11099.0	1562.3	11487.3	10975.6	1.047
M3	12954.5	1822.0	12968.1	12073.2	1.074
X1	21671.1	3042.3	22452.8	45518.4	0.493
X2	7026.0	992.0	7403.3	45518.4	0.163
X3	7133.1	1007.0	7350.7	47088.0	0.156
X4	9701.0	1366.5	10274.7	43948.8	0.234
X5	4677.4	663.2	4703.8	43948.8	0.107
X6	4800.0	680.4	4930.4	43948.8	0.112

Table A1. 21 Results of the TPB tests on TRM strengthened masonry samples

Observing the results of Table A1. 21 it is clear that any strengthening system results in a great improvement respect the unreinforced masonry (samples C1 and C2). Moreover it is noticed that samples strengthened with glass fibre grids (R1 to R3 and M1 to M3) achieved the expected performance as ER coefficient is close to 1. Samples strengthened with carbon fibre which failed by bending (X1 to X4) managed to bear up to 25% of the tensile strength of the fibres provided by the manufacturer before sliding the fibres inside the mortar. This ratio descends to 15% if shear failure was observed.

The average maximum moment the strengthened section could bear was 1.5kN·m for 1 glass fibre grid TRM and 1.6kN·m for 1 carbon fibre grid TRM.

The behaviour of samples R1 to R3 and M1 to M3 was the expected one, showing perfect adherence between the masonry, the mortar and the strengthening fibres. The failure load was always limited by the strength of the fibres whereas in the case of carbon fibre strengthened samples the behaviour changed. It was far stiffer than with glass fibre strengthening. It might be this stiffness of the mortar what prevented all the carbon fibre to work together, loading one portion of the width up to failure when the load was transmitted to the next portion of the width which automatically failed and it continues to the collapse of the sample without any stage when all the fibre had been working together. Furthermore, fibre's sliding was clearly observed in the experimental tests. It may be caused by a poor fibre's wetting by the mortar. So it was concluded that the coating of the glass fibre of the samples R1 to R3 and M1 to M3 was useful at assuring a perfect load transmission between masonry and fibre grid.

The experimental response of each sample is graphically represented in Figure A1. 53 to Figure A1. 55. Each graph corresponds to one type of TRM strengthening: glass fibre with Planitop HDM Restauro, glass fibre with Planitop HDM Maxi and carbon fibre with XMesh M25 mortar respectively. Graphs Figure A1. 53 and Figure A1. 54 show a relative maximum corresponding with the mortar tensile failure. After these, the load increased again and reached the maximum load of the tests which corresponded with the fibre breaking. It caused a sudden descend of the load. In contrast, Figure A1. 55 shows how the

failure of the samples strengthened with carbon fibre is more ductile (except for the case X1) which supports the idea that the failure was due to an internal sliding of the fibres inside the mortar matrix. The progressive descending branch of the curves also shows that not all the fibres worked together at the same time but becoming loaded by parts which made it more difficult to develop the full strength of the system.

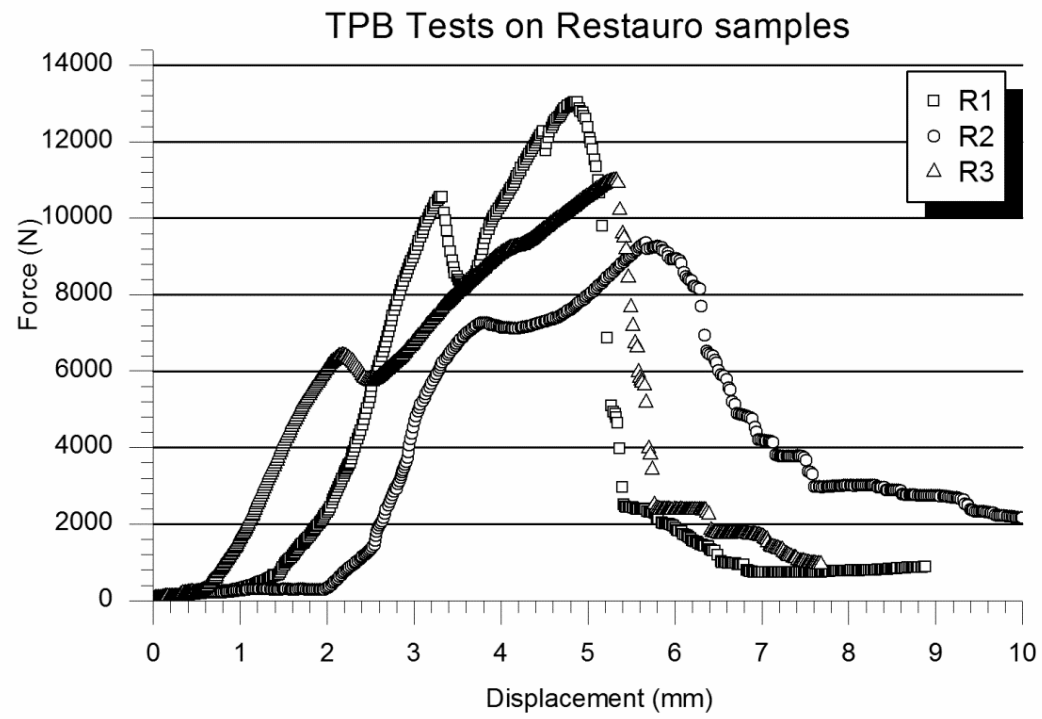

Figure A1. 53 Test results of samples R1 to R3

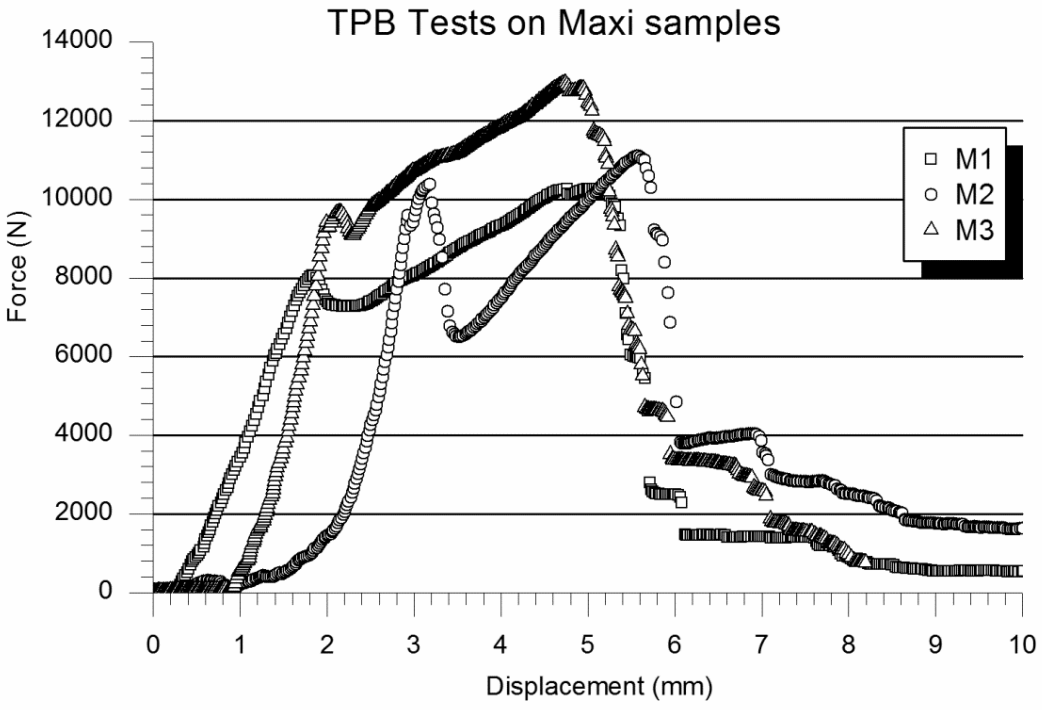

Figure A1. 54 Test results of samples M1 to M3

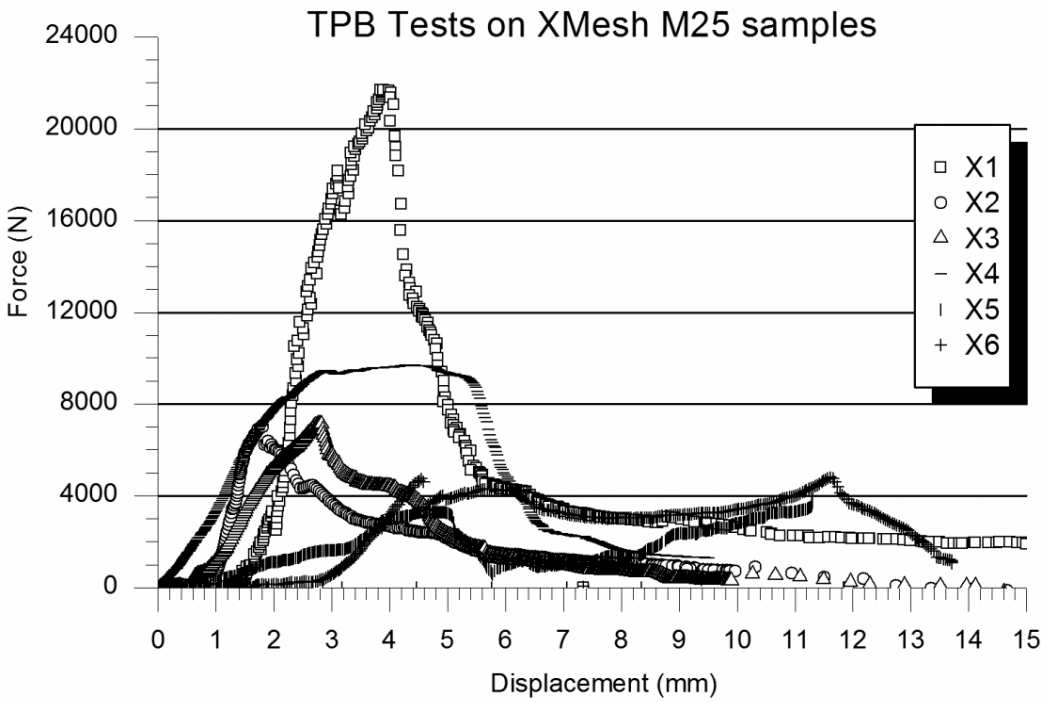

Figure A1. 55 Test results of samples X1 to X6

A1.6 Real scale tests on masonry walls

In this section of the annex a full description of the tests on real scale masonry walls is presented. It is covered from the design of the tests setup and specimens up to the presentation and brief analysis of the results taking into account all the steps followed for developing the experimental campaign. It includes: the design and construction of the walls, the definition of the strengthening variables to analyse and the strengthening particularities, the logistics related with their curing process and transport right to the test position, the test setup and the experimental procedure which slightly varied from test to test.

Particularities found when carrying out the tests are summarised and presented. The subsections below followed the chronological path of the tests:

A1.6.1. Wall's design, variables definition and wall's construction

After a literature overview it was noticed that data about the behaviour of single unreinforced masonry walls under compression when second order bending effects or buckling might appear was lacking. In particular more experimental information acquired with nowadays sensors seemed necessary.

The previous tests (previous sections of this annex) were necessary to characterise the materials that were used to produce the real scale specimens defined here but are not considered as variables but as fixed input values.

A detailed study of the problem recommended maintaining the boundary conditions of the test as clear as possible in order to easily use the obtained data in later on developed numerical models or to contrast with the existing ones. For this reason the walls were pinned at both endings in the test setup configuration.

Furthermore, it was necessary to analyse walls of different slenderness (series H, M, S, F and T according with Table A1. 22) and with different eccentricities of the load application to provide the range of results necessary. All walls except W#17, series T, were single-wythed. Using the same test setup to apply different eccentricities was economically essential so an adjustable system to connect the walls with the test setup was used. It made it necessary to build the walls inside a steel tool called heading element (see Figure A1. 56).

H series was thought to represent real load bearing brickwork walls with height between 2.5m and 3m, and single-wythed whereas M series were produced with height enough to develop the buckling phenomena but far easier to transport and place in position than H series. S walls are the ones with less slenderness and though to compare with cases for which the development of second order bending forces is more complicated and crushing may be more probable. F wall (W#4) was used to prove the effect of the boundary conditions. It has the lower edge fixed and the upper one partially fixed. Finally, W#17 was classified as T series because it was used to qualitatively reveal the effect of having two wythes when a wall is eccentrically loaded in plane.

Geometry type	***Height, H (mm)***	***Wide, b (mm)***	***Thickness, t (mm)***	***Slenderness, λ***	***Walls***
H	2700	900	132	20.5	1-3,5-9
F	2700	900	132	14.4	4
M	1650	900	132	12.5	10-16, 21-29
S	1000	900	132	7.6	18-20
T	1800	900	270	6.7	17

Table A1. 22 Theoretical geometry of the different slenderness series

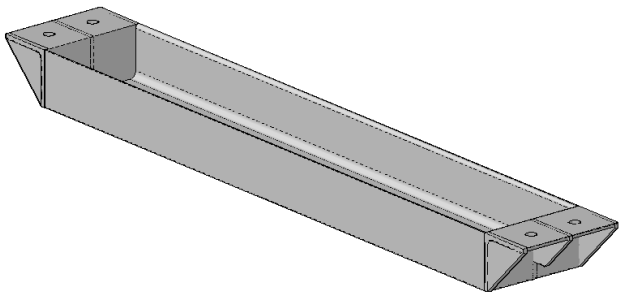

Figure A1. 56 Heading element

20 unreinforced masonry walls (URMW) have been designed, built and tested. These are walls W#1 to W#20. However, knowing the vulnerability of these structural elements in front of out-of plane deformations it was thought essential to study a method to improve their load bearing capacity in front of second order bending or buckling phenomena. Among all possibilities, textile reinforced mortar (TRM) has showed the most promising results (according with the information provided in Chapter 2). For this reason, 9 TRM strengthened walls were tested too. These were W#21 to W#29 and corresponded to M series before strengthening. In this case, the analysed variables were the type of fibre, the type of strengthening mortar, the number of fibre grids in one side and the possibility of installing connectors to assure perfect bonding. The strengthening combinations summarised in Table A1. 23 were applied on the corresponding walls W#21 to W#29 to study all these mentioned variables.

Wall #	***Fibre grid***	***Mortar***	***Fibre layers***	***Connectors***	***TRM System***
W#21	MapeGrid G220	Planitop HDM Maxi	1	0	G_P_1_0
W#22	MapeGrid G220	Planitop HDM Maxi	1	0	G_P_1_0
W#26	MapeGrid G220	Planitop HDM Maxi	2	0	G_P_2_0
W#23	MapeGrid G220	Planitop HDM Restauro	1	0	G_C_1_0
W#24	MapeGrid G220	Planitop HDM Restauro	1	0	G_C_1_0
W#25	MapeGrid G220	Planitop HDM Restauro	2	0	G_C_2_0
W#27	XMesh C10	XMesh M25	1	0	C_X_1_0
W#28	XMesh C10	XMesh M25	1	6	C_X_1_6
W#29	XMesh C10	XMesh M25	1	9	C_X_1_9

Table A1. 23 Strengthening characteristics for TRM strengthened walls

Figure A1. 57 Walls W#4 and W#5 build inside laboratory facilities

Only the first wall (W#1) was constructed by LITEM workers whereas 24 of the walls were built by the same workers from Construcciones Mediterraneo 1994, S.L. These were walls W#2-W#5 (see Figure A1. 57) and W#10-W#29. Walls W#6-W#9 were arisen by a local professional bricklayer.

All walls were built using the same construction procedure:

Preparing the bricks by cutting them with a radial saw. Halves were needed for all walls. Moreover quarters were used in wall W#17. After this, the dust and other alien particles were removed and the bricks immersed for at least 1 minute into water to assure a correct bonding with the mortar at interface contacts.

Preparing the heading element. It is cleaning it with water, drying it and covering its inner part with a thin layer of oil to make it easy to remove the wall's residues after the tests in order to reuse the heading elements.

Levelling the heading element. At least 4 walls were simultaneously built (except for wall W#1) with the purpose of slowing down the construction of the walls which would have caused the application of the gravity load on too fresh joints compared with real execution process. For this reason at least 4 heading elements were levelled to assure the vertical alignment from the very first beginning.

Mixing the mortar. It was Propamsa M7,5 for wall W#1 which, furthermore, was manually mixed. For the rest of the walls the mortar was prepared with a cement mixer and it was Durland M7,5.

Placing a 2cm layer of mortar inside the heading element and constructing the wall over this layer. The purpose of placing a mortar layer was double: firstly to uniformly distribute the stresses and avoid punctual contacts between the steel heading element and the ceramic bricks which could have caused local failures and distorted the structural behaviour. Secondly, it would make it easier to remove the wall's residues from inside the heading element once the tests finished.

Building the walls (at least 4 simultaneously) controlling the vertical and horizontal alignment at each row. All joints were totally filled with mortar.

Regarding the building process it is worth noticing that the most slender walls (H series) were a real challenge for the building professionals as they were very instable due to the slenderness, the reduced width (900mm, see Figure A1. 57) and the lack of out-of-plane tying. This situation complicated the settling of the upper masonry rows.

Figure A1. 58 Construction material for walls W#2 to W#29

Pictures of Figure A1. 58 to Figure A1. 64 show the construction process and the final appearance of the tested walls just after finishing their construction.

Figure A1. 59 Construction of walls W#2 to W#5

Figure A1. 60 Wall W#1

Figure A1. 61 Walls W# to W#5

Figure A1. 62 Walls W#6 to W#9

Figure A1. 63 Walls W#10 to W#17

Figure A1. 64 Walls W#18 to W#29

A1.6.2. Curing and moving the walls

Walls W#1 to W#9 were built inside LITEM laboratory facilities so they were cured in indoor air conditions. They were not wetted nor exposed to windy conditions. In contrast, walls W#10 to W#29 were built outdoors and cured at environmental temperature and exposed to wind. They were under a roof so were not wetted by the rain. Building and testing time for each wall is summarised in Table A1. 24. Strengthening time is also shown if corresponds.

Wall	***Building date***	***Strengthening date***	***Testing date***
W#1	March ‘09	---	July ‘09
W#2 to W#5	July ‘09	---	September ’09 / October ‘09
W#6 to W#9	October ‘09	---	January ’10 / February ‘10
W#10 to W#17	December ‘09	---	February ’10 / March ‘10
W#18 to W#20	December ‘10	---	February ’11 / March ‘11
W#21 to W#29	December ‘10	March ’11 / May ‘11	June ’11 / July ‘11

Table A1. 24 Building, strengthening and testing times

It was necessary to move the walls W#10 to W#29 from outside to inside laboratory facilities. Once the walls were inside they had to be moved again to the test position. The main requirement to undertake these displacements was to carry the weight of the wall through the bottom heading tool in order to prevent the application of tensile forces in the masonry.

Four main displacement procedures were used in the experimental campaign:

A1.6.2.1 Moving walls W#10 to W#29 from outside to inside the laboratory

An elevation tool that had wheels was mounted to slightly elevate the walls from the floor and move them. The elevation tool is shown in Figure A1. 65 to Figure A1. 68. First of all, the wheels of the elevation tool were blocked. With 4 screwed bars the heading tool where the wall was built was elevated and hanged. Then the wall is loaded on the elevation tool. The wall was manually pushed to enter it into the laboratory. The displacement was always in the direction of the wall plane so no out-of-plane forces were applied on the masonry.

Once inside the laboratory the wall was unloaded and left on the floor in a provisional position. The wall was levelled with thin steel plates to prevent any possible balancing movement.

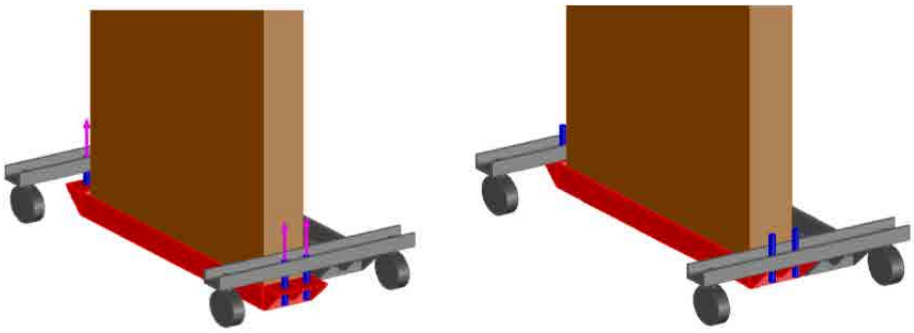

Figure A1. 65 Elevation tool and lifting procedure

Figure A1. 66 Lifting procedure for wall W#17

Figure A1. 67 Displacement of the wall W#17

Figure A1. 68 Elevation and displacement tool. Wall W#10.

A1.6.2.2 Hanging the walls to move them inside the laboratory

To move the walls inside the laboratory from one point to another or to load the walls on the stacking machine to place those in the test positioning (only series M, S and T) the specimens were hanged by a crane.

A heading tool was placed at the top of the wall to be moved. If the wall was going to be positioned in the test setup a mortar layer of 2cm was spread between the wall's top and the upper heading tool with the same purpose as the mortar layer in the base of the wall (see section A1.6.2.1). In this case, at least 4 days were waited before testing the wall. In other cases the upper heading tool was placed with no mortar.

Four bars were fixed to the bottom heading tool and passed through the holes of the upper heading tool. Each bar was fixed to a hook and two short steel bars at each side of the wall connected a pair of hooks. Finally a chain held the group, connected to the short bars. From a crane the chain was lifted and so the full wall was hanged. It is worth noticing that the wall's weight was supported by the bottom heading tool all the time. See Figure A1. 69.

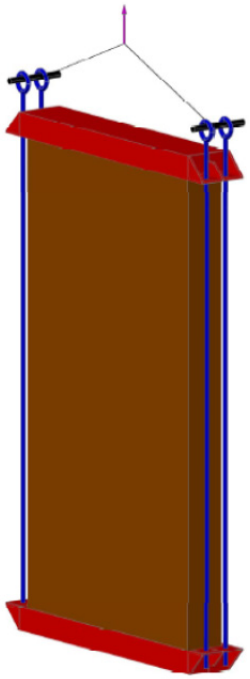

Figure A1. 69 Hanging the walls inside the laboratory to displace them

A1.6.2.3 Placing H and F series walls in test position

Because of height limitation it was not possible to directly put the wall between the two fixed hinges. For these reason, the procedure followed to position samples of series H and F into test spot was slightly fragile. The technique evolved during the campaign but there were two main different strategies:

Using rods to move the wall

The lower hinge was fixed to prevent any rotation. Then it was put over a group of rods on the floor in an area accessible by the overhead crane.

The wall was hanged from the crane as explained in A1.6.2.2 and laid on the lower hinge. The wall and the hinge were connected.

Pushing the wall it slid over the rods and was moved until placed under the upper hinge.

Two manual jacks, one located at each side of the lower hinge, were used in order to elevate this hinge to remove the rods below it. The lower hinge + wall group was laid in position and the alignment was checked. If necessary, the position was adjusted with the aid of cramps and a chain hoist.

Finally, the upper hinge descended and the loading system was connected to the wall leaving the masonry structure in position and ready to test.

The procedure to move the wall and place it on the lower hinge is shown in Figure A1. 70. The use of the rods is illustrated in Figure A1. 71.

Figure A1. 70 Moving wall W#2 with the crane and leaving it on the lower hinge.

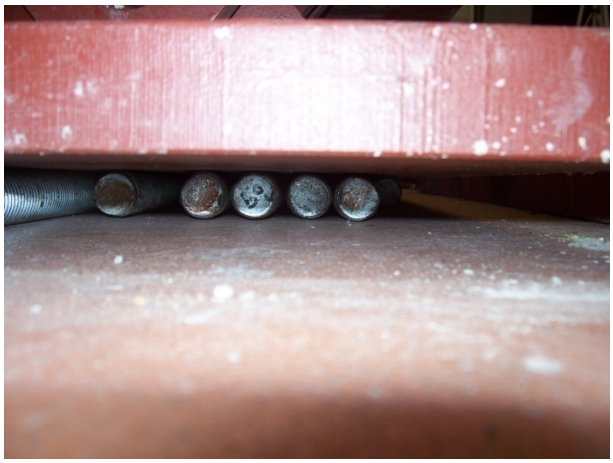

Figure A1. 71 Using rods to move walls of H and F series

Using wheels to move the wall

First of all, the lower hinge was removed from its place under the loading system and it was put on the floor in an area accessible by the overhead crane. Then this lower hinge was blocked to prevent any rotation.

The wall was hanged from the crane, laid on the lower hinge and connected to it.

With two auxiliary tools consisting of a couple of “C” steel profiles which held the upper half of the lower hinge and two wheels connected to each pair of “C” profiles, the wall was lifted screwing 4 M30 bars. The group wall + lower hinge was now loaded on four wheels.

Moving the group under the loading system and aligning it with the fixed upper hinge. When it was in position, the group wall + lower hinge was unloaded and laid on the floor. A second checking of the alignment of the upper side of the wall and the upper hinge was done. If required the group was dragged with the assistance of a chain hoist and a cramp connected to the loading frame

When the wall was correctly placed, the upper hinge descended and was connected to the wall. Now the sample was in the testing position (see Figure A1. 72).

Figure A1. 72 Wall W#3 placed in test position

A1.6.2.4 Placing M, S and T walls in test position

The procedure was different from walls of series H and F because in this case the walls were placed over a steel beam that height the lower hinge up to the required level because the upper hinge was in the same position than in tests of series H and F but the walls were 1m shorter or more. This situation allowed loading the walls on a stacking machine which directly placed them on the lower hinge which

was always fixed to the support steel beam and aligned with the upper hinge. A second checking of the alignment made it possible a repositioning process using cramps and a chain hoist. Finally the upper hinge descended and was connected to the wall which was ready for testing.

A1.6.3. Strengthening procedure

The strengthening procedure of the real scale masonry walls was similar to the one presented in section A1.5.1 which was applied to little samples. The main differences are presented below together with a summary of the general procedure previously presented (see section A1.5.1). It is:

- **Only for walls W#28 and W#29**: Drilling the holes where the connectors were going to be placed crossing the section of the wall and connecting the TRM of the tensile side with the compressed side. These holes were done through the mortar joints as they are the weakest point of masonry. 6 drills were done in W#28 and 9 holes for W#29. The position of the holes is shown in Figure A1. 74 and a picture of the drilling process is presented in Figure A1. 75. The upper and lower rows of holes are in the second mortar joint. The horizontal separation between the holes of the same row is 225mm. For the central row of holes (only for W#29), the two near the edges were drilled in the joint just below the mid-height brick row. The central one is in the immediate upper joint from the mid-height brick row (see Figure A1. 74).

Figure A1. 73 Wall W#13 placed in test position

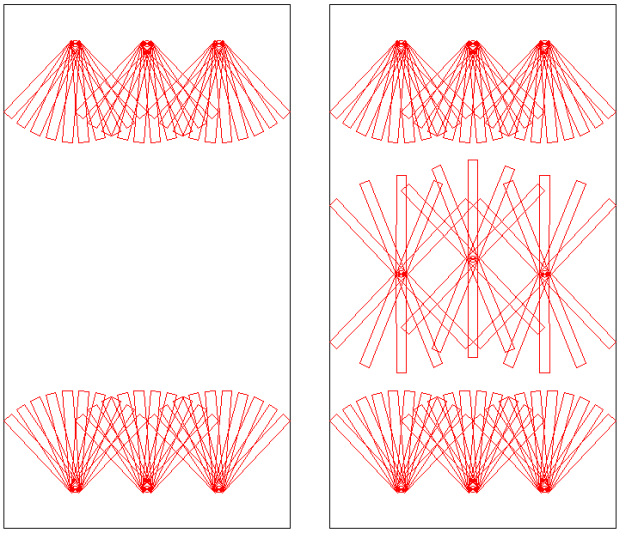

Figure A1. 74 Distribution of the connectors of wall W#28 and W#29

Figure A1. 75 Drilling process of wall W#29

- Cleaning the surface (see Figure A1. 76). To begin with, the mortar bulges were removed with a chisel. This excessive mortar was cut always in vertical descending direction to prevent the debonding of any brick. After this, the cleaning process continued as mentioned before with a metallic brush and compressed air. The area of the non-strengthened side that had to be covered by the connectors was cleaned the same way.

Figure A1. 76 Brushing the masonry surface to remove little mortar irregularities

- Cutting the fibre grid a little shorter in length and width than the wall's side. **Specific considerations:** For walls W#25 and W#26 two fibre grids were cut because they were produced to study the effect of placing two grids in one TRM layer. The connectors for walls W#28 and W#29 were cut and rolled (see Figure A1. 77) to quickly install them with the same mortar layer which would be the TRM matrix. The connectors were positioned in the grid (see Figure A1. 78) to mark and leave the necessary space to pass them (just cut the nylon mounting grid, never the carbon fibre grid) when installing. Connectors were 730mm long to be spread in a 300mm radius (see Figure A1. 74) area in each side of the wall after crossing the wall's thickness (approx. 130mm). The same fibre grid was cut to make the connectors.

Figure A1. 77 Connectors for walls W#28 and W#29

Figure A1. 78 Connectors positioned in the grid XMesh C10

- Wetting the surface pouring water on it (see Figure A1. 79). It took almost half an hour to wet the surface of one M series wall. The wetting procedure was the same than the one presented in section A1.5.1 except for the fact that real scale walls rested up to one hour between wetting them and applying the strengthening mortar. Removing the water exceed with air compressed was not necessary because of the timing.

Figure A1. 79 Wetting M series wall to be strengthened

- Mechanically mixing the mortar according with the guidelines of the mortar manufacturer for each type. However, the mortar for walls W#27, W#28 and W#29 (XMesh M25 strengthening mortar) required only 90% of the water considered by the producer what coincides with the applicator's recommendations. The standard mixing procedure has been already presented in sections A1.2.1.3 to A1.2.1.5. For all cases, the powder component was added to the liquid one (water for XMesh M25) whilst mechanically mixed at low speed.

Figure A1. 80 Mortar Planitop HDM Restauro just after being mixed

- Application of the first layer of the strengthening mortar. The thickness was about 5mm for all mortars. It was planned to keep a uniform thickness in all wall's surface but close to the edges the first mortar layer was approximately 3mm thick. For walls W#28 and W#29 the mortar of this first layer was removed from the drilled holes planned to be filled by the connectors.

It is worth noticing that the first and a half upper masonry row was not strengthened because it was necessary to maintain the wall's thickness to fit the upper heading tool which was indispensable to connect the wall with the loading tools. See Figure A1. 81.

- Putting the fibre grid on the fresh mortar first layer. It required presenting the grid and aligning it with the vertical and horizontal directions. For walls W#25 and W#26 two glass fibre grids were presented simultaneously and positioned alternating the spaces as shown in Figure A1. 82. The grids were slightly embedded into the mortar with little hand pressure and then fully embedded with a trowel trying not to move the grid. See Figure A1. 83. In the case of W#25 andW#26 after embedding the first grid the second one was placed over with no intermediate mortar layer and embedded the same way.

- **Only for walls W#28 and W#29**: after embedding the fibre grid, the connectors were placed in their position through the wall. Then, the free part of each connector was cut to divide it in a few (from 5 to 8 per connector) bands of 300mm length that were spread and embedded into the mortar layer were the full-side fibre grid was already embedded. It is clarified by observing Figure A1. 84.

Figure A1. 81 First layer of Planitop HDM Restauro mortar. Upper are of the wall covered to prevent the mortar to stack on it.

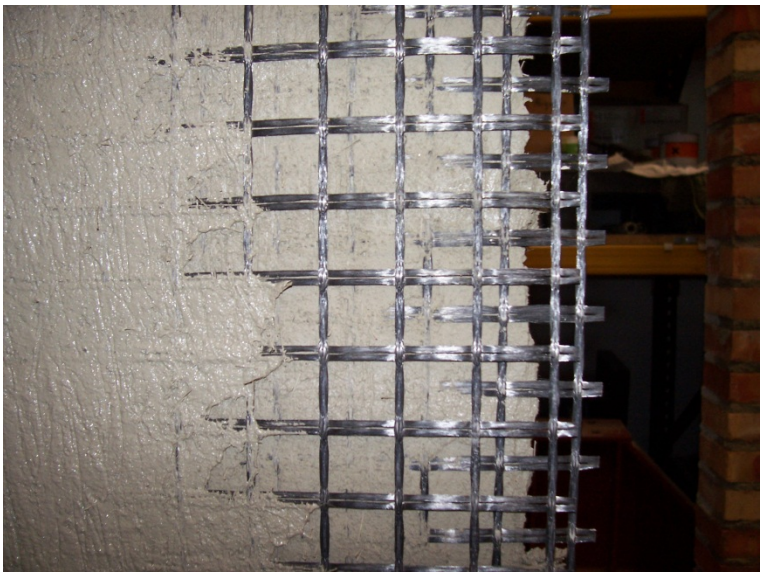

Figure A1. 82 Two glass fibre grids alternately placed

Figure A1. 83 Embedding the glass fibre grid with a trowel

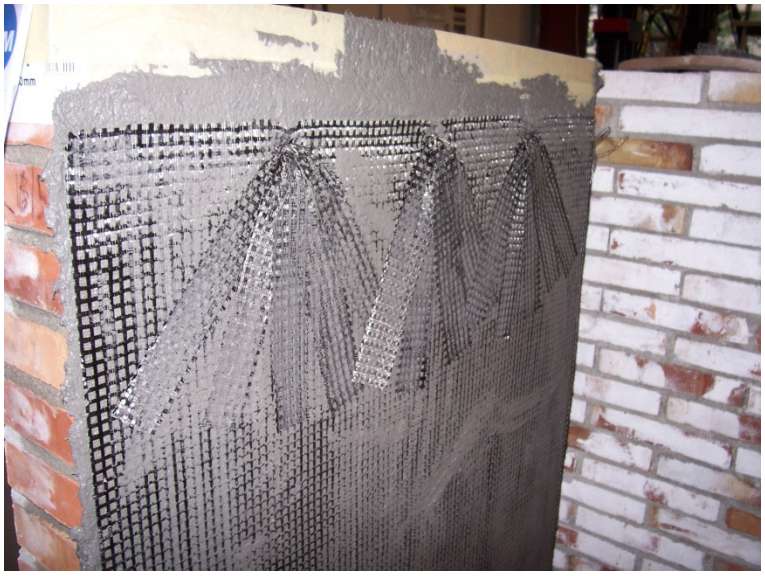

Figure A1. 84 Wall W#28 with the fibre grid and the connectors embedded into the first mortar layer.

- Applying the second mortar layer with a trowel and spreading the product in one direction to prevent the grids from displacing and to avoid the voids formation. The procedure was the same than in section A1.5.1 except for the specific considerations regarding walls W#28 and W#29 for which the presence of connectors required a thicker layer of mortar near the connectors' "root" (where the

connectors crossed the wall). It was difficult to maintain the plane surface as the geometry of the connectors required a thickness of the hole's diameter to be covered with mortar. See Figure A1. 86.

Figure A1. 85 Spreading the second mortar layer of a two grids TRM strengthening (wall W#26)

Figure A1. 86 Final state of a TRM strengthened wall with 6 connectors (W#28)

- **Only for walls W#28 and W#29**: the masonry have to be cleaned and wetted, the connectors spread and the mortar placed to apply a TRM system in the non-strengthened side of the wall in order to bond the connectors. Before bonding them with an equivalent procedure than the one described from a) to h), the holes where the connectors were placed were filled (as much as possible) with the same strengthening mortar. The appearance of the non-strengthened side of the wall W#29 is shown in Figure A1. 87.

Figure A1. 87 Connectors bonding on the non-strengthened face of wall W#29.

- Indoor air curing at laboratory for at least 28 days before testing.

A1.6.4. Test setup and testing procedure

Test setups of real-scale masonry walls are described with detail in this section. Two main setups were used. The first one, intended for walls of series H and F, was characterised by directly supporting the lower hinge on the floor whereas the lower hinge was laid on a steel beam for the second setup. All test used the same loading tools and the upper part of the system was maintained except for the variations described below.

So first of all, the shared upper part is described. After this the particularities for each of the two main setups are presented and finally specific variations from wall to wall are also related.

A1.6.4.1 Loading system. Upper part

The loading system may be divided in four parts: load-transmission part, the load application element, the load-reacting structure and the auxiliary elements. The first one was compound by the upper hinge where the top heading element of the wall was connected with the aid of some plates and the load distribution beam which was fixed to the upper hinge. The load application element was a hydraulic jack

of 1000kN range manually controlled by an oil pressure valve. If the displacement range of the jack was not enough some steel plates where placed under it to height the contact point with the distribution beam. The load-reacting structure was a steel beam where the jack was fixed. This steel beam was connected to the load frame of the laboratory so the loads are always transmitted to this one last. Two main auxiliary elements were used: four steel beams planned to keep the distributing beam always vertically aligned. This steel beams held from two other "L" section beams supported on the loading frame. Some thin steel plates were placed between the distribution beam and these pillars to perfectly adjust the system and maintain the vertical position. The second auxiliary element was 4 bars held by two "H" section steel profiles that were used to temporary held the distribution beam before the wall was placed at its position. For better understanding see Figure A1. 88. This upper part was the same for all the tests with the variations described later on.

A1.6.4.2 Supporting system for H and F series walls. Lower part

The wall was connected to the lower hinge with a pair of steel plates which seized the lower heading tool of the wall. The lower hinge directly laid on the floor.

A1.6.4.3 Supporting system for M and T series walls. Lower part

The setup was the same than for walls H and F except for the fact that the lower hinge laid on a steel beam which was supported by four "V" steel structures. A pair of "C" profiles seized the lower hinge at each side as seen in Figure A1. 88.

A1.6.4.4 Supporting system for S series walls. Lower part

The setup was the same than for walls of M and T series but adding four pillar between the "V" elements and the supporting steel beam to height 500mm the lower hinge.

A1.6.4.5 Particularities of the setup for specific walls

Some tests were carried out with little variations on the test setup described before. The most considerable changes are described below:

Setup for wall W#1 did not count with the auxiliary elements described in section A1.6.4.1. The distribution beam was kept vertically aligned with the aid of just one steel pillar instead of the four of the common setup. A bar connected to a steel plat at each side was also used with this purpose (see Figure A1. 89). Moreover, the holding elements for the distribution beam consisted in a pair of chains in contrast with the bars and steel profiles described before. See Figure A1. 90.

Setup for walls W#2 to W#5 had the same holding system for the distribution beam than test setup for W#1. The particularity was having four steel lattices as elements to maintain the distribution beam vertically aligned. See Figure A1. 91. For walls W#1 and W#2 the loading jack had a hinge installed at the contact with the distribution beam. Wall W#4 had the lower hinge blocked. Wall W#17 (only one of T

series) was connected to the hinges using two “C” steel profiles at each side which seized the heading elements and fixed them to the hinges. See Figure A1. 92.

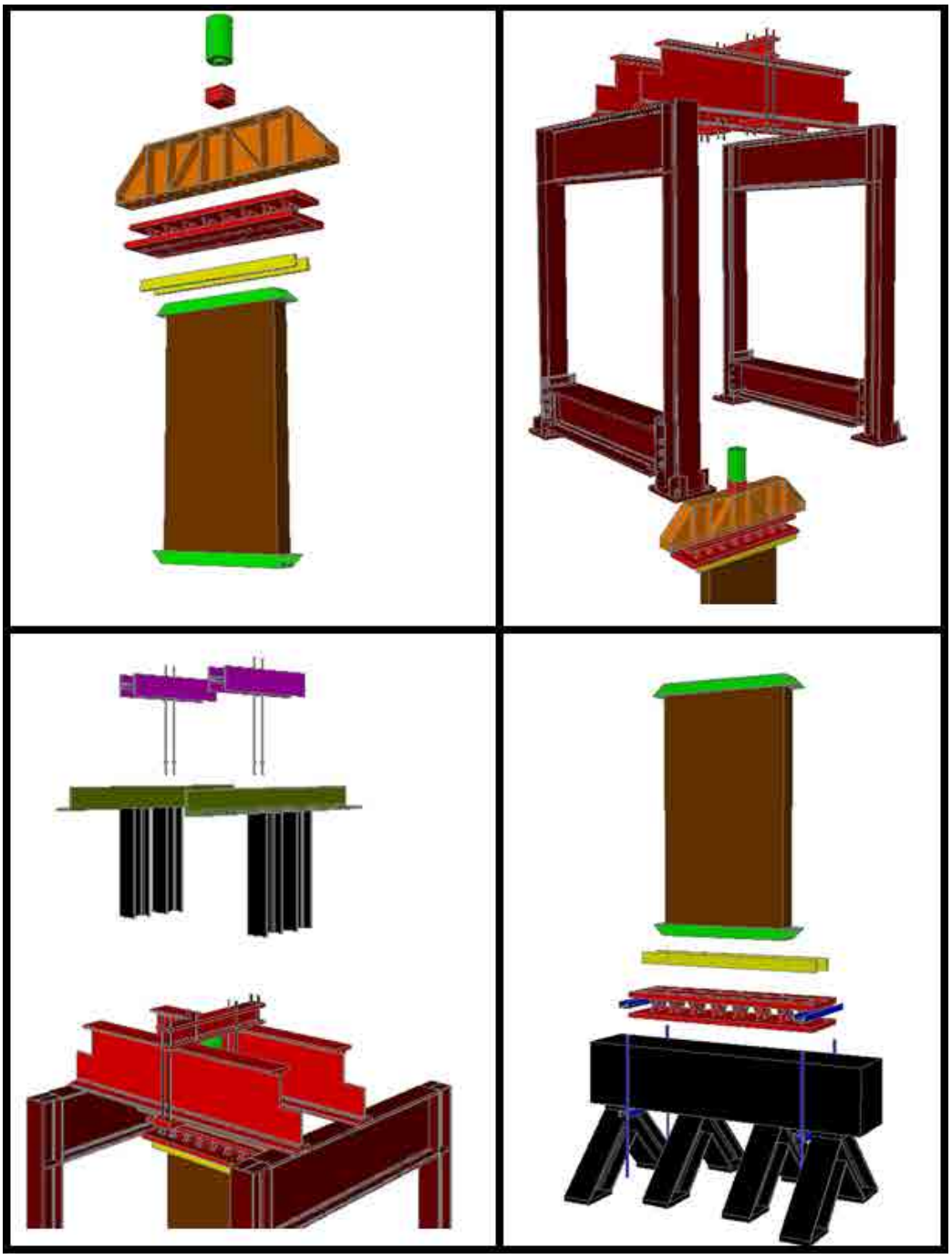

Figure A1. 88 Test setup sketch. Up left: the wall with the heading elements (green), the steel plates (yellow) used to connect the wall to the upper hinge (red) which was fixed to the load distribution beam (orange). The range of the hydraulic jack (green) may be extended with steel plates (red). Up right: the load-reacting structure. Down left: Auxiliary elements to vertically guide (green and black) the load distribution beam and to support it (pink). Down right: supporting system for walls of M and T series with a steel beam over supports (black) where the bottom hinge (right) is fixed with auxiliary elements (blue). The wall with the heading element (green) was connected to the hinge with the steel plates (yellow).

Figure A1. 89 Tool (steel plate and bar) to keep the vertical alignment of the distribution beam in test W#1

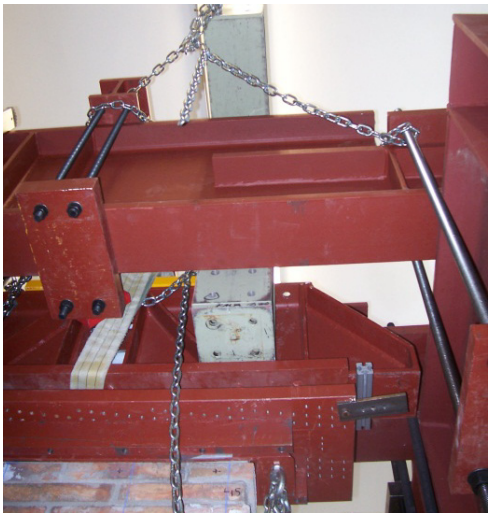

Figure A1. 90 Upper area of the test setup for wall W#1. The distribution beam was held by chains and vertically aligned with only one steel pillar.

Figure A1. 91 Detail of the steel lattice installed in test setup for walls W#2 to W#5 to control the vertical alignment of the distribution beam during the test.

Figure A1. 92. Wall-hinge connection system specially used in wall W#17 (T series)

A1.6.4.6 Sensors

Three types of sensors were used: potentiometers to measure displacements with contact, displacement laser sensors to measure displacements of the wall without contacting it and pressure transmitters to indirectly measure the load applied by the jack.

A brief description of its sensor and application in the tests of real scale walls is herein presented:

Leo-3 was a 700bar range pressure transmitter used to measure the pressure of the oil at the income connection of the hydraulic jack. Its precision was 0.1% of its range what means 1kN. The output signal was electric intensity from 4 to 20 mA. It was used for tests W#1 to W#17. It has a display. See Figure A1. 93.

Wika S-10 was a 1000bar range pressure transmitter with a precision of 0.25% of the full range what means 2.5kN. As the previous one its output was 4...20mA but has no display. Two of them were used in tests W#18 to W#29 to measure the oil pressure at the jack income and to detect any pressure loss in the hydraulic circuit as the other sensor was placed at the output of the pump. See Figure A1. 94.

RF-603 is a laser triangulation position sensor with a measuring range of 500mm, 0.4mm precision and an electrical output of 0...10V. Lasers were protect inside a steel open steel box to prevent any damage by the projection of masonry crushed little elements at wall's failure. Two of them were used in all tests to measure the out-of-plane displacement of the wall at mid-height and ¼ free height. The other two were also used in tests W#6 to W#29 to measure the out-of-plane displacement at ¾ of the buckling free height and the out-of-plane displacement of the distribution beam which was theoretically impeded. See Figure A1. 95. These sensors need an external voltage supply of 12V.

Waycon LWR-100 is a potentiometric displacement sensor consisting in a variable electric resistance of 5kΩ. The analogic measure was output as a voltage. It was used in contact with the element to be measured and fixed to an external element no to take into account the system deformation in the reading. Eight of them were used in all tests: four measuring the descending displacement of the load-distribution beam at the upper four corners so any rotation would be also measured; two indirectly measuring the rotation of the upper hinge by measuring the distance between the two parts of the hinge in the side it closed; two more measuring the rotation of the lower hinge in the same way. See Figure A1. 96.

Figure A1. 93 Keller LEO-3 pressure sensor

Figure A1. 94 Wika S-10 pressure sensor

Concrete strain gages to measure the strain in the surface of the TRM of walls W#21 to W#24 and W#27. Two types of strain gages were used: HBM 1-LY41-50/120 and Vishay N2A-06-20CBW-350 of 120ohms and 350ohms of resistance respectively. Both types were installed on the mortar following the next process: polishing the mortar surface until a perfectly plain area was obtained; preparing the strain gages in a glass plate and covering them with stacking tape used to transfer them to the installation point; marking the position in the TRM mortar surface; positioning the strain gage; mixing the bonding component which was HBM X60 for all cases; applying the glue on the strain gage and transferring it to the mortar surface pressing it; after 24hours the tape was removed and the strain gage was in its position; welding the wires to connect the strain gage to the data acquirement equipment. Seven strain gages were installed in walls W#21, W#23 and W#27 and five in walls W#22 and W#24. See Figure A1. 97.

In Table A1. 25 the use of each sensor depending on the test is summarised. Figure A1. 98 shows the position of the sensors.

Figure A1. 95 Riftek RF-603 laser position sensor

Figure A1. 96 Waycon LRW-100 displacement potentiometric sensor

Figure A1. 97 Strain gage installed on wall W#27

Sensor	***Test wall #***																											
	1	2	3	4	5	6	7	8	9	10	11	12	13	14	15	16	17	18	19	20	21	22	23	24	25	26	27	28	29
Leo-3	X	X	X	X	X	X	X	X	X	X	X	X	X	X	X	X	X												
Wika S-10 #1																		X	X	X	X	X	X	X	X	X	X	X	X
Wika S-10 #2																		X	X	X	X	X	X	X	X	X	X	X	X
RF-603 #1	X	X	X	X	X	X	X	X	X	X	X	X	X	X	X	X	X	X	X	X	X	X	X	X	X	X	X	X	X
RF-603 #2	X	X	X	X	X	X	X	X	X	X	X	X	X	X	X	X	X	X	X	X	X	X	X	X	X	X	X	X	X
RF-603 #3						X	X	X	X	X	X	X	X	X	X	X	X	X	X	X	X	X	X	X	X	X	X	X	X
RF-603 #4						X	X	X	X	X	X	X	X	X	X	X	X	X	X	X	X	X	X	X	X	X	X	X	X
LRW-100 #1	X	X	X	X	X	X	X	X	X	X	X	X	X	X	X	X	X	X	X	X	X	X	X	X	X	X	X	X	X
LRW-100 #2	X	X	X	X	X	X	X	X	X	X	X	X	X	X	X	X	X	X	X	X	X	X	X	X	X	X	X	X	X
LRW-100 #3	X	X	X	X	X	X	X	X	X	X	X	X	X	X	X	X	X	X	X	X	X	X	X	X	X	X	X	X	X
LRW-100 #4	X	X	X	X	X	X	X	X	X	X	X	X	X	X	X	X	X	X	X	X	X	X	X	X	X	X	X	X	X
LRW-100 #5	X	X	X	X	X	X	X	X	X	X	X	X	X	X	X	X	X	X	X	X	X	X	X	X	X	X	X	X	X
LRW-100 #6	X	X	X	X	X	X	X	X	X	X	X	X	X	X	X	X	X	X	X	X	X	X	X	X	X	X	X	X	X
LRW-100 #7	X	X	X	X	X	X	X	X	X	X	X	X	X	X	X	X	X	X	X	X	X	X	X	X	X	X	X	X	X
LRW-100 #8	X	X	X	X	X	X	X	X	X	X	X	X	X	X	X	X	X	X	X	X	X	X	X	X	X	X	X	X	X
Strain Gages																					X	X	X	X			X		
Video Cam.	X	X	X	X	X	X	X	X	X	X	X	X	X	X	X	X	X	X	X	X	X	X	X	X	X	X	X	X	X
Slow Vel. Cam.										X	X	X	X	X	X	X	X	X	X	X	X	X	X	X	X	X	X	X	X

Table A1. 25 Sensor usage in real scale masonry walls tests

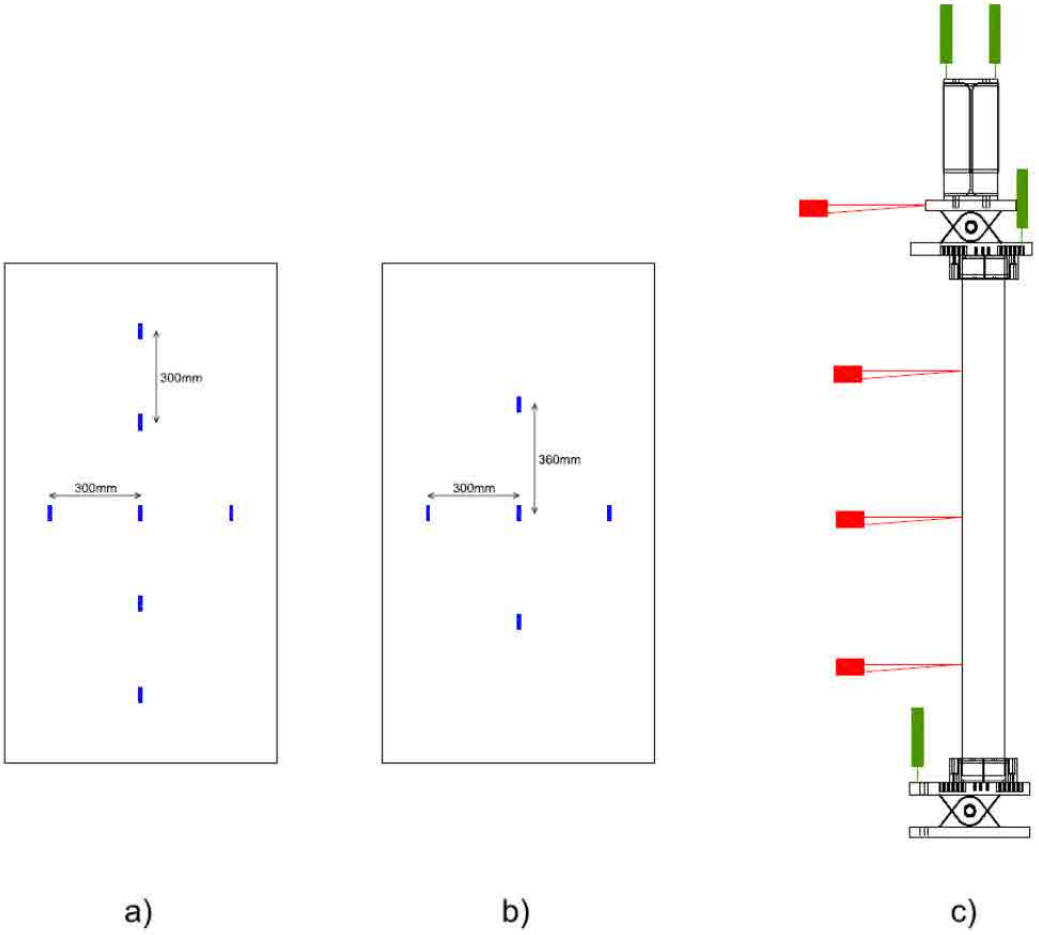

Figure A1. 98 Position of the sensors in the common test setup

Figure A1. 99 Fix video camera to record the test

A part from the sensors two video cameras were used to record the test. The first one is a SONY® Handycam® (see Figure A1. 99) which was used to record the tests from an external fix position. The second one is a MotionBlitz® Cube4 high speed camera which recorded the failure process from one side of the wall. For its correct use an extra light focus was placed at the side of the wall.

Figure A1. 100 MotionBlitz Cube 4 high speed camera

All data was acquired with a HBM MCGPlus data acquiring system controlled by a laptop. All installed sensors were simultaneously recorded at 50Hz. See Figure A1. 101. To provide the required oil pressure for the jack to work a 1000bar pump (see Figure A1. 102) was used.

Figure A1. 101 Voltage supply source for lasers (left), MGCPlus data acquisitor (down) and controlling laptop (up)

Figure A1. 102 1000bar pump for providing the oil pressure needed by the jack

A1.6.4.7 Test procedure

The test procedure slightly varied from one test to another, but the main steps are summarised below. Later on, the particularities of some of the tests are also presented.

With the wall in the test position and having left the upper hinge and the distribution beam laying on it, first of all, it was the time to take the measurements of the real geometry and the position of the wall respect the testing system. With a laser position sensor mounted on an independent and perfectly vertical aligned guide the out of plane initial distance from this vertical guide was measured every two (M, T and S series) or three (H and F series) bricks depending on the height of the wall. The width and the thickness of the walls were also measured in three points at different heights. The height of the wall was measured in four points (each vertical edge) to obtain the effective buckling height, which corresponded with the distance between hinges' rotation points except for wall W#4. This last one had different boundary conditions as described before (see section A1.6.1). The initial rotation of the upper and lower hinges, which was due to the positioning procedure, were measured. Finishing with the initial geometric characterisation, the vertical alignment of the wall which described its initial overall rotation was measured trough the hinges alignment.

The second step was to place, connect and check all sensors and cameras installed as described in previous section. After this, the testing area was covered with a safety mesh to avoid the projection of biggest rubble at wall's failure. All people had the access to the testing area forbidden from this point, specially the area in front of the wall where it was supposed to fall on.

The test data acquisition began (at 50Hz) including the high-speed camera (at 1kHz) recording in case the collapse happened from this time on. The lower hinge was manually freed (removing all the M27 steel bars which fixed the two parts of the lower hinge) and the structure became pinned-pinned.

Once the wall was ready for testing, the hydraulic pump was manually operated and the jack began applying an increasing load. Tests lasted over 5 minutes and the loading rate was constant except for a quicker increase between 50bar and 70 bar (corresponding with a load range from 70kN to 100kN) due to a limitation of the pump.

The load increase was carried on up to the sudden wall failure. After the collapse of the wall, the hydraulic pump and the data acquisition system were stopped. The high-speed camera was stopped a few seconds after the collapse. The tests had finished and data was stored to later on post process.

This test procedure had little variations apart from the sensors' use previously highlighted (section A1.6.4.6). Test on W#1 did not have the safety grid which was introduced later in the test setup. To place the walls W#1 to W#9 it was not necessary to move the upper nor the lower hinge so the initial rotation of the hinges was not measured as they were levelled. For wall W#4 the lower hinge was not freed because the test was carried out with different boundary conditions compared with the others and this hinge was fixed all W#4 test long. For walls W#21 to W#29, the thickness of the TRM strengthening layer as well as the distance from the masonry to the fibre grid was measured after the collapse of the wall.

A1.6.5. Results of real scale masonry walls

In this section the experimental results of the buckling tests on real scale masonry walls are described and presented in detail. These are divided in two parts: those obtained in the tests on unreinforced masonry walls (URMW) and those corresponding with the TRM strengthened walls. All gathered data (including the initial geometry) is summarised in tables and the structural response is graphically presented for each wall. Some qualitatively observations made in life are also included. Little discussion on the results is made but it is mostly extended in Chapter 3.

A1.6.5.1 Results of URMW

The initial significant geometric measurements, the structural response, some qualitative observations and pictures are presented for each wall.

The geometry specifications include the number of brick rows the wall had, its three main dimensions (height between hinges, width and thickness), the theoretical eccentricity fixed by the plates which seized the wall, the horizontal distance between the rotation points of the two hinges that causes some initial overall rotation (positive value if the rotation is oriented to the tensile side of the wall) and the real mid-height eccentricity which included the alignment of the hinges as well as the local constructive imperfections.

Wall W#1

The main geometric variables are summarised in Table A1. 26. The structural response may be observed in Figure A1. 103 to Figure A1. 105, where the force vs. in-plane upper displacement, the force vs. out-of-plane displacement at ¼ and ½ of effective buckling height and the force vs. hinges rotation are presented.

Wall W#1 geometry	
Masonry rows	47
Width	0.900m
Thickness	0.134m
Height between hinges	2.947m
Theoretical eccentricity	20mm
Initial rotation lower hinge	0°
Initial rotation upper hinge	0°
Hinges alignment	-16mm
Real mid-height eccentricity	5.55mm

Table A1. 26 Geometry of wall W#1

This wall was placed trying to keep the two hinges horizontally levelled (see Table A1. 26). To achieve this requirement the hinges alignment was affected and the rotation centre of the lower hinge was placed 16mm more to the tensile side of the wall than the upper hinge. It was due to the geometric imperfections of the wall. This one was the highest of all the walls and was fabricated by LITEM staff.

During the test the in-plane response was almost lineal up to failure as seen in Figure A1. 103. The load loss in this graph is caused by the manual operation of the hydraulic pump and the limitations of this pump to uniformly apply an increasing load at the lower range of pressure. The maximum applied load was 169.34kN which corresponded with less than the 8% of the compressive strength of the wall's section.

The out-of-plane deformation represented in Figure A1. 104 shows how the wall deformed more at ¾ of the buckling height (between rotation centres of the upper and lower hinges) than at mid-height. This situation points out that the wall was turning over as recorded in the video. The upper hinge allowed a far bigger rotation than the lower one.

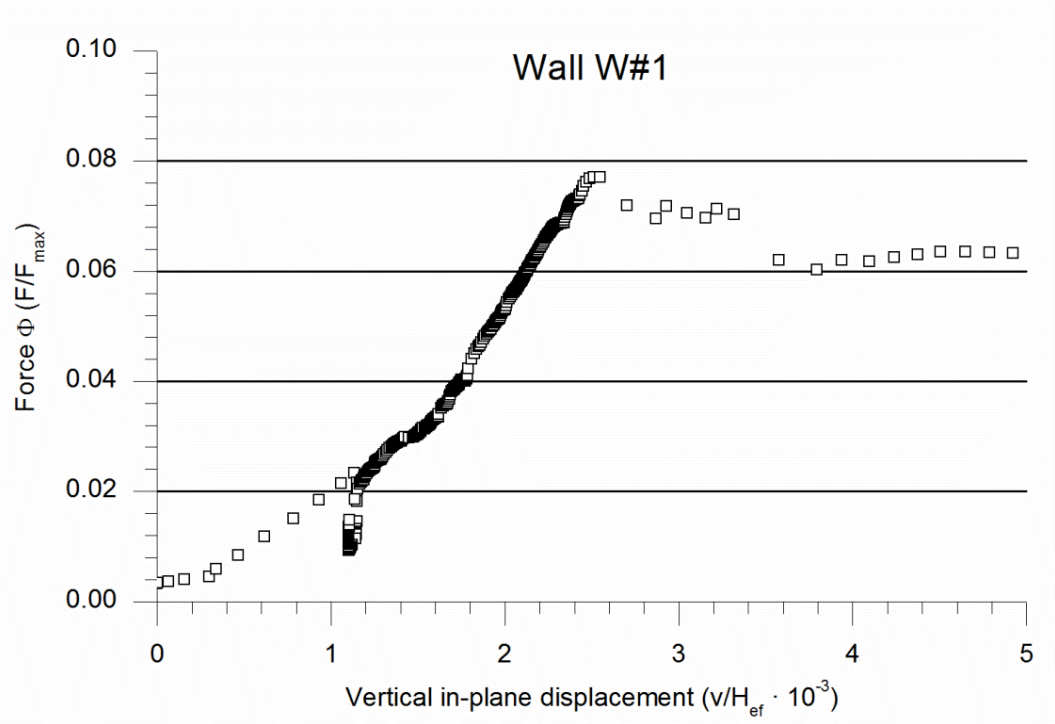

Figure A1. 103 Vertical in-plane response of wall W#1

This asymmetric behaviour was also represented in Figure A1. 105 where can be observed that the lower hinge stayed unmoving (0.14°) while the upper hinge and the upper distribution beam rotated up to 2.53° before the collapse of the wall. It can be explained by the fact that the hydraulic jack had installed its hinge transforming the structural system in a mechanism, where the upper distribution beam and hinge could rotate easier than the lower hinge.

In fact, the failure seemed to be caused by the rotation of the upper loading system (geometric instability) which leaded to the rotation of the wall (turn over). Then the wall laid on the horizontal restraining tools that suddenly stopped it causing the flexion breaking that was captured by the cameras.

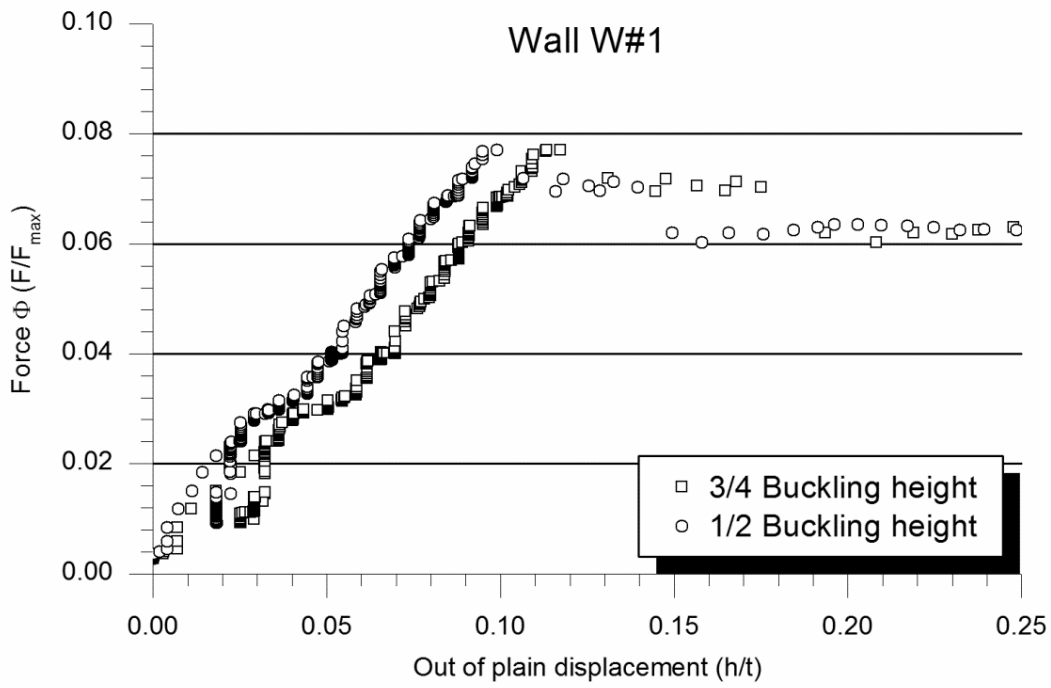

Figure A1. 104 Out-of-plane response of wall W#1

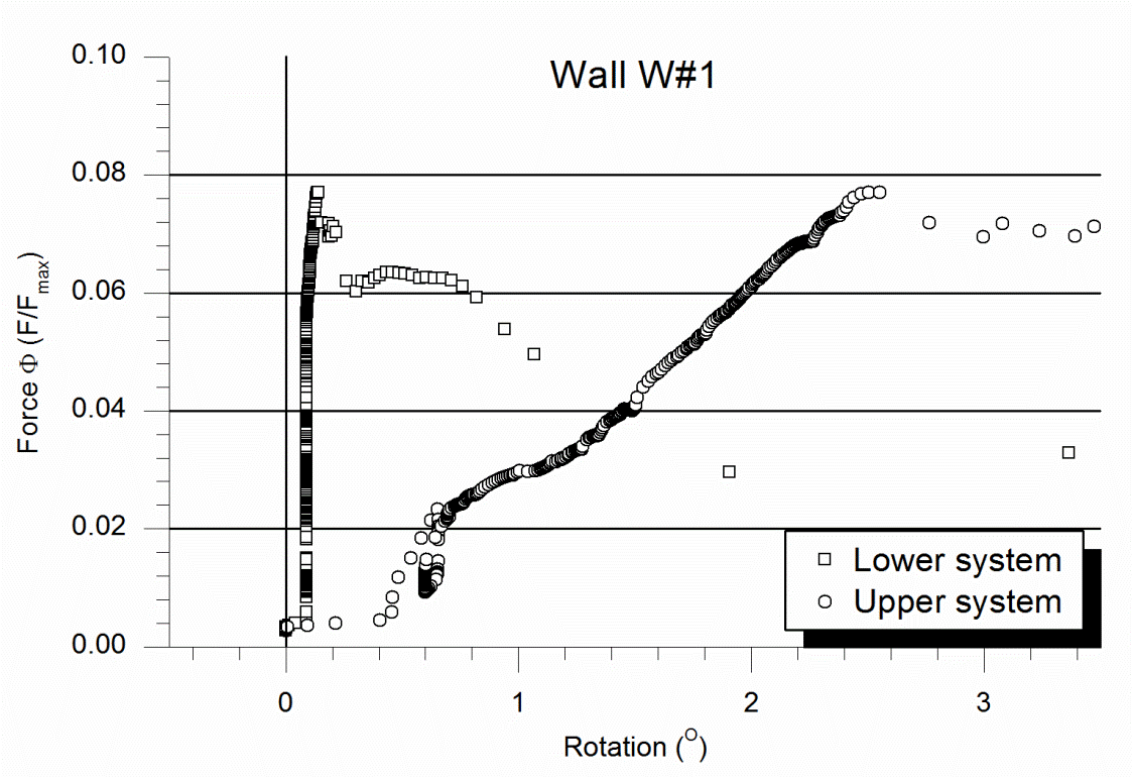

Figure A1. 105 Rotation at wall's endings for wall W#1

As it is the first wall tested of the series H, some pictures are provided to graphically describing the measurement tasks of the out-of-plane initial imperfections (Figure A1. 106), the measuring system for the rotation of the lower and upper hinges (Figure A1. 107 and Figure A1. 108 respectively).

The position of the potentiometers installed for controlling the descending movement of the distribution beam is shown in Figure A1. 109.

Finally, the collapse shape was characterised by the formation of a unique horizontal crack slightly below mid-height as can be seen in Figure A1. 110. However, before this, the wall turned over rotating around the lower hinge at maximum load which caused the structure impact the horizontal restraining system. It was this impact what broke the wall as presented in Figure A1. 110. After the wall's collapse, it completely broke into little pieces.

From the experience of the video recording, the next walls would have the tensile face white-painted.

Figure A1. 106 Measuring the geometry of wall W#1

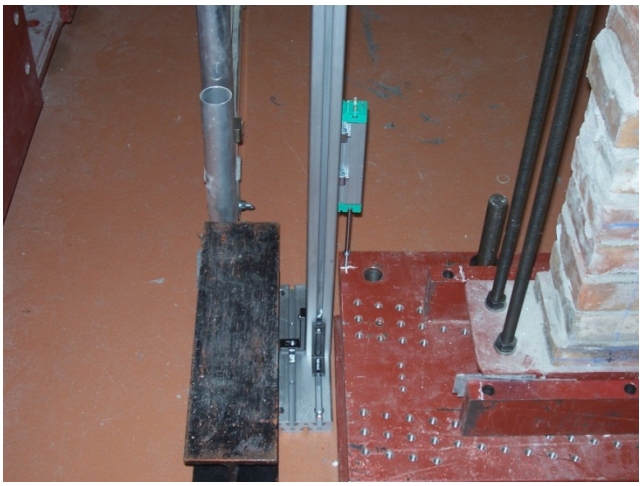

Figure A1. 107 Potentiometer for the measure of the rotation of the lower hinge valid for H series walls

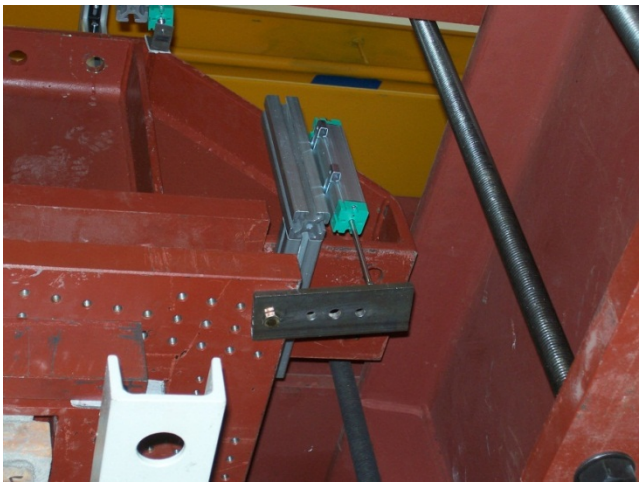

Figure A1. 108 Potentiometer for the measure of the rotation of the upper hinge valid for H series walls

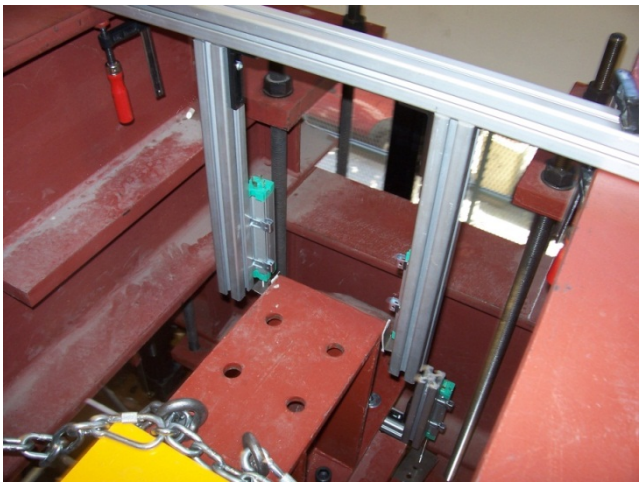

Figure A1. 109 Two of the four potentiometers used for measuring the descending movement and rotation of the distribution beam. Valid for H series walls

Figure A1. 110 Wall W#1 at the beginning of the test (left) and failing (right)

Wall W#2

Table A1. 27 Summarises the geometry of wall W#2. It is shown that although this wall is almost the same height than the previous one, W#2 has 4 masonry rows less than W#1 what points out the mortar joints were approximately a 30% thicker.

As for the previous wall, the hinges were initially levelled. This caused a greater hinges' misalignment. The real eccentricity at mid-height almost coincides with the theoretical eccentricity (the real at the extremes of the wall) what proves this wall had a better vertical alignment.

The wall W#2 failed at lower load (65.7kN) than the previous one and the in-plane deformation (see Figure A1. 111) was also less: 4.1mm. However, the behaviour was almost the same with a linear response up to failure.

Wall W#2 geometry	
Masonry rows	43
Width	0.900m
Thickness	0.134m
Height between hinges	2.927m
Theoretical eccentricity	20mm
Initial rotation lower hinge	0°
Initial rotation upper hinge	0°
Hinges alignment	15mm
Real mid-height eccentricity	19.63mm

Table A1. 27 Geometry of wall W#2

Observing Figure A1. 112 it is noticed that the wall presented a clearly different response than the previous wall as the out-of-plane displacement was far larger in mid-height than at ¼ height. Moreover, the out-of-plane response was not proportional to the applied load. Near the collapse load, the deformation increased faster proving the second order effects. The mid-height out of plane displacement at maximum load was 17.3mm.

Regarding the behaviour of the boundary conditions, it is observed (Figure A1. 113) that during the test the two hinges rotate in different directions. The lower hinge rotate in the expected direction but the upper one did the opposite movement. It may be caused by the problems of constraining the horizontal out-of-plane displacement of the distribution beam together with the extra rotation possibility of the hinge of the jack which was not used for the next tests.

Near the failure both hinges rotate in the same direction (the one associated with the theoretical eccentricity). Analysing the results in detail it was observed that almost all the rotation of the upper supporting system was due to the rotation of the distribution beam.

After the test the little adherence between the bricks and the mortar joints is evidenced as there was possible to manually separate these two components of the masonry. From this test and until the test on

wall W#5 the system to avoid the horizontal displacement of the upper distribution beam was the one presented in Figure A1. 91.

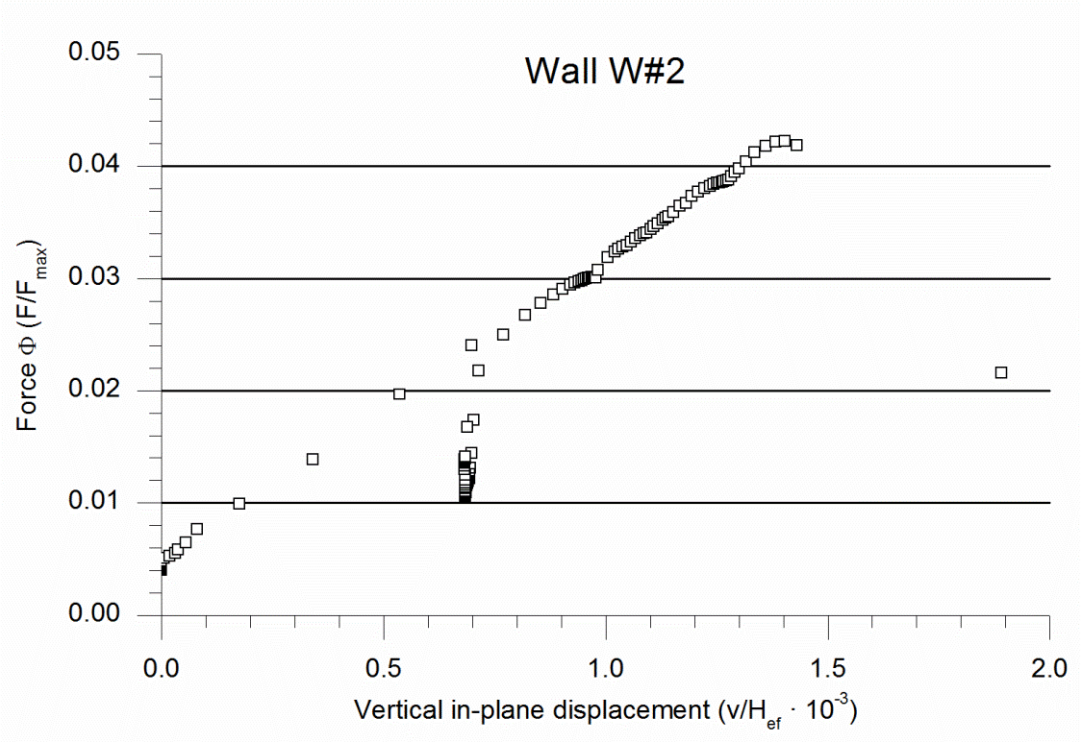

Figure A1. 111 Vertical in-plane response of wall W#2

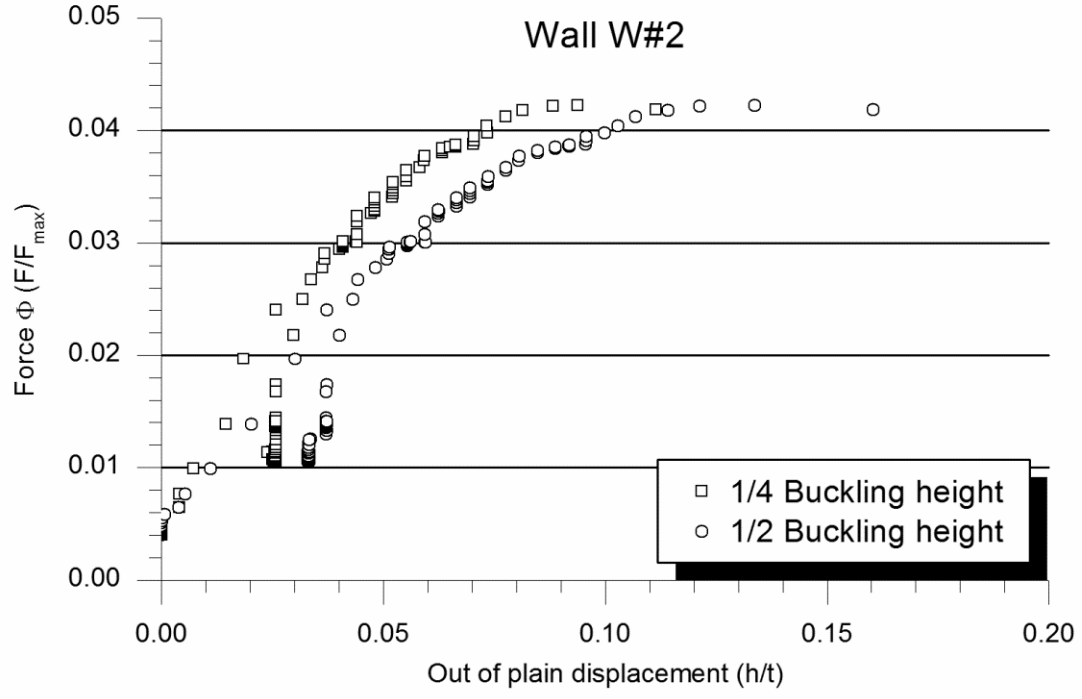

Figure A1. 112 Out-of-plane response of wall W#2

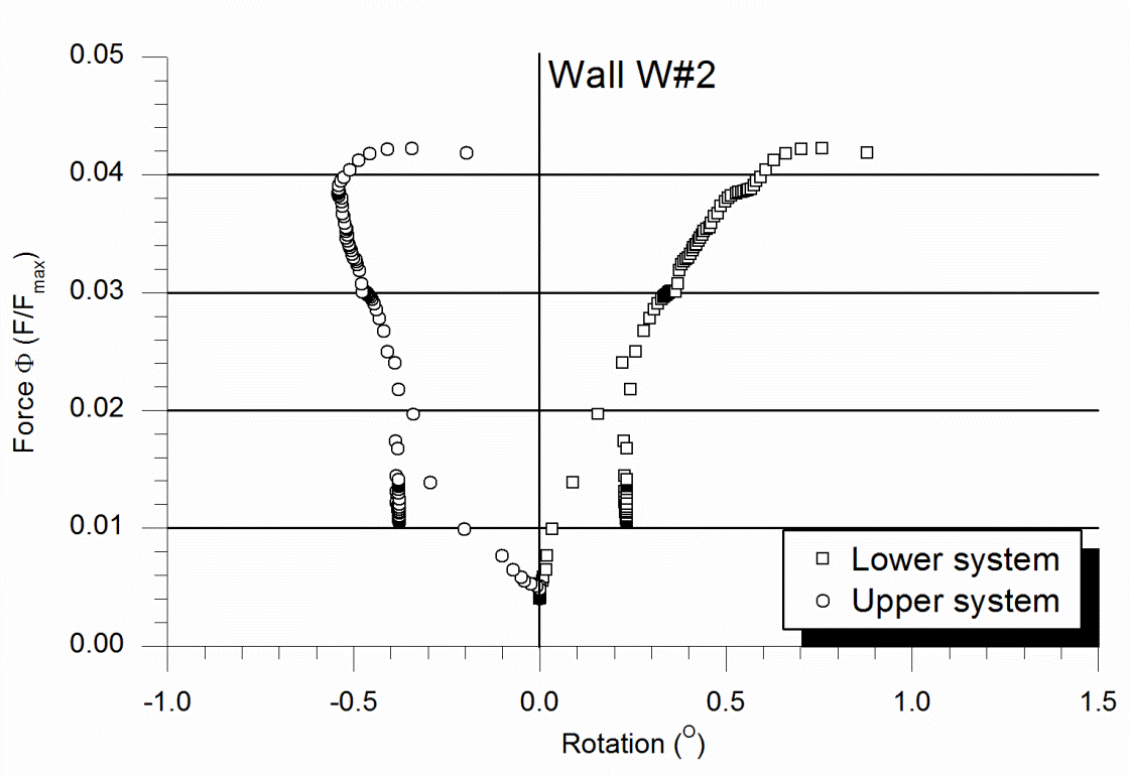

Figure A1. 113 Rotation at wall's endings for wall W#2

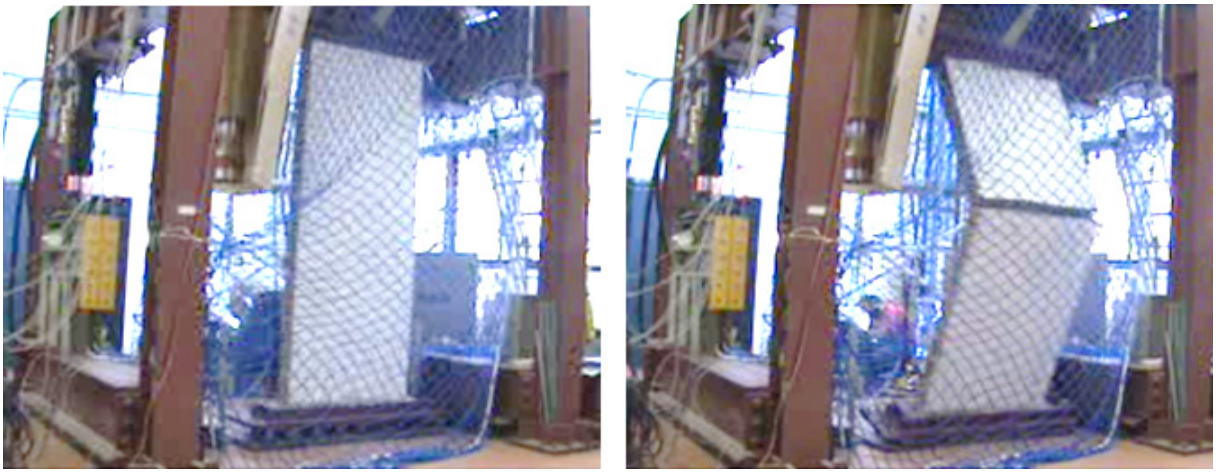

Figure A1. 114 Wall W#2 at the beginning of the test (left) and failing (right)

The wall W#2 collapsed in the expected direction and by the expected mode: opening a unique horizontal crack following a mortar joint in the tensile side of the wall, see Figure A1. 114. It has to be highlighted that the side with some horizontal joints not completely filled with mortar was placed at the compression side.

Wall W#3

As the previous walls, for this one the initial position of the hinges was levelled (see Table A1. 28) although this caused more difficulties to align the hinges. Geometry is very similar to wall W#2 but in this case the eccentricity at the hinges was only of 10mm. An initial wall deformation made that the initial md-height eccentricity was 1.2mm instead of the theoretical 10mm.

Wall W#3 geometry	
Masonry rows	43
Width	0.870m
Thickness	0.134m
Height between hinges	2.922m
Theoretical eccentricity	10mm
Initial rotation lower hinge	0°
Initial rotation upper hinge	0°
Hinges alignment	10mm
Real mid-height eccentricity	1.20mm

Table A1. 28 Geometry of wall W#3

Observing the in-plane response of the wall the linear behaviour was clear for the initial loads. However, for loads over the 6% of the maximum compression load the masonry could bear in uniform compression, the slope of the graph increased what means that the system became stiffer for major loads. A final relaxation was observed very close to the collapse load.

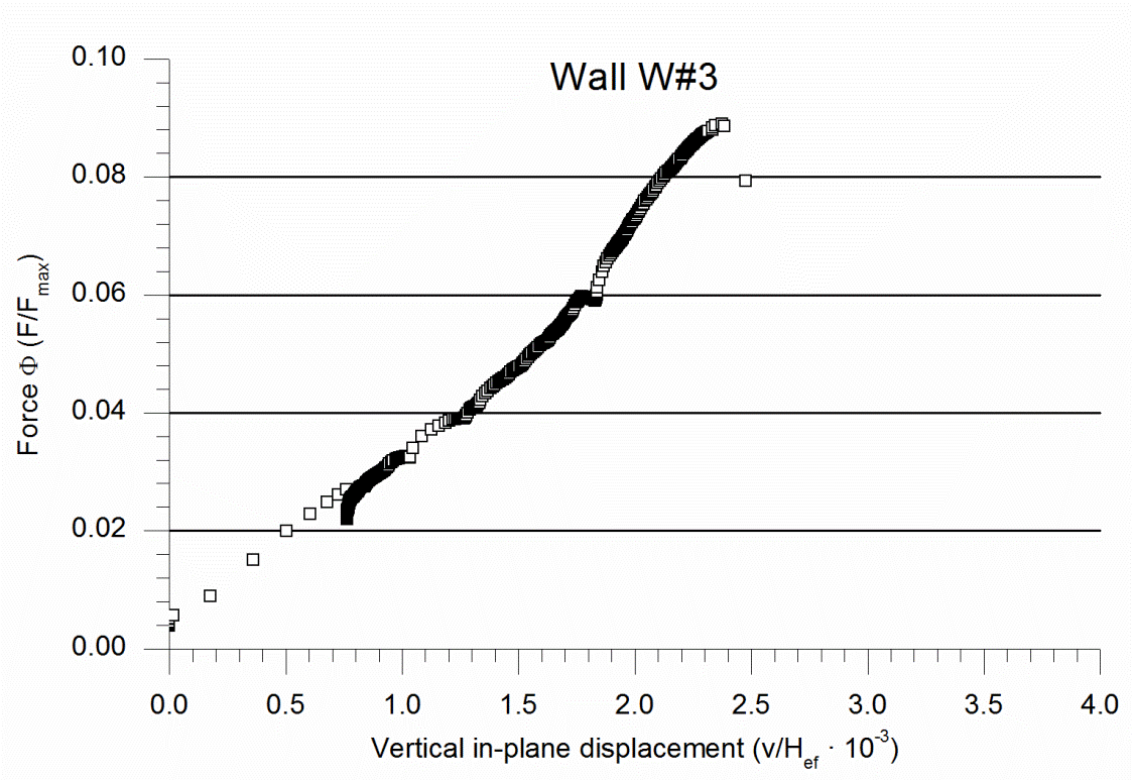

Figure A1. 115 Vertical in-plane response of wall W#3

Regarding the out-of-plane displacement (see Figure A1. 116), it shows a clear non-linear behaviour. When increasing the load the out-of-plane increasing ratio rises. The second order bending effects are evident. Moreover, the mid-height displacement is always greater than the ¼ height and the difference grow up when increasing the load which corresponded with the expected deformed shape.

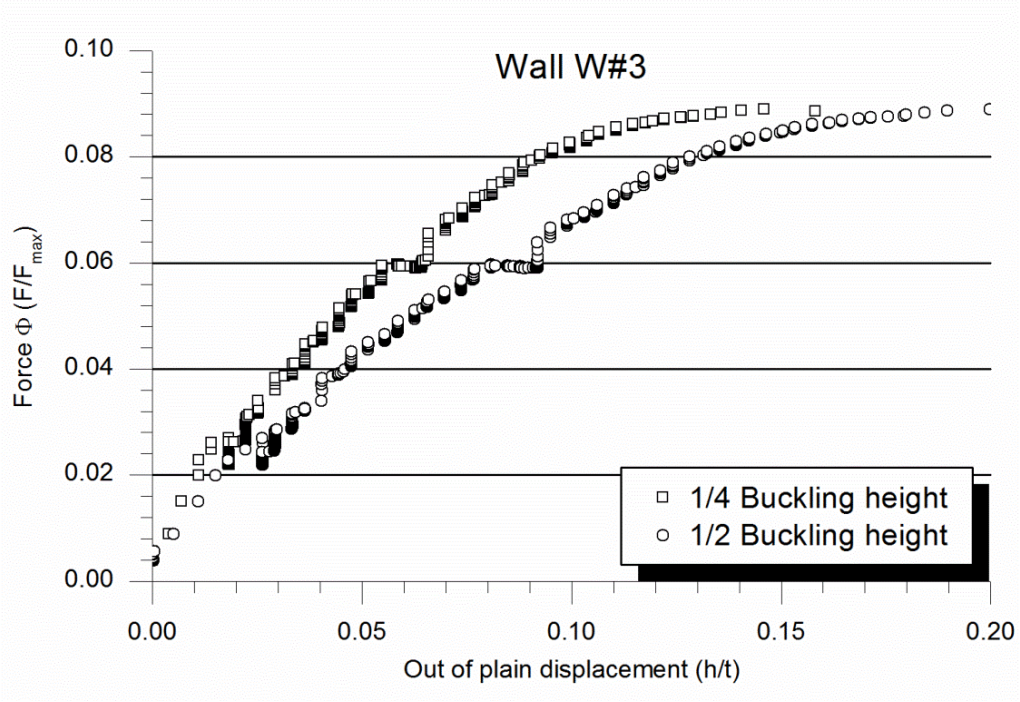

Figure A1. 116 Out-of-plane response of wall W#3

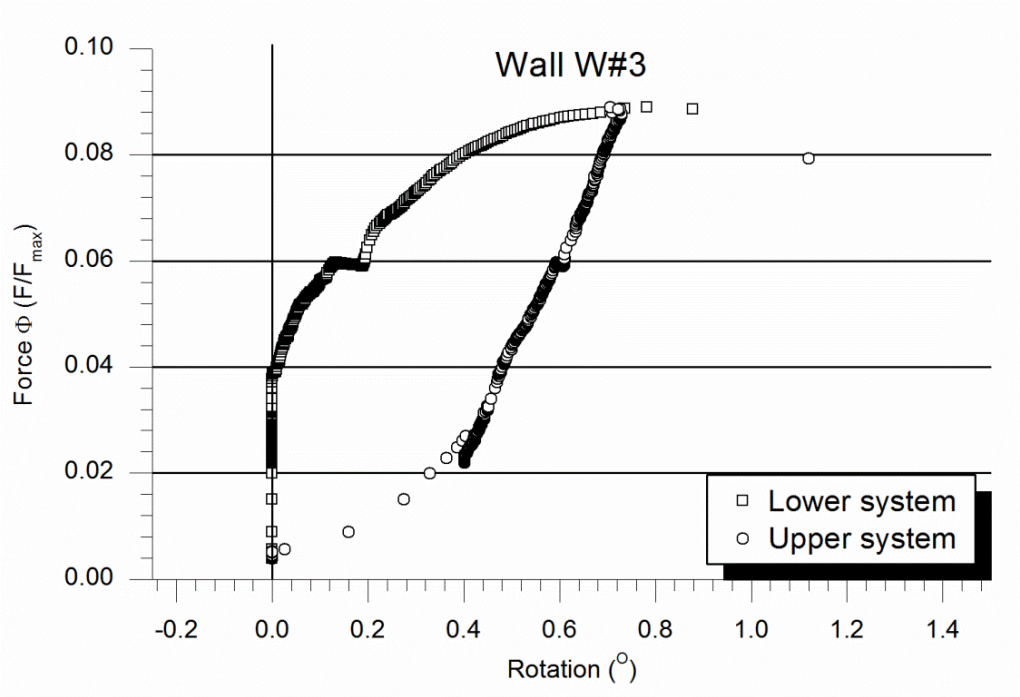

Figure A1. 117 Rotation at wall's endings for wall W#3

Observing the graph in Figure A1. 117 it is clear that the rotation of the upper system (specially the distribution beam) was fast at the beginning corresponding with the initial settling movements and being observed as an overturning of the wall. After the initial stages, the rotation of the upper supporting system was almost linear with the load increase whereas the rotation of the lower hinge was negligible up to half the maximum load when a non-linear response began. The rotation speed increased with the load. Finally, at the collapse load (133.8kN), the rotations of the extremes of the wall were the same so a symmetric failure shape was produced as shown in Figure A1. 118. One horizontal crack opened following one mortar joint.

In contrast with wall W#2, W#3 had the side with the completely mortar filled joints at the compression side. This may allow better using the thickness of the wall.

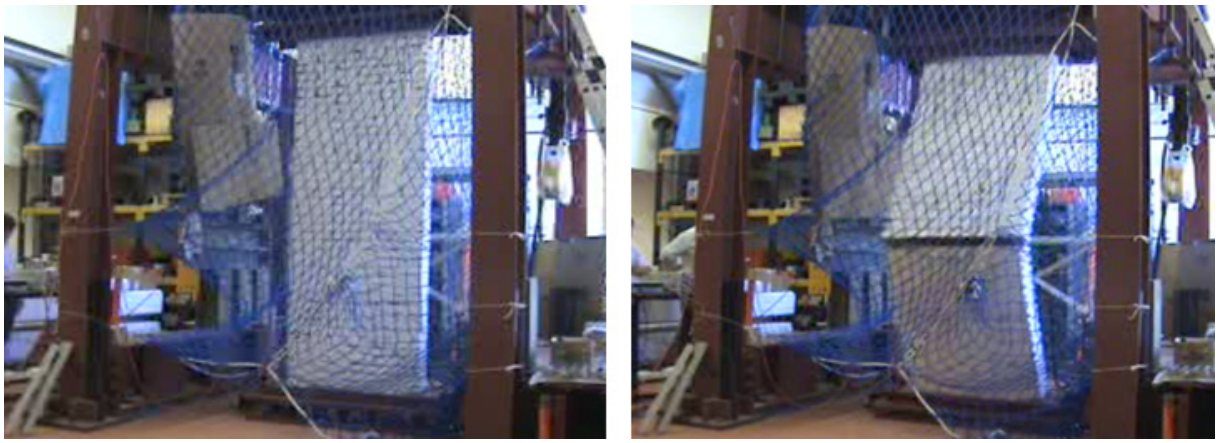

Figure A1. 118 Wall W#3 at the beginning of the test (left) and failing (right)

Wall W#4

In contrast with walls W#2 and W#3, W#4 had two more brick rows what indicates using thinner mortar joints. This wall was the only one of the F series and had the particularity of varying the boundary conditions respect the rest of the tests on real scale walls.

In this case, the corresponding buckling length was not the distance between hinges but a shorter one. It was approximately 2.05m as the lower hinge was fixed.

Wall W#4 geometry	
Masonry rows	45
Width	0.870m
Thickness	0.134m
Height between hinges	2.922m
Theoretical eccentricity	0mm
Initial rotation lower hinge	0°
Initial rotation upper hinge	0°
Hinges alignment	6.5mm
Real mid-height eccentricity	3.90mm

Table A1. 29 Geometry of wall W#4

Like previous tests, the hinges were levelled at the beginning (see Table A1. 29). The little geometric imperfections make it possible to place the wall W#4 with only 6.5mm of vertical misalignment between the hinges. For W#4 the specimen was centred respect the theoretic rotation axis of each hinge. For this reason a uniform compression test affected by the buckling phenomena originated by the little initial geometric imperfections was expected.

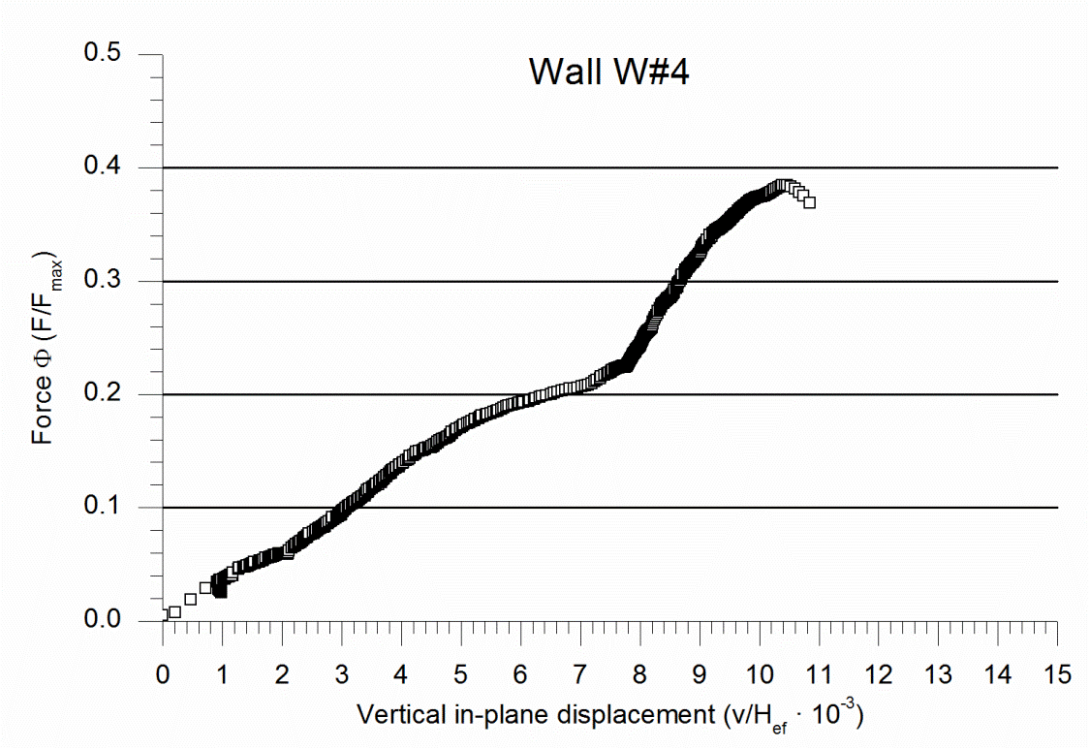

Figure A1. 119 Vertical in-plane response of wall W#4

Focusing on Figure A1. 119 the linear in-plane deformation response is more or less observed up to half the maximum load. After this point, the slope of the curve in Figure A1. 119 suddenly grew and the response became stiffer to finally present a relaxation effect near the collapse load. This complex behaviour may be influenced by the boundary conditions and some crushing effects that lead to the final softening not observed so clear before.

Regarding the out-of-plane behaviour (see Figure A1. 120), it is shown that the deformation of the mid-height point was almost lineal up to 80% of the maximum load (578.6kN) when the buckling effects appeared and the deformation increasing rate grew respect the applied load. Focusing on the deformation of one point placed at ¼ of the wall's height, a backwards displacement was observed at the initial loading steps. However, it deformed to the same direction than mid-height point and according with initial mid-height real eccentricity. Compared with previous tests, the out-of-plane displacement of the ¼ height measurement point is far lower what indicates the correct of the fixed lower hinge. According with this, the rotation of this hinge was zero all the test as shown in Figure A1. 121. The upper hinge, however,

began rotating with the opposite direction of the final deformed shape maybe due to the initial settling effects. The change of slope observed in Figure A1. 119 was also noticed when analysing the rotation of the upper supporting system.

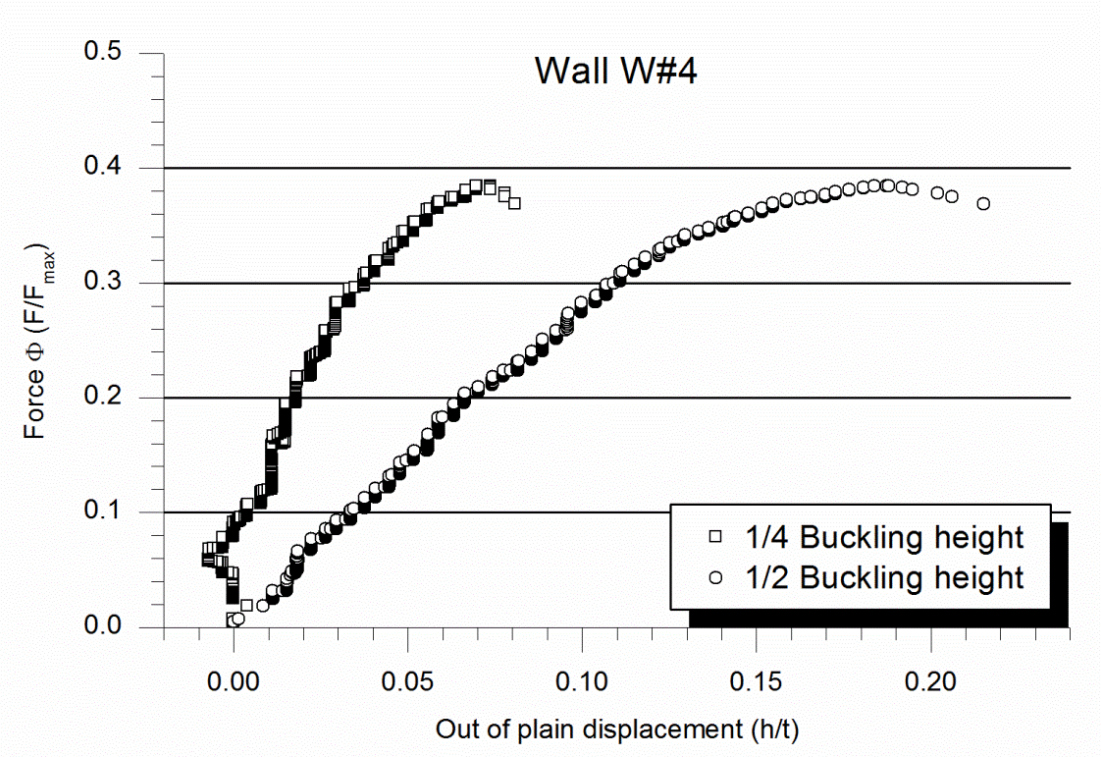

Figure A1. 120 Out-of-plane response of wall W#4

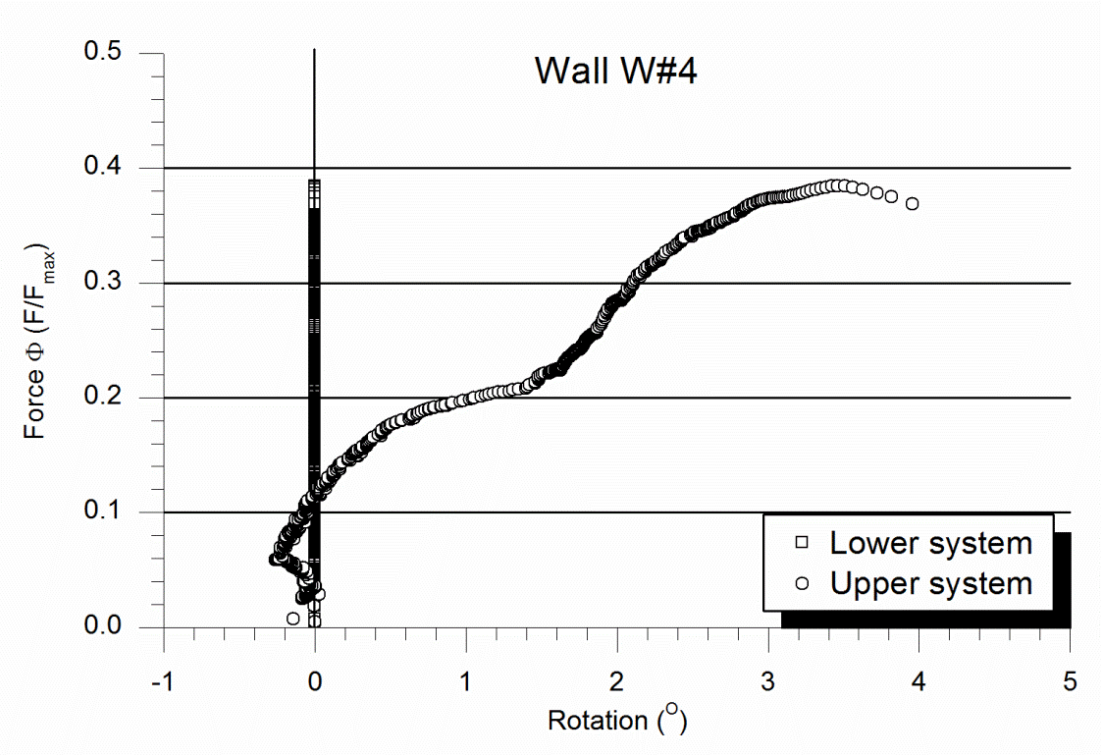

Figure A1. 121 Rotation at wall's endings for wall W#4

At the failure moment the vertical displacement of the load distribution beam was 21.4mm and the out-of-plane displacement at mid-height was 25.2mm. The failure happened when one of the steel lattices placed to control the horizontal displacement of the distribution beam failed. This was analogue to freeing an important horizontal force which broke the upper masonry row by shear. With the wall disconnected, it overturned and fell. It can be seen in Figure A1. 122.

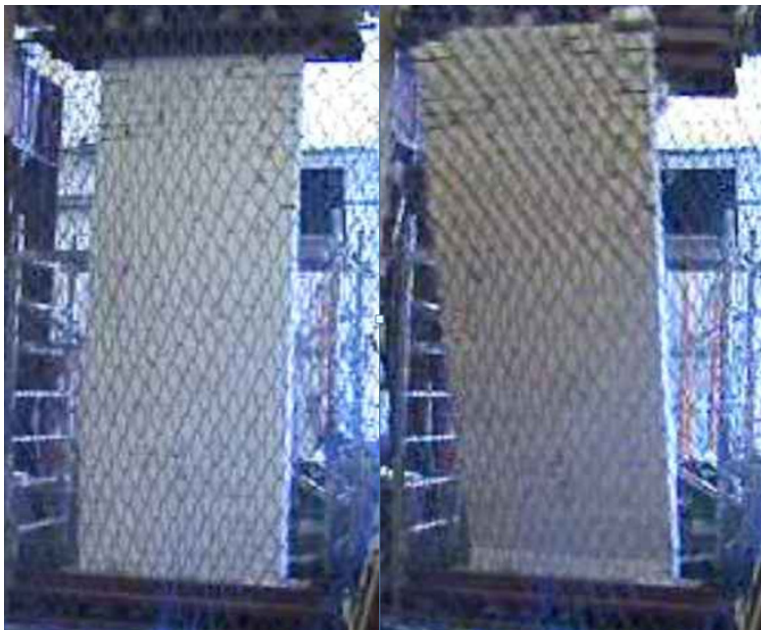

Figure A1. 122 Wall W#4 at the beginning of the test (left) and failing (right)

Wall W#5

This was the first test carried out without the hinge of the hydraulic jack. All following tests were performed without this hinge so the system was statically determined. And the possibility of having an initial mechanism was avoided.

This wall, like the previous ones, had the two hinges horizontally levelled at the beginning of the test (see Table A1. 30). The real eccentricity at mid-height (7mm) almost coincided with the theoretically eccentricity (5mm).

Observing Figure A1. 123, the in-plane response is characterised by an initial settling which corresponded with and increasing of the curve's slope followed by a linear response (from 75kN to 225kN) that near to the collapse load changes again presenting a relaxation effect. The maximum load was 239.8kN and the associated in-plane descending movement of the distribution beam was 6.3mm.

Wall W#5 geometry	
Masonry rows	45
Width	0.900m
Thickness	0.134m
Height between hinges	2.917m
Theoretical eccentricity	5mm
Initial rotation lower hinge	0°
Initial rotation upper hinge	0°
Hinges alignment	7mm
Real mid-height eccentricity	7.00mm

Table A1. 30 Geometry of wall W#5

Regarding the out-of-plane response (Figure A1. 124) it is observed that the deformation at mid-height was always greater than the deformation at ¼ the height. Moreover, the difference grew during the test indicating the presence of second order effects. At the initial loading stage, the deformation grew but suddenly it stopped while the load was increasing. After that, the deformation raised at its maximum rate to finally change again the slope in the graph and returning to the initial growing rate. The final out-of-plane deformation at mid-height was 9.6mm.

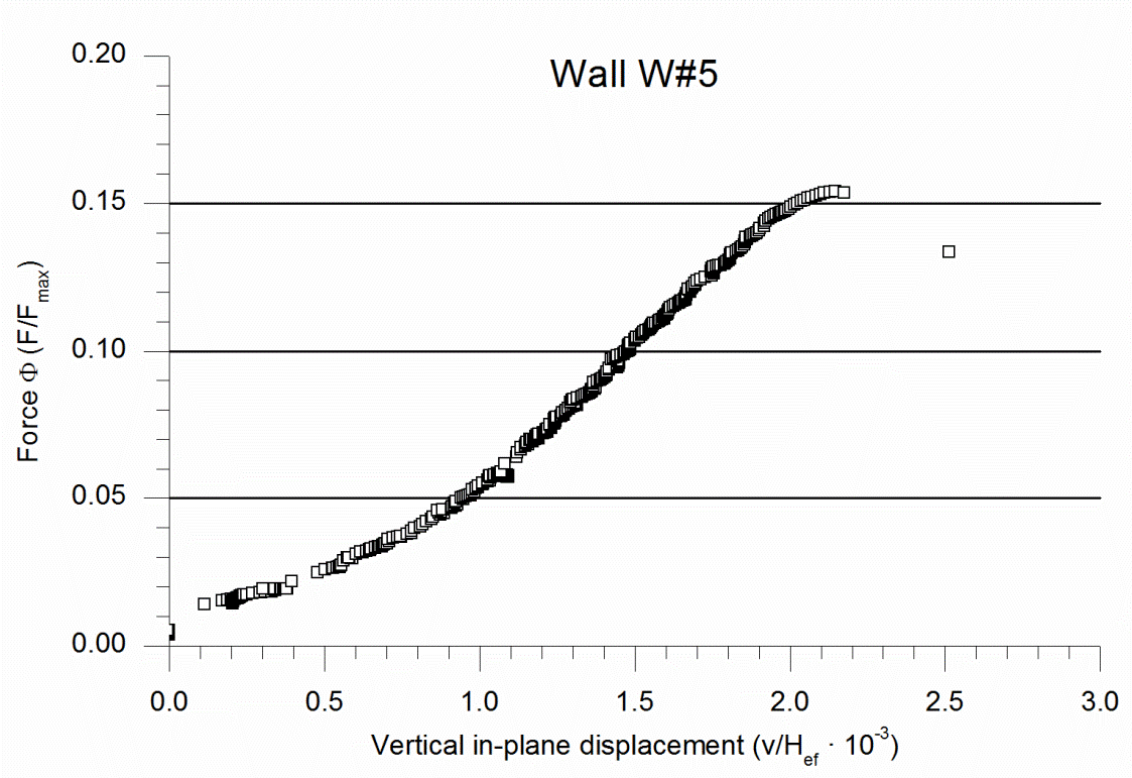

Figure A1. 123 Vertical in-plane response of wall W#5

Looking at Figure A1. 125 it is noticed that the system deformed asymmetrically with the upper hinge rotating at a far greater velocity than the lower one from the very first beginning. At the collapse point, the upper hinge had rotated like 10 times the angle of the lower hinge which rotation was almost zero. Most of the rotation of the upper supporting system was due to the movement of the distribution beam what indicates that the horizontal restrain of this element had to be improved.

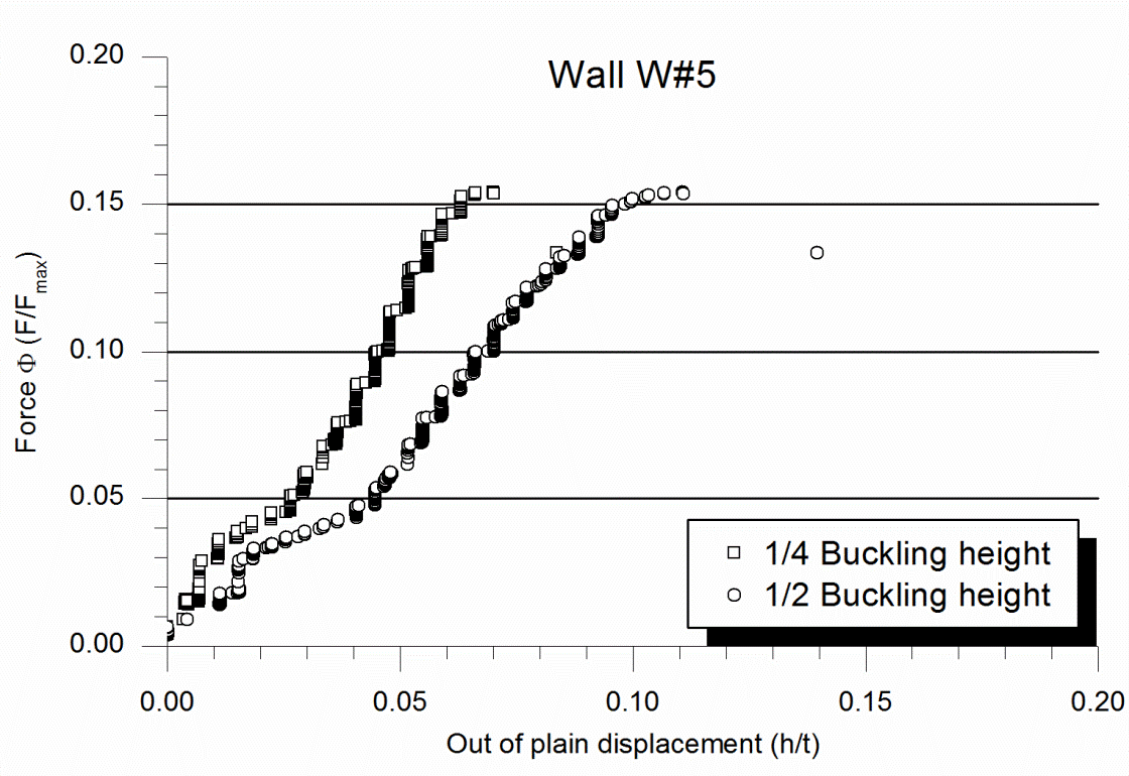

Figure A1. 124 Out-of-plane response of wall W#5

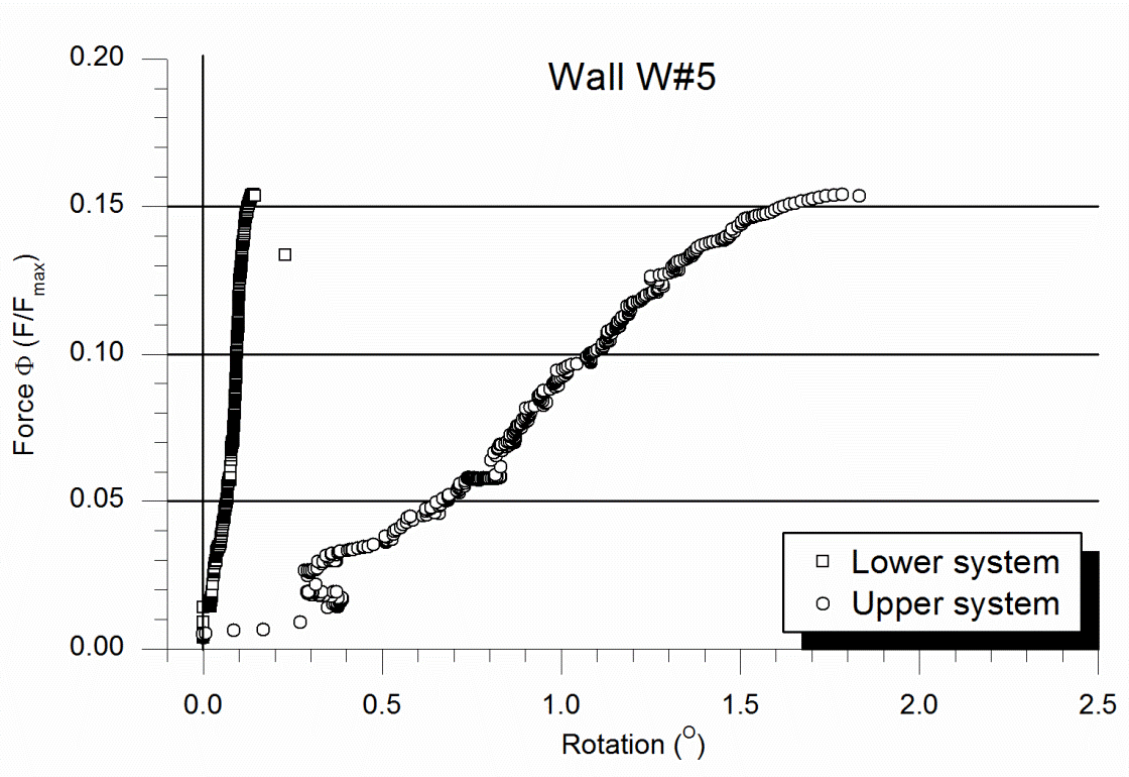

Figure A1. 125 Rotation at wall's endings for wall W#5

Finally, in relation with the failure mode, the following observations were made during the test: the wall overturned respect the lower hinge so the upper head was displaced out-of-plane. When this movement stabilised, the bending of the wall became more and more evident up to the final failure due to the opening of a mortar joint more or less at ¾ of the height (see Figure A1. 126).

Figure A1. 126 Wall W#5 at the beginning of the test (left) and failing (right)

Wall W#6

This was the first test with the definitive restraining system of the out-of-plane horizontal movement of the distribution beam. As explained before it consisted in four steel profiles as shown in Figure A1. 127. In addition, the upper fixation plates had screws incorporated to better adjust and grab the upper heading tool (see Figure A1. 127). Moreover, two additional laser displacement transducers were added to sensors of the previous tests. These two new lasers measured the out-of-plane displacement at ¾ of the effective height and checked the distribution beam did not move in out-of-plane direction.

Wall W#6 geometry	
Masonry rows	42
Width	0.875m
Thickness	0.134m
Height between hinges	2.857m
Theoretical eccentricity	25mm
Initial rotation lower hinge	0°
Initial rotation upper hinge	0°
Hinges alignment	-12.5mm
Real mid-height eccentricity	33.73mm

Table A1. 31 Geometry of wall W#6

Wall W#6 was placed with the upper and lower hinges perfectly levelled but the horizontal gap between the rotation axes of the hinges was 12.5mm. The upper hinge was backwards respect the in-test out-of-

plane deformation direction. Although the eccentricity at the wall's extremes was 25mm, at mid-height it was 33.7mm due to the construction geometric imperfections.

Figure A1. 127 Vertical steel profiles to constrain the horizontal movement of the distribution beam and screws placed in the hinge plate to grab the upper heading tool

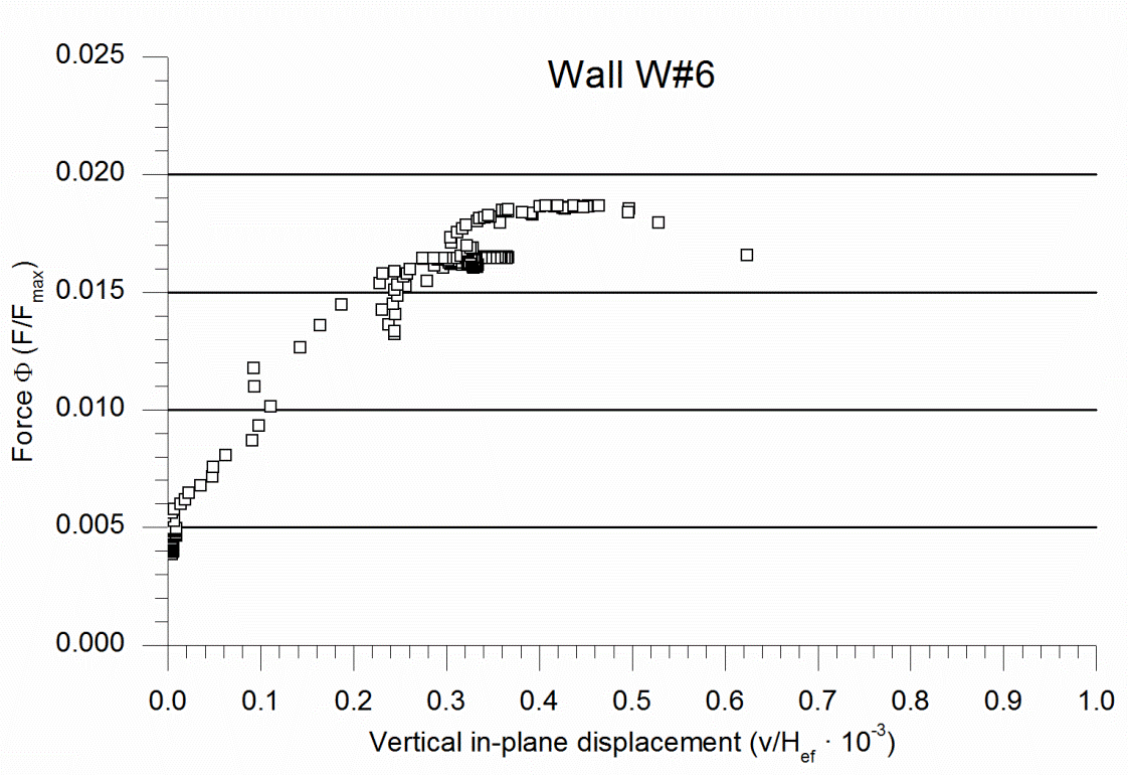

Figure A1. 128 Vertical in-plane response of wall W#6

Looking at Figure A1. 128, it is shown that the initial linear response rapidly changed because of relaxation effects near the collapse load, when the in-plane descending displacement was 1.3mm. In contrast (see Figure A1. 129), the out-of-plane deformation was always non-linear with an increasing

deformation rate. For each load increment the out-of-plane deformation at all measured heights grew more than for the previous increase. Deformation at ¼ and ¾ of the effective height was approximately the same during all test what points out the symmetric response of the system. In addition, mid-height out-of-plane deformation was always bigger than the measured at ¼ or ¾ which coincided with the expected second order response. The maximum was 13.9mm.

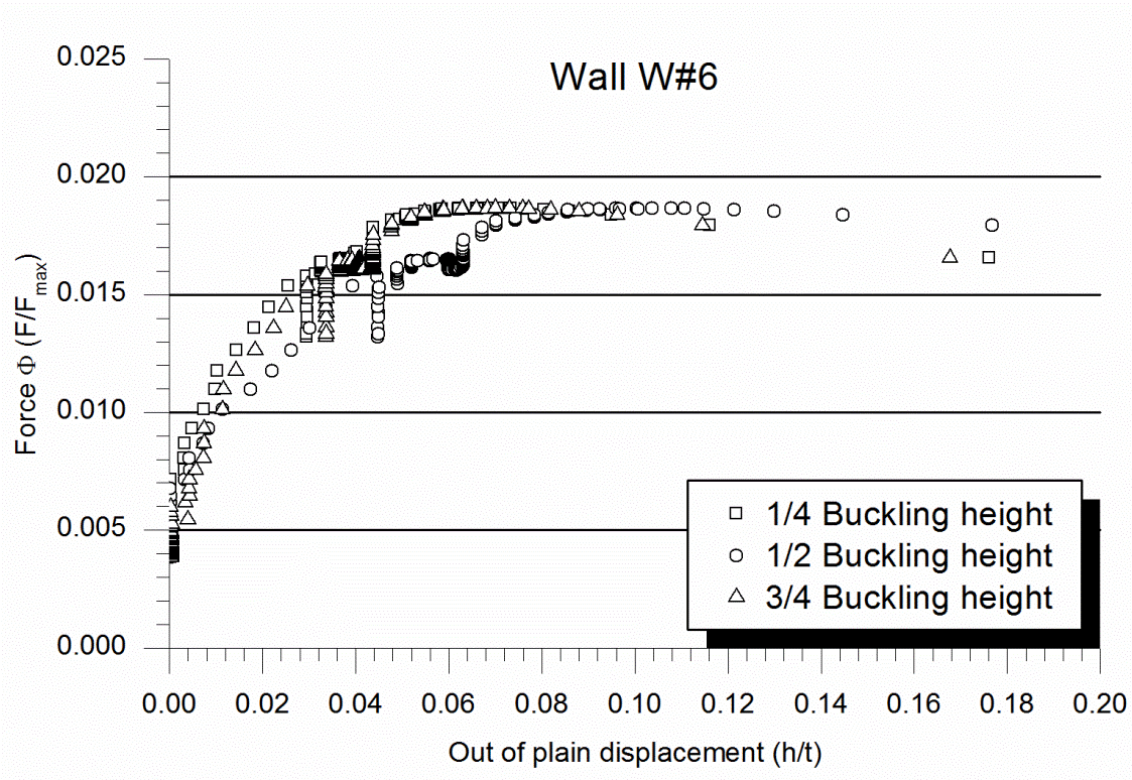

Figure A1. 129 Out-of-plane response of wall W#6

Observing Figure A1. 130, the symmetry of the structural response is clear although at the beginning the upper supporting system rotated faster than the lower hinge which remained fixed up to 1/3 of the maximum load: 30kN.

The collapse mode was associated with second order bending and buckling processes as shown in Figure A1. 131. The wall failed by the formation of a unique horizontal crack following a mortar joint placed little below the mid-height. This appeared after observing a second order bending due to the eccentrically applied vertical compressive force.

It is worth noticing that the distribution beam did not move in the out-of-plane direction and did not rotate either.

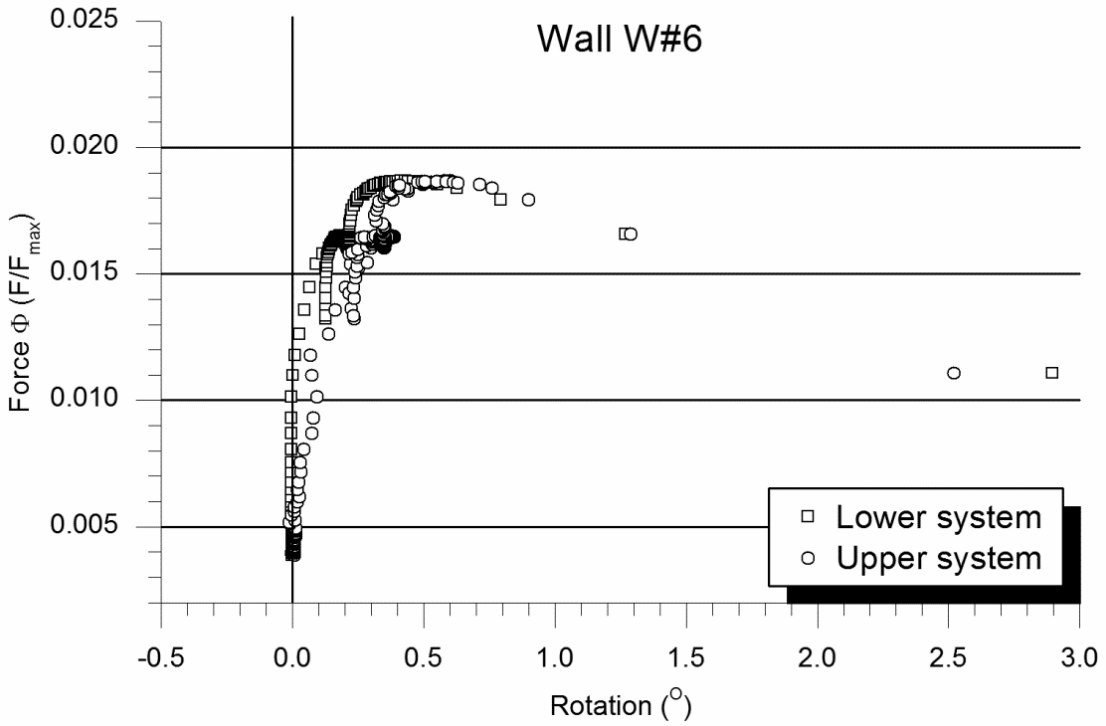

Figure A1. 130 Rotation at wall's endings for wall W#6

Figure A1. 131 Wall W#6 at the beginning of the test (left) and failing (right)

Wall W#7

For wall W#7, the hinges were initially levelled and the mid-height real eccentricity was approximately the eccentricity at wall's extremes (10mm) what showed a better execution with less geometric irregularities. Like in the previous test, the hinges horizontal misalignment (6mm) was due to the backwards position of the upper hinge respect the lower one taking the out-of-plane deformation direction as the reference. See Table A1. 32.

Wall W#7 geometry	
Masonry rows	42
Width	0.885m
Thickness	0.134m
Height between hinges	2.872m
Theoretical eccentricity	10mm
Initial rotation lower hinge	0°
Initial rotation upper hinge	0°
Hinges alignment	-6mm
Real mid-height eccentricity	13.08mm

Table A1. 32 Geometry of wall W#7

Analysing the in-plane response (Figure A1. 132) it was linear up to failure after an initial increase of slope. The descending displacement at maximum load (134.7kN) was 5.4mm. This behaviour seemed a little stiffer than previous wall.

Regarding the out-of-plane deformation (Figure A1. 133), it was symmetric. Measures at ¼ and ¾ of the effective height were approximately the same and always under the value of the deformation measured at mid-height which reached 19.3mm for the maximum load.

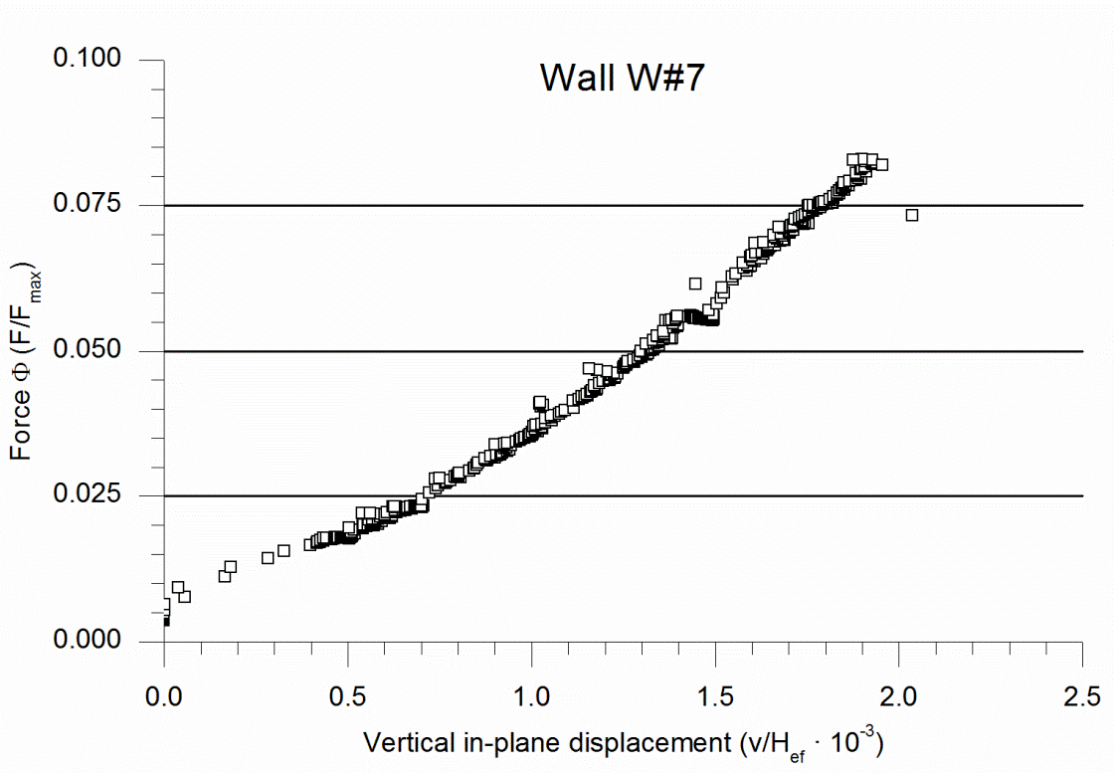

Figure A1. 132 Vertical in-plane response of wall W#7

The mentioned symmetric response is not shown in Figure A1. 134 where the rotation of the lower hinge stayed close to zero while the upper hinge rotated during the initial stages of the test. Near the collapse the lower hinge began to rotate.

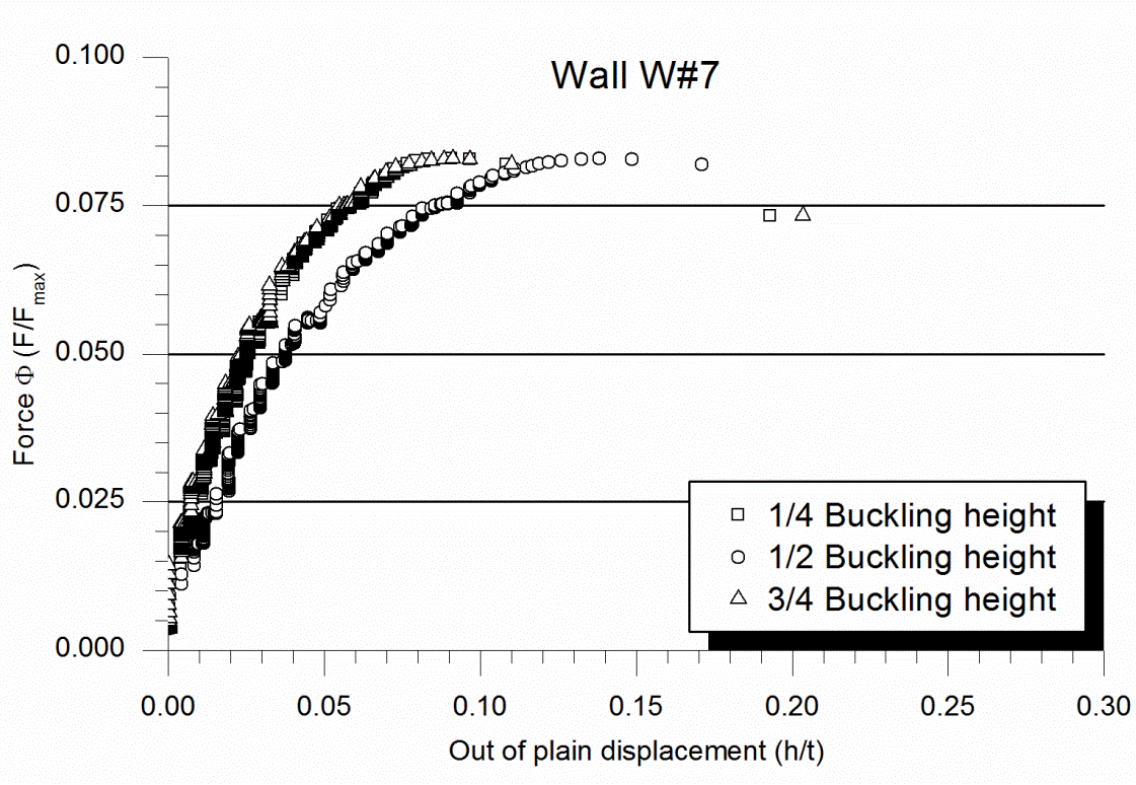

Figure A1. 133 Out-of-plane response of wall W#7

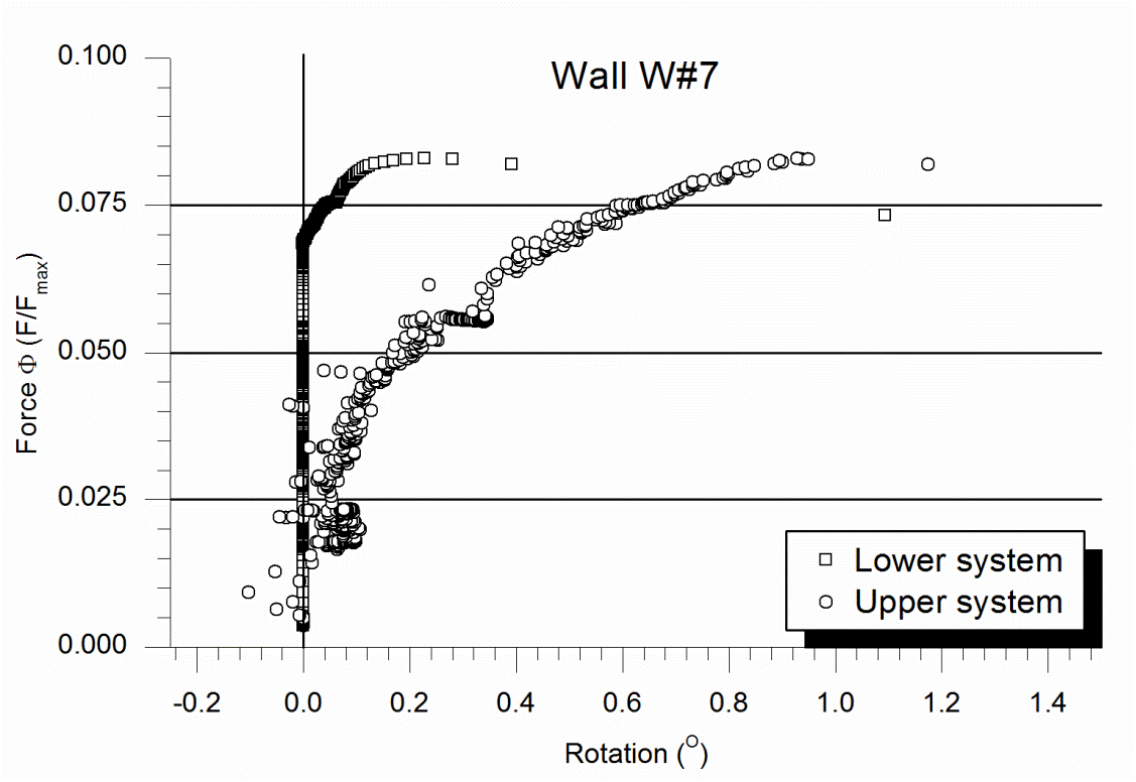

Figure A1. 134 Rotation at wall's endings for wall W#7

In fact, the asymmetric rotation was not observed in life test. The failure (see Figure A1. 135) occurred like in the previous test with the opening of just one crack following a horizontal mortar joint. For wall W#7 the failure cracking was placed at mid-height what contrast even more with the asymmetric rotation of the hinges.

Figure A1. 135 Wall W#7 at the beginning of the test (left) and failing (right)

Wall W#8

This wall was tested the same way than the previous ones: the hinges were kept levelled until the beginning of the test and the horizontal gap in the alignment of the hinges was 8mm (the upper hinge was displaced to the tensile side of the wall). Although the eccentricity at the wall's endings was 10mm, the eccentricity at mid-height was 7.55mm in the opposite direction due to the construction geometric imperfections. It is, the real eccentricity at the mid-height was favourable to break the wall in the opposite direction than the eccentricity at the endings. See Table A1. 33.

The in-plane response was linear (see Figure A1. 136) up to failure at 129.4kN when the distribution beam had descended 4.4mm. It indicates that the system's settling was little compared with other tests like, for example, W#5.

Wall W#8 geometry	
Masonry rows	43
Width	0.879m
Thickness	0.134m
Height between hinges	2.942m
Theoretical eccentricity	10mm
Initial rotation lower hinge	0°
Initial rotation upper hinge	0°
Hinges alignment	8mm
Real mid-height eccentricity	-7.55mm

Table A1. 33 Geometry of wall W#8

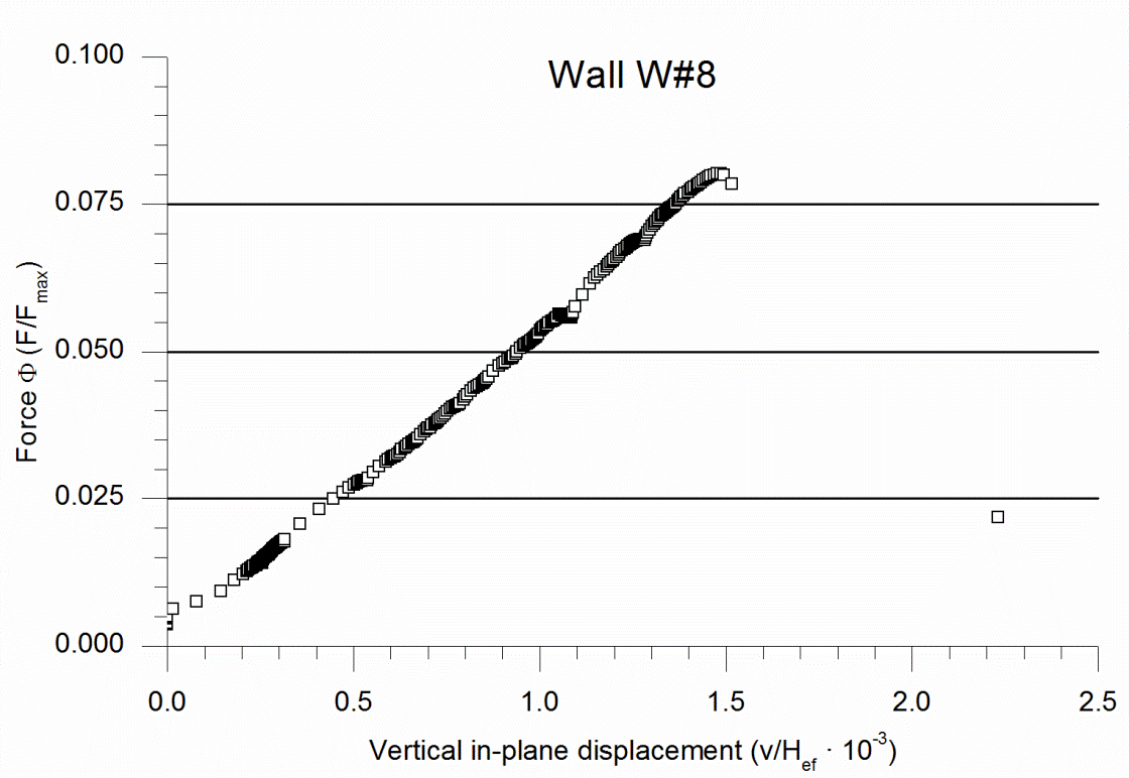

Figure A1. 136 Vertical in-plane response of wall W#8

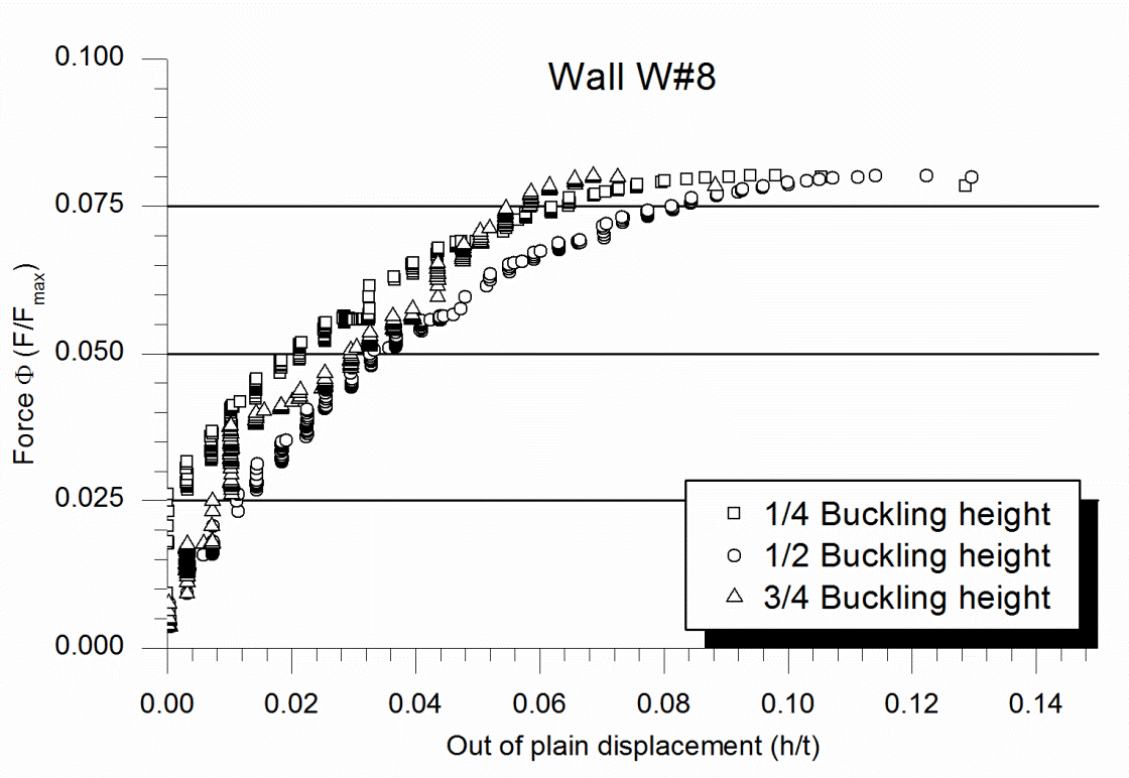

Figure A1. 137 Out-of-plane response of wall W#8

Regarding the out-of-plane behaviour (see Figure A1. 137), it was observed that, initially, the deformation at ¾ of the height grew as fast as the deformation at mid-height. This tendency changed and, at the end of the test, the measured point with less deformation was the ¾ of the height. The greater displacement was at the mid-height and the final configuration was not symmetric with more out-of-plane deformations at the lower part of the wall. It coincided with the failure pattern, suddenly cracking a horizontal mortar joint below the mid-height (see Figure A1. 138).

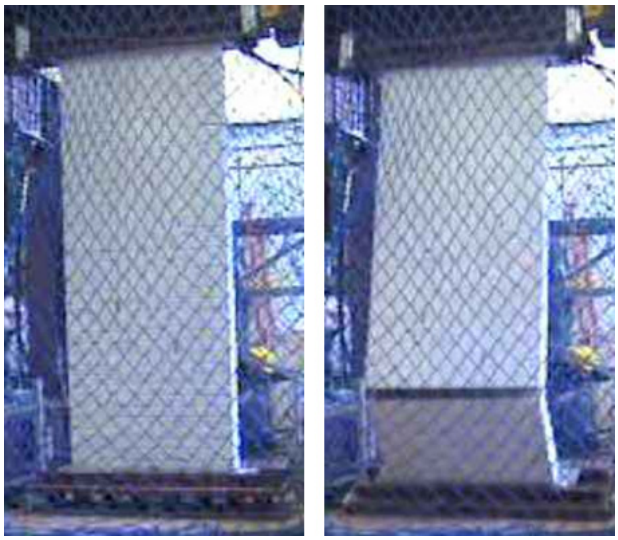

Figure A1. 138 Wall W#8 at the beginning of the test (left) and failing (right)

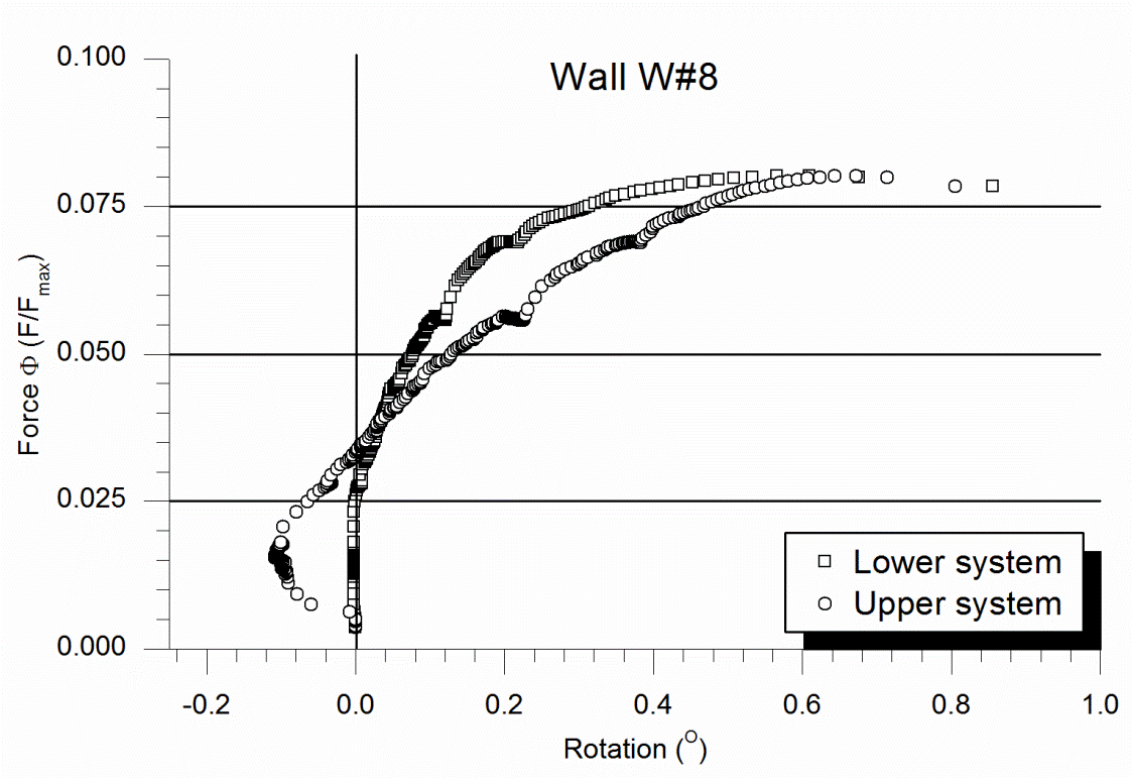

Figure A1. 139 Rotation at wall's endings for wall W#8

An exceptional behaviour (Figure A1. 139) was observed in relation with the hinges rotation at the beginning of the test. Initially, the upper supporting system rotated in the opposite direction than the final rotation. After that, this system turned with a constant velocity almost up to the collapse when it had the maximum rotation of the whole structure. In contrast, the lower hinge began the test with no movements and slowly its rotation got faster. During the test, the rotation rate of the lower hinge was increased.

Wall W#9

Because of the considerable geometric imperfections of wall W#9, the hinges were initially rotated to achieve a better positioning inside the testing system (see Table A1. 34). The effect of the geometric irregularities is proved by comparing the eccentricity at the endings (5mm) with the real eccentricity at mid-height (21.5mm). In addition, the lower hinge was 8.5mm displaced to the tensile side of the wall respect the upper hinge.

Wall W#9 geometry	
Masonry rows	43
Width	0.888m
Thickness	0.134m
Height between hinges	2.892m
Theoretical eccentricity	5mm
Initial rotation lower hinge	2,72°
Initial rotation upper hinge	-4,86°
Hinges alignment	-8,5mm
Real mid-height eccentricity	21.48mm

Table A1. 34 Geometry of wall W#9

The vertical descending movement is shown in Figure A1. 140. The response was linear most of the time but near the collapse load, 109.8kN, some relaxation was observed. At failure, the distribution beam had descended 3.6mm.

An asymmetric response is observed in Figure A1. 141. The out-of-plane deformation at ¼ of the buckling height was always bigger than the deformation at ¾ of the buckling height. At mid-height, the deformation was the largest. At collapse point, it was 12.9mm. This asymmetric behaviour may be associated with the initial different rotation of the hinges or even with the considerable geometric irregularities of wall W#9.

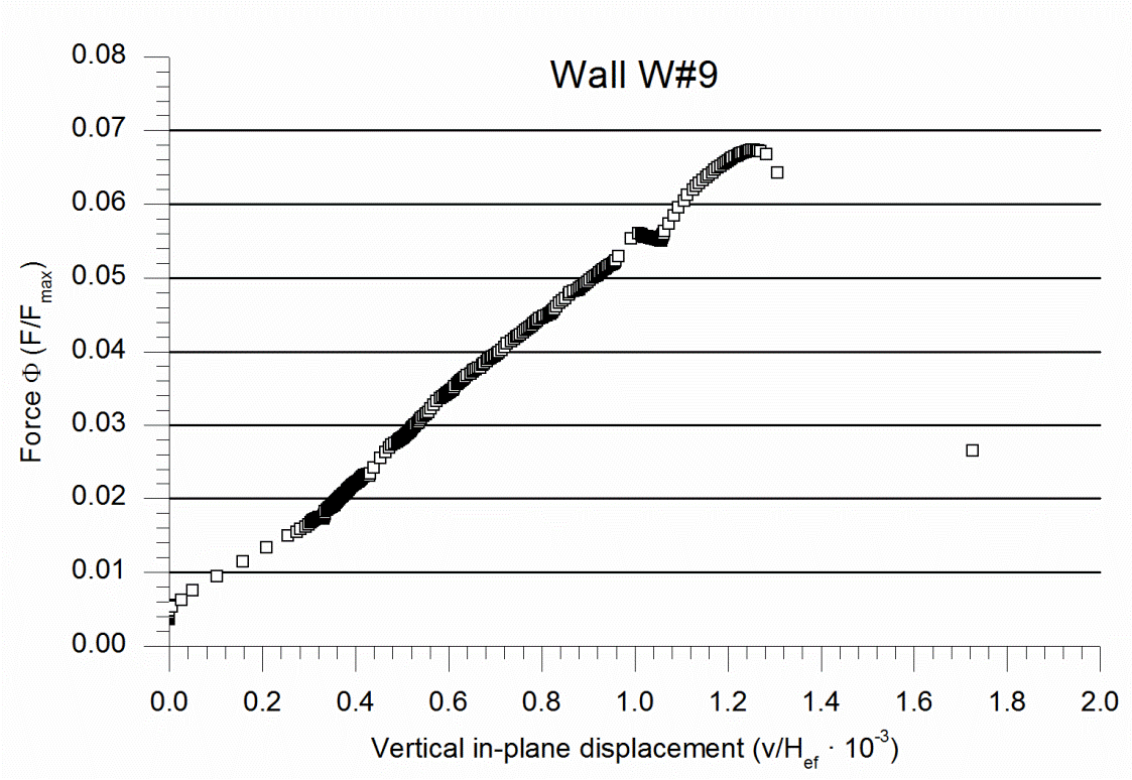

Figure A1. 140 Vertical in-plane response of wall W#9

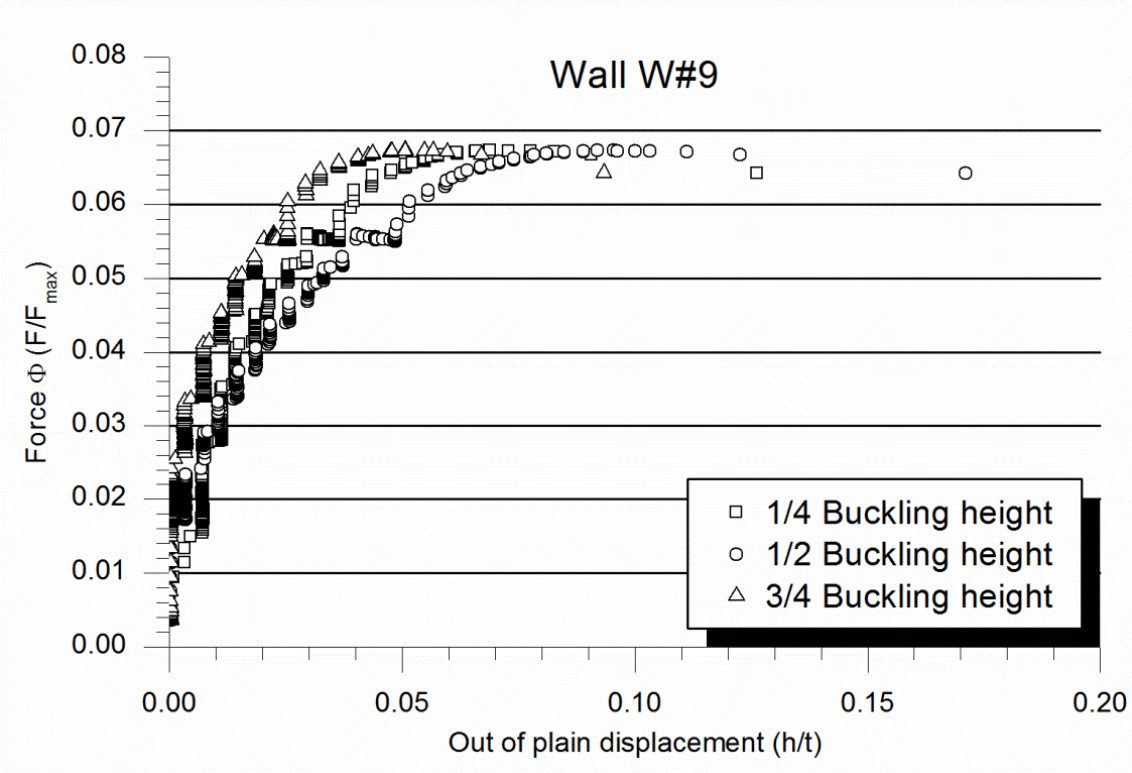

Figure A1. 141 Out-of-plane response of wall W#9

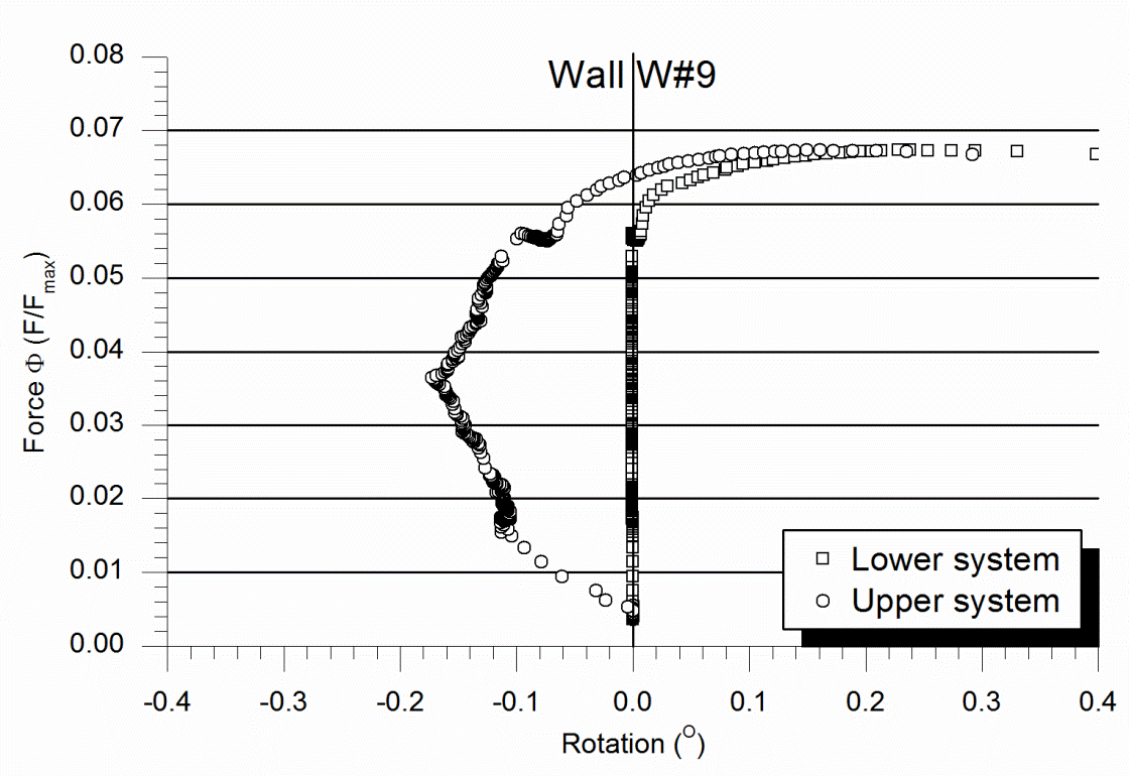

Figure A1. 142 Rotation at wall's endings for wall W#9

Figure A1. 143 Wall W#9 at the beginning of the test (left) and failing (right)

About the rotation (see Figure A1. 142), the same behaviour than previous walls was observed. It is the lower hinge stayed at the initial condition while the upper one rotates. However, in this case, the upper hinge began its rotation to the opposite direction than the buckling failure had associated. It would have

caused the asymmetric behaviour commented before for wall W#9. At half the maximum load, the rotation of the upper hinge changed its direction and, finally, the collapse was associated with the expected rotation sign. It was only at the collapse that the lower hinge rotated from its initial unlevelled position. During the test, the upper system rotated because of the movement of the distribution beam which had little more freedom than in previous comparable tests.

Although all the reasons for asymmetric behaviour, the collapse pattern respected the symmetry of the system as seen in Figure A1. 143.

Wall W#10

This one was the first of the M series. It was also the first test recorded with the high-speed camera. When placing it at the testing position both hinges turned to better fit the wall in its position (see Table A1. 35). However, the horizontal distance between the rotation axes of the hinges was, for this case, 10.5mm. The upper hinge was initially displaced to the same side where the tensile stresses would appear during the test. Due to the construction imperfections, the real mid-height eccentricity was almost 0 although at the wall's headings it was 10mm.

Wall W#10 geometry	
Masonry rows	27
Width	0.888m
Thickness	0.134m
Height between hinges	1.865m
Theoretical eccentricity	10mm
Initial rotation lower hinge	0.14°
Initial rotation upper hinge	0.86°
Hinges alignment	10.5mm
Real mid-height eccentricity	0.19mm

Table A1. 35 Geometry of wall W#10

The in-plane vertical displacement (Figure A1. 144) showed an initial settling stage that lasted up to 25% of the maximum load, followed by a linear response that finally relaxed near the collapse point. The vertical displacement of the distribution beam was 11.3mm for the applied load of 423.9kN.

At the beginning of the test the upper part of the wall moved backwards as shown in Figure A1. 145. The out-of-plane displacement of the mid-height point and the ¼ height point was almost the same up to half the maximum load when the buckling effects began to be more appreciable and the mid-height point deformed more than the one placed at ¼ height.

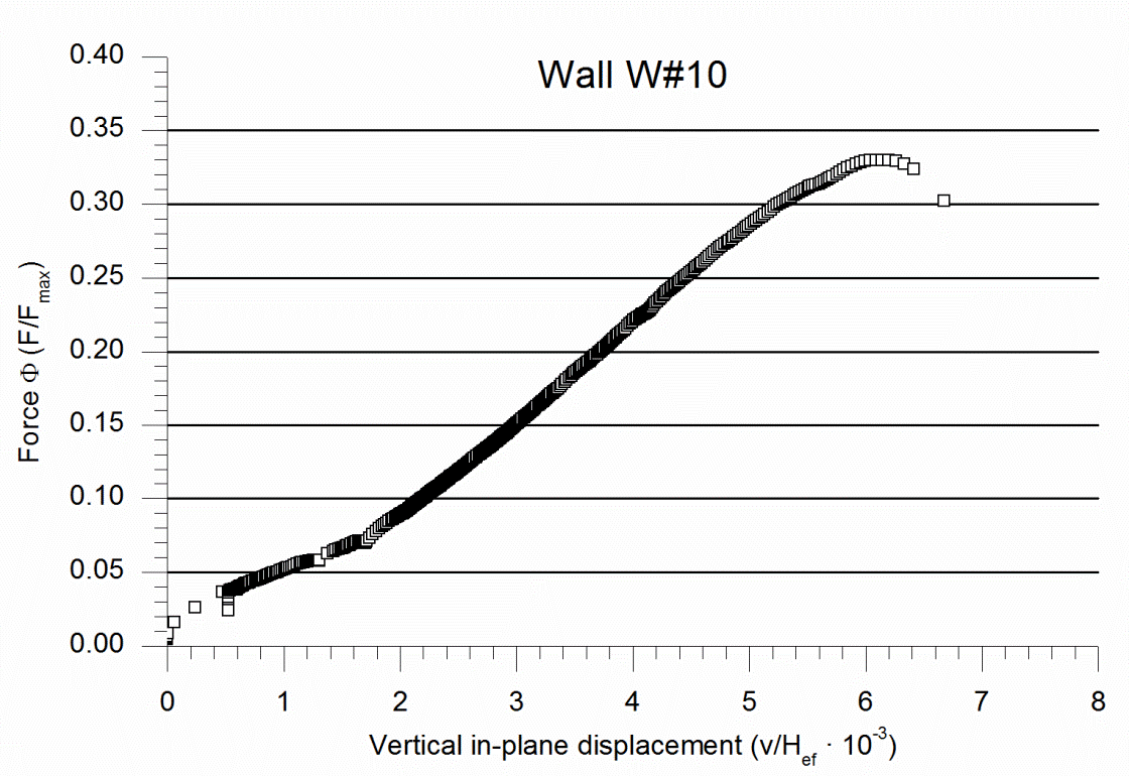

Figure A1. 144 Vertical in-plane response of wall W#10

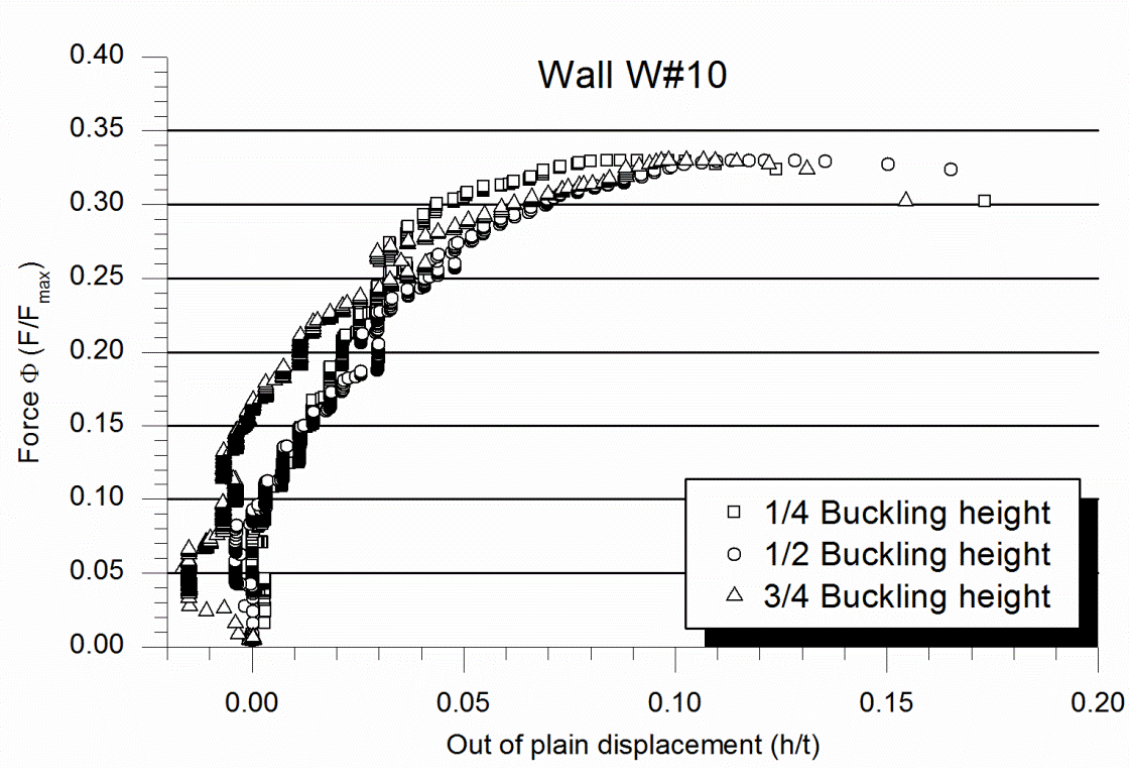

Figure A1. 145 Out-of-plane response of wall W#10

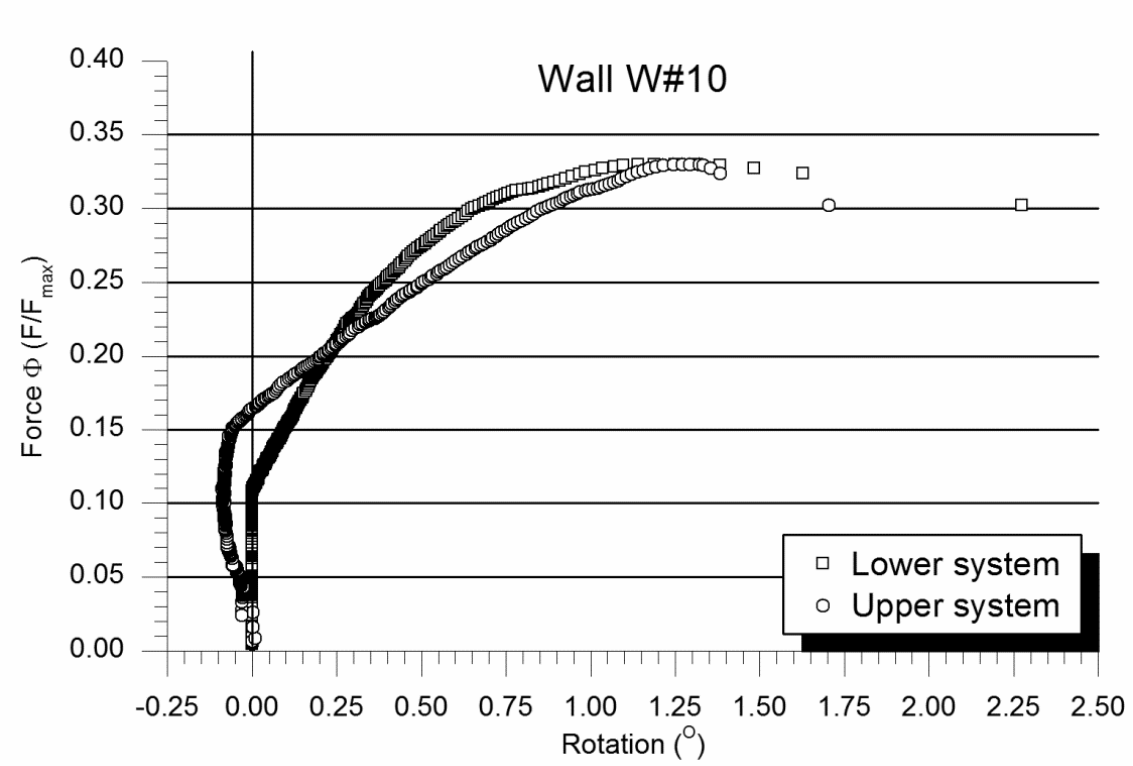

Figure A1. 146 Rotation at wall's endings for wall W#10

Figure A1. 146 shows the rotation of the supporting systems at each extreme of the wall W#10. It is noticed that the lower hinge remained up to 30% of the maximum load when it began to grow with and increasing velocity. In contrast, the upper system was rotating from the very first loading step but it was in the opposite direction from the expected. After this a linear response was observed and the upper system overturned with a constant rate up to the collapse point.

Figure A1. 147 Wall W#10 at the beginning of the test (left) and failing (right)

The collapse mode was extremely fragile, observing a suddenly loss of the vertical stability. The formation of a hinge at approximately mid-height of the wall is clear observing Figure A1. 147 and specially Figure A1. 148.

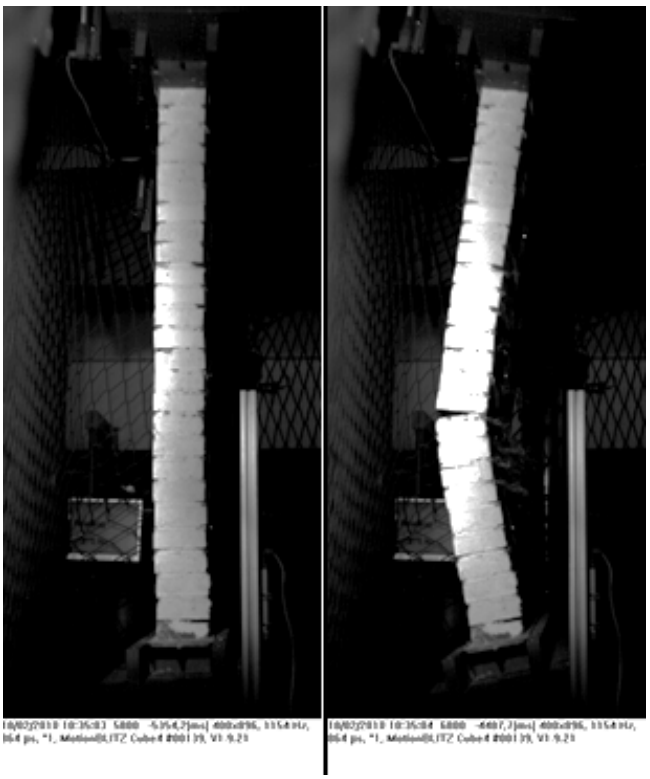

Figure A1. 148 Failure of the wall W#10. Opening of a horizontal mortar joint below mid-height

Wall W#11

The initial geometry of this wall was closer to the theoretical than the previous one (Table A1. 36). For this reason it was not necessary to rotate the lower hinge before the test. However, the upper hinge was slightly turned. The geometric irregularities made that the eccentricity at the wall's endings (20mm) was less in the mid-height position (13.9mm). At the beginning of the test, the upper hinge was placed 10mm to the tensile side of the wall respect from the lower hinge.

Wall W#11 geometry	
Masonry rows	27
Width	0.870m
Thickness	0.134m
Height between hinges	1.892m
Theoretical eccentricity	20mm
Initial rotation lower hinge	0°
Initial rotation upper hinge	-1.29°
Hinges alignment	10mm
Real mid-height eccentricity	13.9mm

Table A1. 36 Geometry of wall W#11

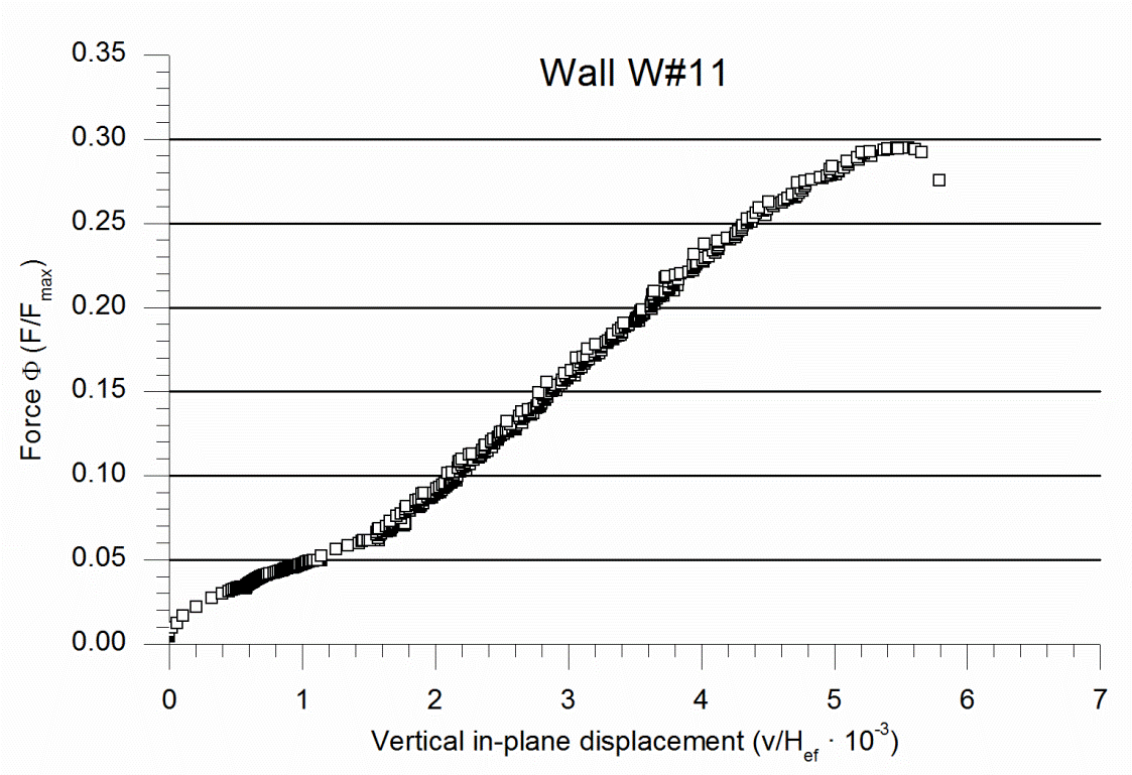

Figure A1. 149 Vertical in-plane response of wall W#11

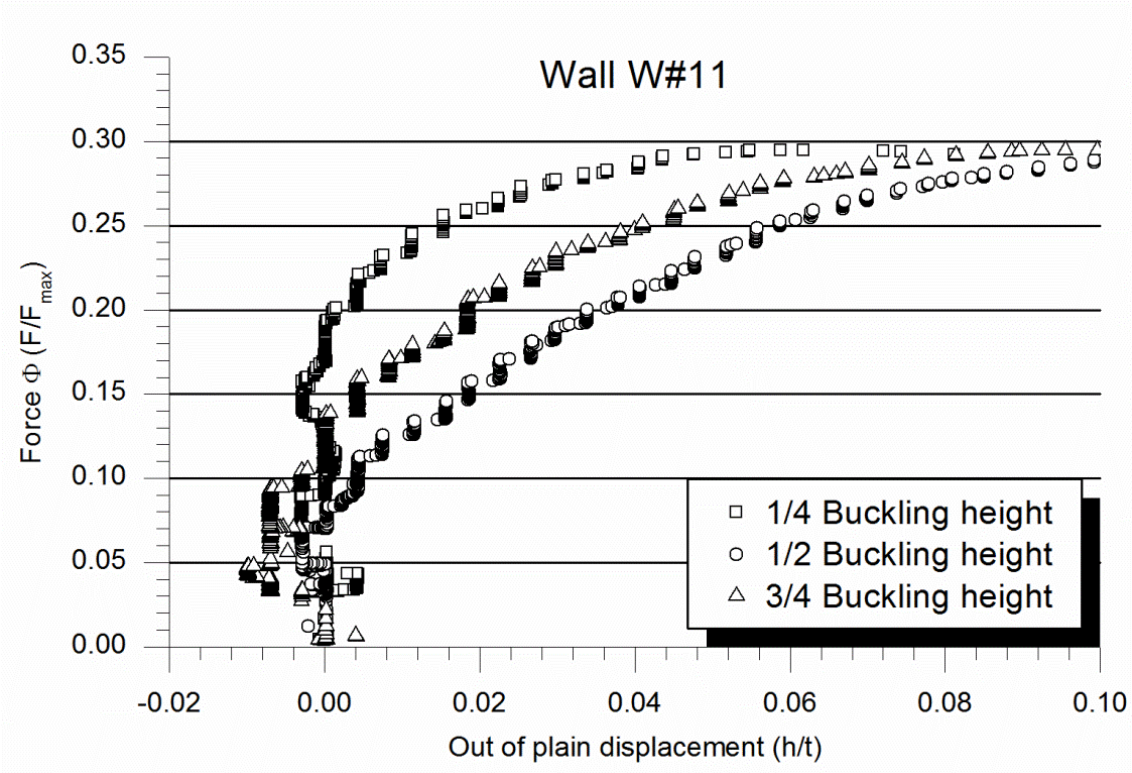

Figure A1. 150 Out-of-plane response of wall W#11

In plane descending movement of the top of the wall (Figure A1. 149) was characterised by an initial settling stage up to approximately 1/5 of the maximum load (371.2kN), followed by a linear response which finished with a relaxation near the collapse (vertical displacement in collapse was 10.5mm).

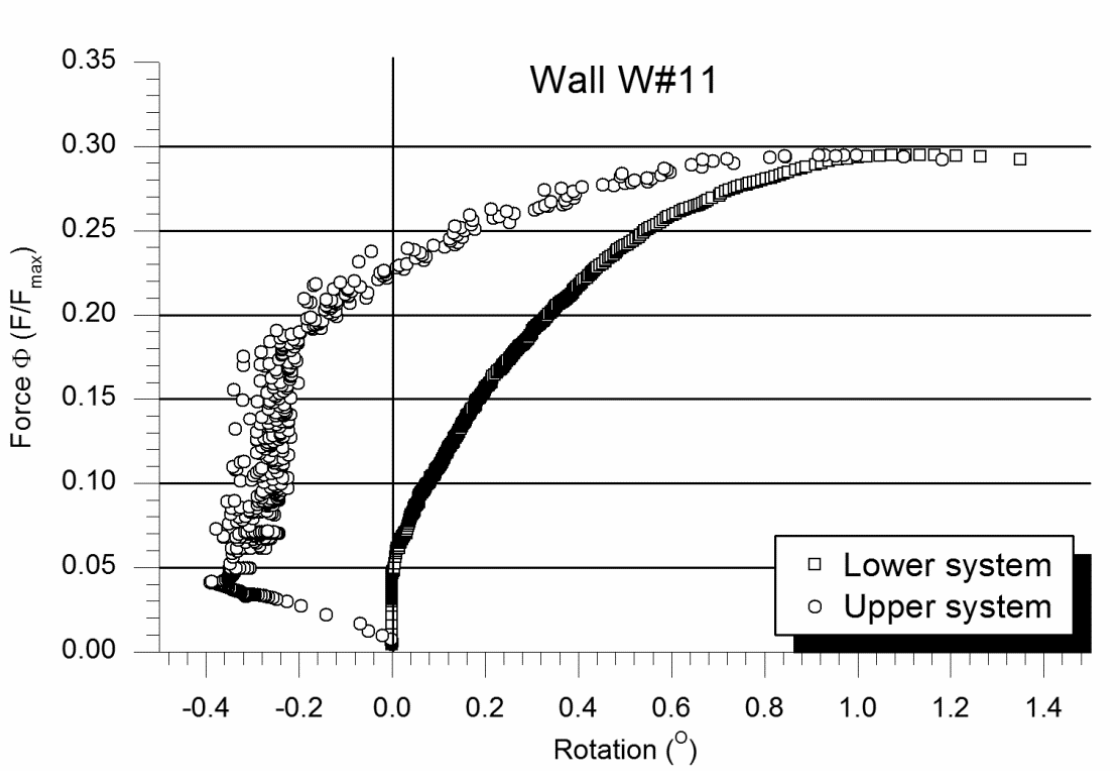

Figure A1. 151 Rotation at wall's endings for wall W#11

In relation with the out-of-plane deformation, Figure A1. 150, all sensors presented an instable behaviour up to 30% of the maximum load. The first sensor to stabilise was the positioned at mid-height and it always measured the maximum values for the three lasers. Secondly, the laser placed at ¾ of the effective height began to read increasing values and finally the sensor at ¼ of the height stabilised its readings. All measures were non-linear with a rising deformation velocity. The maximum out-of-plane deformation (for the mid-height sensor) was 17.4mm.

Regarding the rotation of the supporting systems (Figure A1. 151) it is noticed that the measures of the upper system were unstable although the whole tendency can be studied. The upper hinge, together with the distribution beam rotated in the opposite direction from the expected according with the observed failure mode. However, the direction changed near the collapse load. In contrast, the lower hinge rotated always in the same direction it moved during the wall's failure. The measurements of this hinge's rotation were more stable than the upper ones. At the first stage the lower hinge stay still but then it began to rotate with an increasing rate up to failure.

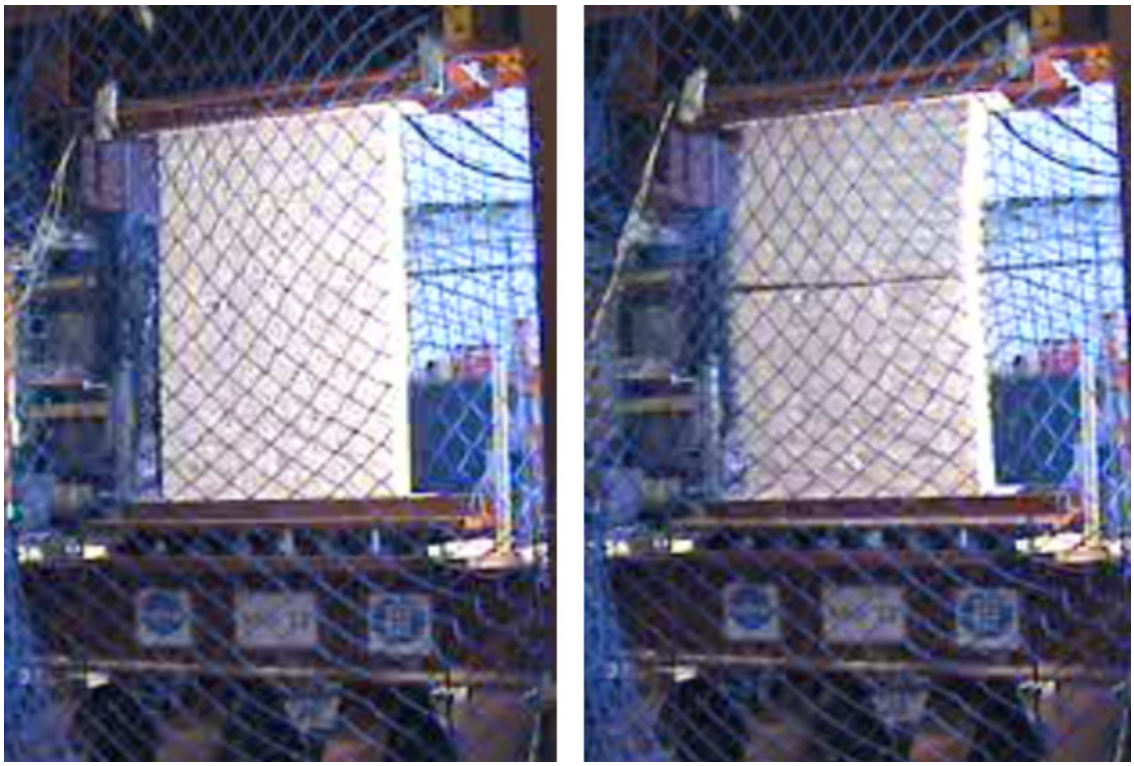

Figure A1. 152 Wall W#11 at the beginning of the test (left) and failing (right)

The failure was caused by buckling or geometric instability when one mortar joint opened slightly over mid-height (see Figure A1. 152 and Figure A1. 153). The collapse was suddenly although second order caused bending deformation was previously noticed during the test. Moreover, looking at Figure A1. 152 (failing) an clear asymmetry along the wall's width was observed as the crack opened from one side and grew to the other.

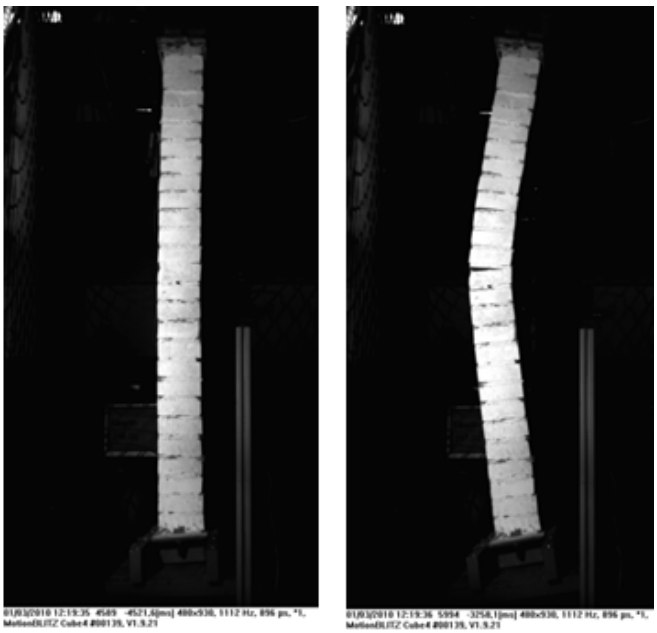

Figure A1. 153 Failure of the wall W#11. Opening of a horizontal mortar joint over mid-height

Wall W#12

This wall was placed in testing position with a slight adjustment on the hinges levelling and a good alignment between the upper and lower hinges was achieved. The eccentricity at the extremes (10mm) was clearly reduced at mid-height (1.6mm) due to geometric irregularities. See Table A1. 37.

The in-plane behaviour (Figure A1. 154) was very similar to the previous two tests, with an initial settling stage followed by a linear response which finished with a relaxation. The in-plane displacement of the distribution beam corresponding with the maximum applied load was (471.1kN) 11.1mm.

Wall W#12 geometry	
Masonry rows	27
Width	0.882m
Thickness	0.134m
Height between hinges	1.841m
Theoretical eccentricity	10mm
Initial rotation lower hinge	0.72°
Initial rotation upper hinge	1.79°
Hinges alignment	5mm
Real mid-height eccentricity	1.63mm

Table A1. 37 Geometry of wall W#12

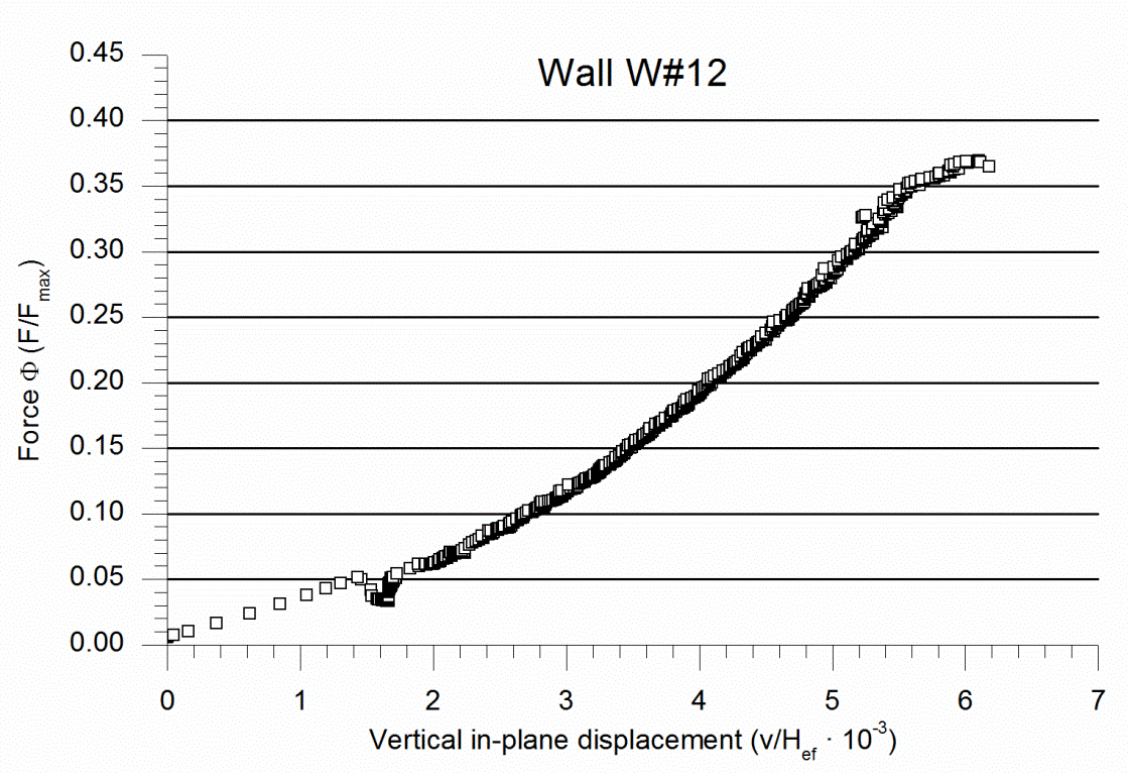

Figure A1. 154 Vertical in-plane response of wall W#12

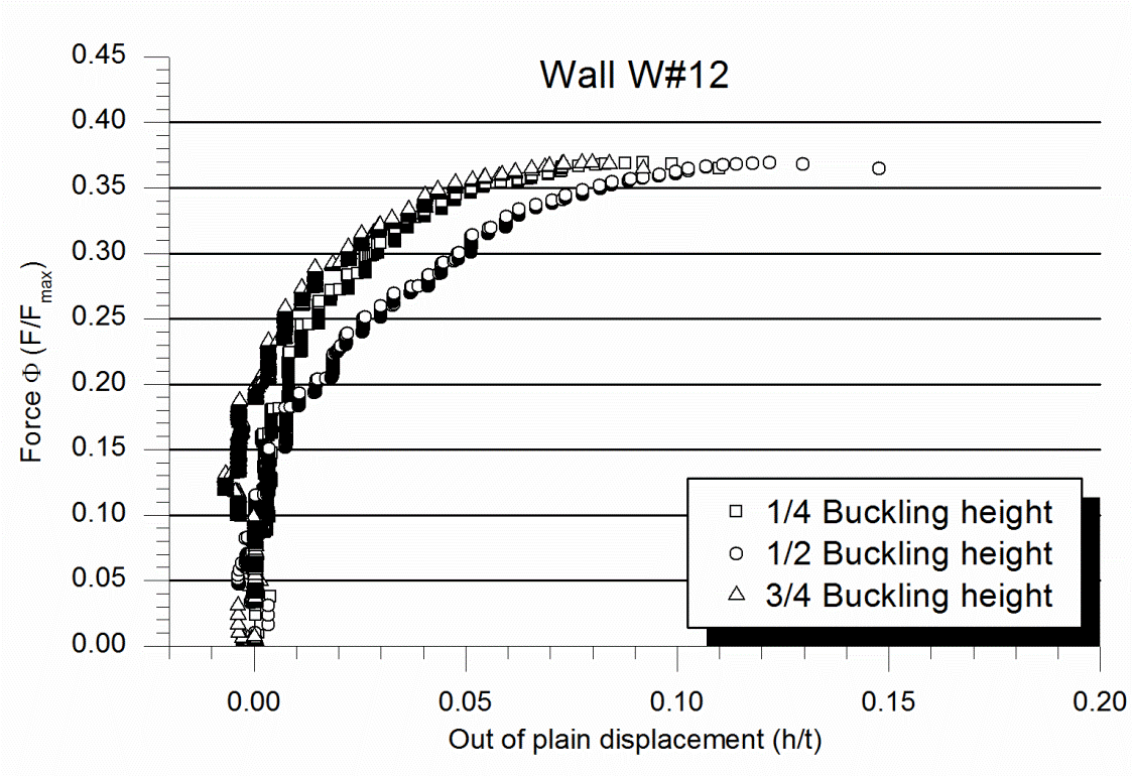

Figure A1. 155 Out-of-plane response of wall W#12

For wall W#12, the out-of-plane deformations were symmetric so the lasers placed to measure the deformation at ¼ and ¾ of the effective height read approximately the same. The major out-of-plane displacements corresponded with the measures at the mid-height (see Figure A1. 155). At collapse this point deformed 16.3mm. It has to be noticed that at the beginning of the test the three lasers measured a deformation of opposite sign than the final deformation. It may be caused by initial settling effects.

Measuring the rotation of the supporting systems, Figure A1. 156, it is observed the same behaviour than wall W#11. The lower hinge stays still while the upper system rotates with the opposite direction than the final collapse pattern. The main difference with the previous test is that for W#12 the lower hinge stays still for most of the test duration and only began its movement when reaching over the 60% of the maximum load. The upper hinge rotated in the expected direction only on the failing stage.

The asymmetry on the supports rotation seems to influence more than the symmetric of the out-of-plane deformations as the collapse pattern was clearly asymmetric (see Figure A1. 157). Wall W#12 failed by opening a horizontal mortar joint placed near ¼ of the effective height. Although the failure was sudden large deformations were observed before achieving the maximum load.

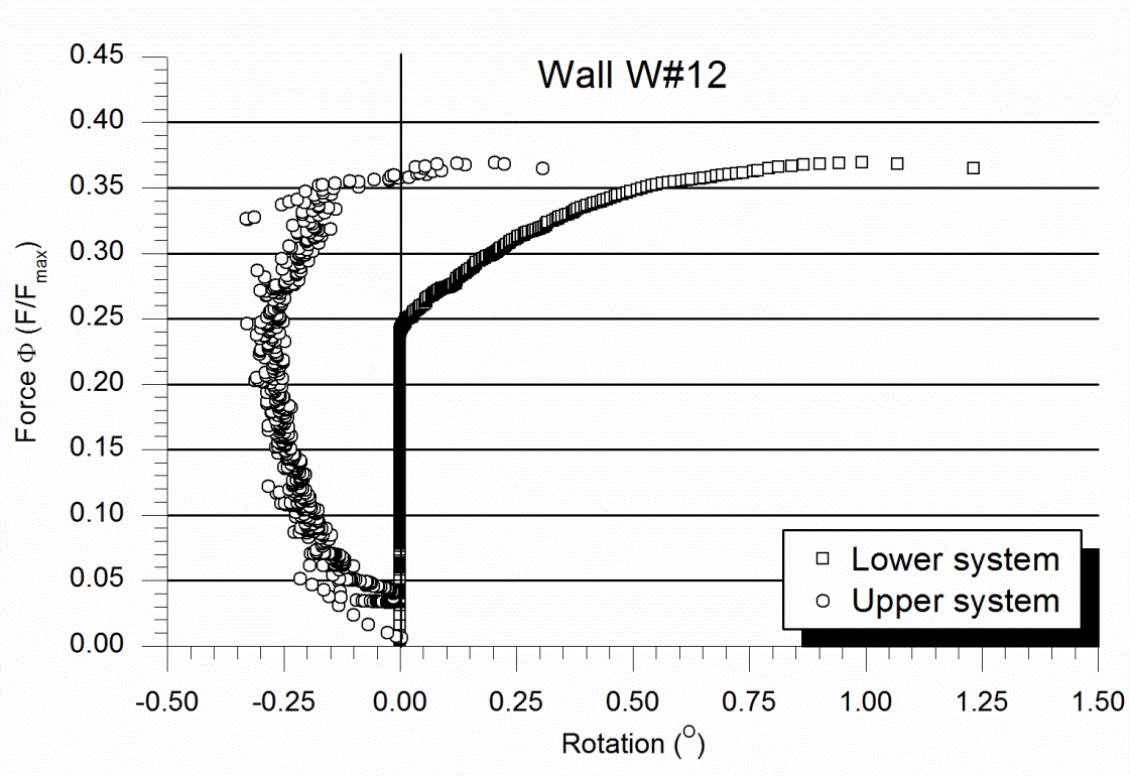

Figure A1. 156 Rotation at wall's endings for wall W#12

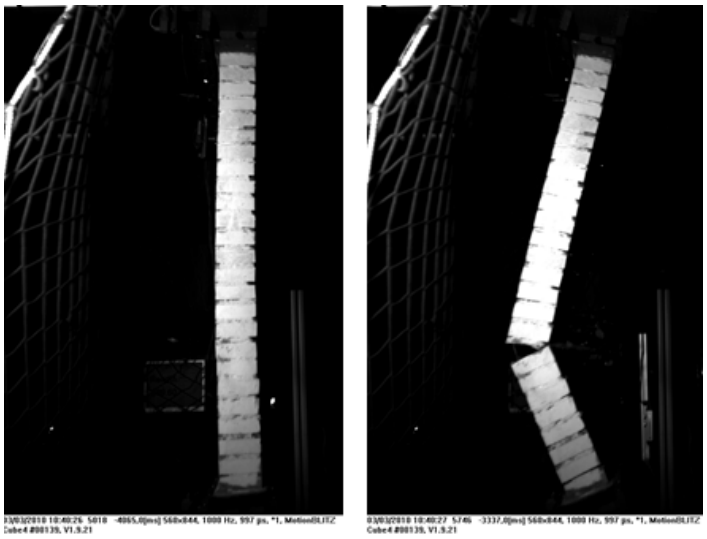

Figure A1. 157 Failure of the wall W#12. Opening of a horizontal mortar joint at approximately ¼ height

Wall W#13

This wall was tested with the two hinges initially rotated to the opposite direction the extremes of the wall were supposed to rotate during the test according with the eccentricity of the load. Moreover, this eccentricity was the biggest and the real mid-height eccentricity was even larger because of geometric irregularities from the construction procedure. However, the two hinges were practically aligned (see

Table A1. 38). All these facts considered together may be the cause for the unusual low load bearing capacity of wall W#13 (83.8kN).

Wall W#13 geometry	
Masonry rows	27
Width	0.900m
Thickness	0.134m
Height between hinges	1.660m
Theoretical eccentricity	30mm
Initial rotation lower hinge	-0,36°
Initial rotation upper hinge	-0,72°
Hinges alignment	2mm
Real mid-height eccentricity	31.75mm

Table A1. 38 Geometry of wall W#13

The vertical displacement vs. force graph (Figure A1. 158) shows a linear behaviour up to failure what was expected given the low value of the stresses as the applied force was relatively little compared with previous tests. The vertical displacement of the distribution beam when the wall collapsed was 4.1mm.

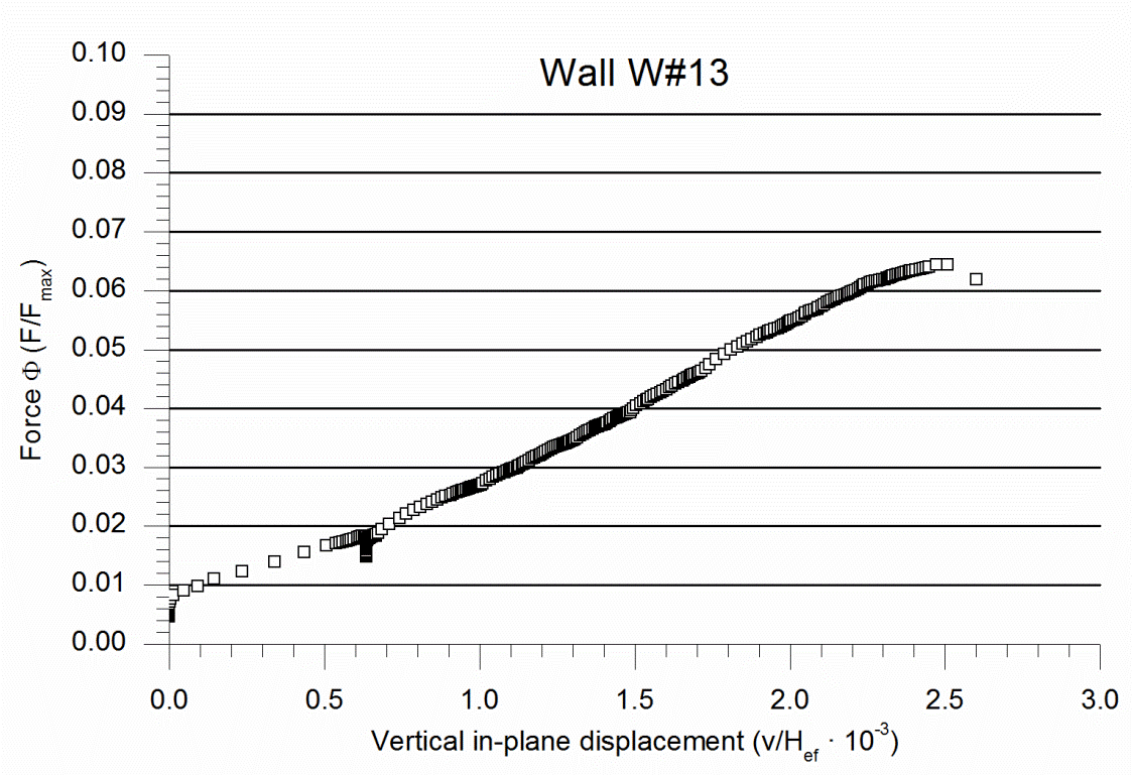

Figure A1. 158 Vertical in-plane response of wall W#13

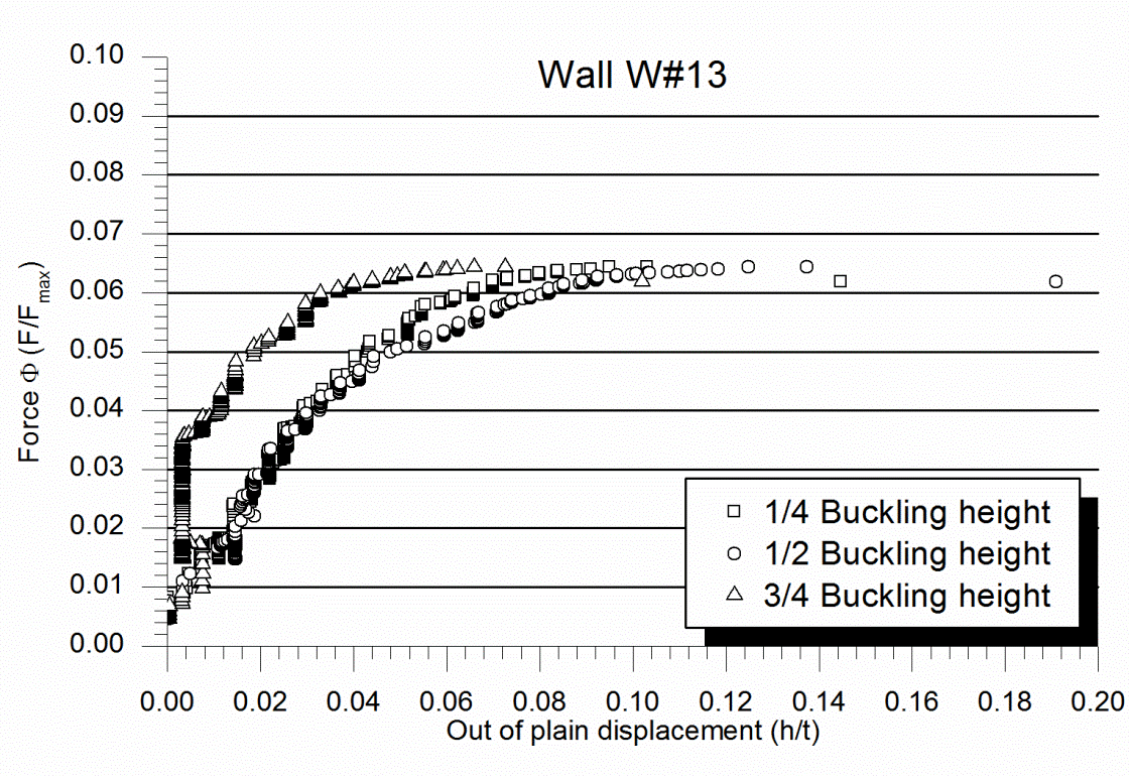

Figure A1. 159 Out-of-plane response of wall W#13

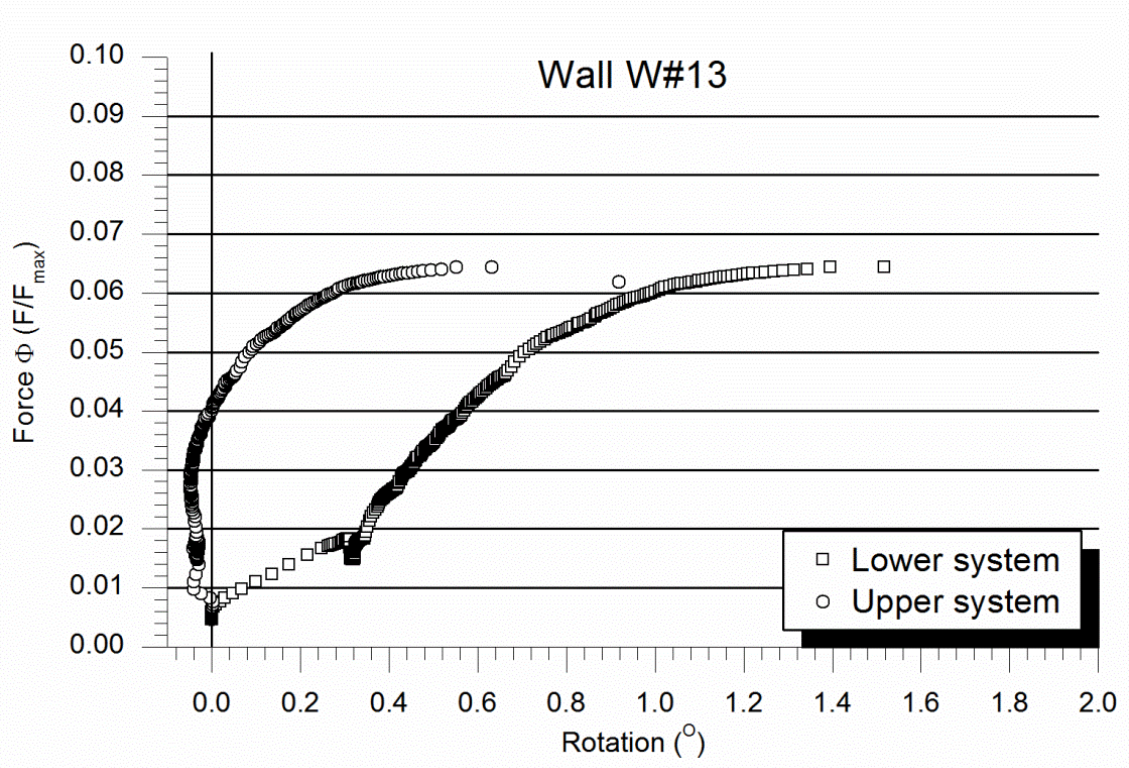

Figure A1. 160 Rotation at wall's endings for wall W#13

Analysing the out-of-plane deformations (Figure A1. 159), it is observed that mid-height and ¼ height placed points deformed approximately the same whereas laser measuring the displacement at ¾ of the height was always reading minor values. In fact, it seems the upper area of the wall did not move until half the maximum force was applied. At the failure time the mid-height out-of-plane deformation was 17.6mm.

The behaviour of the supporting system (Figure A1. 160) was different from previous tests as the lower hinge rotated from the very first moment. This hinge began its movement with a high velocity but then the rotation slowed down to progressively increase again up to failure. The upper supporting system behaved different with an initial rotation opposite to the expected direction (not following the out-of-plane deformation pattern) followed by a constant position phase and finishing with a rotation in the direction associated with the failure with increasing velocity up to failure.

The wall W#13 failed when opening a mortar joint below the mid-height (see Figure A1. 161). The difference with previous tests is that, for W#13 case the wall supported increasing loads even when the joint was opened. The failure mechanism was not as sudden as the previous tests. In the other hand, it is worth mentioning that the out-of-plane deformation and the hinges rotation presented both asymmetric responses which agree with the asymmetric collapse pattern.

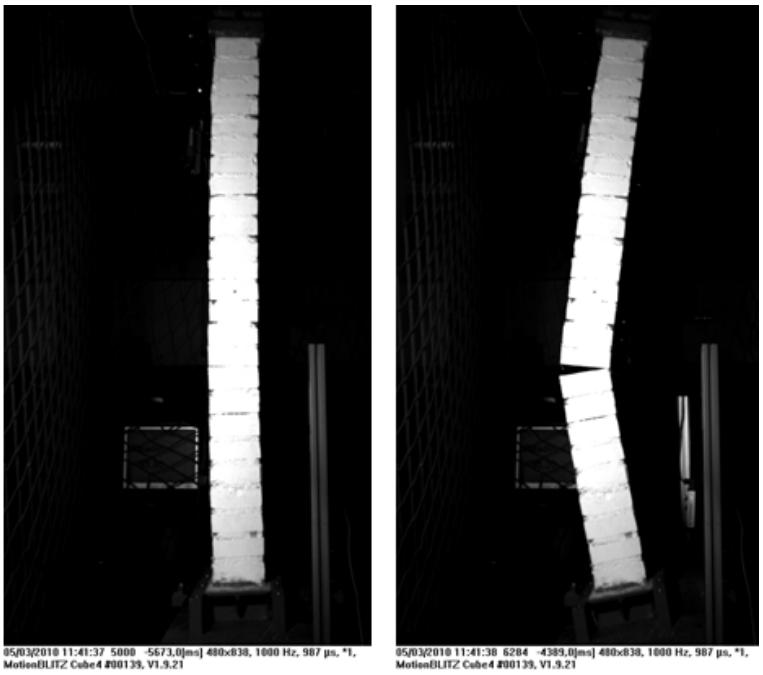

Figure A1. 161 Failure of the wall W#13. Opening of a horizontal mortar joint at approximately 1/3 height

Wall W#14

Wall W#14 was placed rotating both hinges following the direction the hinges were expected to rotate near the failure. This initial rotation was less than other cases (see Table A1. 39). Furthermore, the average verticality of the wall was better than most of the previous wall tested. In fact, the eccentricity at mid height was almost the same than the eccentricity at the extremes of the wall (theoretical). However, the hinges alignment at both sides had the same value but opposite directions (so the average alignment was 0mm) describing a helicoid shape. Finally, wall W#14 was the only one which presented a crack in the masonry before testing it. There was one stepped crack in the tensile side of the wall near the lower ending (see Figure A1. 162).

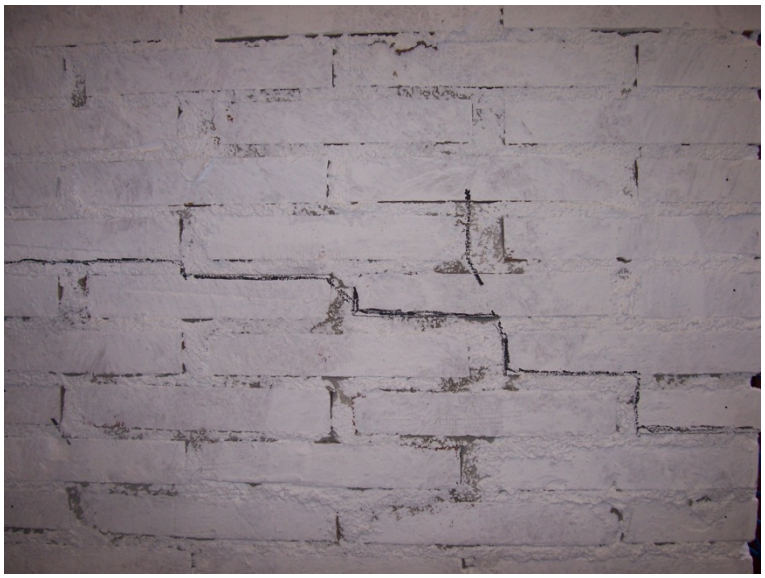

Figure A1. 162 Initial crack at the tensile side of the wall W#14 before testing

Wall W#14 geometry	
Masonry rows	27
Width	0.900m
Thickness	0.134m
Height between hinges	1.861m
Theoretical eccentricity	20mm
Initial rotation lower hinge	0.07°
Initial rotation upper hinge	1.86°
Hinges alignment	0mm
Real mid-height eccentricity	21.18mm

Table A1. 39 Geometry of wall W#14

Looking at the in-plane response (Figure A1. 163) the behaviour was similar to that observed for walls W#10, W#11 and W#12, with an initial settling phase followed by a linear response stage and finishing with a material relaxation. For the maximum load (518.5kN) the vertical descending displacement of the distribution beam was 10mm.

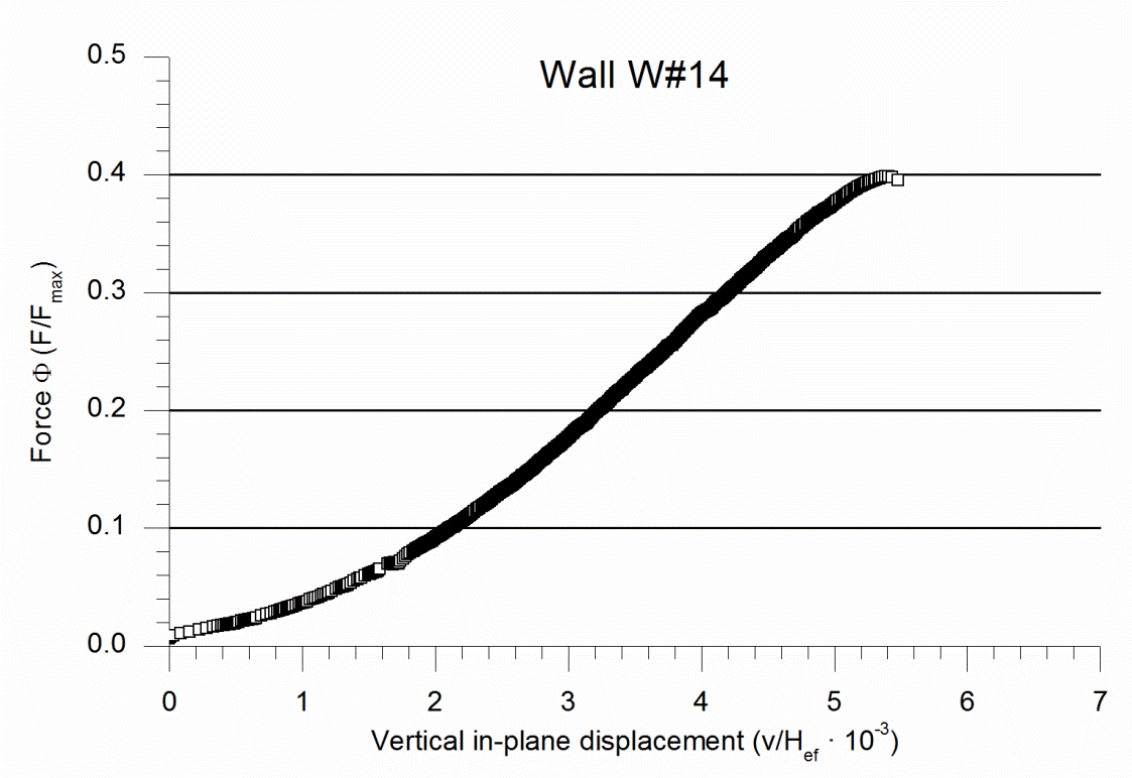

Figure A1. 163 Vertical in-plane response of wall W#14

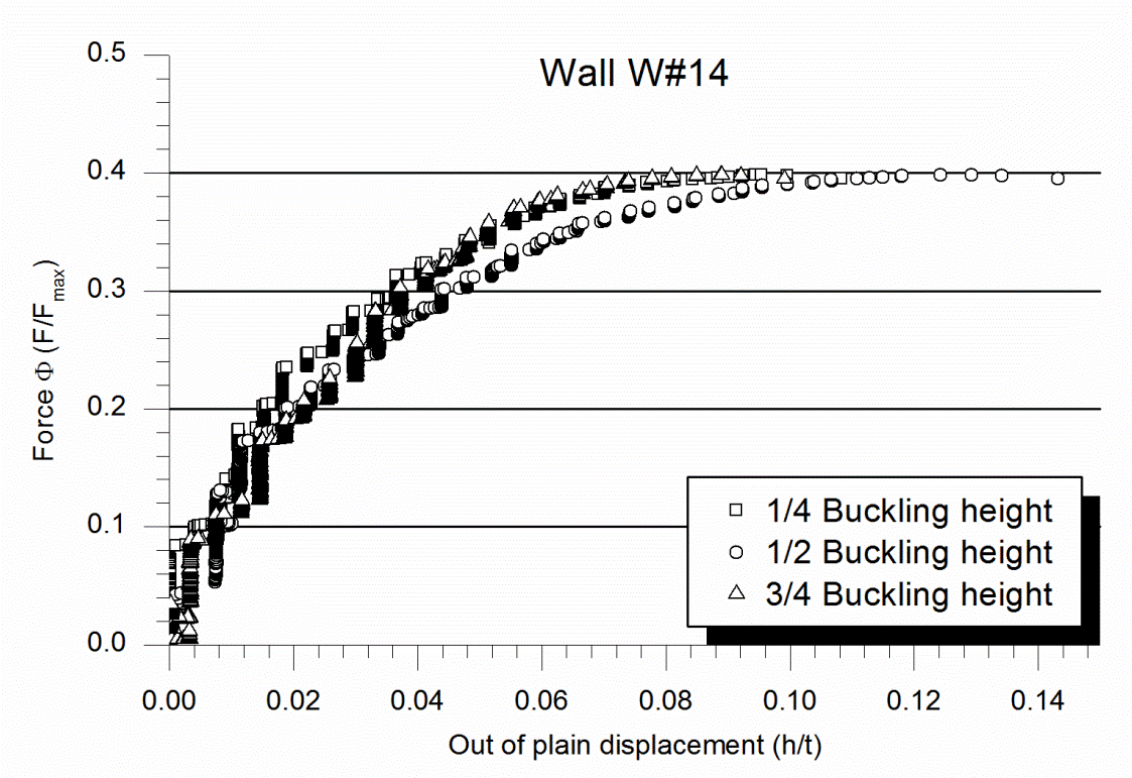

Figure A1. 164 Out-of-plane response of wall W#14

Regarding the out-of-plane response (Figure A1. 164), it is observed that the deformation at ¾ and ½ of the effective height was the same up to the half of the maximum load. From this point and on, the deformation at ½ was always the biggest and from the 80% of the maximum load the out-of-plane displacement at ¼ and ¾ of the height was the same. It indicates an initial asymmetric behaviour which became symmetric at increasing the applied load. The mid-height out-of-plane deformation at maximum load was 16.7mm.

Looking at the response of the supporting systems (Figure A1. 165) it is observed that the upper hinge began rotating to the opposite direction of the expected one whilst the lower hinge remained still. After that, the upper system rotated with an increasing speed. A clear change in the slope of the curve of the lower system is observed at loading more than 80% of the maximum load.

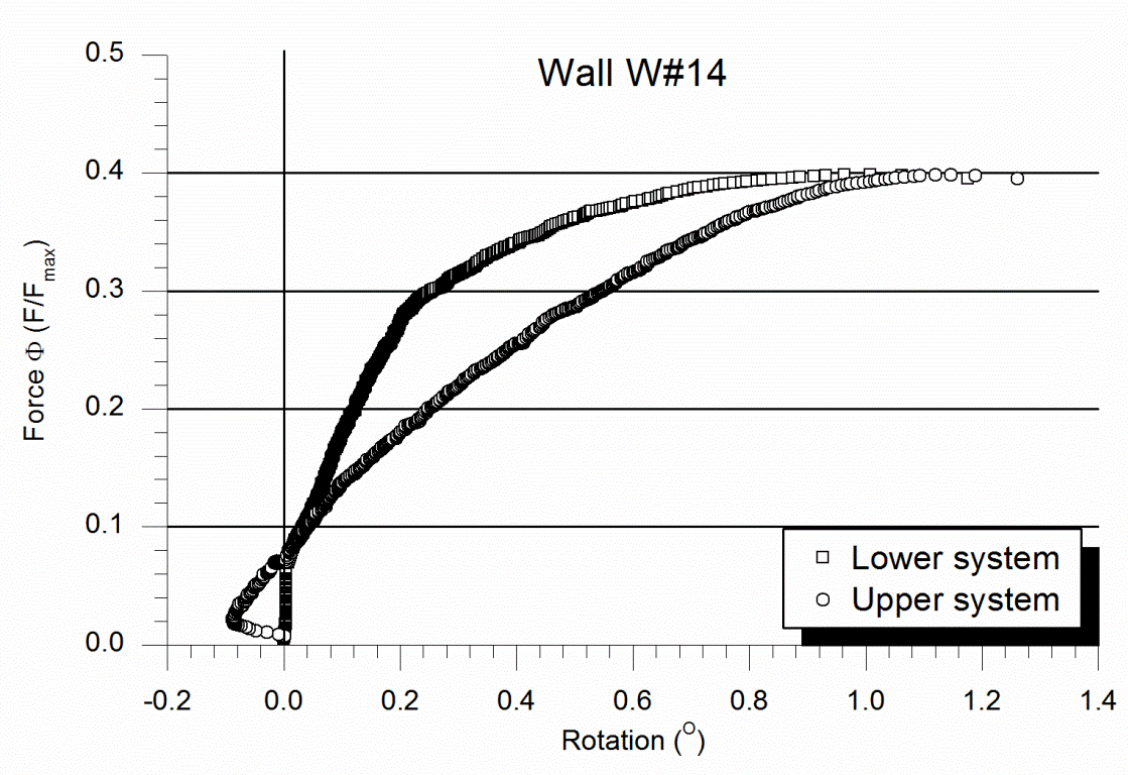

Figure A1. 165 Rotation at wall's endings for wall W#14

The three previous graphs showed a change in the wall response from 80% of the maximum load. The failure process of wall W#14 was different from the rest of the walls of the M series because a crushing-buckling mixed mode was observed (see Figure A1. 166). The collapse was sudden.

Figure A1. 166 Failure of the wall W#14. Crushing at compression side and opening of a horizontal joint

Wall W#15

As observed in Table A1. 40, to place wall W#15 in testing position with little hinges alignment gap (3mm) it was necessary to rotate the upper hinge to the expected rotation direction at collapse while the lower hinge was rotated in the opposite direction. The vertical shape of the wall was better than the average as the eccentricity at the hinges (30mm) was more or less the same at mid-height (29.03mm). As the previous wall, this one also presented a helicoidally shape.

Wall W#15 geometry	
Masonry rows	27
Width	0.895m
Thickness	0.134m
Height between hinges	1.845m
Theoretical eccentricity	30mm
Initial rotation lower hinge	-0.14°
Initial rotation upper hinge	1.15°
Hinges alignment	3mm
Real mid-height eccentricity	29.03mm

Table A1. 40 Geometry of wall W#15

Observing the response of the wall W#15 (see graphs in Figure A1. 167, Figure A1. 168 and Figure A1. 169) the fast increase of the load at the beginning of the test is noticed. The in-plane behaviour was lineal up to failure at 236.7kN when the top of the wall had descended 5.9mm.

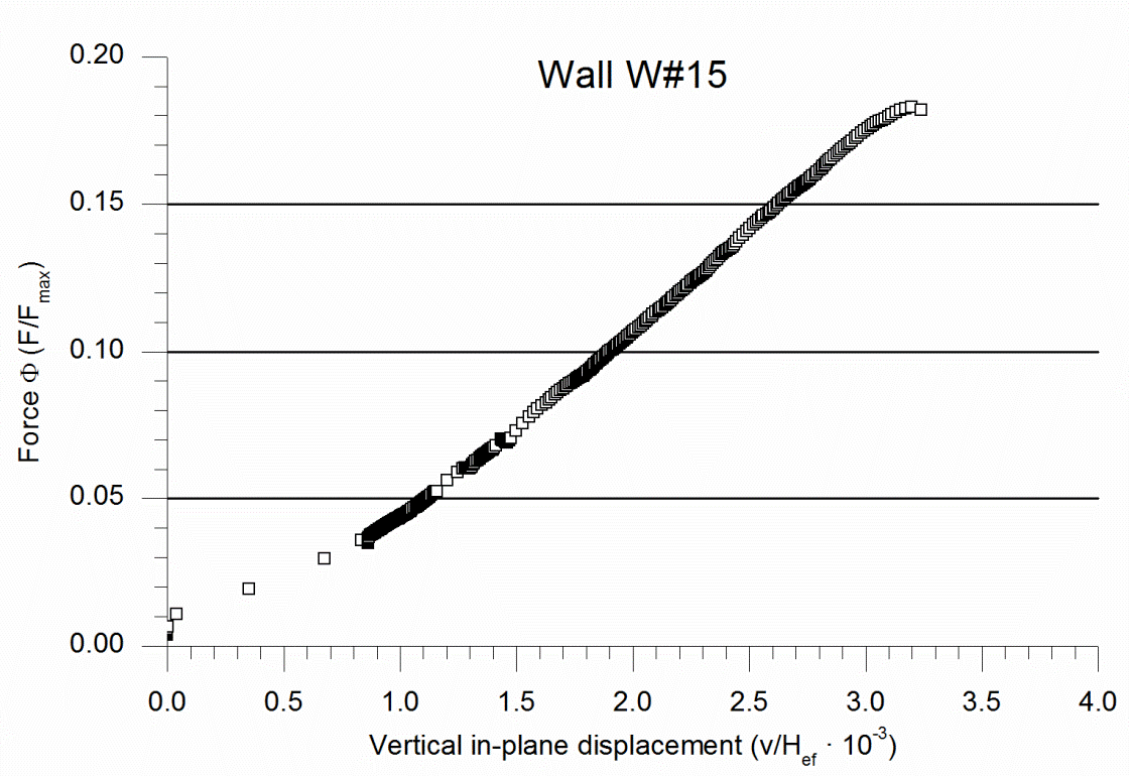

Figure A1. 167 Vertical in-plane response of wall W#15

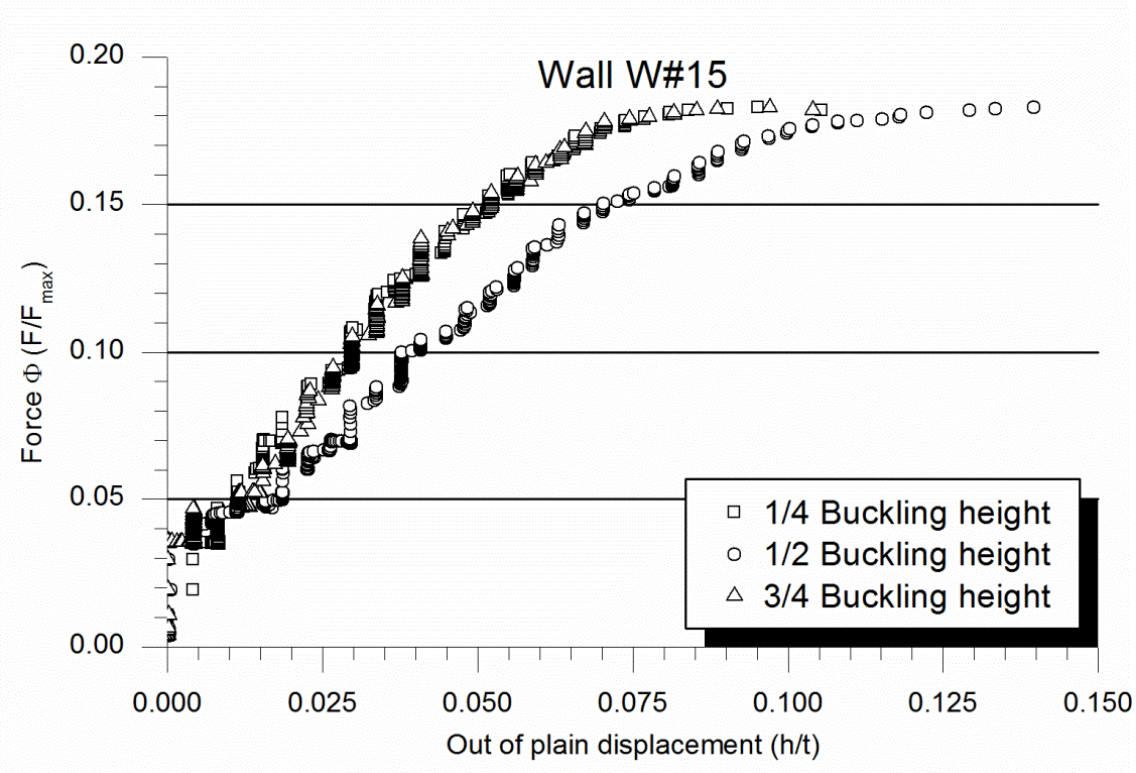

Figure A1. 168 Out-of-plane response of wall W#15

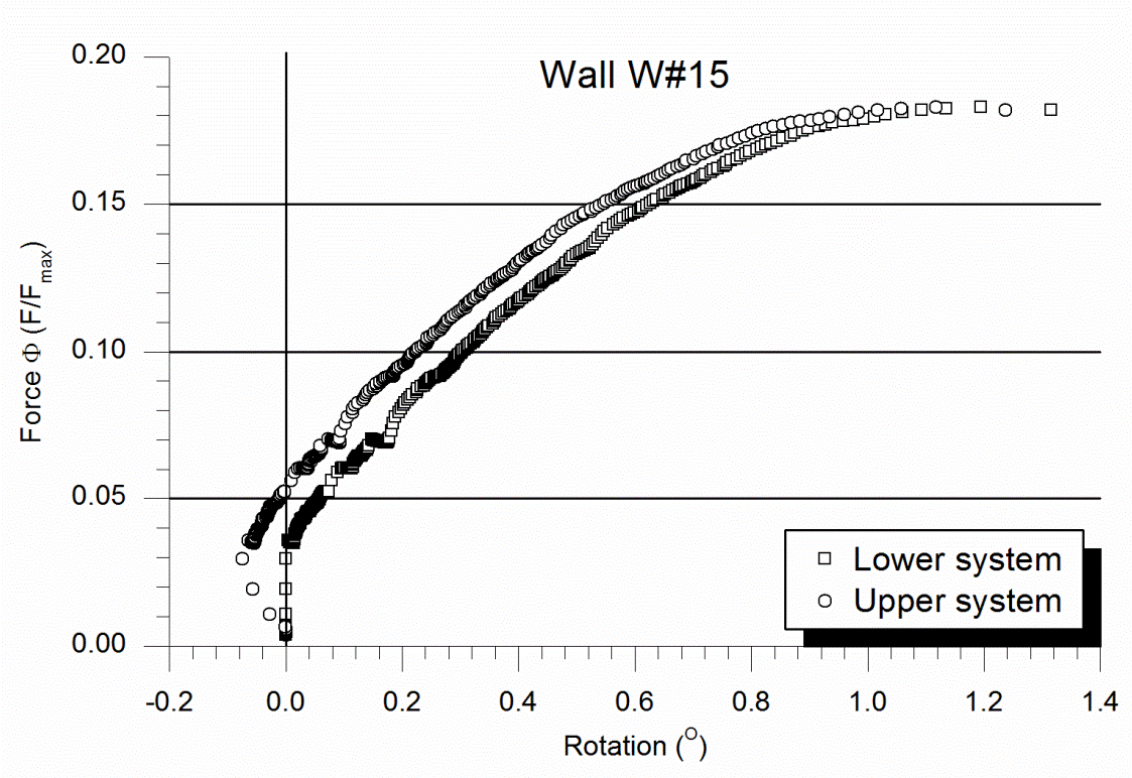

Figure A1. 169 Rotation at wall's endings for wall W#15

Figure A1. 170 Failure of the wall W#15. Opening of a horizontal joint at mid-height.

The out-of-plane response is clearly symmetric with the same deformation at ¼ and ¾ of the effective height and a bigger deformation always at mid-height. Although the behaviour was lineal during the test, near the collapse point the out-of-plane displacement grew faster up to 18.7mm for the maximum load.

Regarding the rotation of the supporting systems it was observed that similarly to the previous tests, the upper hinge rotated to the opposite direction of the expected one at the very first beginning of the test but after that, both hinges rotated with the same rate and the same direction most of the duration of the test. The rotation at the failure point was more or less the same for both hinges. It indicates a symmetric response which agreed with the observed failure mode associated with the tensile failure of a horizontal mortar joint placed at mid-height (see Figure A1. 170).

It has to be noticed that the distribution beam moved 2.5mm in the out-of-plane direction during the test which was far more than the previous tests for which the movement was insignificant.

Wall W#16

Like the previous two walls, for wall W#16, the vertical straightness is proved at observing the eccentricity at extremes practically coincided with the real eccentricity at mid-height. In addition, to place the wall in position respecting the hinges alignment, just a little (by comparing with previous tests) initial rotation of the hinges was necessary. However, this test had the particularity of having a negative hinge's alignment (see Table A1. 41) what means that the upper hinge was horizontally displaced to the opposite direction of the out-of-plane bending displacement respect with the lower hinge.

Wall W#16 geometry	
Masonry rows	27
Width	0.894m
Thickness	0.134m
Height between hinges	1.864m
Theoretical eccentricity	20mm
Initial rotation lower hinge	-0.43°
Initial rotation upper hinge	-0.29°
Hinges alignment	-3mm
Real mid-height eccentricity	19.52mm

Table A1. 41 Geometry of wall W#16

The force vs. in-plane descending deformation of the distribution beam (Figure A1. 171) shows a similar behaviour to walls W#10, W#11, W#12 and W#14 with a clear settling initial stage followed by a linear response which changed due to a softening of the structure near the maximum load (408.2kN) when the descending deformation of the top of the wall was 8.5mm.

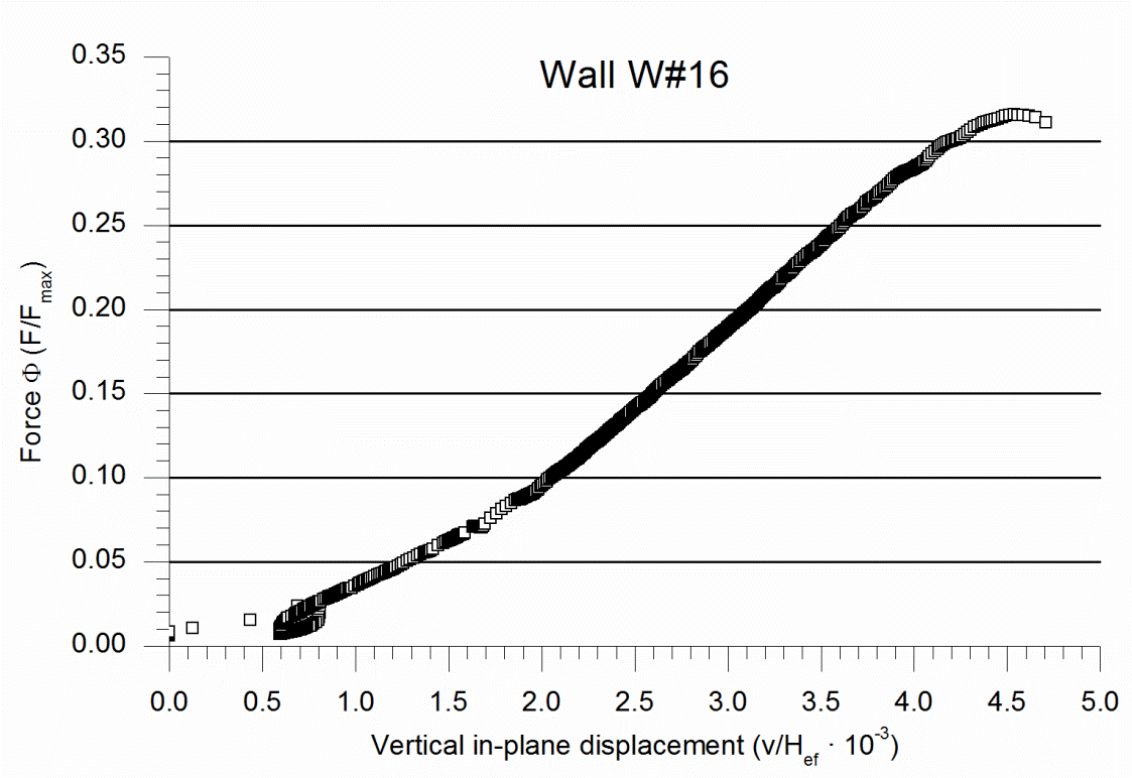

Figure A1. 171 Vertical in-plane response of wall W#16

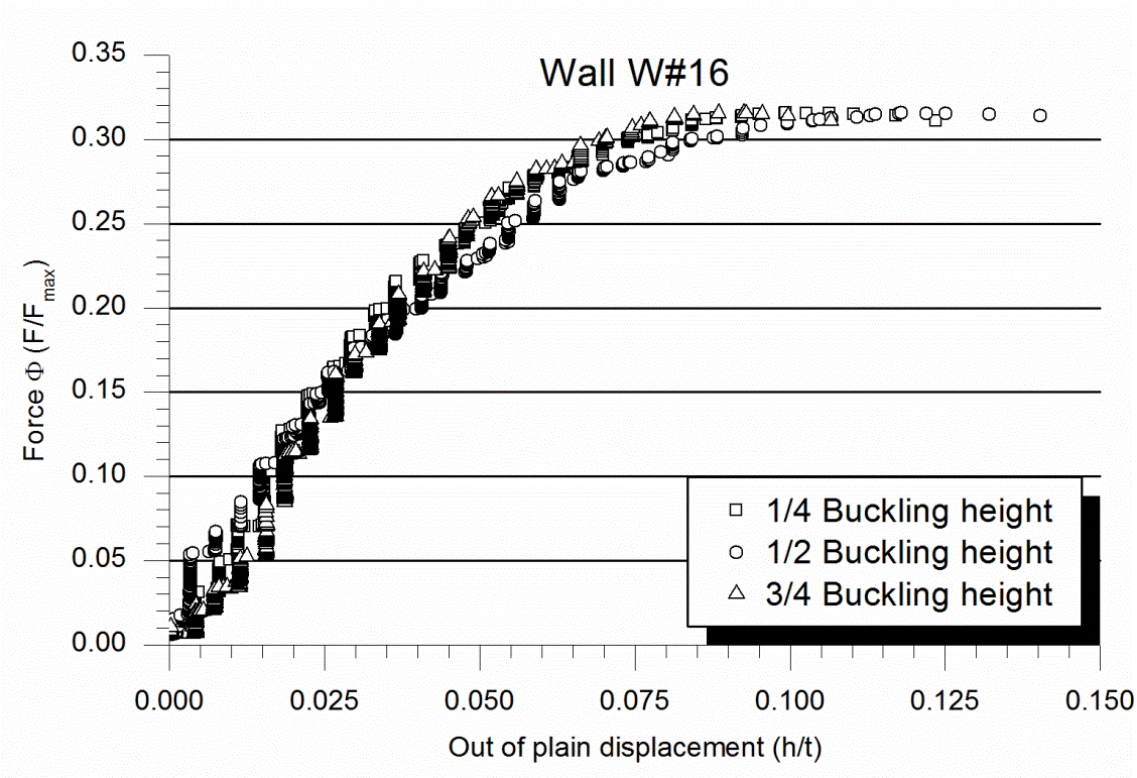

Figure A1. 172 Out-of-plane response of wall W#16

Observing the out-of-plane response (Figure A1. 172), it is noticed that the three measured points (at ¼, ½ and ¾ of the effective height) deformed almost the same during the test although from the 60% of the maximum load the mid-height displacement was slightly higher. It reached 15.8mm at the collapse point.

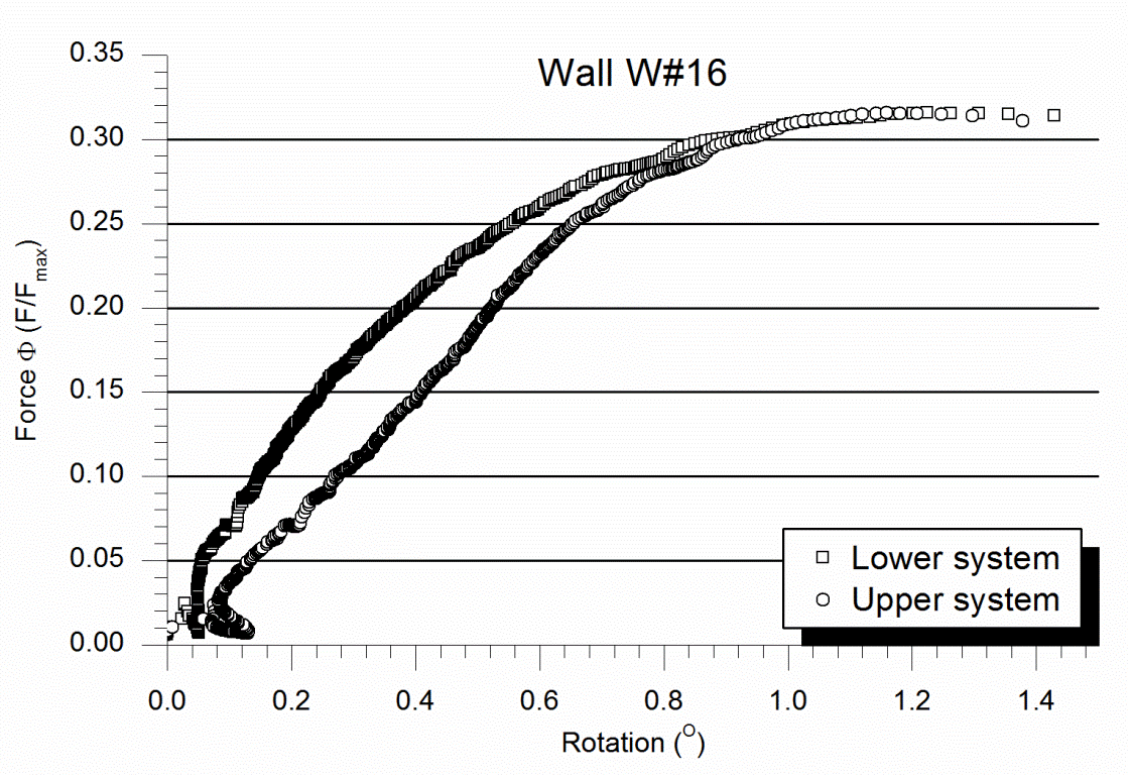

Figure A1. 173 Rotation at wall's endings for wall W#16

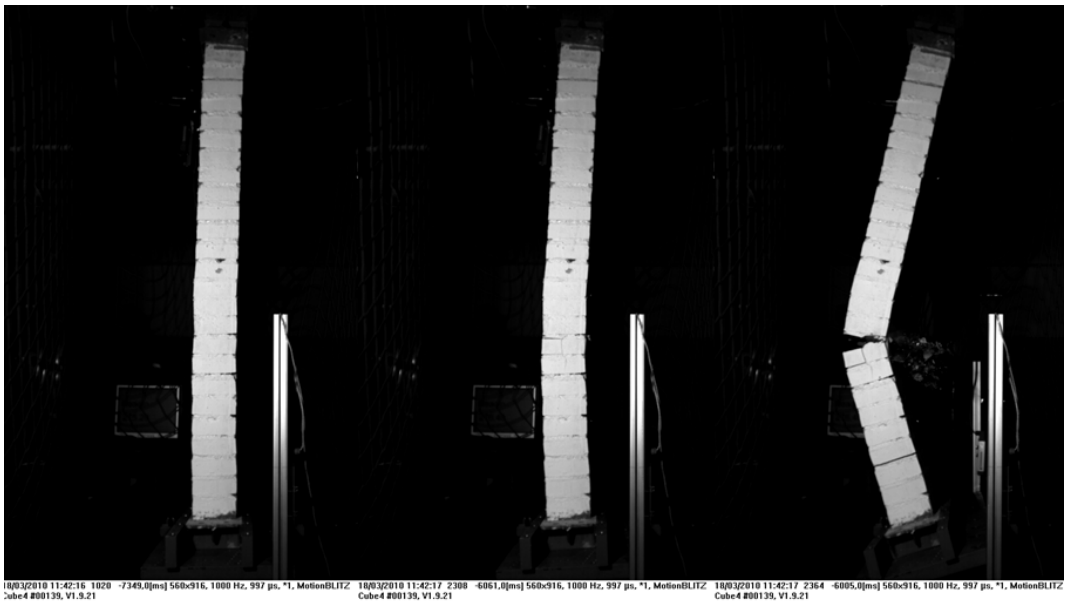

Figure A1. 174 Failure of the wall W#16. Opening of a horizontal joint at 1/3 of the height.

In contrast with previous tests, both hinges of the test of wall W#16 rotated in the expected direction from the beginning. However, a discontinuity may be observed in the early response of the upper system (see Figure A1. 173) which finally rotated at a constant rate whilst the lower hinge moved with an increasing speed. Close to the failure both hinges had the same rotation proving a symmetric response of the structure.

The failure mode was asymmetric (see Figure A1. 174) although the previous evidences in the response during the test. Material and construction heterogeneities may explain this collapse shape. Little compression crushing was also observed. The failure was sudden.

Wall W#17

This wall had two wythes internally connected by transversal bricks. The measured thickness is presented in Table A1. 42. Like the previous test, both hinges were rotated in the opposite direction of the associated with the expected bending. However, the hinges alignment was difficult and the upper rotation centre was 12mm more to the out-of-plane bending direction than the lower hinge at the beginning of the test. This agreed with the poor vertical straightness proved comparing the eccentricity at endings (80mm) with the mid-height real eccentricity (88mm). Initial cracks in the joints (vertical and horizontal) were observed before the test.

Wall W#17 geometry	
Masonry rows	28
Width	0.894m
Thickness	0.282m
Height between hinges	1.905m
Theoretical eccentricity	80mm
Initial rotation lower hinge	-0.43°
Initial rotation upper hinge	-1.00°
Hinges alignment	12mm
Real mid-height eccentricity	88mm

Table A1. 42 Geometry of wall W#17

Vertical in-plane response (Figure A1. 175) followed the same behaviour than previous tests with an initial settling, a final softening and a large linear response during most of the test. In this case, the descending displacement for the maximum load (491.1kN) was 9.2mm.

The out-of-plane response (Figure A1. 176) at the beginning of the test was characterised with the displacement of the points placed at ¼ and ½ of the effective height to the opposite direction of the bending deformation according with the fixed eccentricity. This tendency changed most of the experiment and all measured points displaced to the expected direction. However, the mid-height out-of-plane displacement was not the biggest one until higher loads closer to the collapse. The value at maximum

load was 16.8mm. All test long, deformation at ¼ of the height was always bigger than at ¾ which indicated an asymmetric response.

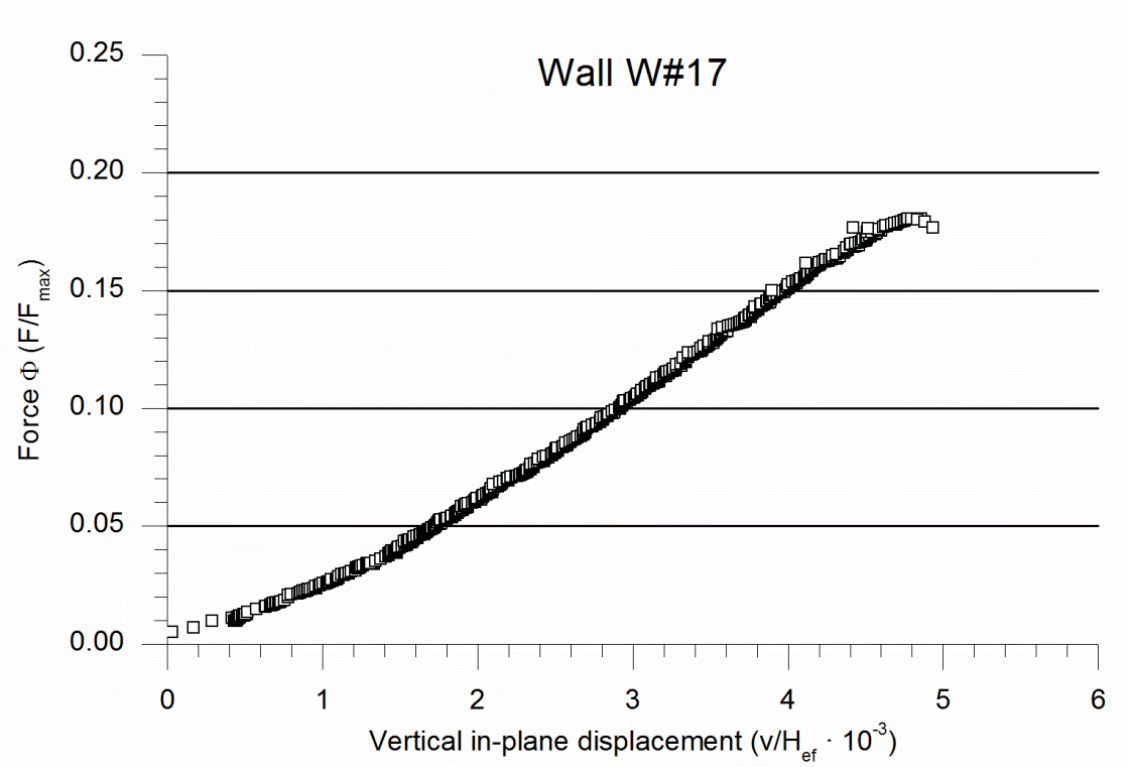

Figure A1. 175 Vertical in-plane response of wall W#17

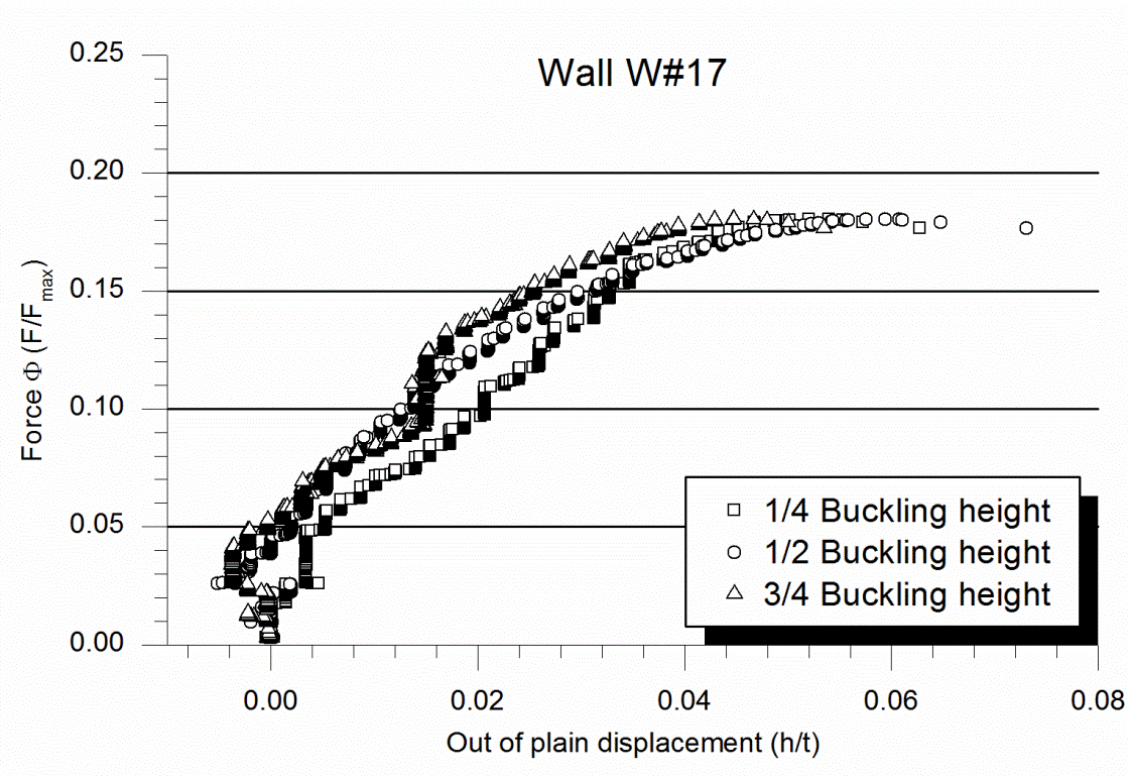

Figure A1. 176 Out-of-plane response of wall W#17

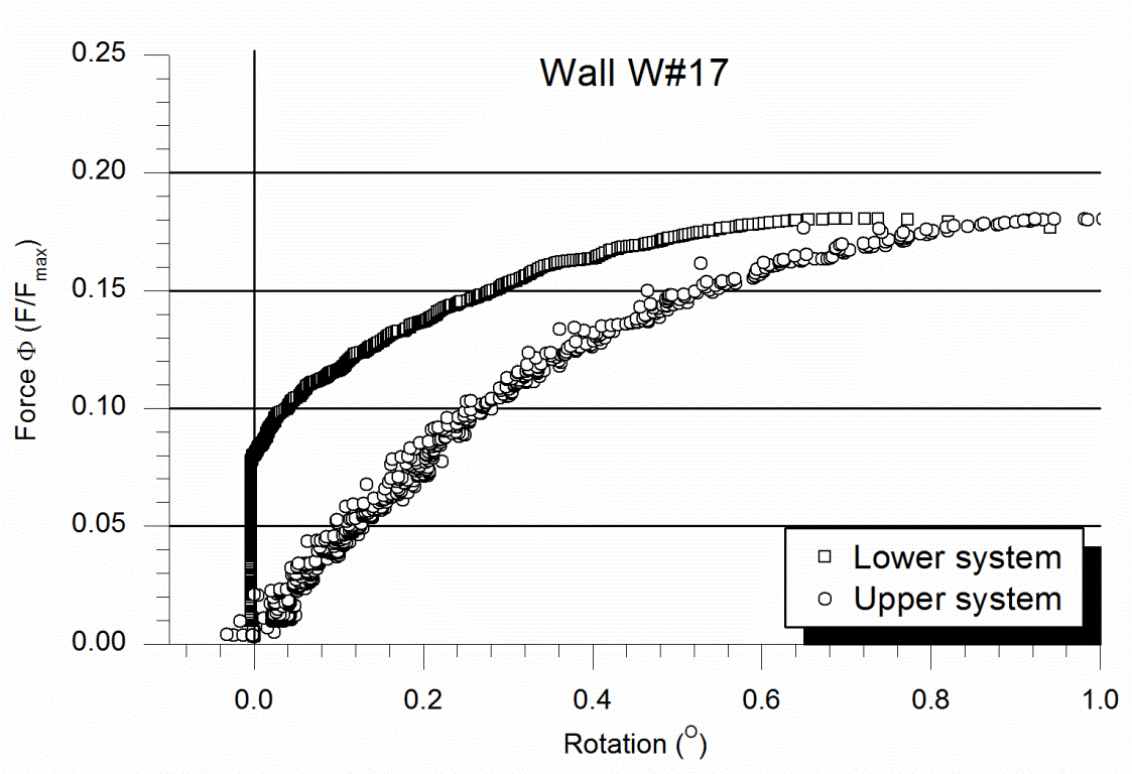

Figure A1. 177 Rotation at wall's endings for wall W#17

Figure A1. 178 Failure mode of wall W#17. Beginning with tensile cracking and final masonry crushing.

The behaviour of the supporting systems recovered particularities observed in the first tests of M series (walls W#10, W#11 and W#12). It was characterised (see Figure A1. 177) by the upper system rotating while the lower hinge remained still up to approximately half the maximum load. When moving, the two hinges showed and increasing rotation speed.

Finally, the wall collapsed combing a masonry crushing in the compression side and the buckling (geometric instability) associated with a second order bending which caused the opening of a horizontal joint in the tensile side of the wall. According with having always a greater out-of-plane displacement at the lower part of the wall W#17, the collapse associated damage appeared at the lower part of the structure as shown in Figure A1. 178.

Wall W#18

Wall W#18 was the first of the three which belonged to S series. The effective height was approximately 1.2m (see Table A1. 43). Rotation of the two supporting systems was necessary to achieve a good hinge's alignment. The wall was straight with constant eccentricity along the height (less than 1mm difference between the extreme eccentricity and the eccentricity at mid-height).

Wall W#18 geometry	
Masonry rows	16
Width	0.871m
Thickness	0.134m
Height between hinges	1.197m
Theoretical eccentricity	20mm
Initial rotation lower hinge	0.72°
Initial rotation upper hinge	1.00°
Hinges alignment	3mm
Real mid-height eccentricity	20.8mm

Table A1. 43 Geometry of wall W#18

In plane behaviour was similar to some previous tests on walls of series H and S (Figure A1. 179). There was an initial settling stage under 10% of the maximum load (803.4kN) followed with a linear response which finished with a material softening. The main difference with previous test was the material relaxation part covered almost the last 30% of the loading process whilst it was just a final little portion for previous tests of other series. It may indicate the increasing importance of the compressive response of masonry for tests on walls which bore bigger loads. The descending displacement of the distribution beam was 6.4mm at the maximum load.

The out-of-plane behaviour (Figure A1. 180) showed a response which is typically associated with a turn over process. The out-of-plane deformation at ¾ of the height was bigger than the same movement at mid-height. The out-of plane deformation at ¼ of the effective height was the littlest. In fact, up to 60% of the maximum load, the wall deformed in the opposite direction of the typically associated with the bending caused by the fixation of the eccentricity at wall's endings. The displacement at ¾ of the height was almost constant all test and only increased when the applied load was close to the maximum. The mid-height deformation reached positive values (according with the induced second order bending) only near the collapse. It deformed 3.4mm with the maximum load applied.

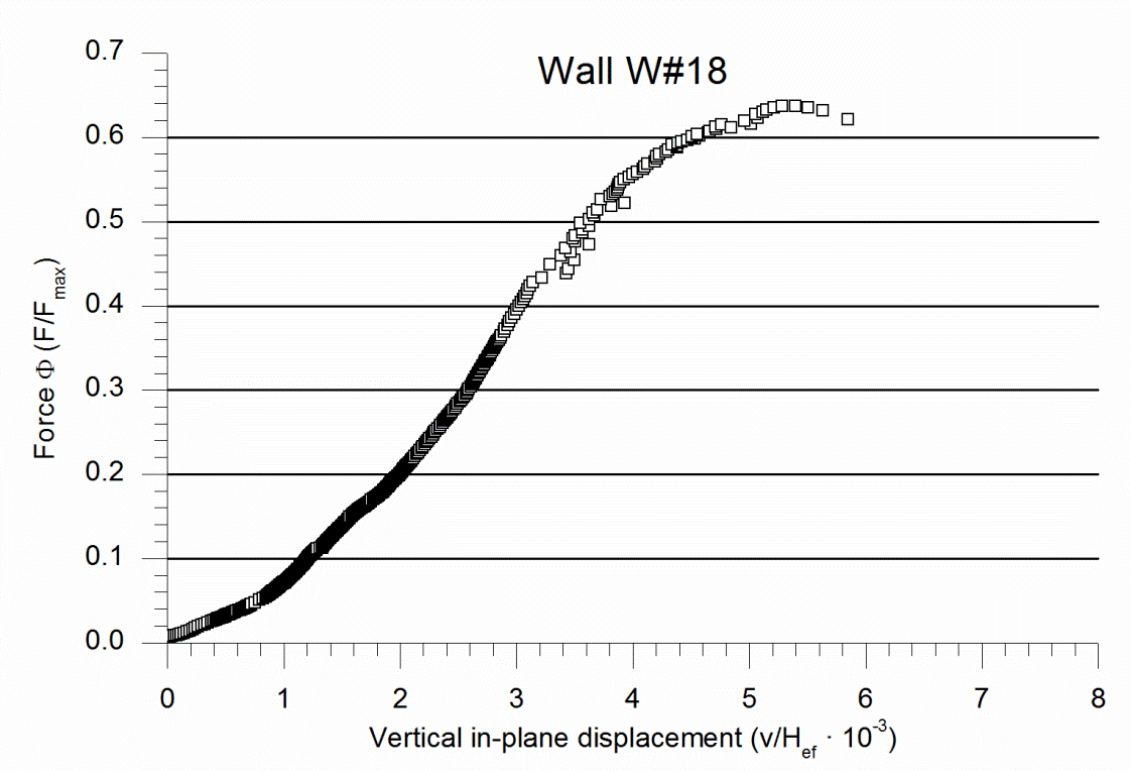

Figure A1. 179 Vertical in-plane response of wall W#18

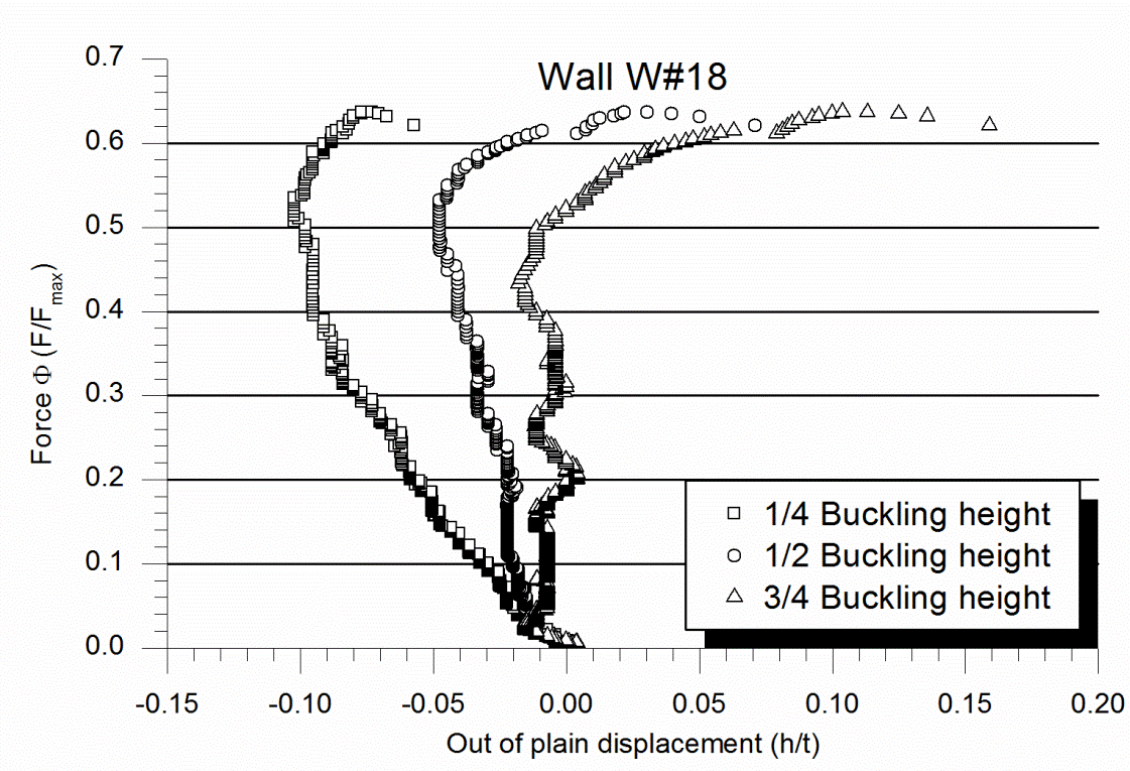

Figure A1. 180 Out-of-plane response of wall W#18

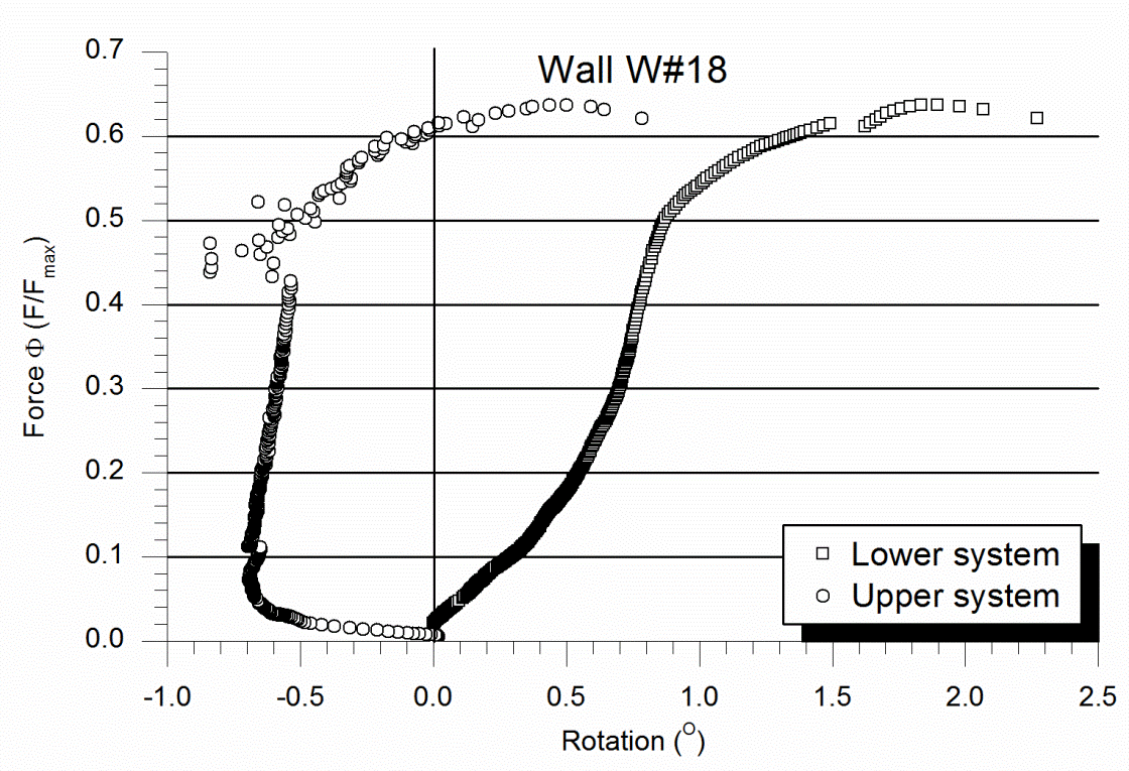

Figure A1. 181 Rotation at wall's endings for wall W#18

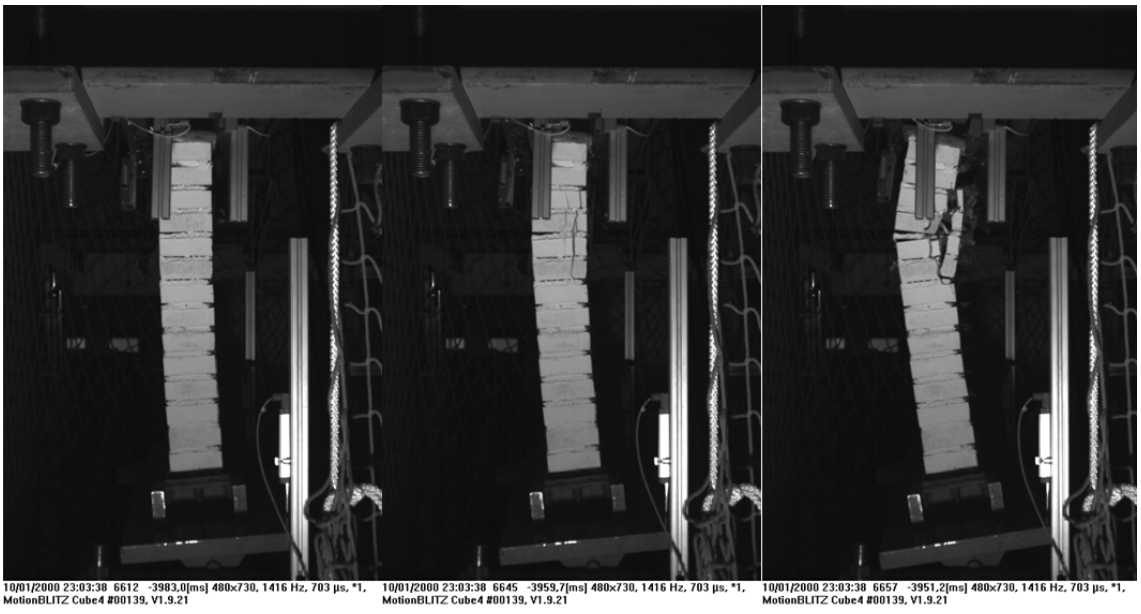

Figure A1. 182 Failure of the wall W#18. Crushing of the masonry near the wall's top.

The upper supporting system rotated opposite to the bending associated direction at the beginning of the test. After this, the rotation followed the expected direction at a constant speed. Near the collapse both hinges experienced a clear increase of the rotation velocity. The lower hinge showed a more continuous

response during the test, always in the same direction and changing only the rotation speed according with the same pattern showed by the upper supporting system. See Figure A1. 181.

The failure mode (Figure A1. 182) was characterised by crushing the masonry. The opening of the horizontal joint seems a consequence of the collapse. The asymmetric failure shape agrees with the previously mentioned asymmetric out-of-plane response.

Wall W#19

To place wall W#19 in its testing position the hinges were rotated in the direction associated with the expected second order bending (Table A1. 44). The upper hinge had a noticeable rotation in comparison with all previous tests and contrasting with the lower hinge. However, the wall's vertical straightness is showed observing the perfect alignment of the hinges rotation centres and noticing the real eccentricity at mid-height was almost the same than the theoretical eccentricity applied at both endings of the wall.

Wall W#19 geometry	
Masonry rows	17
Width	0.871m
Thickness	0.133m
Height between hinges	1.220m
Theoretical eccentricity	30mm
Initial rotation lower hinge	0.57°
Initial rotation upper hinge	2.00°
Hinges alignment	0mm
Real mid-height eccentricity	30.28mm

Table A1. 44 Geometry of wall W#19

The in-plane vertical deformation of the wall W#19 (Figure A1. 183) showed a similar response to wall W#18 except for the fact that the relaxation associated with the material failure appeared only in the very last loading steps. It might be caused by having a littler load applied because of the larger eccentricity. The distribution beam had descended 10.6mm at the collapse load (686.1kN).

As happened with wall W#18, the out-of-plane response (Figure A1. 184) corresponded with a turn over movement. During the test, the mid-height sensor registered no movement whilst the one placed at ¾ of the height displaced to the direction associated with the expected bending. The lower measured point (¼ of the effective height) displaced to the opposite direction. Only near the collapse all the wall moved to the out-of-plane direction associated with the second order bending. The mid-height out-of-plane deformation corresponding to the maximum load was 5.5mm.

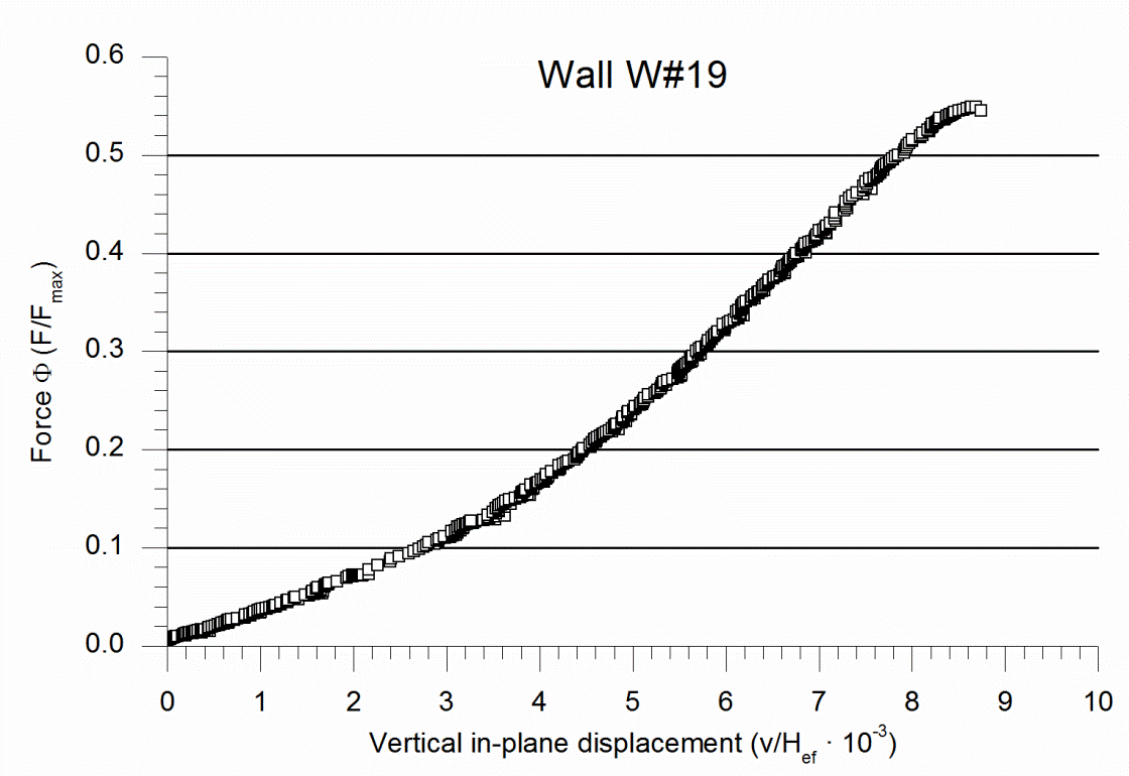

Figure A1. 183 Vertical in-plane response of wall W#19

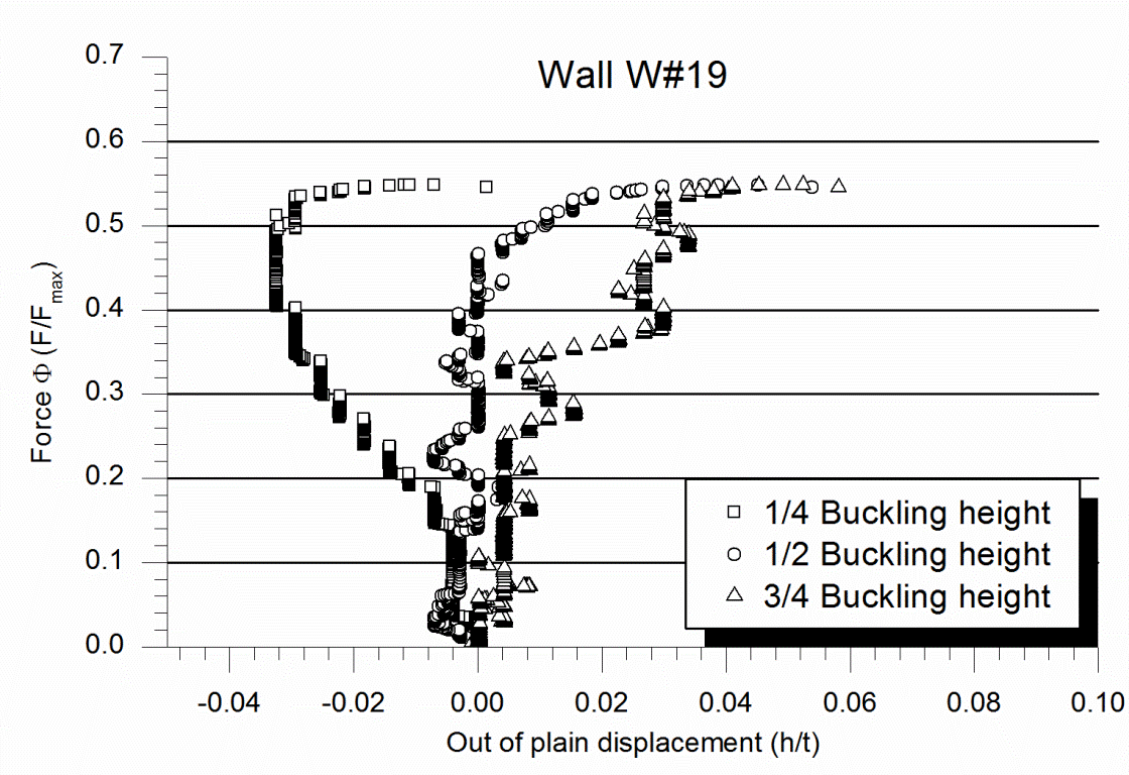

Figure A1. 184 Out-of-plane response of wall W#19

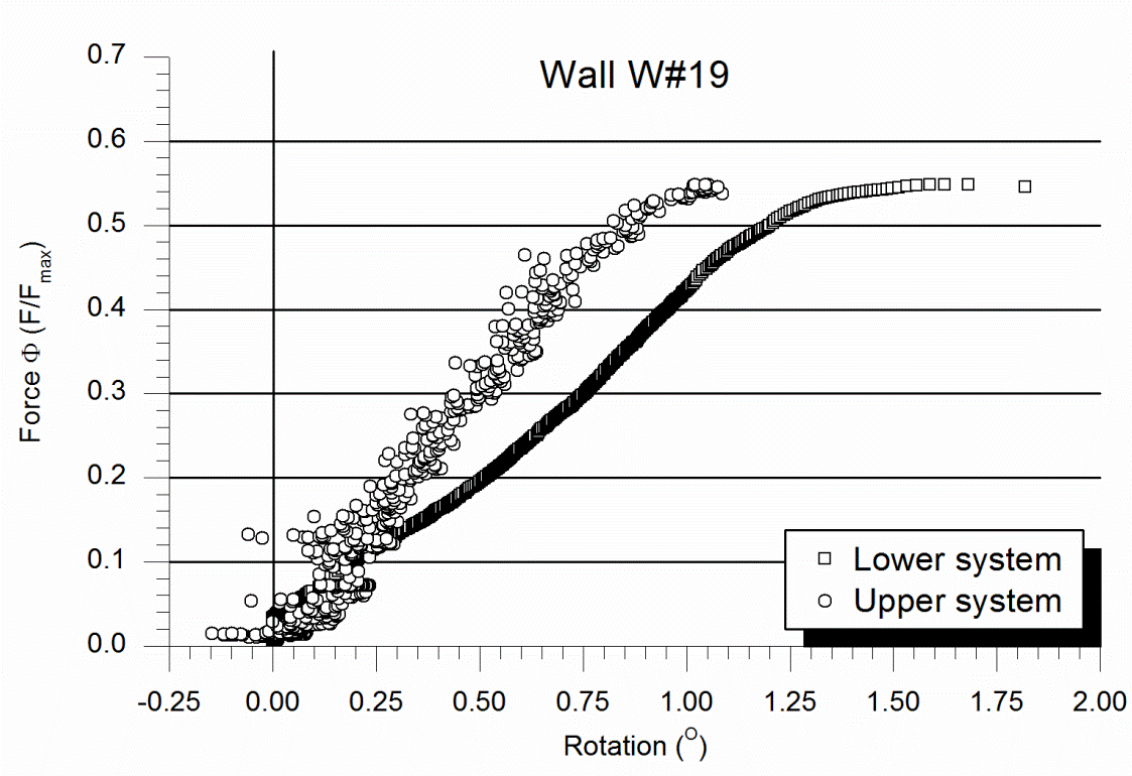

Figure A1. 185 Rotation at wall's endings for wall W#19

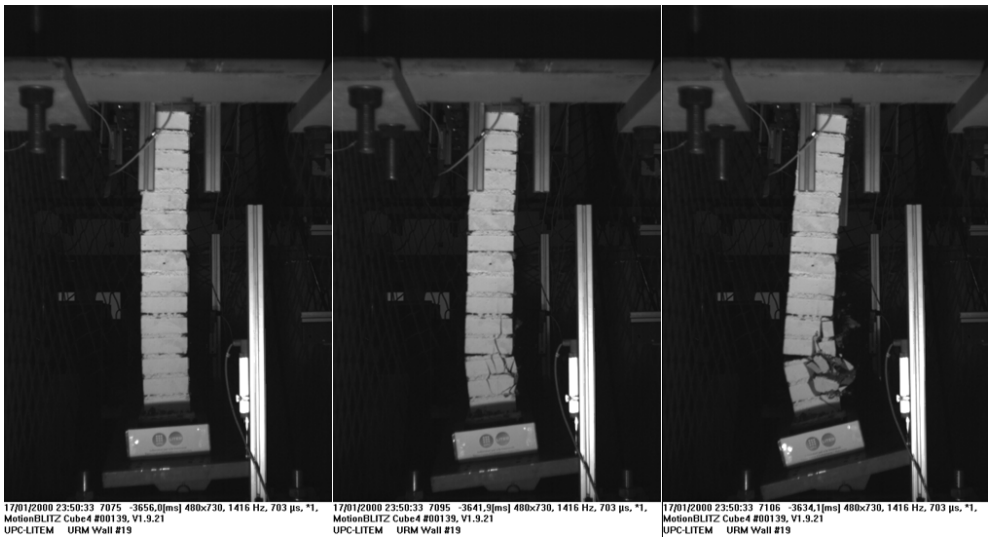

Figure A1. 186 Failure of wall W#19. Masonry crushing at the lower part.

The supporting systems' rotation (Figure A1. 185) was similar to the observed with W#17. Both endings of the wall rotated in the direction of the second order bending from the very first beginning of the test. Although the upper system was more instable in the lectures, the response of both extremes was analogue with a constant rotation velocity up to reaching load closer to the collapse.

Finally, the failure mode (Figure A1. 186) was a combination of a material crushing in the compression side with a tensile failure associated with the opening of a horizontal joint and caused by the second order bending. The asymmetry of the measured values is reflected in the asymmetric collapse pattern.

Wall W#20

The last unreinforced masonry wall, W#20, was placed at testing position by rotating the hinges in the direction they were expected to rotate according with the initial eccentricity. However a perfect hinge's alignment was not possible. This wall had bigger geometric imperfections than the other two of the S series (W#18 and W#19). It is noticed (Table A1. 45) that the eccentricity at wall's extremes (40mm) was different from the mid-height real eccentricity (33mm) indicating a poor initial straightness.

Wall W#20 geometry	
Masonry rows	17
Width	0.868m
Thickness	0.133m
Height between hinges	1.220m
Theoretical eccentricity	40mm
Initial rotation lower hinge	0.93°
Initial rotation upper hinge	0.57°
Hinges alignment	3mm
Real mid-height eccentricity	33mm

Table A1. 45 Geometry of wall W#20

The in-plane response (Figure A1. 187) was linear up to failure. No softening effects associated with material non-linearity were observed in contrast with the two previous tests of the same series. The in-plane displacement at maximum load (152.6kN) was 5.3mm. In the same way, the out-of-plane behaviour (Figure A1. 188) was also different from tests W#18 and W#19. In the case of W#20, the three measured points (at ¼, ½ and ¾ of the effective height) moved in the direction associated with the second order bending (bigger effect because of the bigger initial eccentricity). Values recorded at ¼ of the height were always littler than at the other two points. Values at mid-height and ¾ of the height were almost the same what indicates an asymmetric response. The mid-height out-of-plane displacement at the maximum load time was 9.2mm.

Regarding the rotation of the supporting systems (Figure A1. 189), behaviour similar to that observed in test on wall W#3 was detected. Whilst the lower hinge rotated with an increasing speed, the upper system showed a fast initial rotation followed by a constant rotation rate up to failure.

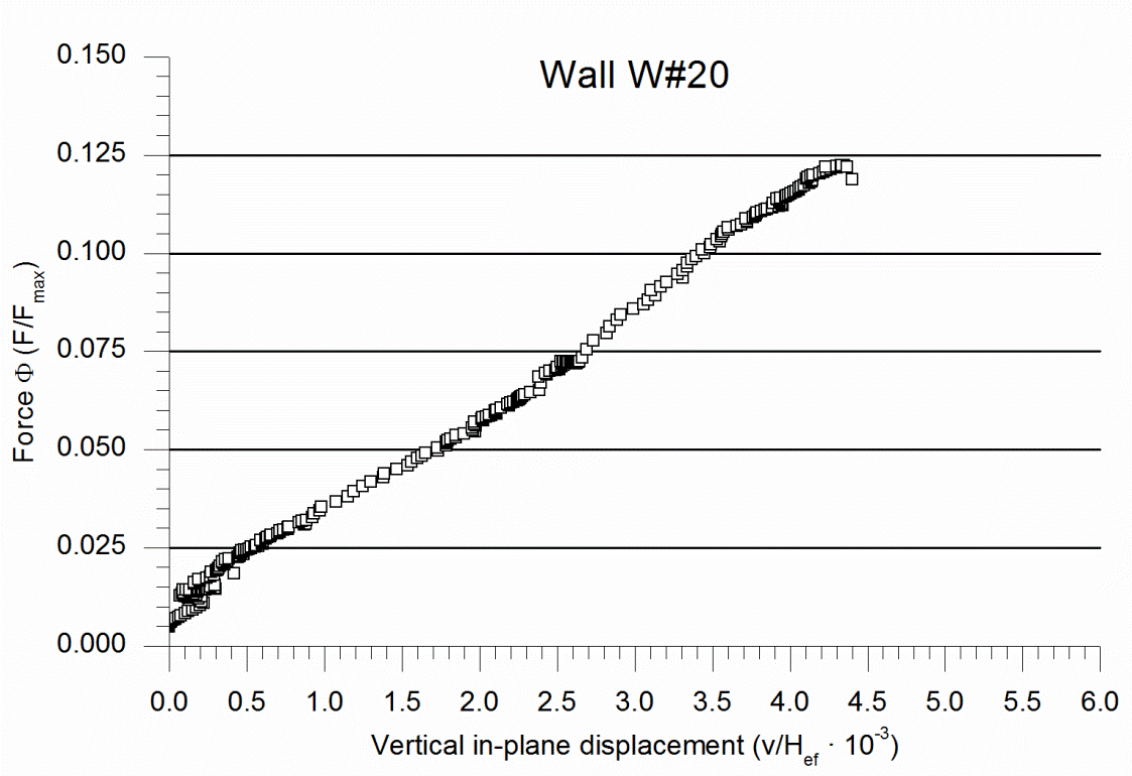

Figure A1. 187 Vertical in-plane response of wall W#20

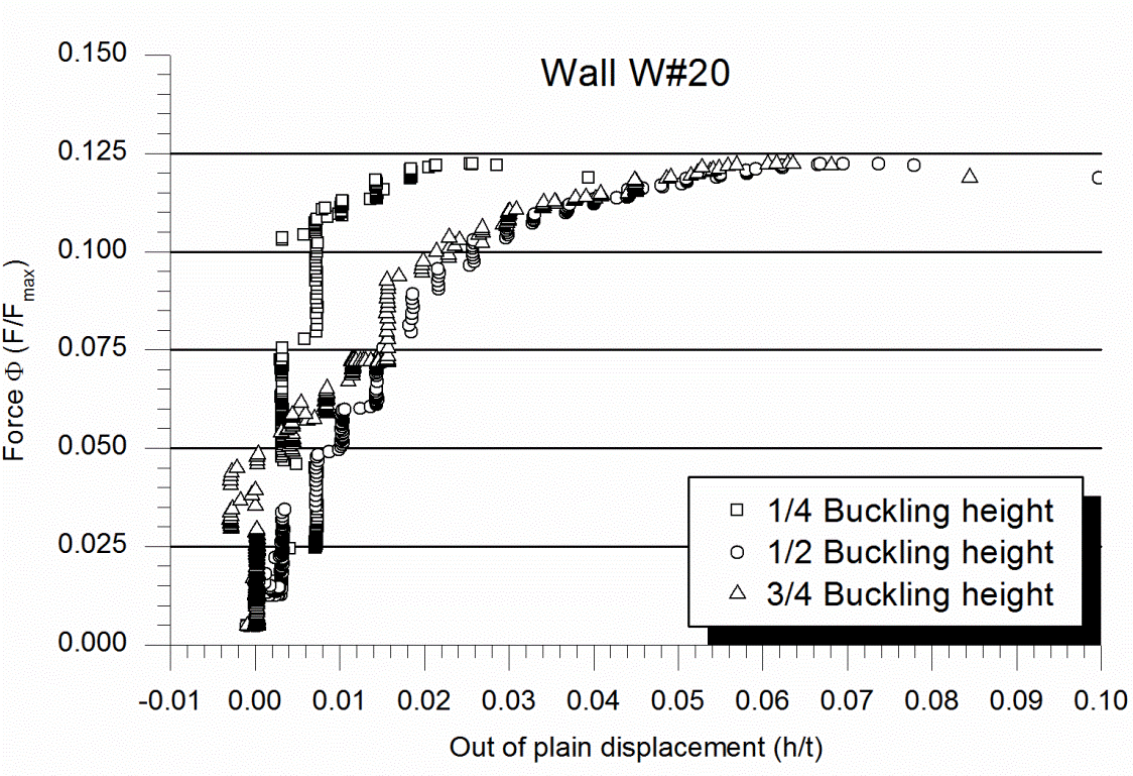

Figure A1. 188 Out-of-plane response of wall W#20

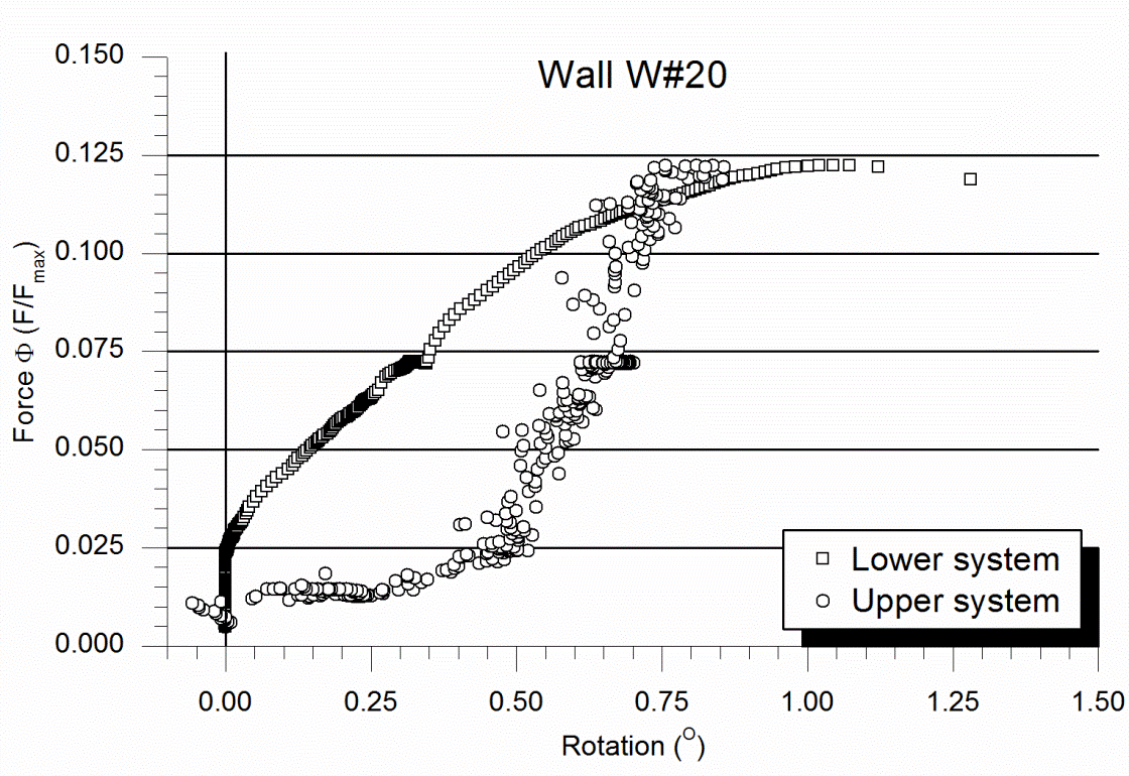

Figure A1. 189 Rotation at wall's endings for wall W#20

The failure mode of wall W#20 was different from walls W#18 and W#19. A horizontal joint near the mid-height position opened due to buckling process and no crushing of the material was observed (see Figure A1. 190). The asymmetric behaviour was slightly present at the failure shape as the crack appeared little over the mid-height.

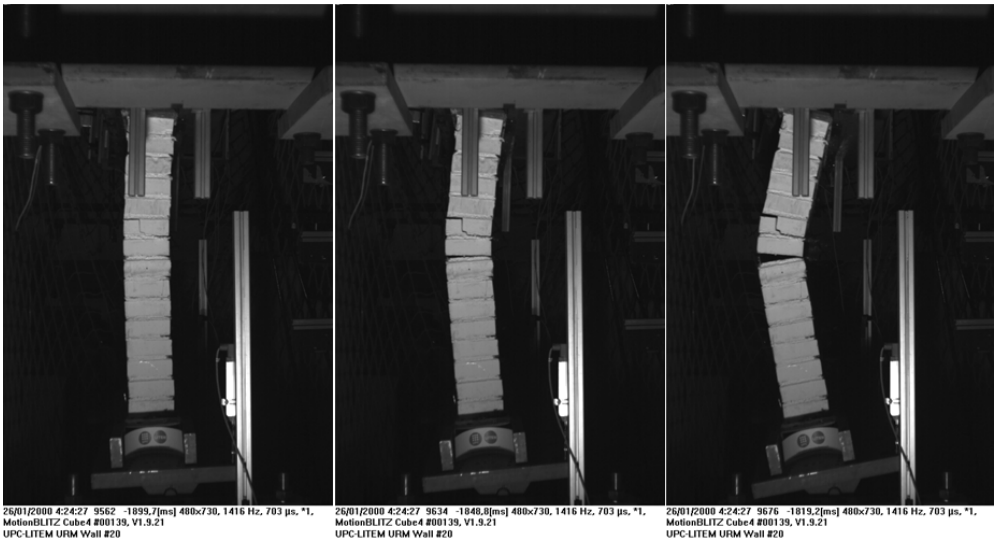

Figure A1. 190 Failure of the wall W#20. Opening of a crack near the mid-height.

A1.6.5.2 Results of TRM strengthened walls

The same data shown in previous section is now presented for the tests corresponding with the strengthened walls.

Wall W#21

Wall W#21 was strengthened with one layer of MapeGrid G220 embedded into a Planitop HDM Maxi mortar layer. The thickness of the TRM system measured on the residues corresponding to the section at mid-height is presented in Table A1. 46. This chart also summarises the main geometric characteristics of the wall W#21. It may be observed that the fibre grid was placed at 10mm from the masonry surface what is more than the expected gap according with the manufacturer's recommendations. It is also worth noticing that rotating the hinges a perfect alignment of them was achieved although the initial rotation of the upper hinge was significant. Moreover, it might be observed that the lateral levelling of the wall was particularly good as the eccentricity at the supports and the real eccentricity at mid-height coincided.

Observing the in-plane behaviour of wall W#21, no difference with previous tests on unreinforced masonry walls may be observed (see Figure A1. 191). This agrees with the fact that the mode of failure was the same than most of the tests on unreinforced walls: second order bending and buckling failure. There is an initial settling stage followed by a more or less linear response which finalises with a softening near the collapse of the wall. The descending displacement of the distribution beam at maximum load (299.7kN) was 7.9mm.

Wall W#21 geometry	
Masonry rows	26
Width	0.865m
TRM thickness	13mm
Grid position	10mm
Height between hinges	2.832m
Theoretical eccentricity	30mm
Initial rotation lower hinge	-0.36°
Initial rotation upper hinge	-2.58°
Hinges alignment	0mm
Real mid-height eccentricity	30.28mm

Table A1. 46 Geometry of wall W#21

Regarding the out-of-plane response of the wall (Figure A1. 192), a clearly asymmetric behaviour was observed for wall W#21. During the test, the out-of-plane deformation at mid-height was always the greatest, but at ¾ of the effective height there was a bigger out-of-plane displacement than at ¼ of the height. The deformation at mid-height when reaching the maximum load was 19.7mm. It is higher than the deformation observed in the previous unreinforced walls.

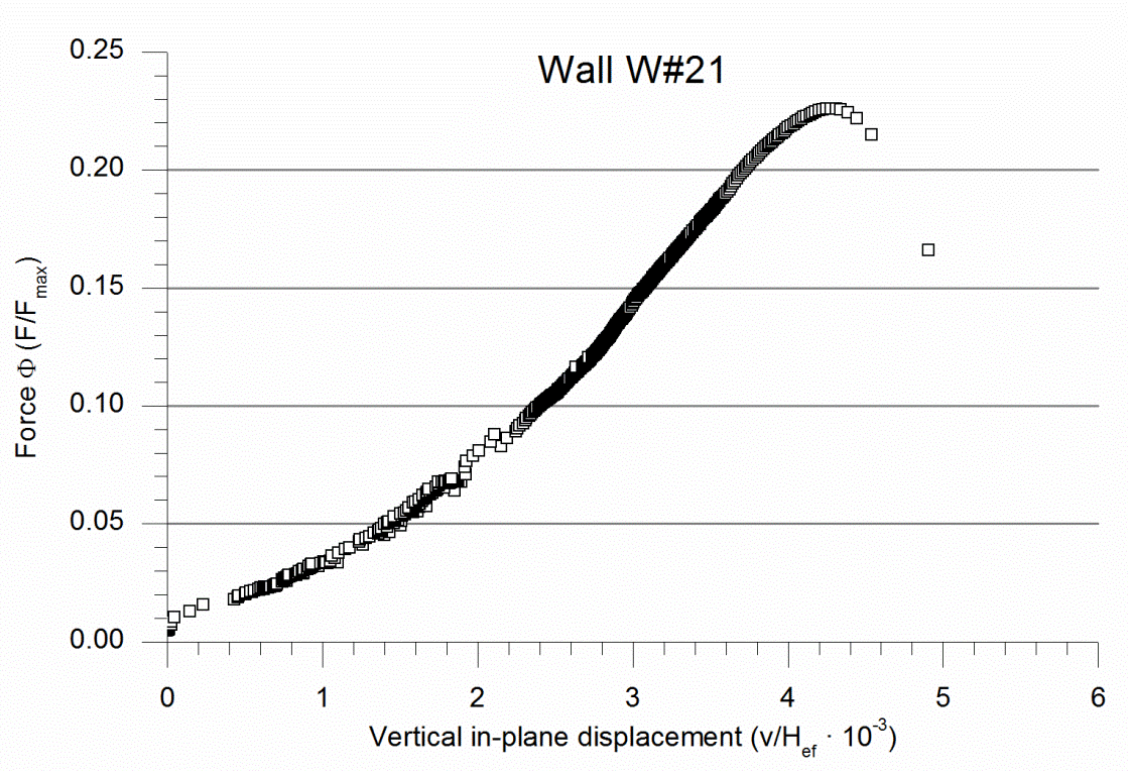

Figure A1. 191 Vertical in-plane response of wall W#21

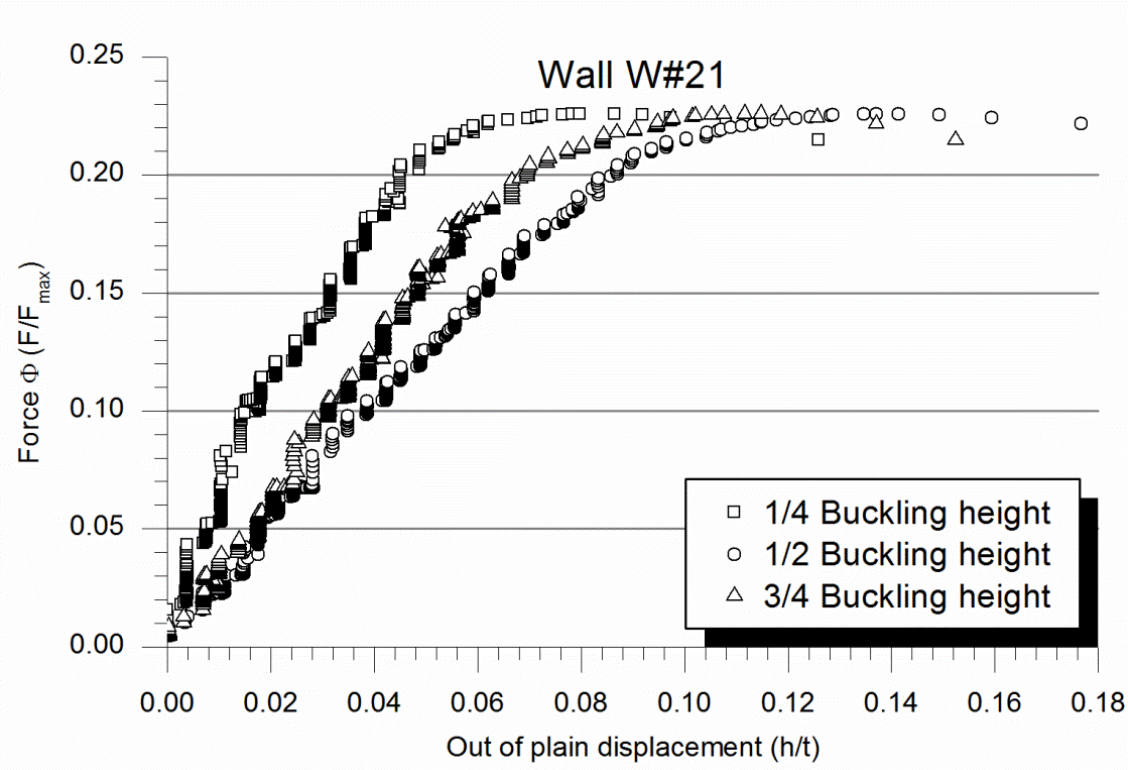

Figure A1. 192 Out-of-plane response of wall W#21

Looking at graph in Figure A1. 193, it is observed that the upper supporting system rotated faster than the lower one at the beginning of the test. The lower hinge moved at a constant speed up to load values close to the failure load and showed a continuous curve response. In contrast, the upper system behaved in an irregular way, with little oscillations up to 40% of the maximum load when the response became more stable. It is worth noticing that the two supporting system rotated in the expected direction from the beginning of the test.

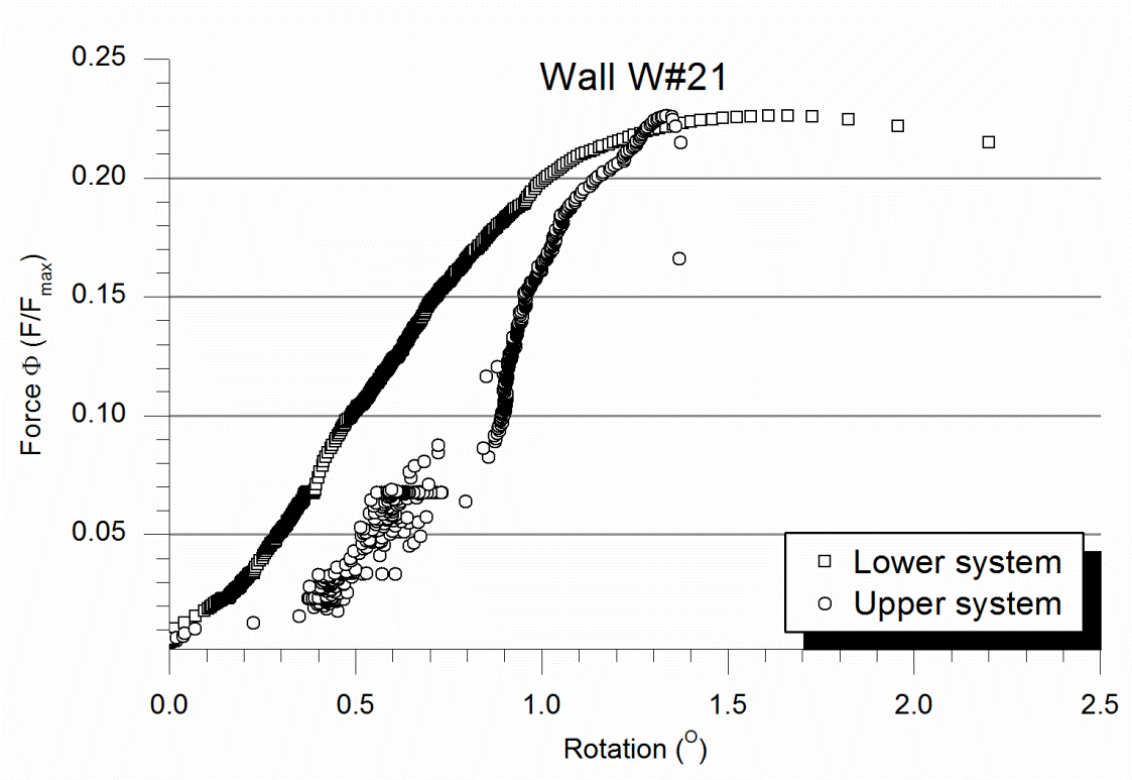

Figure A1. 193 Rotation at wall's endings for wall W#21

From the out-of-plane displacement and load values, and taking into account the horizontal reaction forces, the bending moment associated which each applied compressive load was calculated. All sections of the structure bore an axial compressive effort combined with a bending moment, so the section resistance depended on the combination of these two efforts. The maximum interaction curves (commented in Chapter 5) and the experimental axial-bending response are plotted in Figure A1. 194. The experimental response of wall W#21 clearly showed the second order bending effects as the slope of the curve is always increasing with the load growing.

Finally, the graph in Figure A1. 195 presents the strain measured in the five points detailed in section A1.6.4.6. The same asymmetric response showed by figures Figure A1. 192 and Figure A1. 193 is observed. The lower strain gage registered higher values than the upper sensor and the strain gage installed at the left side of the wall (looking in front of the strengthened face) measured larger strains than

the analogue sensor at the right side. However, the maximum strains were always measured at the centre of the wall. The strain at the central position when maximum load was applied was 0.48%.

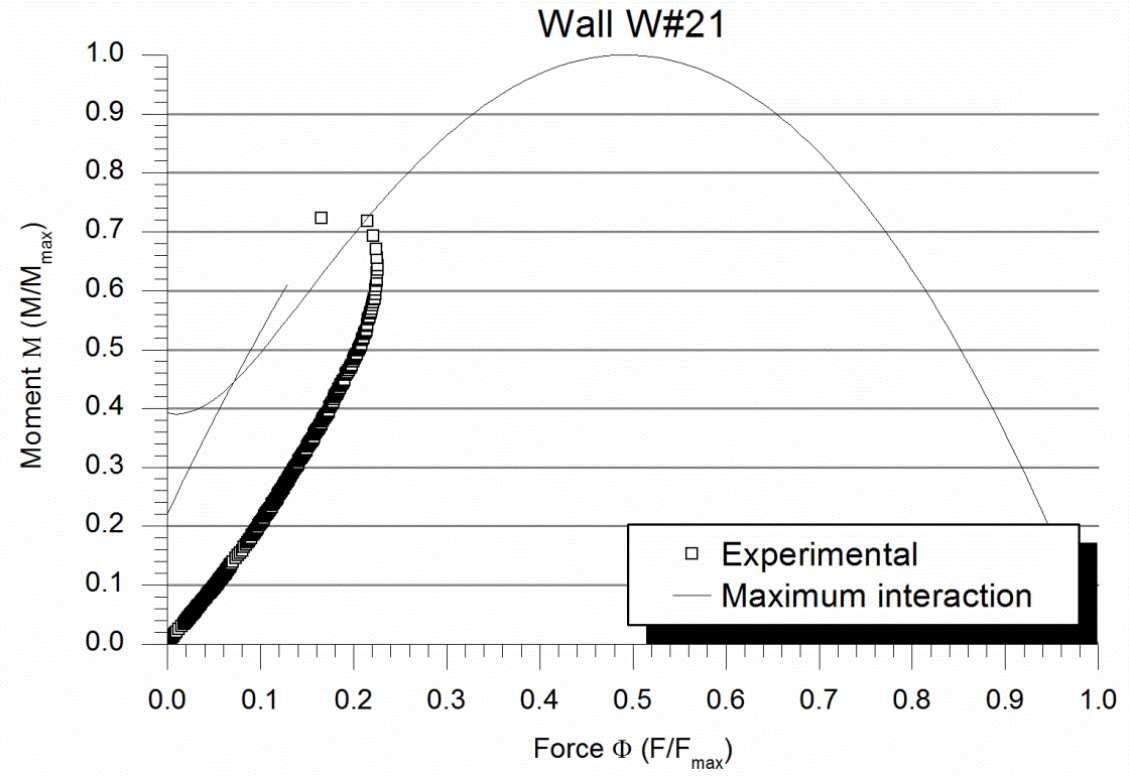

Figure A1. 194 Bending moment vs. Force response and interaction curve for wall W#21

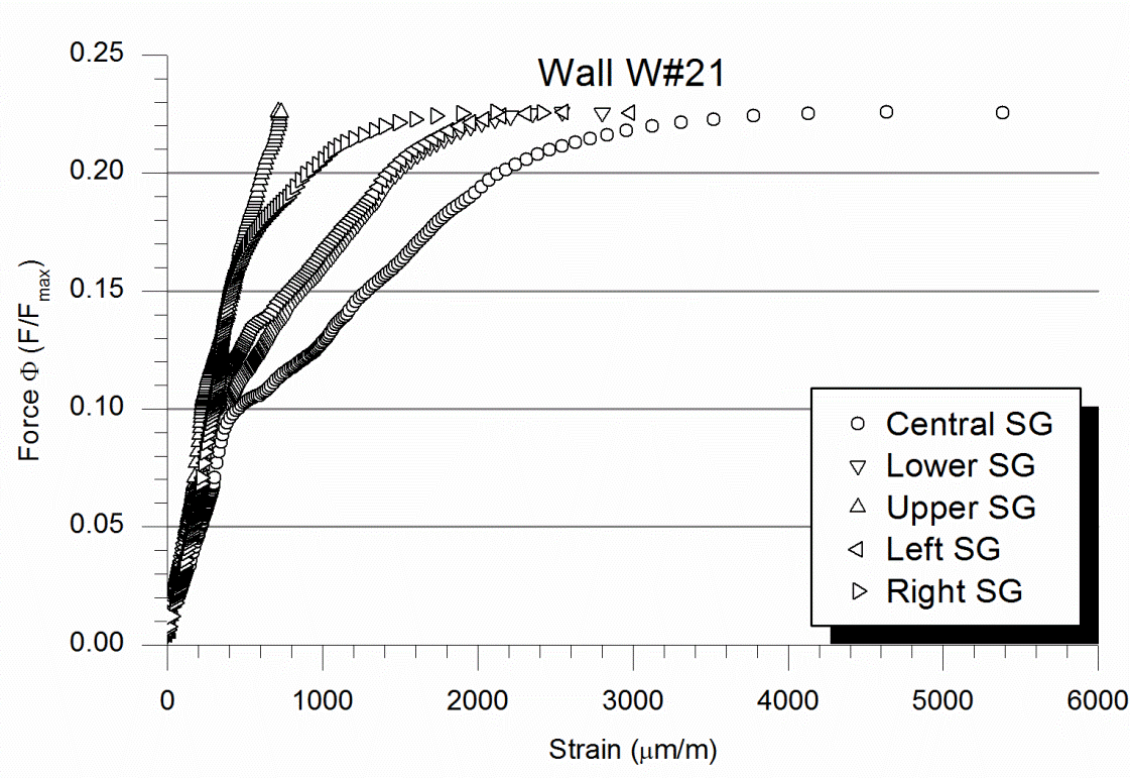

Figure A1. 195 Strains measured on the TRM for wall W#21

Observing Figure A1. 196, the significant out-of-plane deformation of the wall before appearing any visible damage 8second picture) might be noticed. The failure mode was associated with the tensile rupture of the TRM strengthening and the consequent opening of a horizontal masonry joint. This failure was located below the mid-height agreeing with the strain measurements. The collapse was sudden breaking the structure in a fragile way.

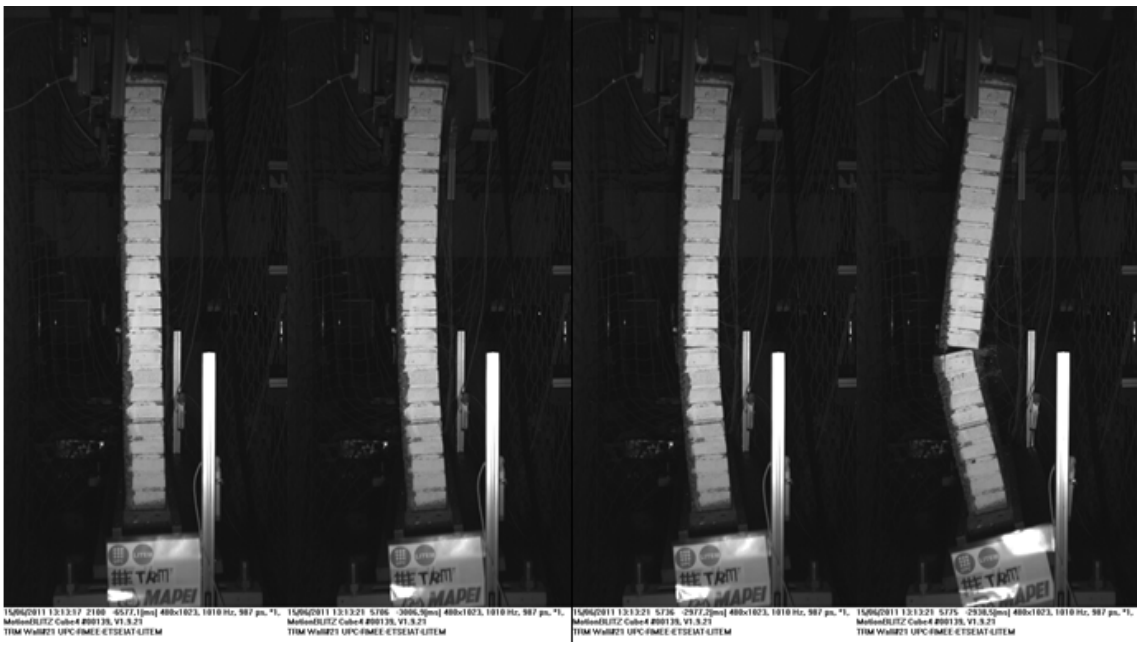

Figure A1. 196 Failure of the wall W#21. TRM tensile fracture and horizontal joint opening

Wall W#22

Wall W#22 was strengthened in the same way than W#21. However, the mortar thickness was less and the grid was positioned closer to the masonry face. Although the hinges alignment in Table A1. 47 is 0mm, the wall showed a meaningful helicoidally shape. The alignment in Table A1. 47 is an average value. It is worth noticing this fact for this particular wall because the real hinges alignment was 15mm at one side and -15mm at the other. This irregularity should be added to the poor out-of-plane levelling as it is proved by the difference existing between the real mid-height eccentricity and the eccentricity at the wall's endings. To place the wall in the testing position the two hinges were rotated in the opposite direction respect the rotation associated with the bending caused by the fixed eccentricity.

About the in-plane response of the wall W#22 (Figure A1. 197), it was analogue to the behaviour described for wall W#21 what agrees with the repeatability assumption. However, little changes at the last steps of the test made the wall W#22 to maintain its stiffness a little more and to show less relaxation. The descending movement of the distribution beam for the maximum load (328.6kN) was 6.7mm.

Wall W#22 geometry	
Masonry rows	27
Width	0.872m
TRM thickness	8mm
Grid position	6mm
Height between hinges	1.827m
Theoretical eccentricity	30mm
Initial rotation lower hinge	-0.86°
Initial rotation upper hinge	-0.86°
Hinges alignment	0mm
Real mid-height eccentricity	33.15mm

Table A1. 47 Geometry of wall W#22

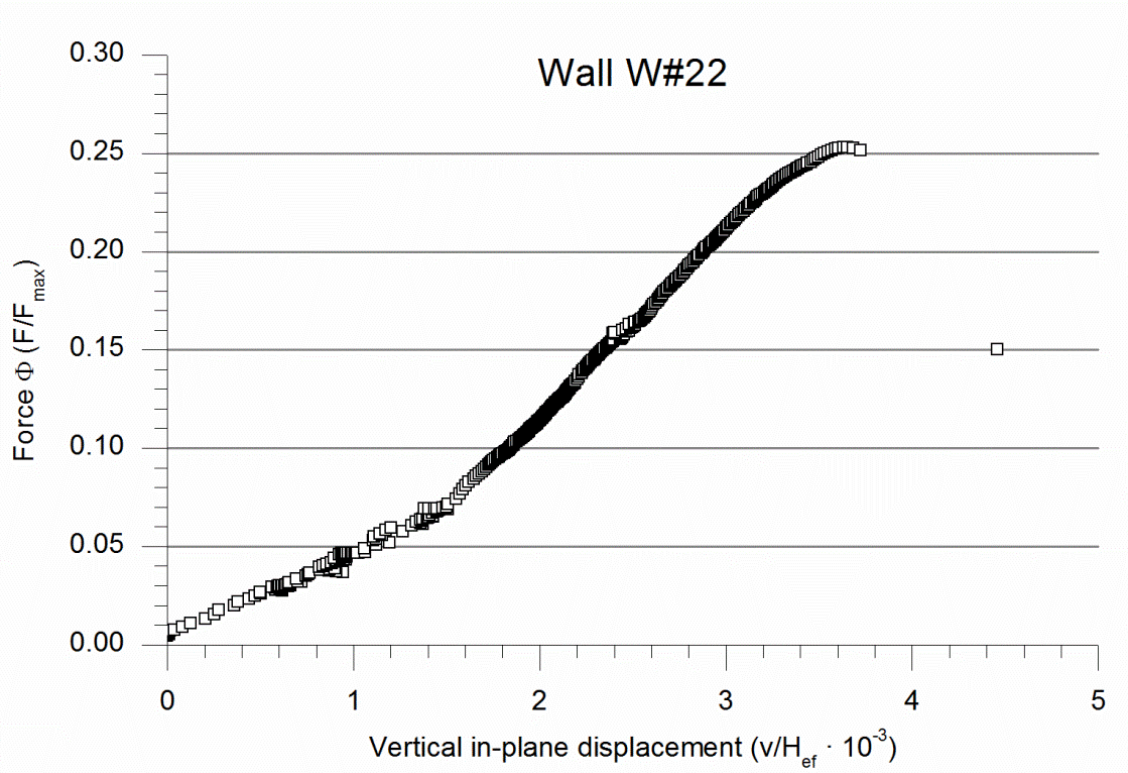

Figure A1. 197 Vertical in-plane response of wall W#22

Regarding the out-of-plane response of the wall W#22 (Figure A1. 198) it presented an asymmetric response. The deformations at mid-height and ¾ of the effective height are almost the same during the test. A clear increase in the deformation rate was observed when the load reached its maximum. At this point the mid-height out-of-plane displacement was 20.1mm, so a significant flexural deformation was observable when the cracks appeared.

In relation with the rotation of the supporting systems (Figure A1. 199), the irregular response of the upper system previously observed in other test is also present for wall W#22. The upper system rotated half the final rotation just at the beginning of the test due to settling effects. After that, it rotated with a constant velocity as the lower hinge did. Closer to the maximum load both supporting systems accelerated its rotations.

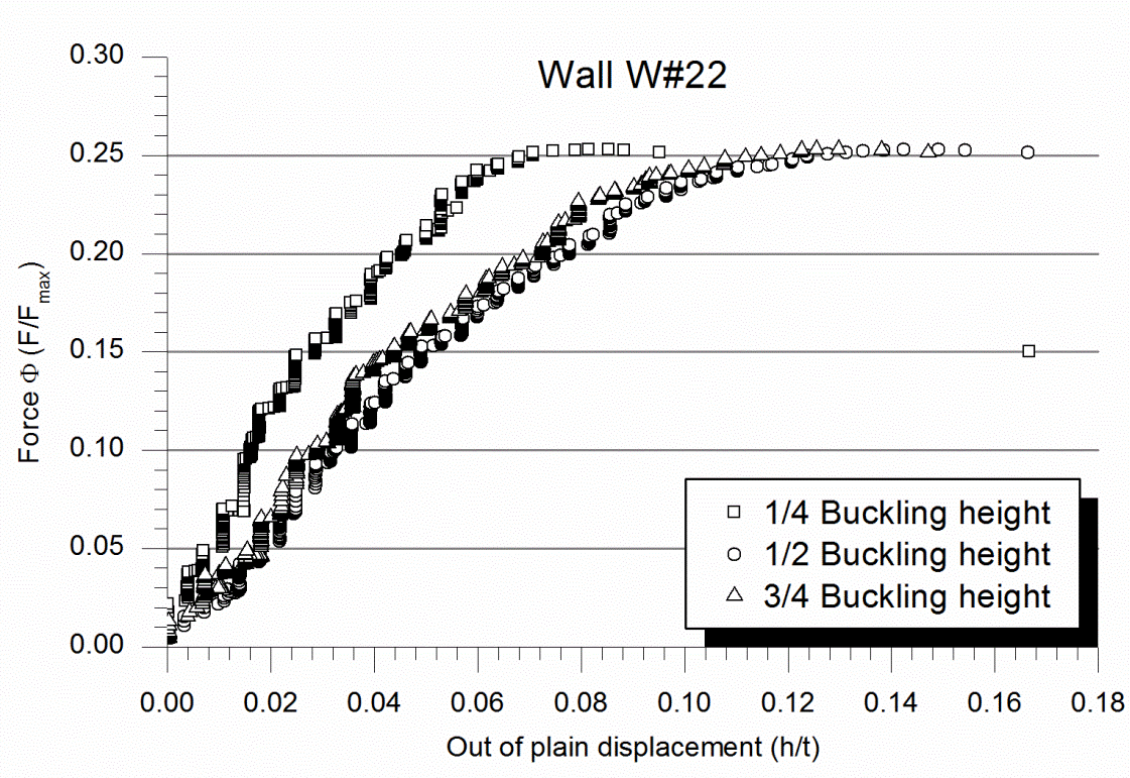

Figure A1. 198 Out-of-plane response of wall W#22

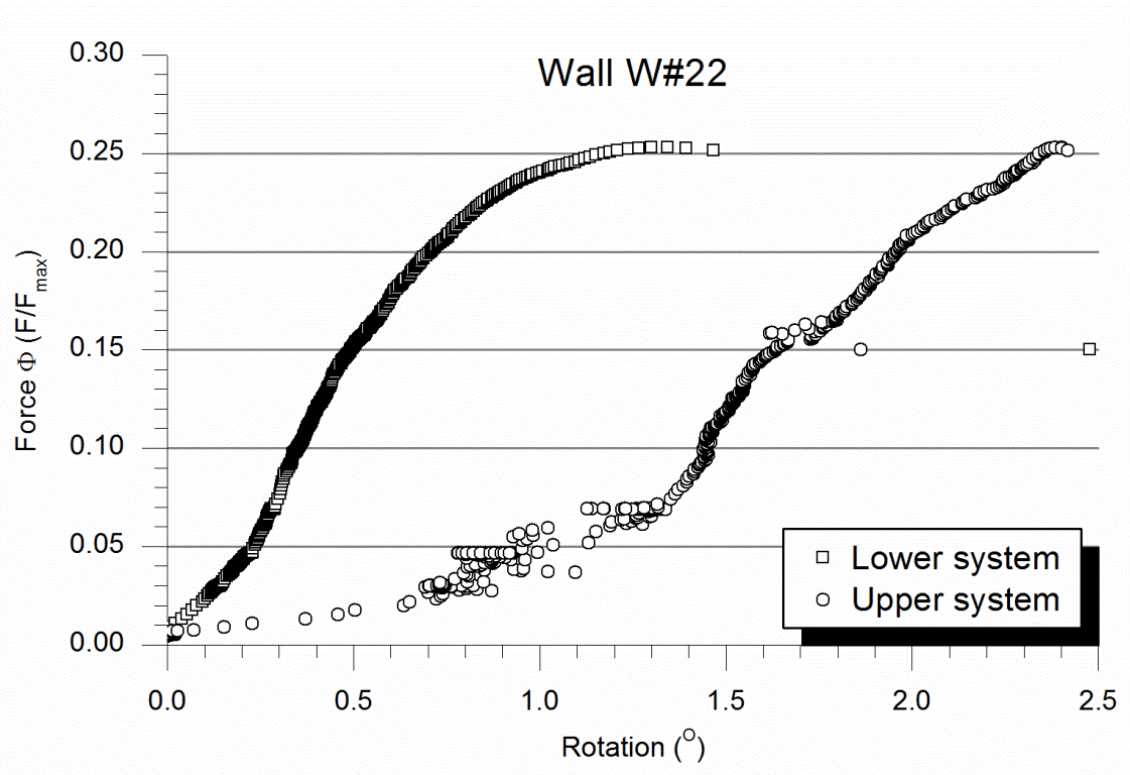

Figure A1. 199 Rotation at wall's endings for wall W#22

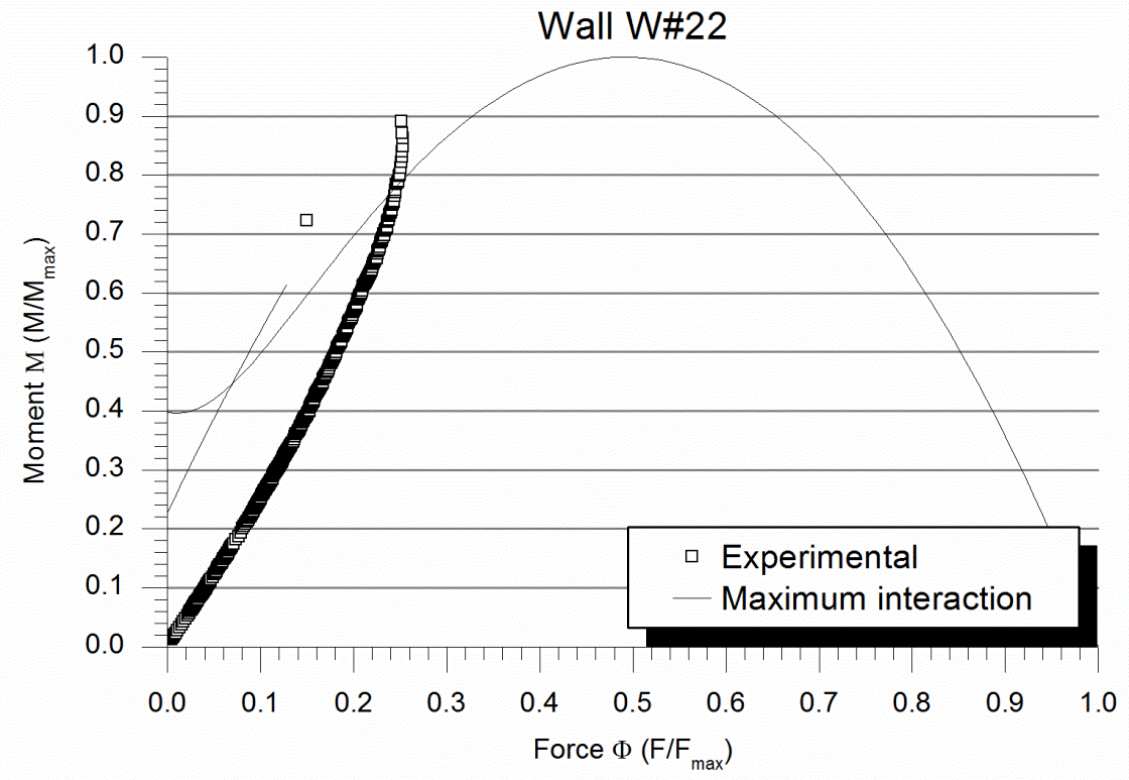

Figure A1. 200 Bending moment vs. Force response and interaction curve for wall W#22

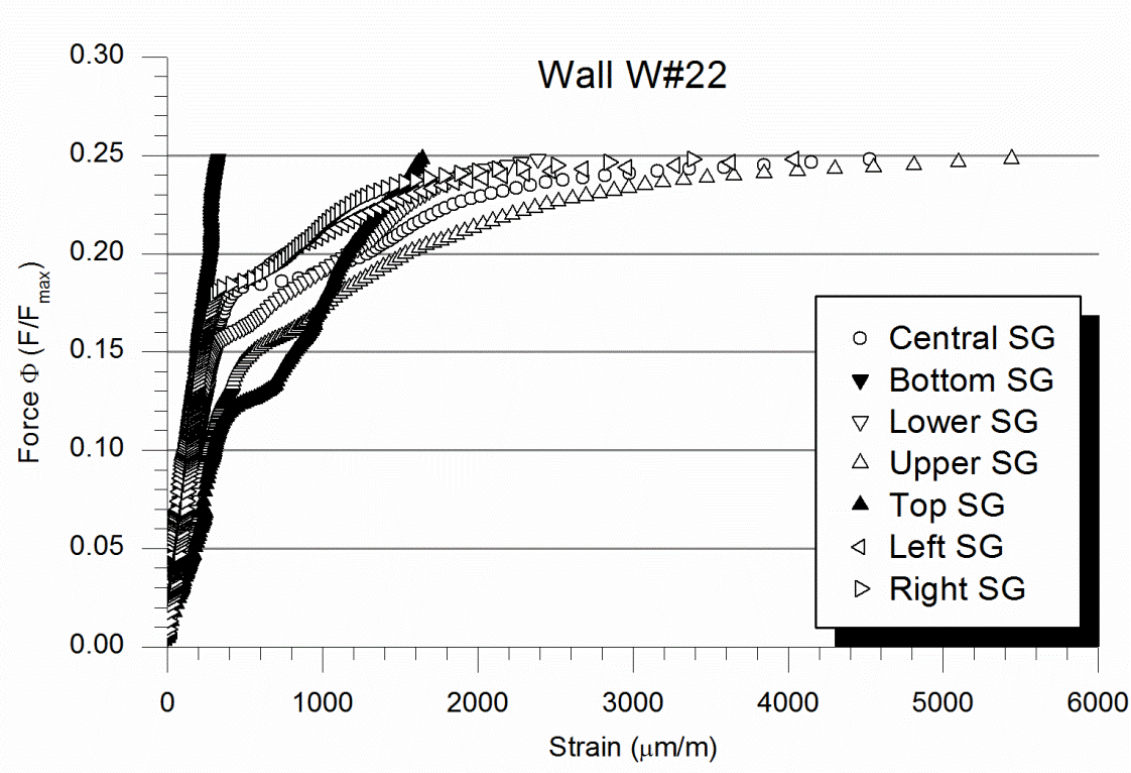

Figure A1. 201 Strains measured on the TRM for wall W#22

The axial force versus flexural moment is plotted in the graph presented at Figure A1. 200. An initial linear relationship is observed up to approximately 40% of the maximum load. After this point the moment increased faster than the applied axial load what indicated the second order eccentricity growing. This change in the behaviour corresponded with the raising of the out-of-plane deformation at a higher rate.

Looking at the measured strains (Figure A1. 201) the asymmetric behaviour in vertical direction is clear. The sensor placed 25cm over the mid-height measured the greatest strains. Between 50% and 60% of the maximum load, approximately, most of the strains changed their measures and the growing rate of the strains increased. This fact was not observed for the strain gage placed at the bottom of the wall. The order the gages changes their response was: first of all the top one, followed but the one placed 25cm over the mid-height, the one located 25 cm below the mid-height and finally the three at mid-height.

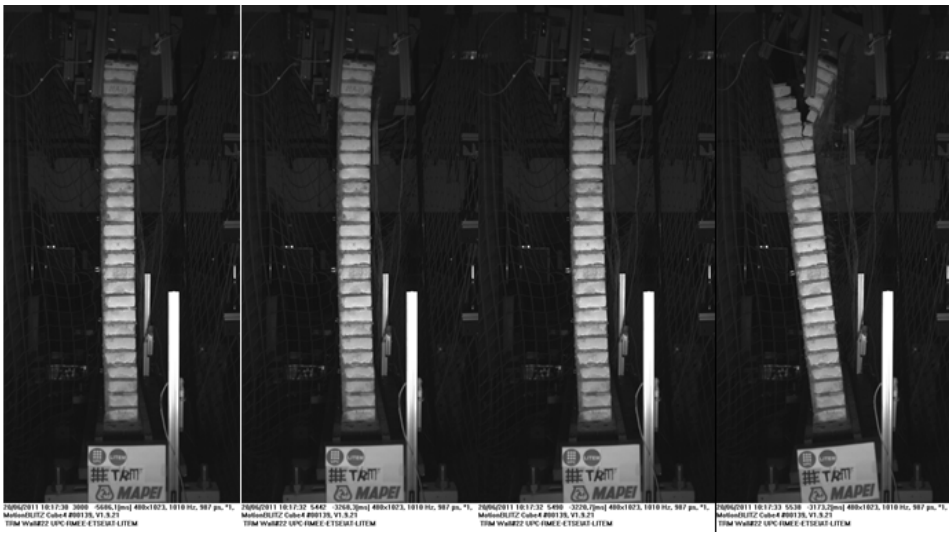

Figure A1. 202 Failure of the wall W#22. Masonry failure at wall's top.

The failure mode was by breaking the masonry with a compression/shear unique crack at the top. A stress concentration due to high compression loads and the pulling effort of the TRM on the masonry near the endings are causes of the damage. The collapse was sudden, breaking the upper part of the wall (7 masonry rows). The crack began at the tensile side and crossed the masonry section (see Figure A1. 202) to finish in the compression side of the wall. Then the wall was disconnected from the upper supporting system and it fell as a solid rigid. Thus, the failure mode was localised to the upper supporting area although the significant bending deformation during the test.

Wall W#23

Wall W#23 was strengthened with one woven sheet of glass fibre (MapeGrid G220) embedded into a layer of hydraulic-lime-based mortar (Planitop HDM Restauro). The position of the fibre grid (see Table A1. 48) was closer to the masonry face than the manufacturer's specifications. The horizontal levelling of this wall was better than W#22 although the difference between the real mid-height eccentricity and the eccentricity at the wall's endings was almost the same. What changes from W#22 is the hinges' alignment which practically might fully explain the increase of eccentricity at mid-height. Moreover this wall has a plane shape.

Wall W#23 geometry	
Masonry rows	26
Width	0.868m
TRM thickness	9.5mm
Grid position	6mm
Height between hinges	1.822m
Theoretical eccentricity	30mm
Initial rotation lower hinge	-1.29°
Initial rotation upper hinge	-0.86°
Hinges alignment	5.5mm
Real mid-height eccentricity	33.93mm

Table A1. 48 Geometry of wall W#23

Regarding the in-plane behaviour (Figure A1. 203), it is, like in previous test, continuous with an initial settling, followed by a linear response that finally changes (softening) when the load is close to its maximum. For the maximum load (270.9kN), the descending displacement of the distribution beam was 7.6mm. This pair of values is close to the obtained for wall W#21.

Observing the graph in Figure A1. 204, a clearly asymmetric response, comparable with the behaviour obtained for wall W#22, is noticed. It is, the out-of-plane displacement at ¾ of the effective height was just slightly less than the same deformation at mid-height. The minimum out-of-plane deformation was always at ¼ of the height and corresponding with the maximum applied load, the out-of-plane displacement at the centre of the wall was 20.6mm.

The fact that the out-of-plane displacement at ¼ of the effective height is always the minimum of the measured agreed with the response of the supporting systems (see Figure A1. 205). The rotation of the lower hinge was less than the rotation of the upper system during test. Only near the collapse this tendency changed. Furthermore, as seen in previous tests, the behaviour of the upper system was more irregular than the response of the lower hinge because of the connection between the distribution beam and the upper hinge. For wall W#23, moreover, the behaviour of the upper system was more or less linear so the rotation speed was constant whereas the lower hinge rotational speed increased with the load.

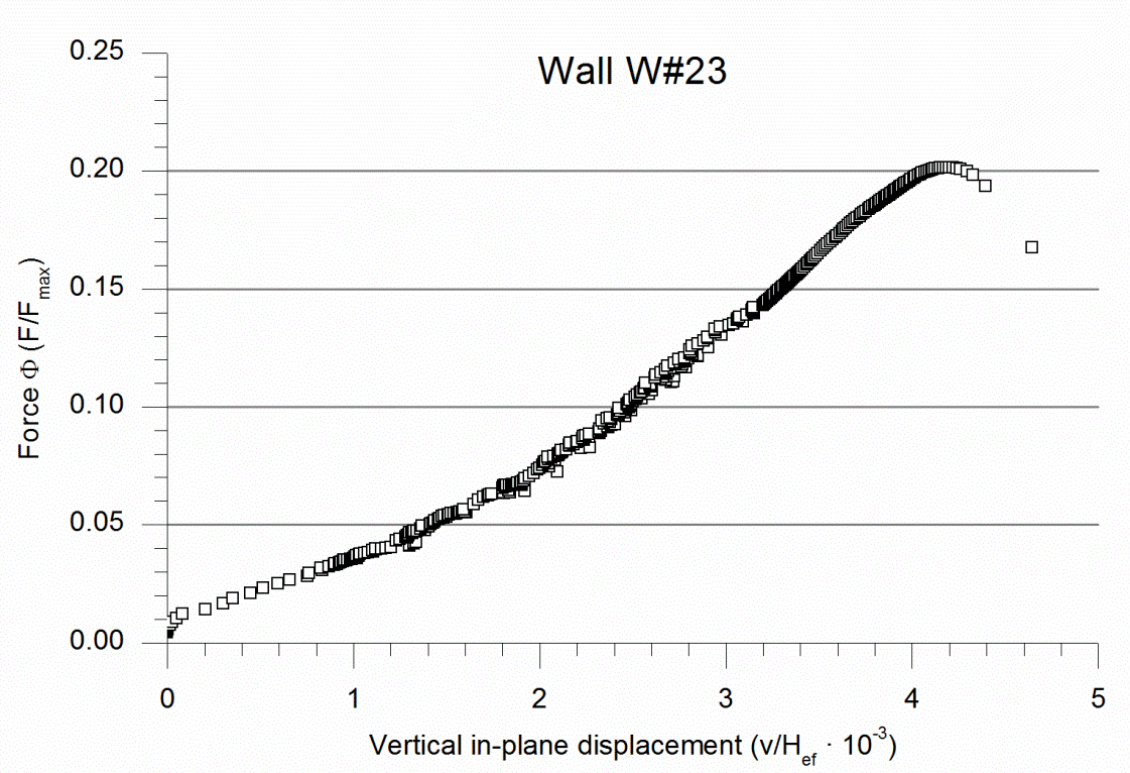

Figure A1. 203 Vertical in-plane response of wall W#23

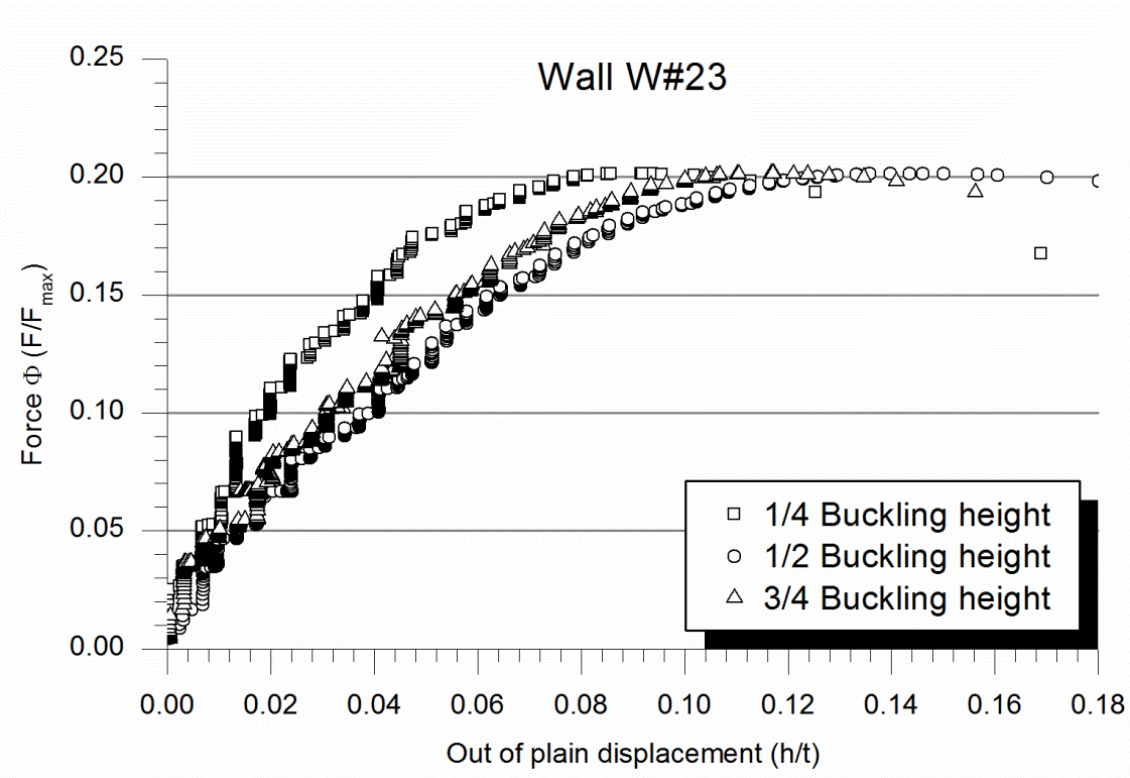

Figure A1. 204 Out-of-plane response of wall W#23

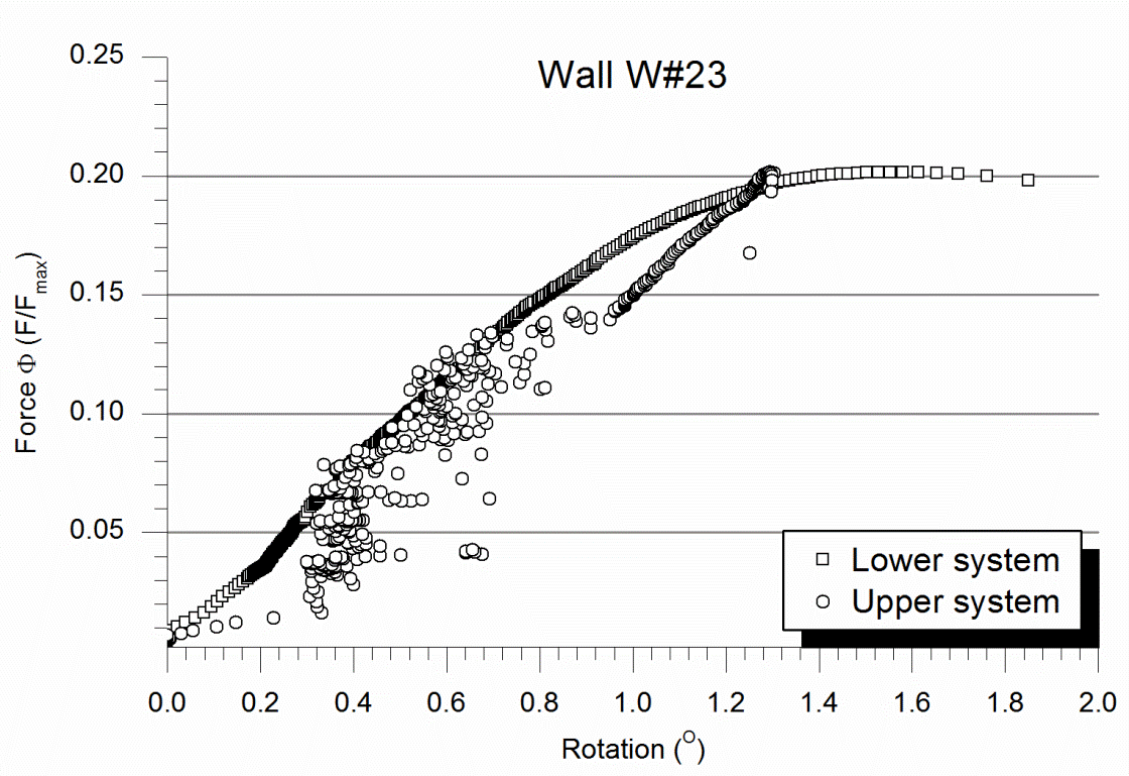

Figure A1. 205 Rotation at wall's endings for wall W#23

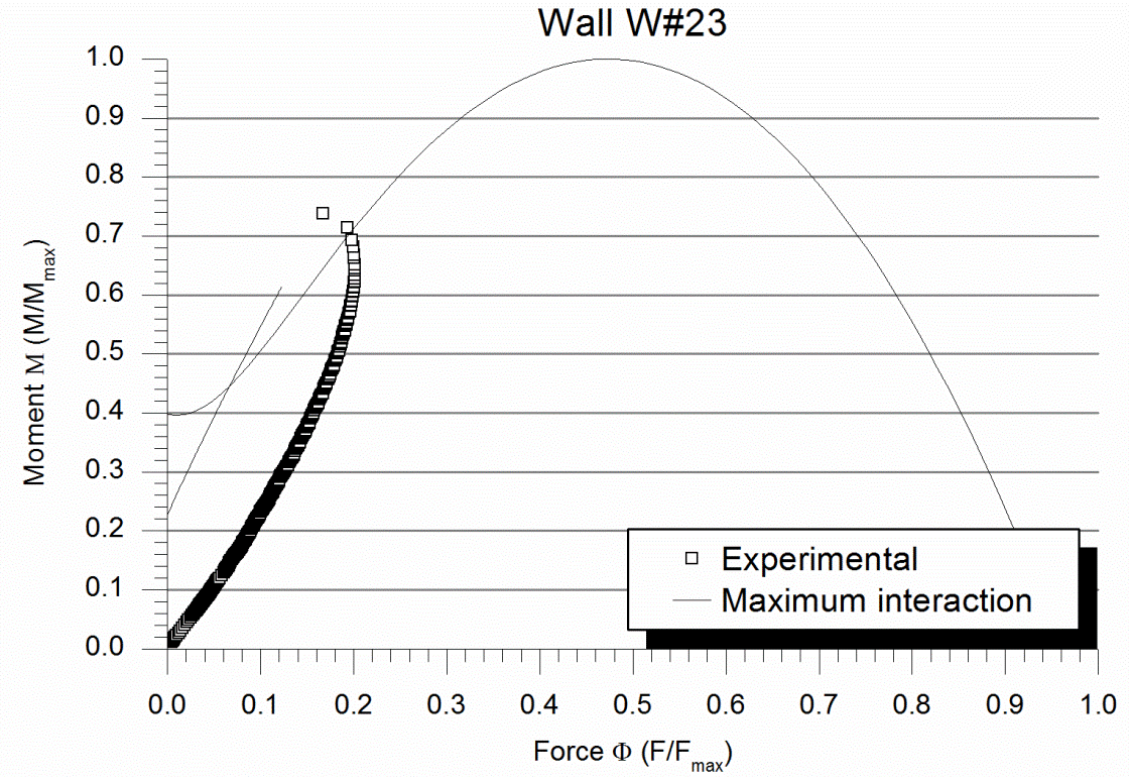

Figure A1. 206 Bending moment vs. Force response and interaction curve for wall W#23

Observing the bending moment versus the applied axial load for wall W#23 (see Figure A1. 206), the second order effect is visible from the very first beginning of the test so the behaviour was the expected from the start. It is worth mentioning that the wall reached the 70% of the maximum bending moment whilst the axial load was only the 20% of its capacity what proves the great effect of both, the initial and the second order generated eccentricities.

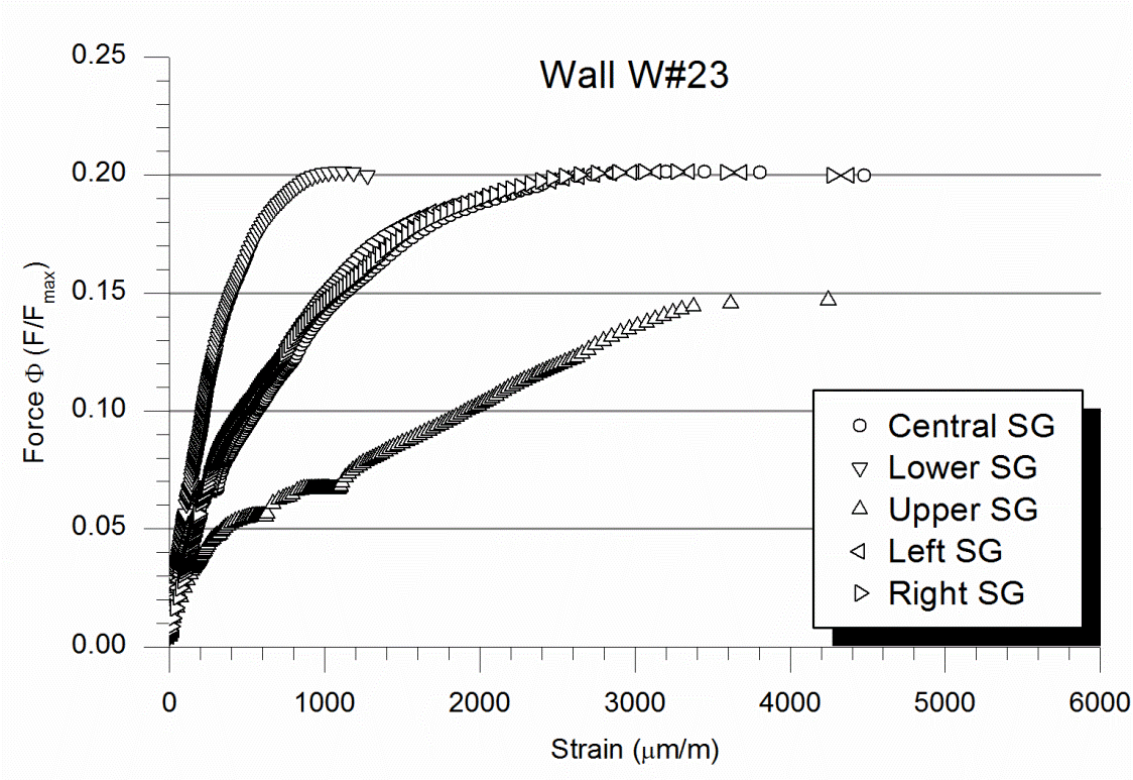

Figure A1. 207 Strains measured on the TRM for wall W#23

According with graphs in Figure A1. 204 and Figure A1. 205, where it is showed that the lower part of the wall deformed less than the upper one, in Figure A1. 207 it is noticed that the minimum measured strains corresponded also to the gage placed at the lower part. In the strains reading for wall W#23 it is worth noticing that the three placed at mid-height (central, left and right) measured practically the same during the test proving in this case were not torsion efforts like in in the two previous tests with TRM. However, the asymmetry along the height of the wall is clear when observing that the strain gage which recorded greatest values was always the one installed at the upper part of the wall.

In Figure A1. 208 it is shown that the wall's failure corresponded with the tensile breaking of the TRM at a position slightly below the mid-height. It is also important to comment the naked eye visible bending deformation before the sudden collapse of the wall.

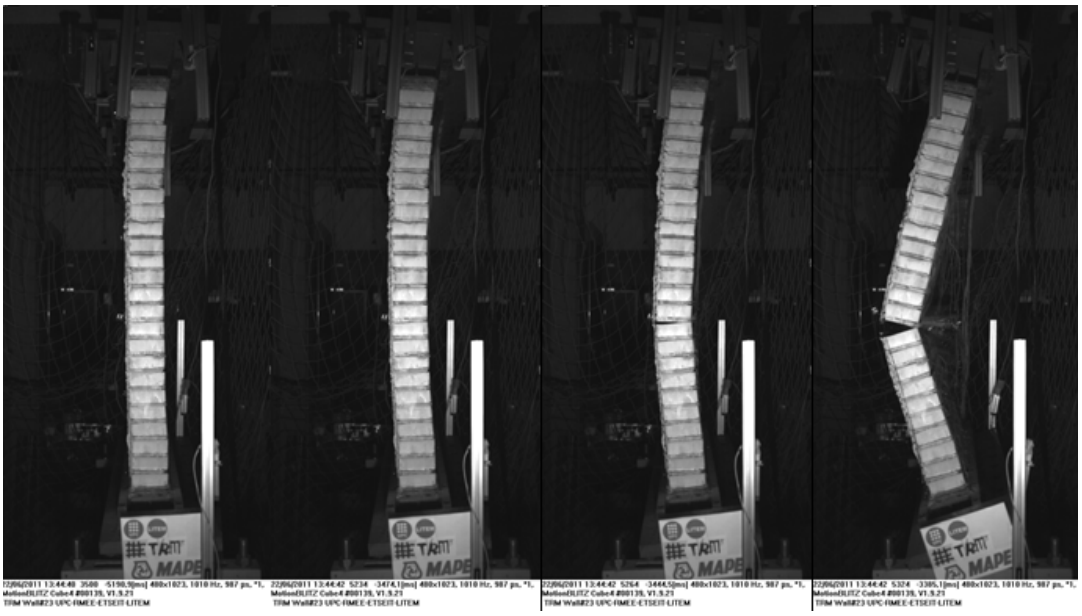

Figure A1. 208 Failure of the wall W#23. TRM tensile fracture and horizontal joint opening

Wall W#24

Wall W#24 was strengthened in the same way than wall W#23 but the position of the fibre grid was slightly closer to the masonry face in W#24 case (see Table A1. 49). The poor vertical straightness of wall W#24 is proved at observing the large initial rotation of the upper hinge (in opposite direction respect the associated with the bending that would appear during the test) to place the wall in the testing position respecting the hinges alignment as much as possible. Moreover, the real mid-height eccentricity is lower than the fixed eccentricity at wall's endings. It indicates that the initial shape had an opposite curvature of the developed during the test.

Wall W#24 geometry	
Masonry rows	27
Width	0.867m
TRM thickness	9mm
Grid position	4.5mm
Height between hinges	1.840m
Theoretical eccentricity	30mm
Initial rotation lower hinge	-0.21°
Initial rotation upper hinge	-2.72°
Hinges alignment	0.5mm
Real mid-height eccentricity	25.36mm

Table A1. 49 Geometry of wall W#24

The in plane response of wall W#24 (Figure A1. 209) was similar to the obtained from other similar walls. However, more instable values were recorded in the first half of the test. It might be caused by settling effects associated with bigger initial rotations. The final values were comparable with previous

tests with a maximum descending displacement of the distribution beam of 8.3mm for the maximum load (285.6kN).

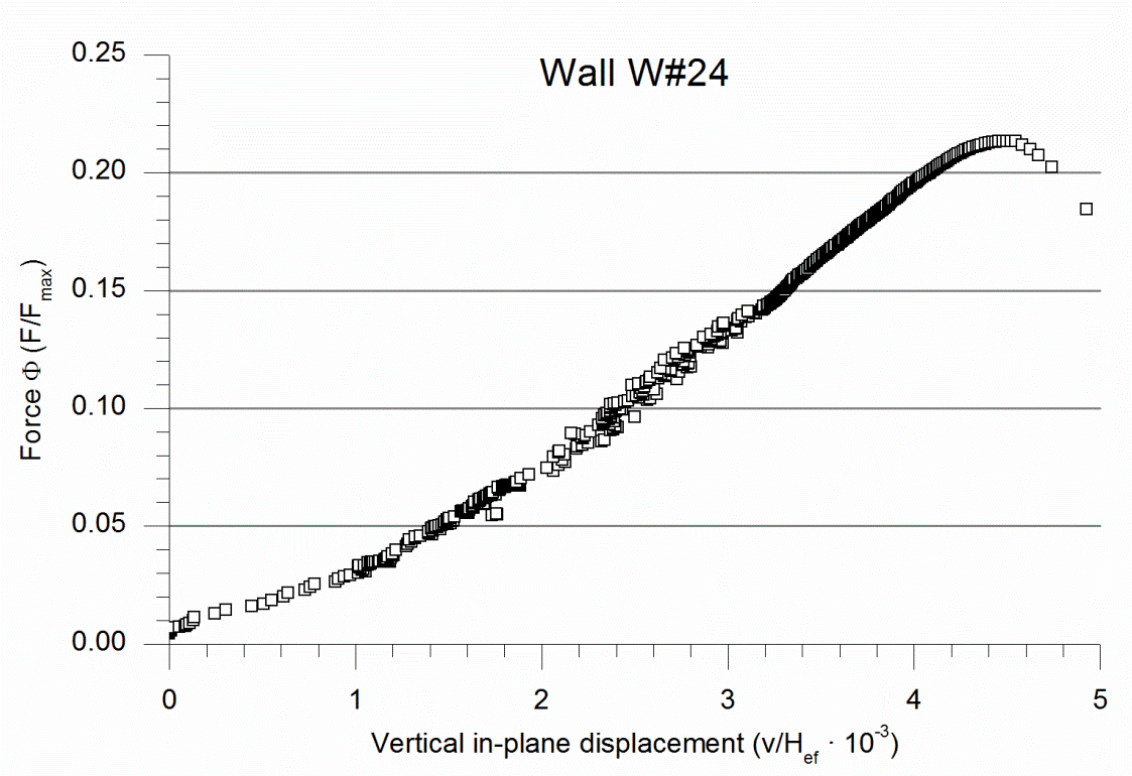

Figure A1. 209 Vertical in-plane response of wall W#24

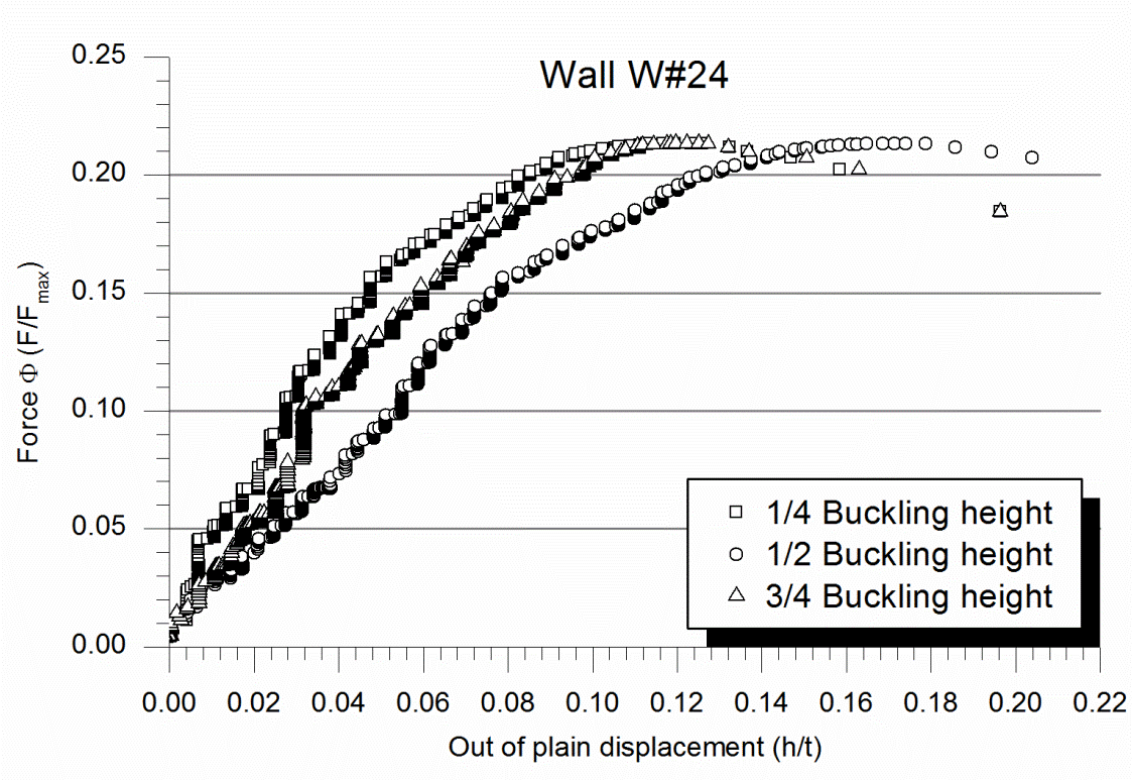

Figure A1. 210 Out-of-plane response of wall W#24

Observing Figure A1. 210, a more symmetric behaviour than walls W#22 and W#23 is noticed for the out-of-plane displacements. The mid-height deformation was the greater one and it reached 24.3mm for the maximum load. Although the deformation at ¾ of the buckling height was slightly bigger than the deformation measures at ¼ of the effective height, near the collapse load these two values converged reaching a symmetric response.

Regarding the rotation of the supporting systems (see Figure A1. 211) a clear difference on the behaviour is observed between the upper system and the lower hinge. Whilst the first one is unstable and the rotation speed decreased with the load increase, the lower hinge showed a more continuous response accelerating the rotation with the load growth.

In the graph at Figure A1. 212 the second order effects are clearly represented by the slope increase of the plot. Moreover, the experimental load-moment interaction intersected the maximum interaction curve (commented in Chapter 5) accurately for the maximum applied load value. The experimental moment is relatively higher than the axial load compared with the possible maximum values.

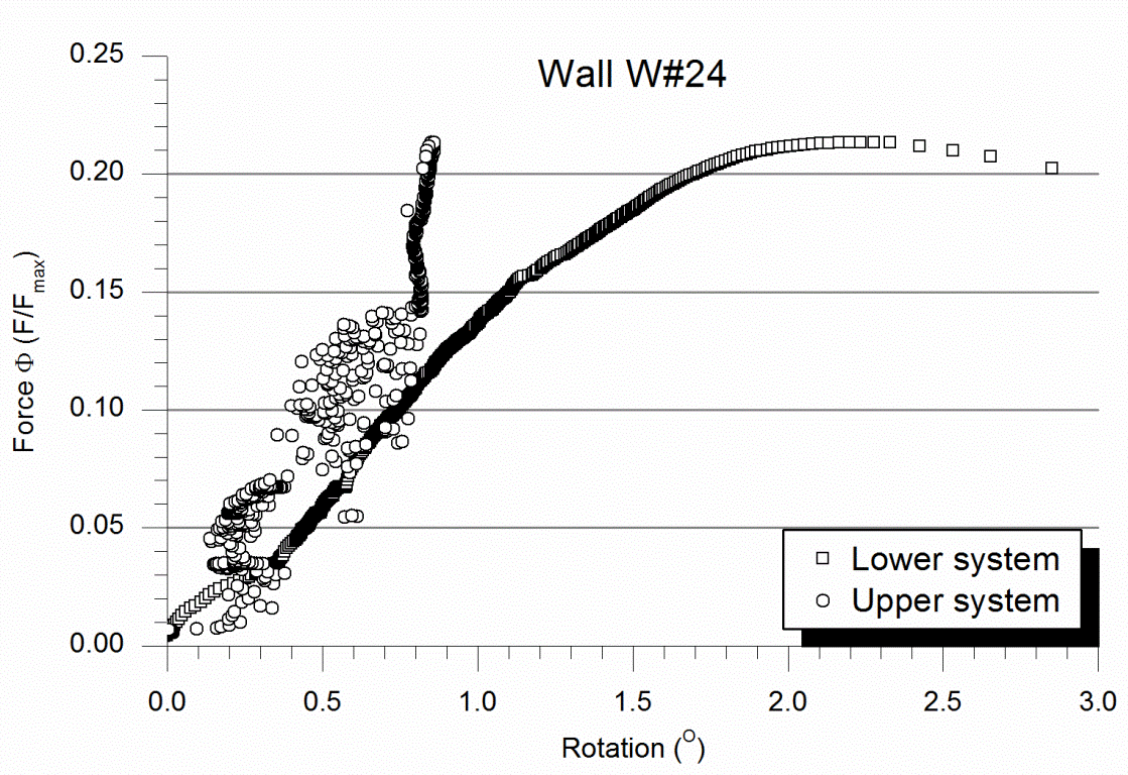

Figure A1. 211 Rotation at wall's endings for wall W#24

Figure A1. 213 shows the strain measures on the seven points corresponding with the seven installed strain gages. The gages placed at mid-height measured the lower strain values (there is also asymmetric response in the width of the wall) whilst the upper and lower gages recorded higher values. The maximum strains were measured at the top of the wall. A clear asymmetric response is reflected in the graph.

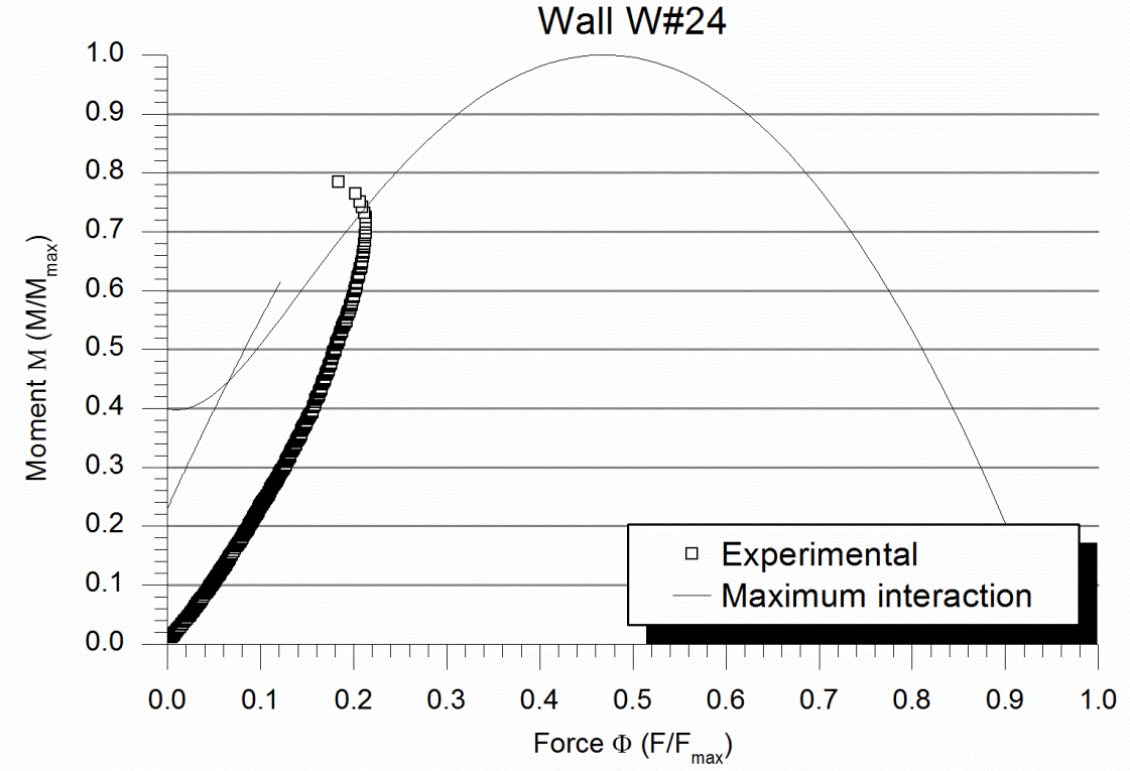

Figure A1. 212 Bending moment vs. Force response and interaction curve for wall W#24

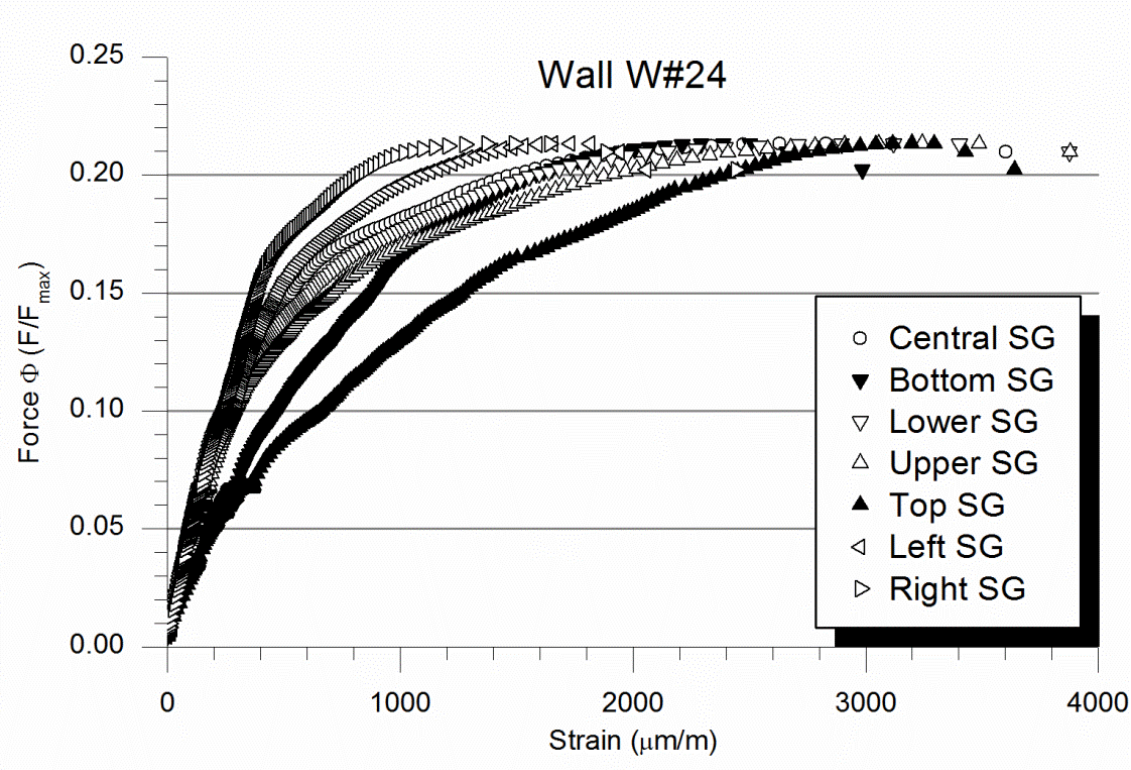

Figure A1. 213 Strains measured on the TRM for wall W#24

The failure mode was also asymmetric as the wall broke by masonry cracking from the tensile face, trough the wall's thickness to the compressive side (see Figure A1. 214). Breaking one of the endings of the wall corresponded with the distribution of strains which were bigger near these areas. The collapse was sudden although a great flexural deformation was observed before.

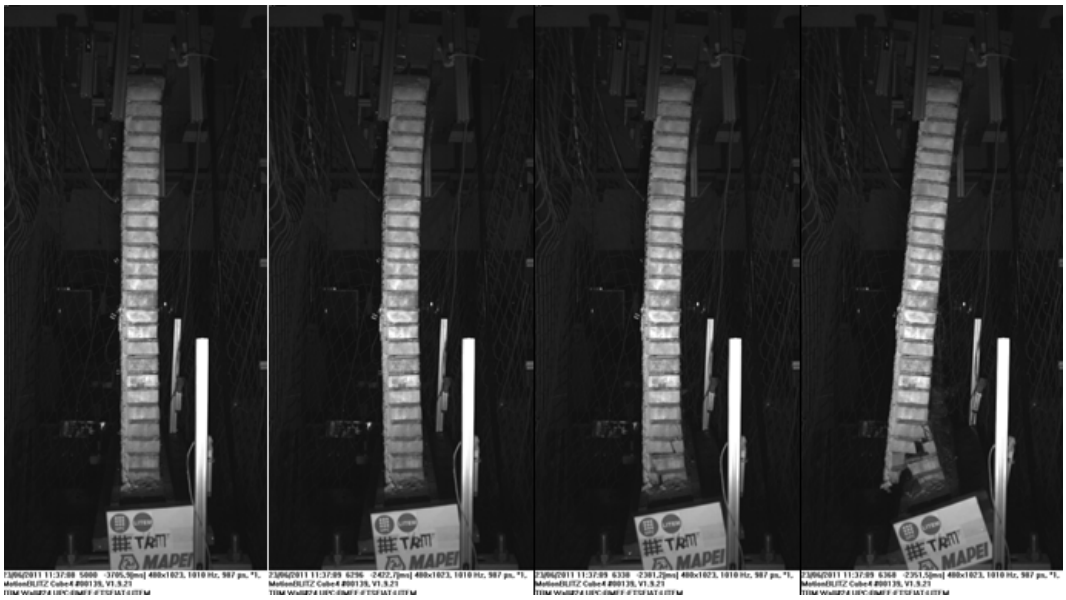

Figure A1. 214 Failure of the wall W#24. Masonry failure at wall's bottom.

Wall W#25

Wall W#25 was strengthened with two layers of glass fibre (MapeGrid G220) embedded into a thin layer (7.5mm, see Table A1. 50) of Planitop HDM Restauro Mortar. The gap between the two fibre grids was 3mm (Table A1. 50). In contrast with previous tests on TRM strengthened walls, for wall W#25 the lower hinge was rotated in the same direction it would move when the wall was loaded. The hinges alignment was accurate but a significant initial rotation of the upper supporting system was required. Furthermore, this wall showed an initial deformed shape which caused an increase on the eccentricity at the mid-height section.

Wall W#25 geometry	
Masonry rows	26
Width	0.868m
TRM thickness	7.5mm
Grid position	3.5mm/6.5mm
Height between hinges	1.828m
Theoretical eccentricity	30mm
Initial rotation lower hinge	0.21°
Initial rotation upper hinge	-1.58°
Hinges alignment	0.5mm
Real mid-height eccentricity	32.66mm

Table A1. 50 Geometry of wall W#25

Graph in Figure A1. 215 shows the in plane response of the wall W#25. As previous tests, the descending movement of the distribution beam was linearly dependent on the applied load during most of the test. However, the initial settlement and final softening effects are qualitatively less important than in previous tests. The in plane displacement of the top of the wall at the maximum load (414.0kN) was 7.4mm.

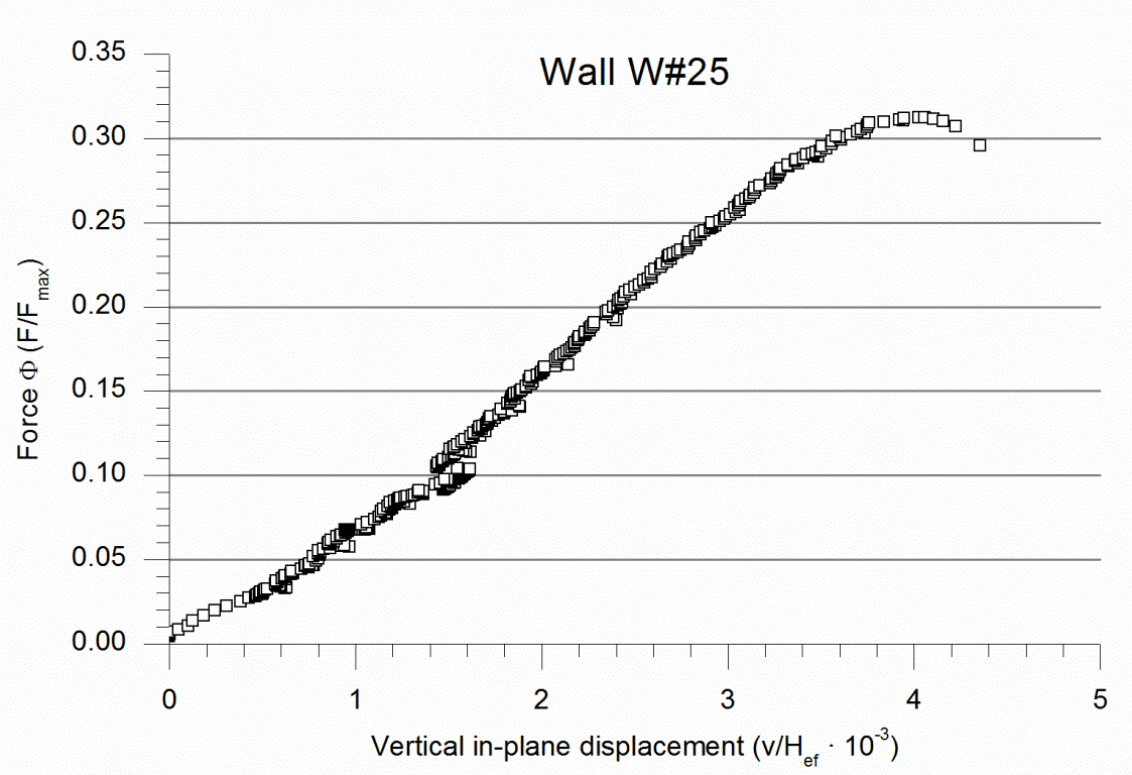

Figure A1. 215 Vertical in-plane response of wall W#25

In Figure A1. 216, the symmetric out-of-plane response of the wall W#25 is observed. The reading of the laser sensor placed at mid-height was always bigger than the other two measures which read equal values corresponding to ¼ and ¾ of the effective height. An initial linear response is observed for the three sensors up to 75% of the maximum load when the out-of-plane displacement rose faster. The out-of-plane deformation at mid-height corresponding with the maximum height was 23.9mm.

In contrast with the out-of-plane response, observing Figure A1. 217, an asymmetric behaviour of the supporting systems was observed. Whilst the lower hinge rotated at a constant speed up to 50% of the maximum load and the accelerated its movement, the upper supporting system began with a quick rotation followed by an almost linear response up to failure. This response is similar to the one observed for wall W#20.

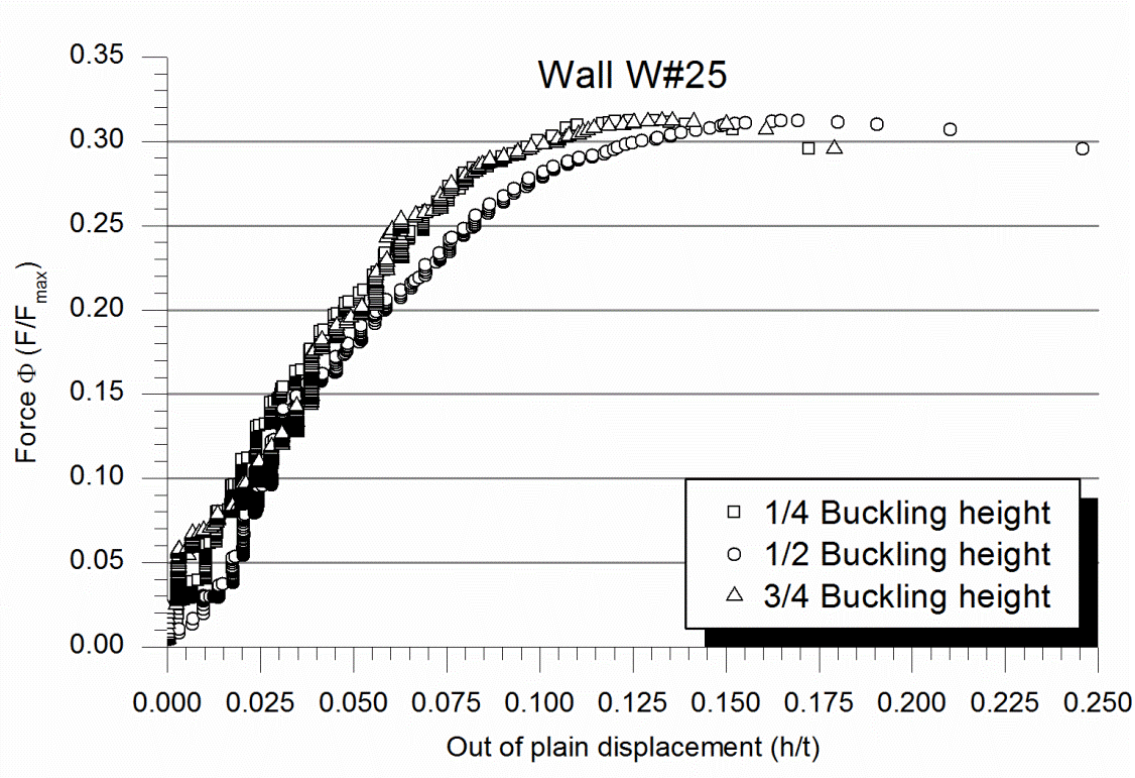

Figure A1. 216 Out-of-plane response of wall W#25

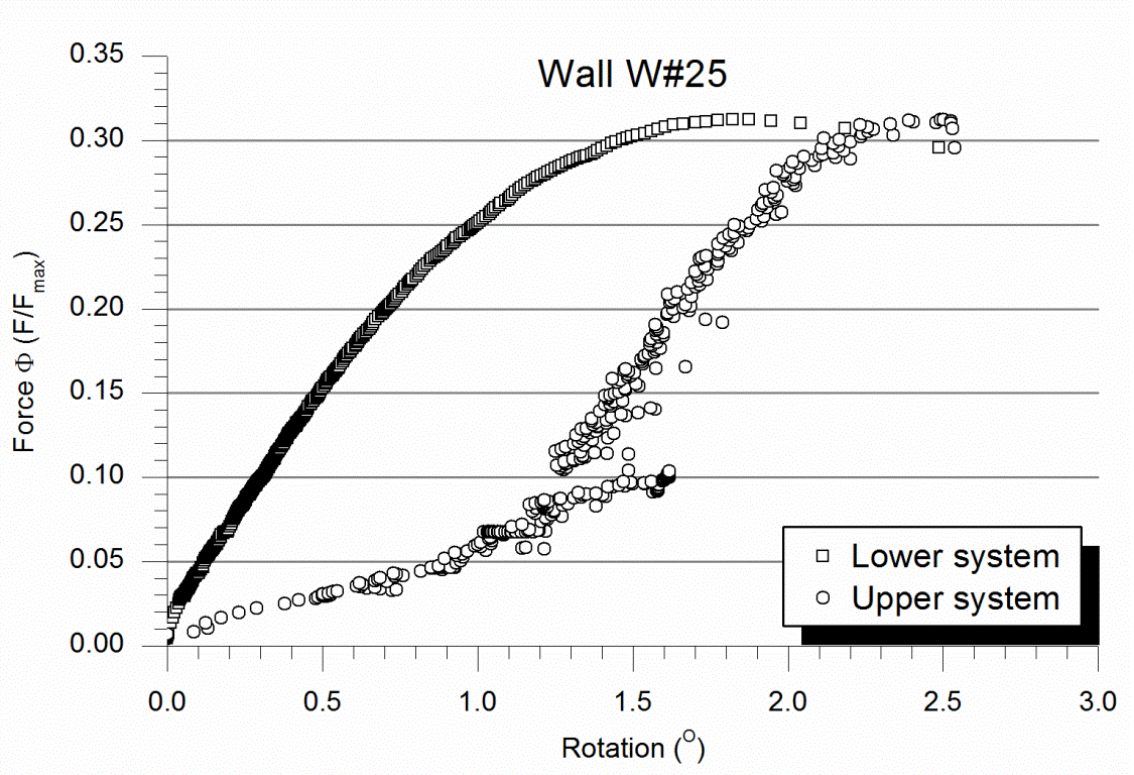

Figure A1. 217 Rotation at wall's endings for wall W#25

The bending moment – axial force interaction experimental curve (Figure A1. 218) showed an initial linear response corresponding with the stage the second order effects were not significant. It was up to 30% of the maximum bending and almost the 50% of the maximum applied load. The constant slope of the curve at this moment contrasted with the increase of the out-of-plane displacement. From this point (over 50% of the maximum load) and on, the second order effects got more and more noticeable so the bending moment increased faster than the applied load.

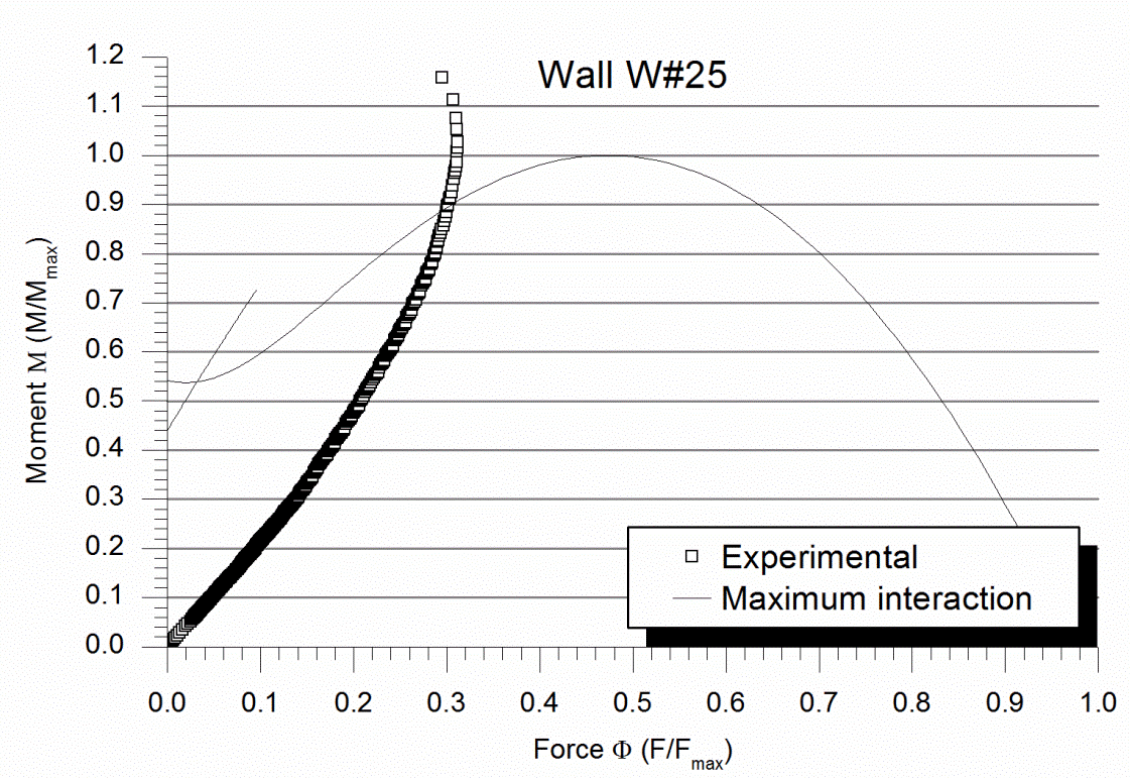

Figure A1. 218 Bending moment vs. Force response and interaction curve for wall W#25

Figure A1. 219 Failure of the wall W#25. Masonry failure at wall's bottom.

It was the second order bending moment what caused the naked eye visible out-of-plane deformation (see second picture in Figure A1. 219). Finally, the failure mode was the masonry cracking at the bottom part. The crack began at the tensile side just above the heading element and grew to the compressive side which was reached between the 6th and 7th masonry rows. It separated the wall from the lower hinge. After that the structure simply fell as a rigid solid.

Wall W#26

The strengthening system of wall W#26 was similar to the used for wall W#25 except the strengthening mortar, which was Planitop HDM Maxi. In this case, the thickness of the mortar layer was slightly bigger than for wall W#25 and the mortar between the masonry surface and the grids was little thicker (see Table A1. 51). Although the initial rotation of both supporting systems (in the opposite direction from the expected to be developed during the test) the hinges alignment was not as good as in previous test. However, the geometrical imperfections compensated these deviations as can be seen by comparing the theoretical eccentricity (real at the ends of the wall) with the experimental eccentricity at mid-height.

Wall W#26 geometry	
Masonry rows	26
Width	0.869m
TRM thickness	8mm
Grid position	4mm/6mm
Height between hinges	1.823m
Theoretical eccentricity	30mm
Initial rotation lower hinge	-0.29°
Initial rotation upper hinge	-1.58°
Hinges alignment	6mm
Real mid-height eccentricity	29.73mm

Table A1. 51 Geometry of wall W#26

Observing the graph in Figure A1. 220 it is noticed that the in plane behaviour was similar to walls W#23 and W#24 which were strengthened with the same mortar but only one fibre grid. So the application of extra fibre layers seems not to influence the wall response for this TRM application case. The curve shape is characterised by a proportional response after an initial settling process and before the final relaxation of the structure. The descending displacement of the loading beam at the maximum load (390.3kN) was 8.4mm.

The out-of-plane response began asymmetric but during the test the structure adapted its response and near the collapse the symmetry was almost perfect (see Figure A1. 221). The same out-of-plane deformation values were recorded for ¼ and ¾ of the effective height of the wall. The maximum out-of-plane displacement was measured at mid-height and it was 19.1mm for the maximum load what indicates a stiffer response than walls W#23 and W#24.

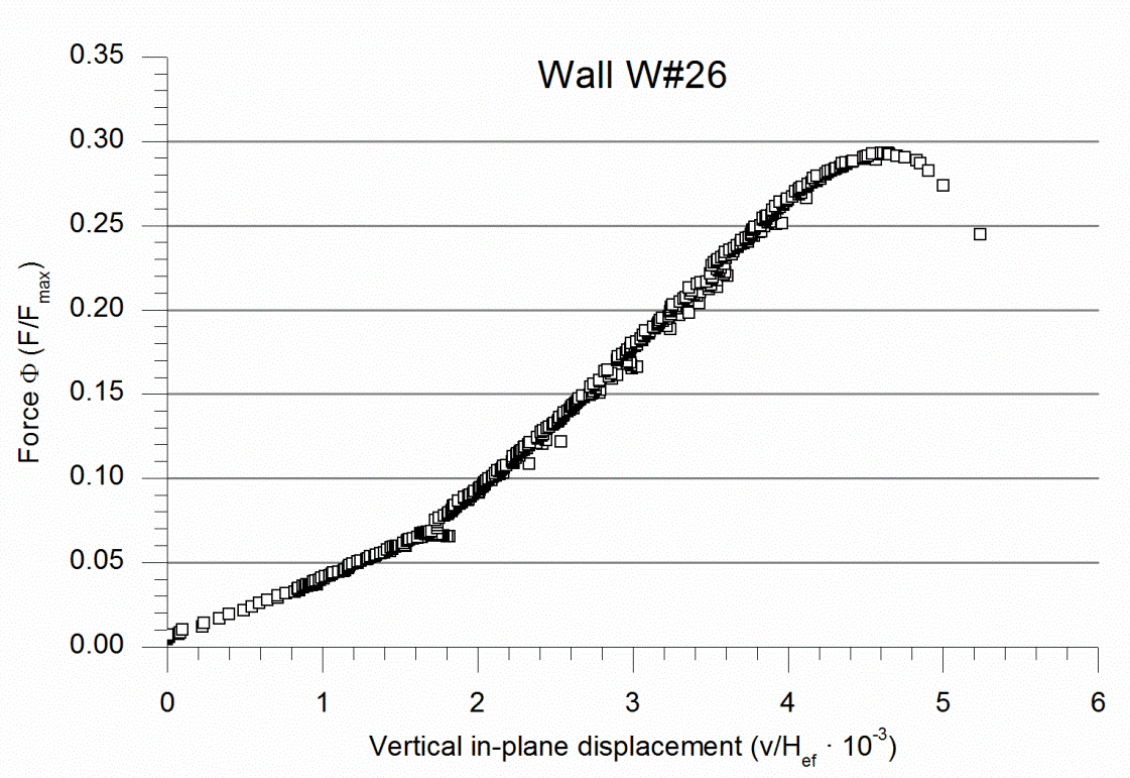

Figure A1. 220 Vertical in-plane response of wall W#26

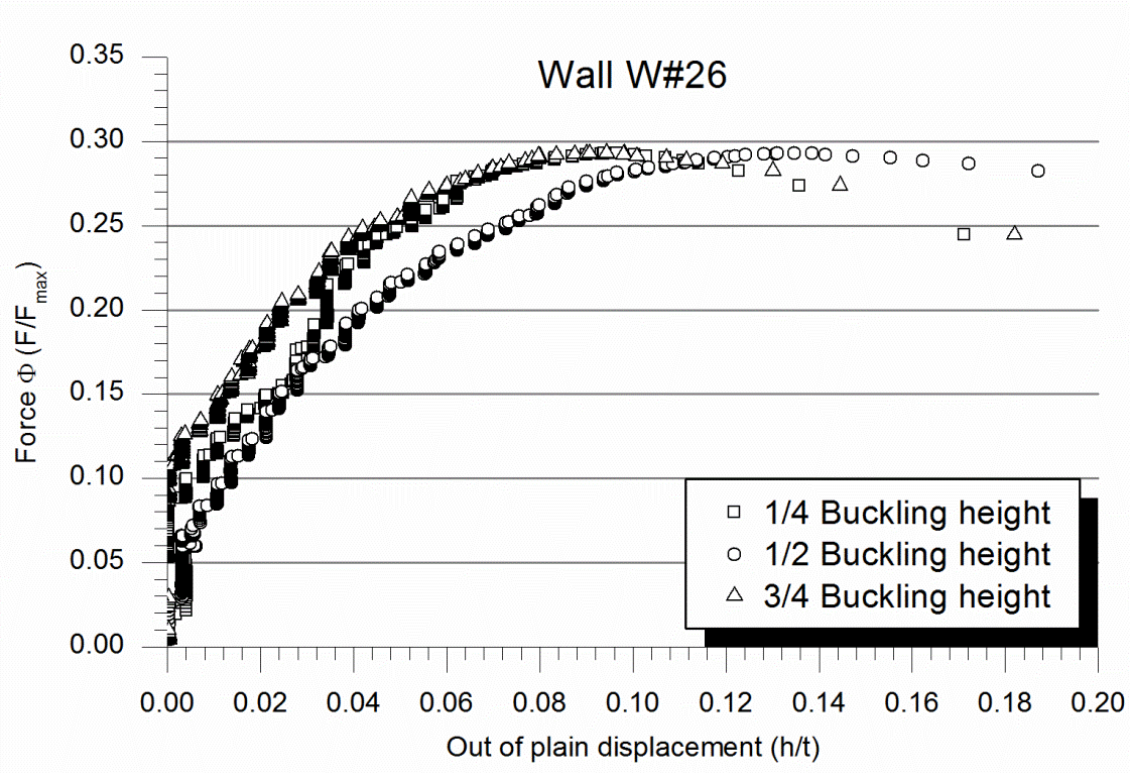

Figure A1. 221 Out-of-plane response of wall W#26

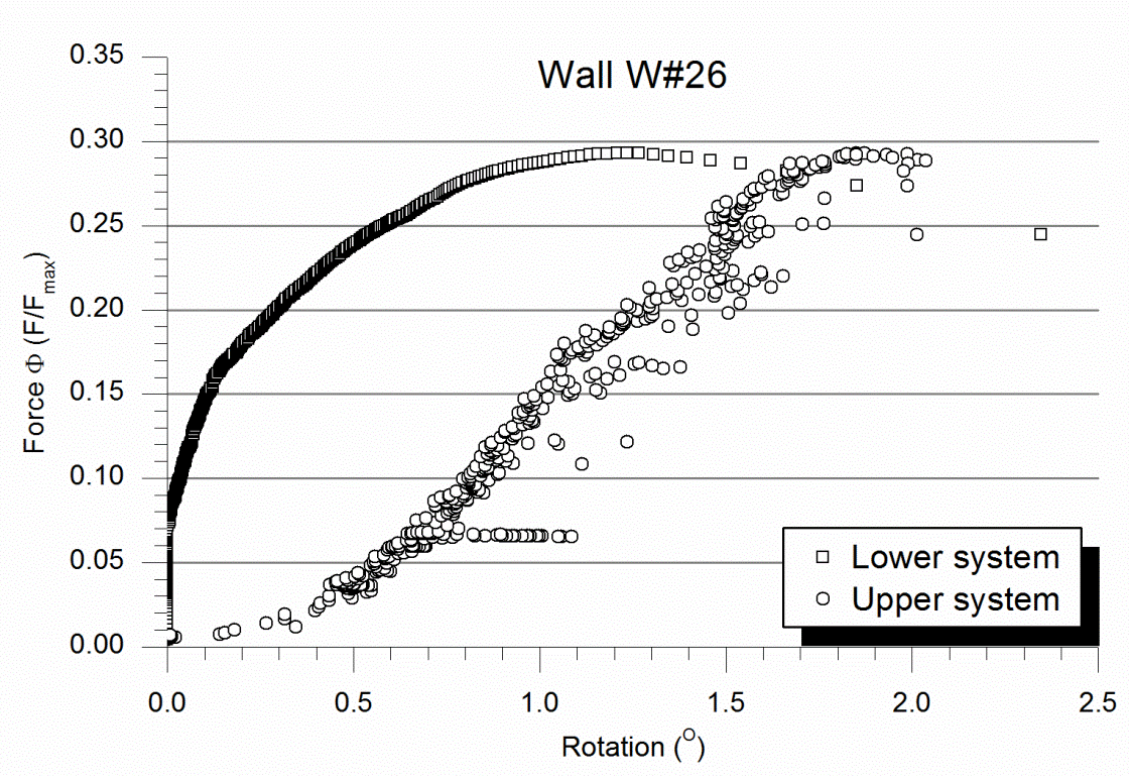

Figure A1. 222 Rotation at wall's endings for wall W#26

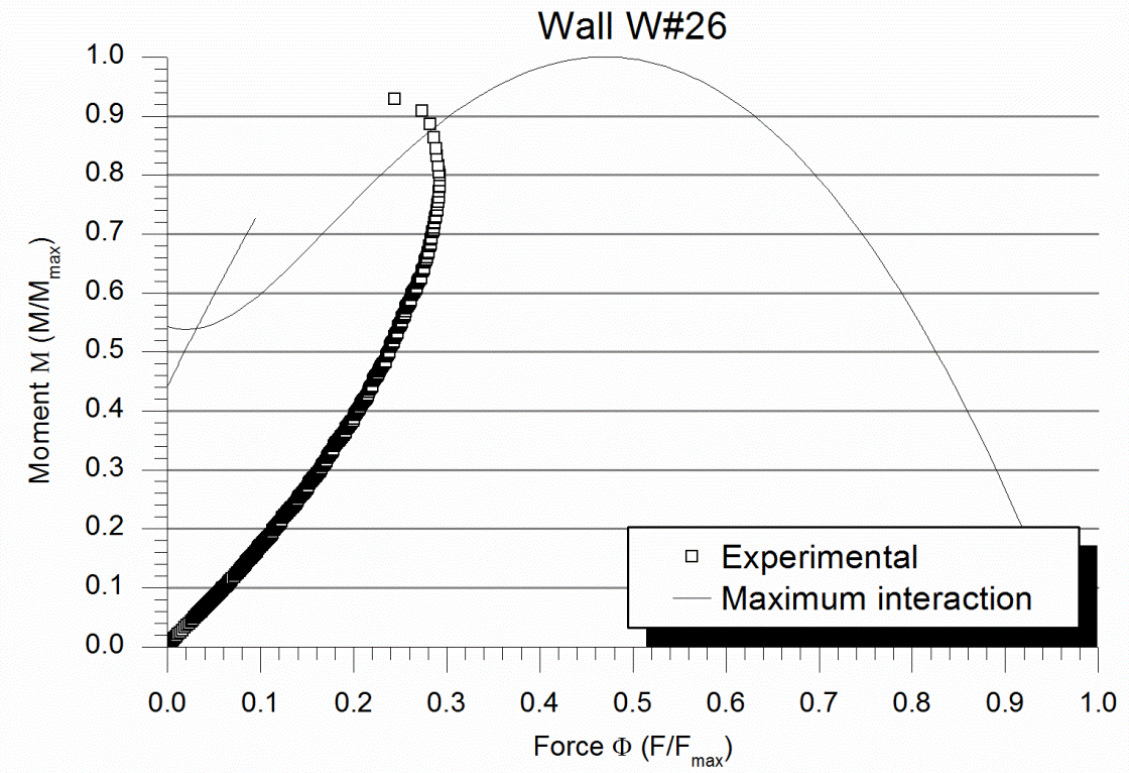

Figure A1. 223 Bending moment vs. Force response and interaction curve for wall W#26

Regarding the rotation of the extreme supporting systems a clearly asymmetric response was noticed (see Figure A1. 222). The lower hinge rotated with increasing speed during all test whereas the upper system (affected by the movement of the load distribution beam) began with a quick rotation followed by a constant speed movement maintained until almost the end of the test when the rotation accelerated.

In Figure A1. 223 the axial-bending response of wall W#26 is plotted. As in previous cases, the effect of the second order moment is clearly observed throughout the increasing slope of the curve. The initial proportional response (associated with little out-of-plane deformation) is limited to the initial 30% of the load. The maximum load-moment is placed near the maximum theoretical interaction.

Although the wall W#26 had littler out-of-plane deformations compared with wall W#23 and W#24, these displacement were still clearly noticeable by naked eye (see Figure A1. 224) before the collapse. The failure was due to the masonry failure at the bottom extreme of the wall. The crack began at the tensile side at the joint between the strengthening system and the masonry and propagated throughout the wall's thick up to the 5th masonry row when it reached the compressive side separating the wall in two parts that fell independently.

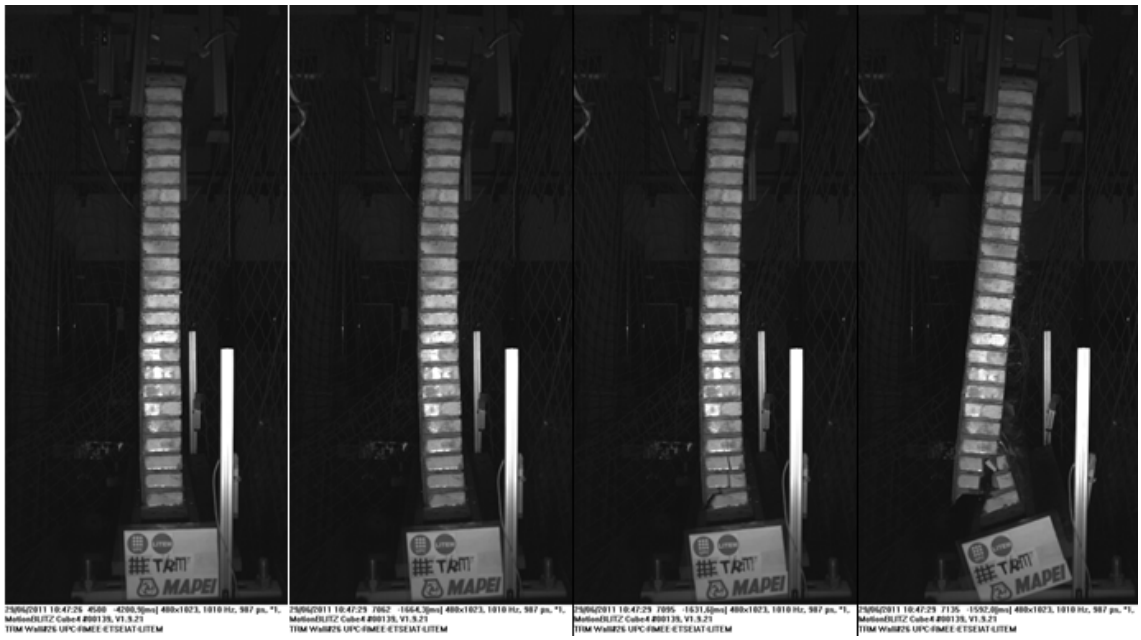

Figure A1. 224 Failure of the wall W#26. Masonry failure at wall's bottom.

Wall W#27

Wall W#27 was the first wall strengthened with a carbon fibre grid that was tested. About its geometry (see Table A1. 52) it is worth mentioning that it was the only strengthened wall which required rotating both hinges in the expected movement direction during the test to adjust its alignment. However, the horizontal distance between the rotation axes of the hinges at the two endings of the wall was 9mm before

testing wall W#27. Nevertheless, at the beginning of the test the wall was straight as the eccentricity was constant along its height.

Wall W#27 geometry	
Masonry rows	27
Width	0.873m
TRM thickness	8mm
Grid position	4mm
Height between hinges	1.822m
Theoretical eccentricity	30mm
Initial rotation lower hinge	0.93°
Initial rotation upper hinge	0.43°
Hinges alignment	9mm
Real mid-height eccentricity	30.43mm

Table A1. 52 Geometry of wall W#27

The in plane response (Figure A1. 225) was very similar to most of the previous test, with an initial settling range followed by a force proportional descending movement that finally showed a relaxation. However, in this case, the last stage was littler than in others. It means that the wall broke in a more brittle way and its behaviour seemed almost linear up to failure. The descending displacement of the distribution beam at the collapse (345.7kN) was 10.4mm.

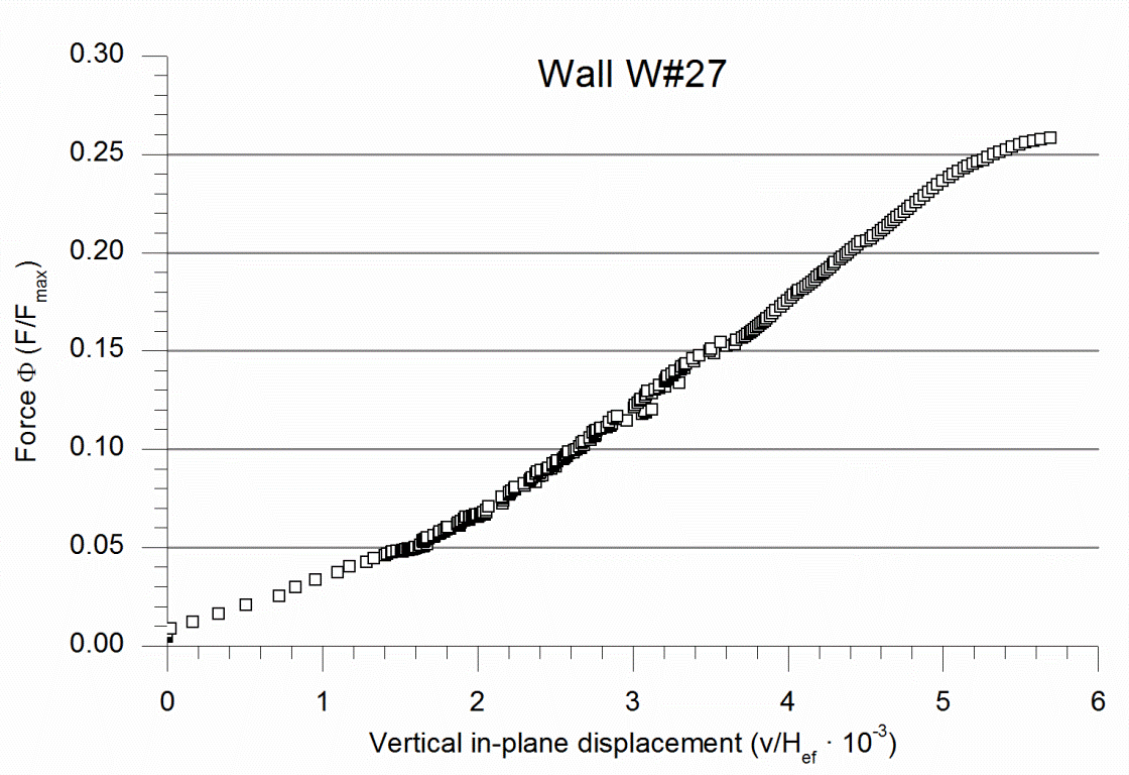

Figure A1. 225 Vertical in-plane response of wall W#27

Regarding the out-of-plane response (see Figure A1. 226) it was asymmetric during almost all the test. The deformation at ¾ of the buckling height began with values comparable with the out-of-plane displacement at mid-height. However, during the test these two measures diverged and the deformation at ¾ of the effective height became closer to the out-of-plane deformation at ¼ of the buckling height. That means that close to the collapse the out-of-plane deformation of the wall was symmetric although it was not that way during most of the experiment. The maximum out-of-plane deformation was always measured at mid-height, reaching the maximum of all tests, 26.1mm, for the maximum load.

According with the graph in Figure A1. 227, the rotation of the upper system was irregular up to 60% of the maximum load when it stabilised and described a constant rotation movement. In contrast, the lower hinge behaved as the previous tests, with an increasing rotation speed. No symmetry might be observed in the response of the supporting systems for wall W#27.

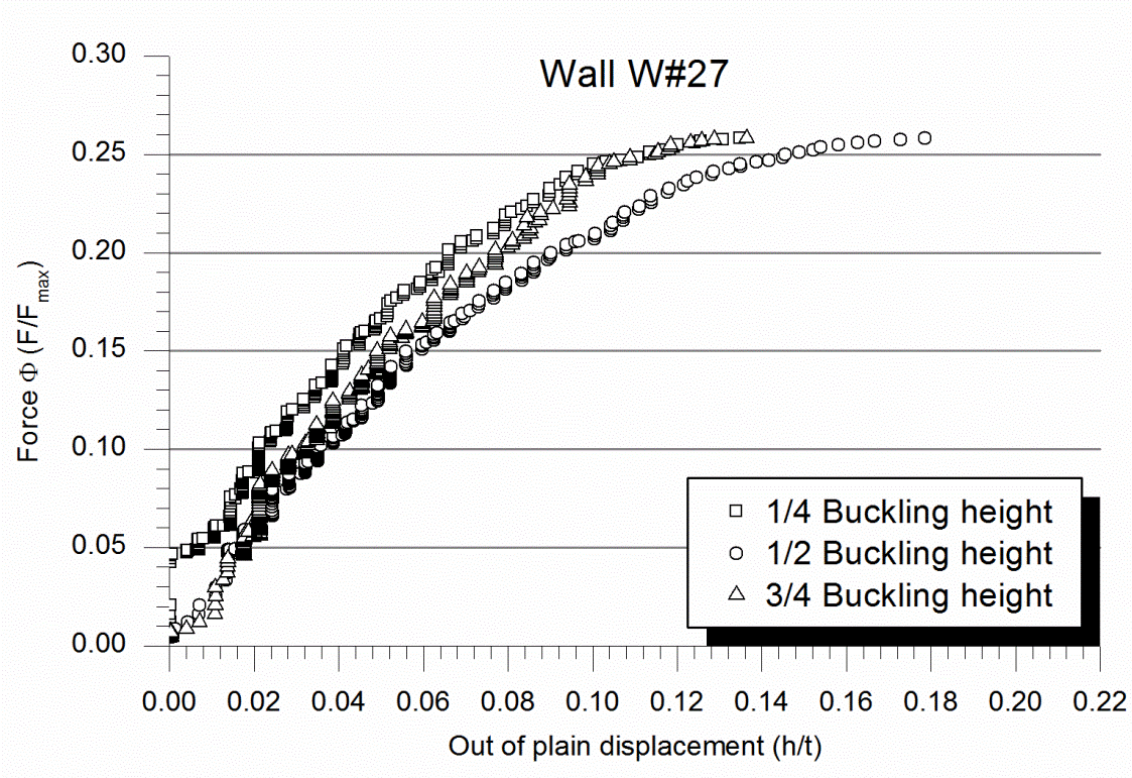

Figure A1. 226 Out-of-plane response of wall W#27

The axial force vs. bending moment interaction curve plotted in Figure A1. 228 showed the effects of the second order bending (increasing slope of the curve) and pointed out the prevalence of the bending moment in front of the axial compressive effort as the first one reached the 80% of its maximum corresponding with less than 30% of the compressive maximum force. Compared with previous cases, the collapse point is no so close to the theoretical maximum interaction curve defined according with Chapter 5.

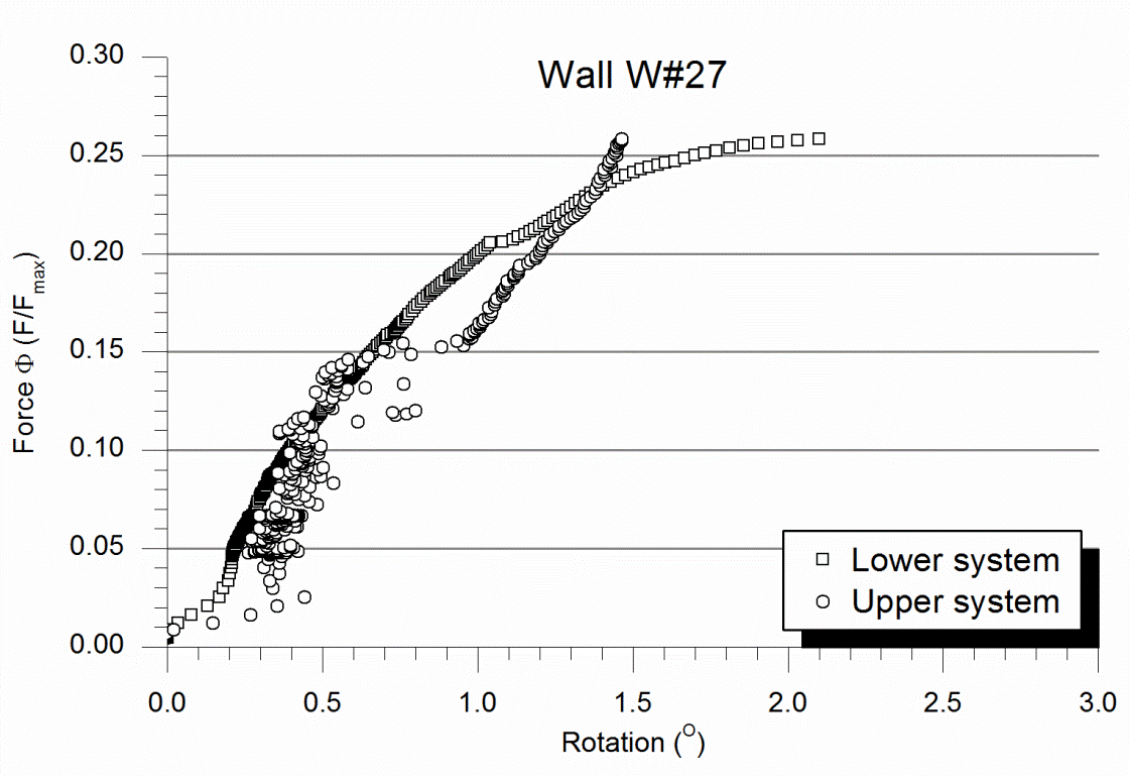

Figure A1. 227 Rotation at wall's endings for wall W#27

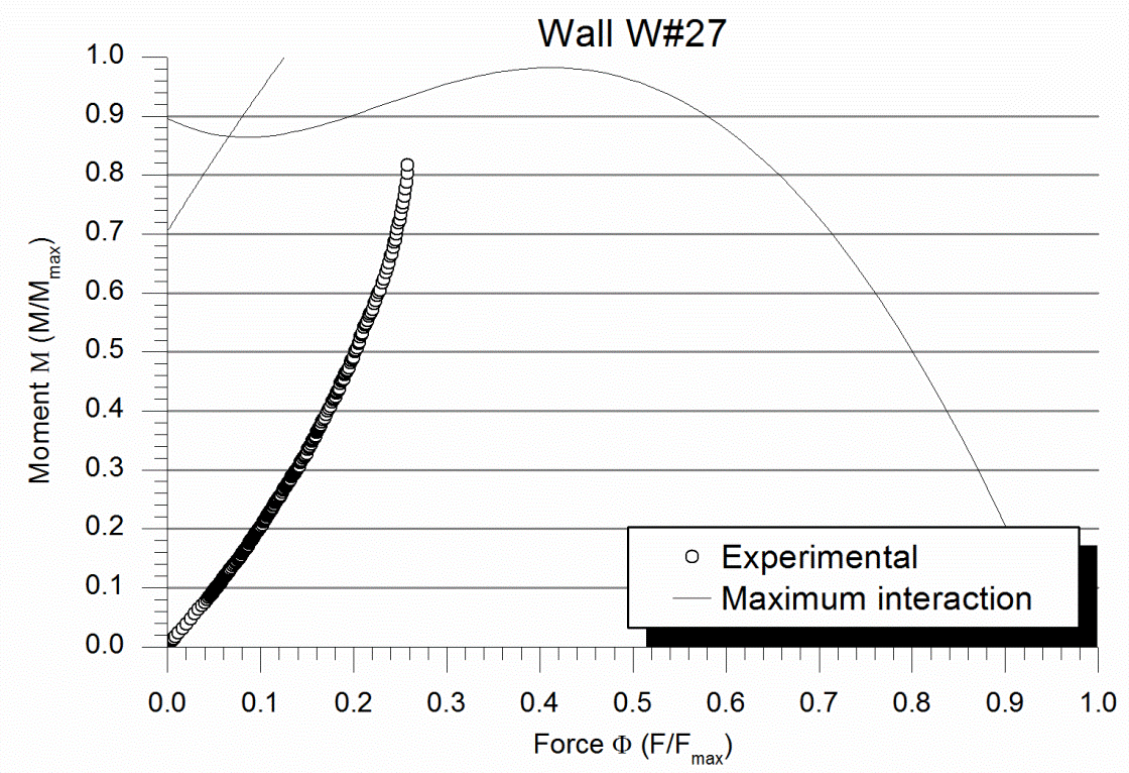

Figure A1. 228 Bending moment vs. Force response and interaction curve for wall W#27

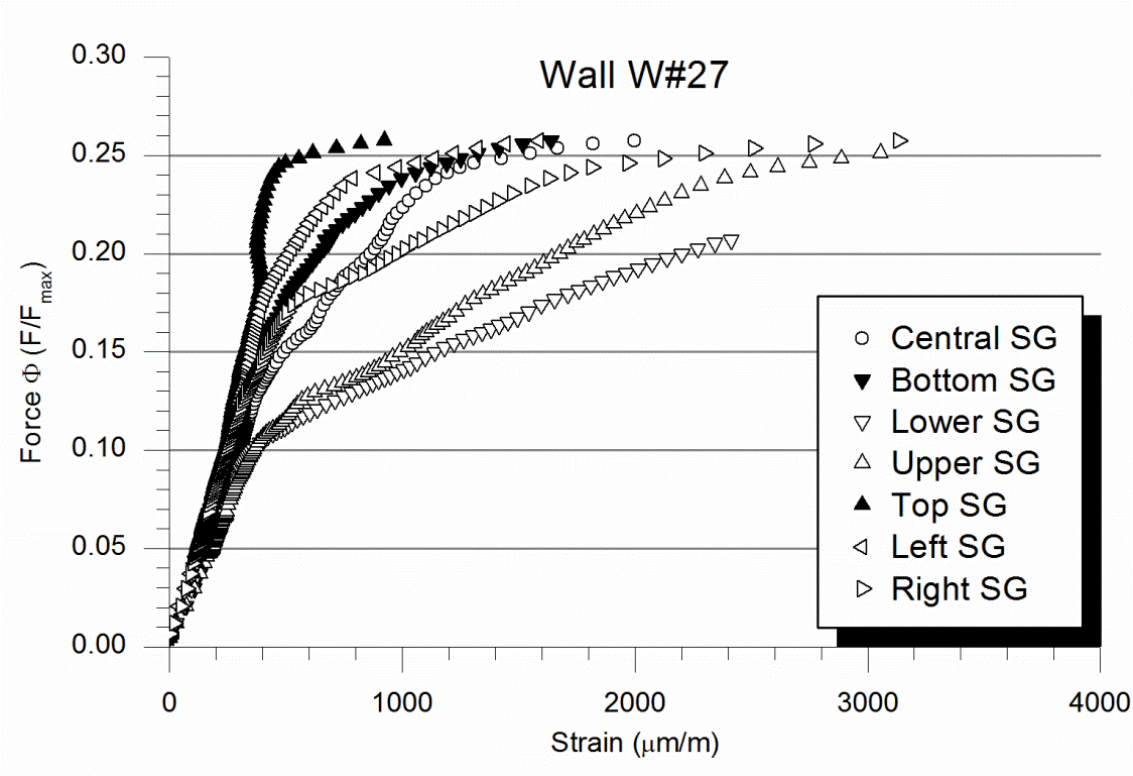

Figure A1. 229 Strains measured on the TRM for wall W#27

Observing Figure A1. 229, the distribution of the strains in the TRM strengthening system may be analysed. The first thing to be highlighted is that there is no much difference between the strains in different points of the wall until reaching the 30% of the maximum load. From this point and on, the maximum strains corresponded with points placed over and below the mid-height but not the ones closer to the extremes of the wall, which, in fact, had the lower measured values. Observing the strain at the three points placed at mid-height, an asymmetric response of the wall is noticed. Analysing the overall behaviour it can be concluded that TRM was not working the most at mid-height and that it was around this position of maximum out-of-plane deformation that the TRM worked more efficiently, when the anchorage length was developed and it could absorb the tensile force.

Finally, observing Figure A1. 230, the failure mode was associated with the developing of a unique big crack throughout the thick of the wall near the bottom, beginning at the tensile side and finishing at the compressive side. It was like previous failure of strengthened walls except for the fact that it began upper (at the third masonry row) and finished at an even higher position (between the 8th and the 9th rows). Compared with wall reinforced with glass fibre, wall W#27 showed a meaningful minor out-of-plane deformation before the collapse.

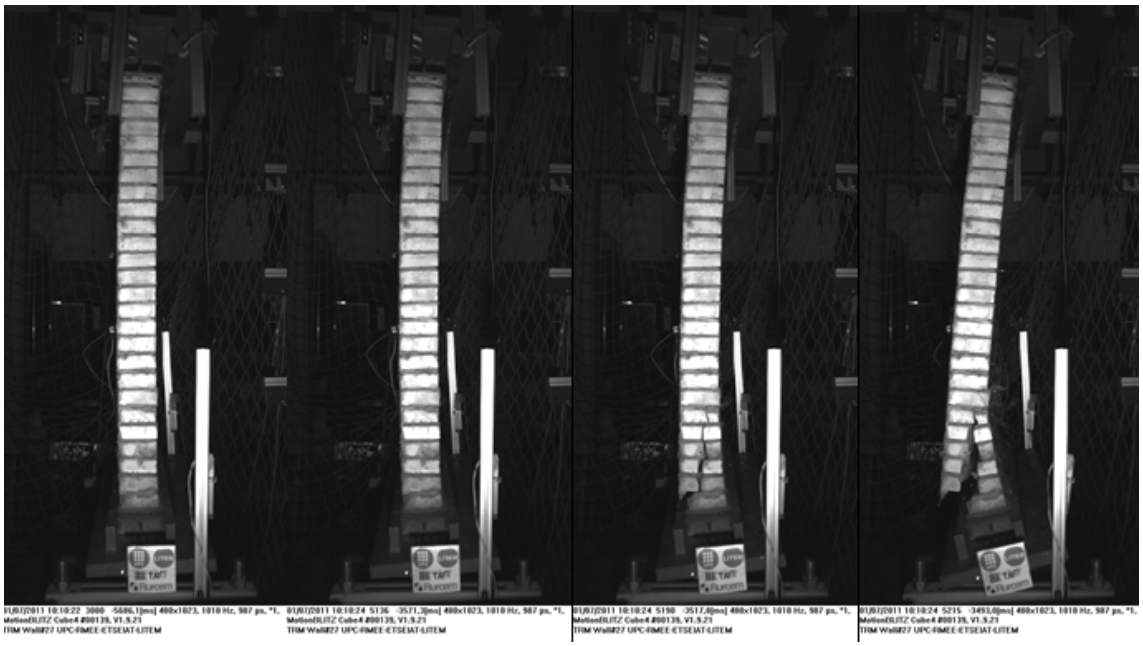

Figure A1. 230 Failure of the wall W#27. Masonry failure at wall's bottom.

Wall W#28

The strengthening method for wall W#28 was the same than for wall W#27 but including six connectors that pass through the wall's section connecting the TRM with the masonry in the compressive side to assure the bonding. Placing wall W#28 in position and with an almost perfect alignment between hinges required rotating both supporting systems in the opposite direction from the ones expected to follow during the loading process (see Table A1. 53). Although the alignment was good, the poor straightness of the wall make the eccentricity to vary along the height, changing from the fixed 30mm at the endings to just 24mm at the mid-height. It means the wall was initially bended in the opposite direction it was expected to bend during the test due to the fixed eccentricities.

Wall W#28 geometry	
Masonry rows	27
Width	0.871m
TRM thickness	9mm
Grid position	4mm
Height between hinges	1.828m
Theoretical eccentricity	30mm
Initial rotation lower hinge	-0.21°
Initial rotation upper hinge	-1.29°
Hinges alignment	0.5mm
Real mid-height eccentricity	23.73mm

Table A1. 53 Geometry of wall W#28

Regarding the in-plane behaviour (Figure A1. 231), it has to be noticed that wall W#28 deformed less than W#27 although the structural response followed the same pattern. At the beginning the wall settled and after that, the response was proportional to the applied force up to values close to the collapse load when the wall deformed more. The in-plane descending displacement of the distribution beam corresponding to the maximum applied load (313.5kN) was 6.8mm.

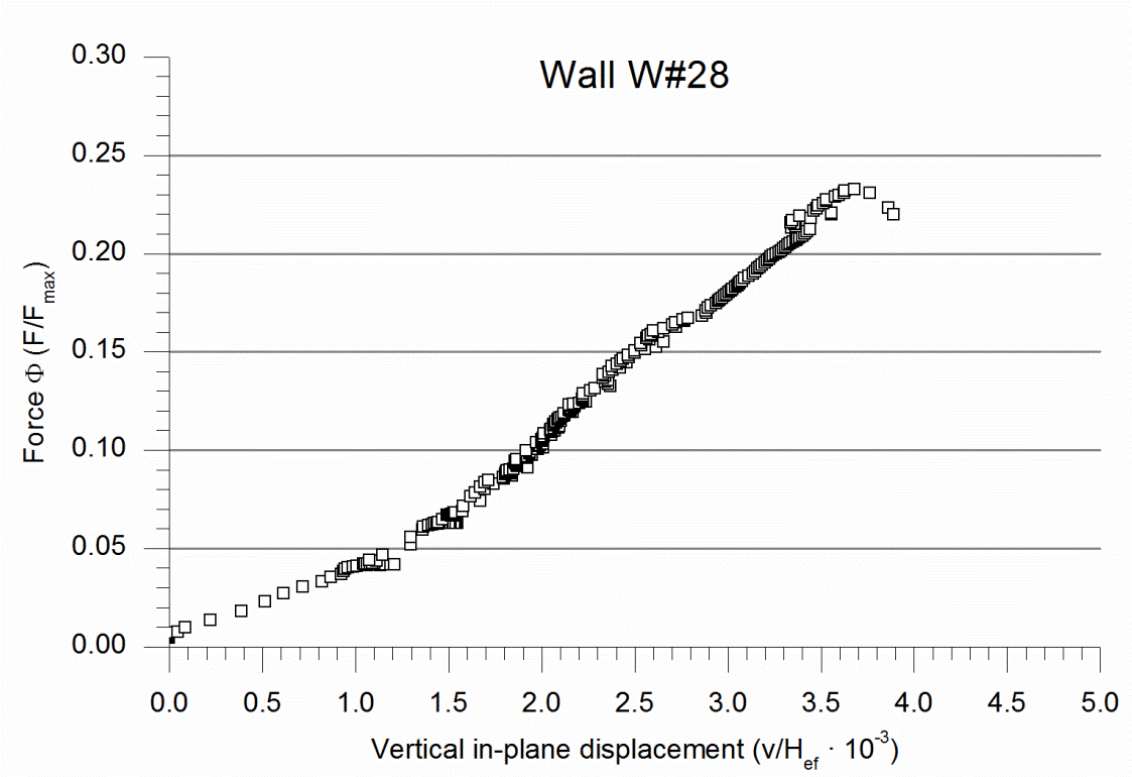

Figure A1. 231 Vertical in-plane response of wall W#28

Observing the graph in Figure A1. 232, it is observed that there were no big differences between the out-of-plane deformations at different heights for wall W#28. This behaviour contrasts with the observed in the previous strengthened walls. However, it might be said that the maximum out-of-plane displacement was measured at the mid-height whereas the minimum movement corresponded to the sensor placed at ¼ of the buckling height at the beginning of the test and it was equal at ¾ of the effective height near the collapse showing a symmetric response. Nevertheless, the main difference with previous walls is the less bending deformation during the test. At collapse the out-of-plane displacement at mid-height was 13.3mm.

The two supporting systems behaved approximately the same way although the upper system rotated with a more instable response and began with a quick rotation which makes the two curves in Figure A1. 233 to be plotted in parallel. The higher rotation of the upper system corresponded with the failure mode cracking the lower part.

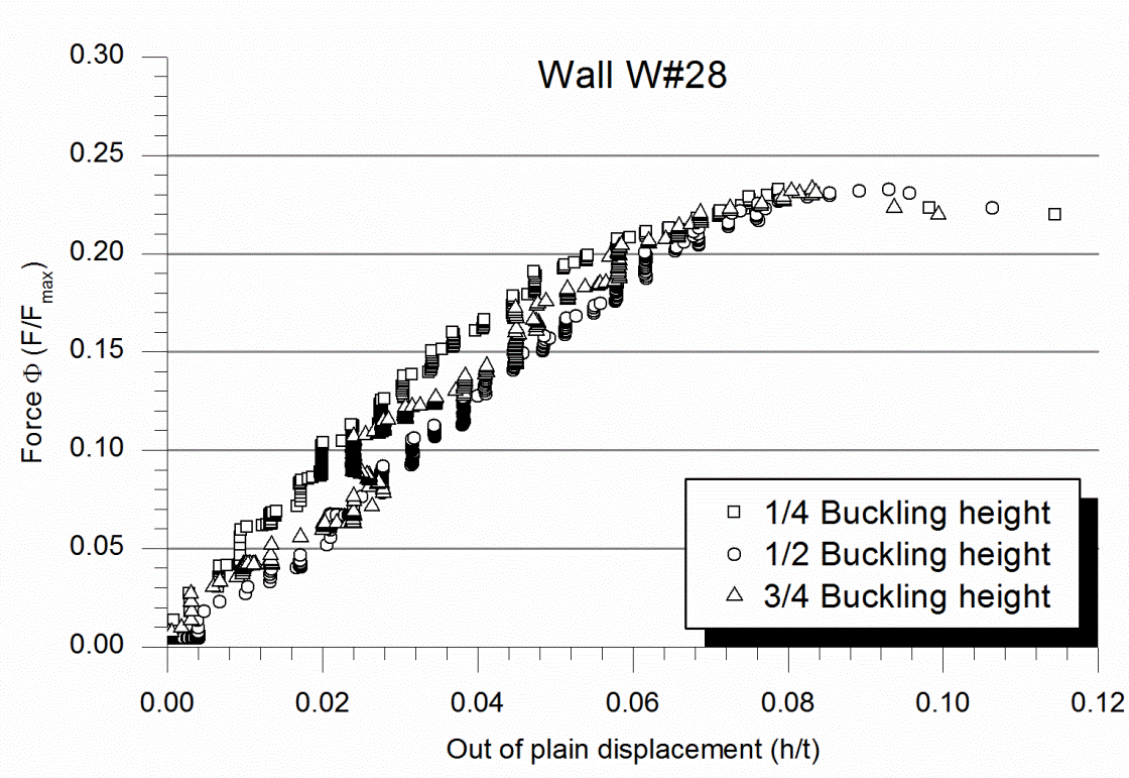

Figure A1. 232 Out-of-plane response of wall W#28

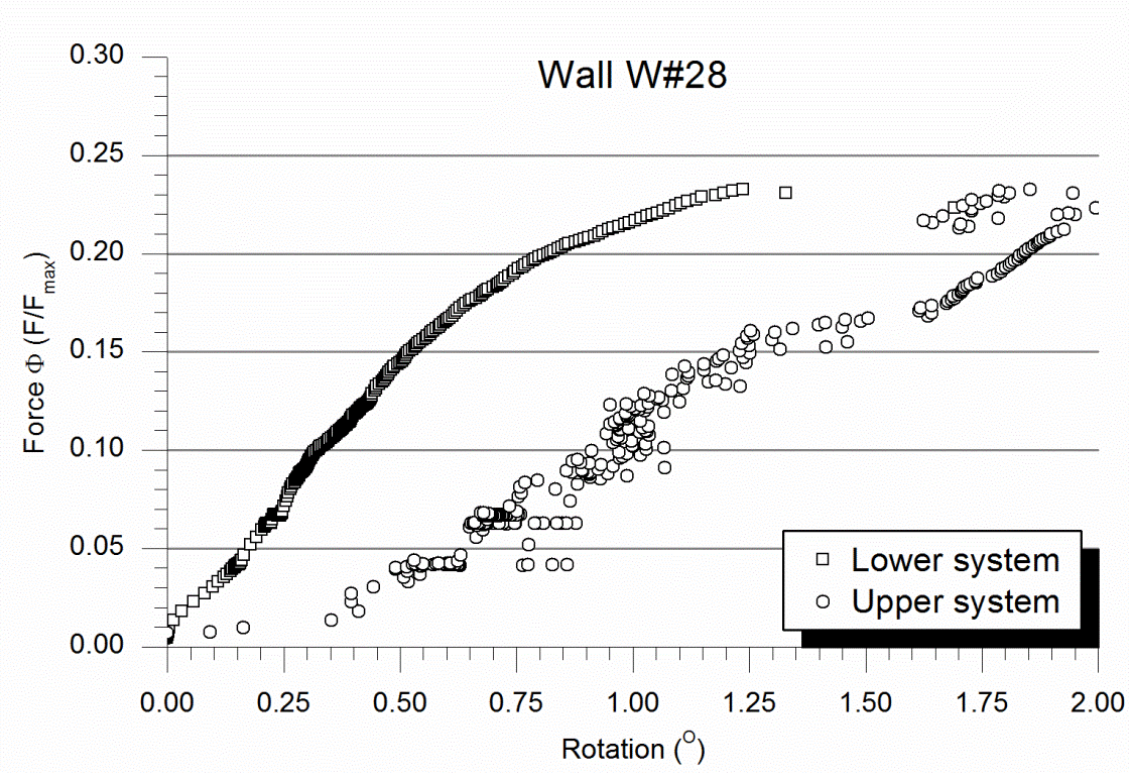

Figure A1. 233 Rotation at wall's endings for wall W#28

A practically linear force-bending moment response was registered for wall W#28 (see Figure A1. 234). It means the eccentricity did not grow so much due to second order effects as in previous walls. This analysis agrees with the fact that the wall presented little bending deformation as commented before observing the out-of-plane deformations. Only at the end of the test the bending moment increased much more that the applied load. Nevertheless, it has to be noticed that the maximum applied axial load was just the 25% of the theoretically maximum whereas the bending moment was over the 50% indicating the prevalence of this effort. In contrast with wall W#27, the axial-bending combination was far from the theoretical limit at the experimental failure point.

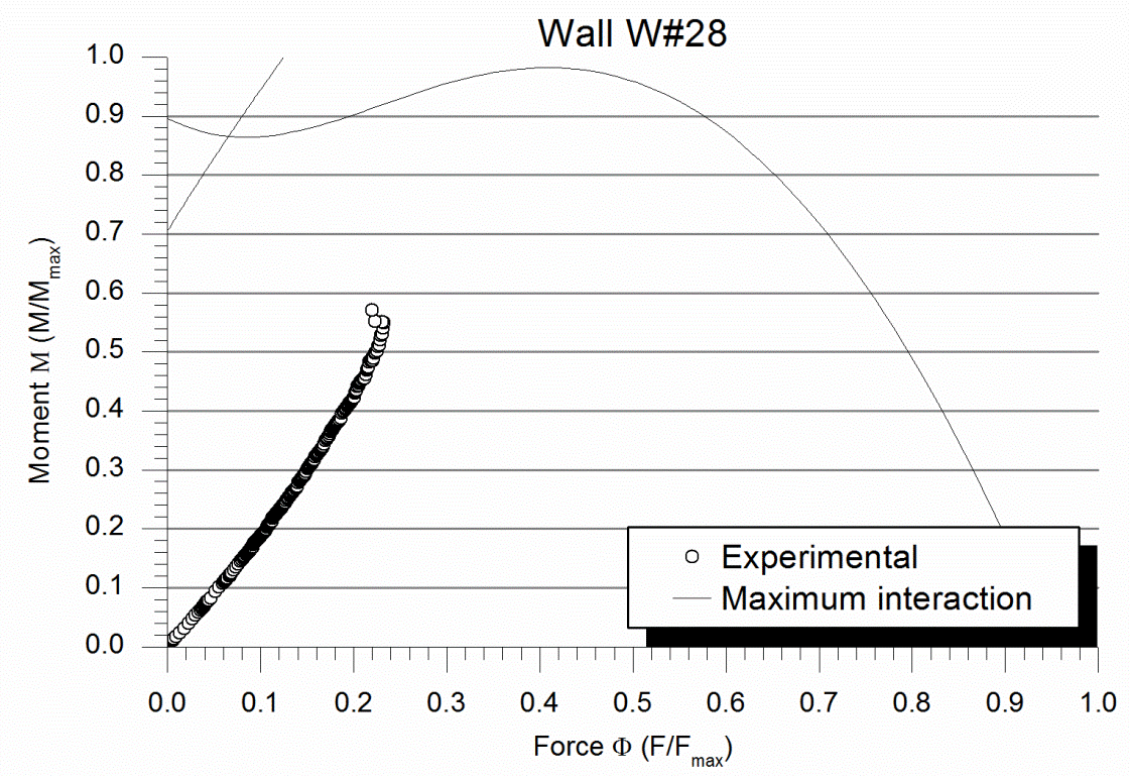

Figure A1. 234 Bending moment vs. Force response and interaction curve for wall W#28

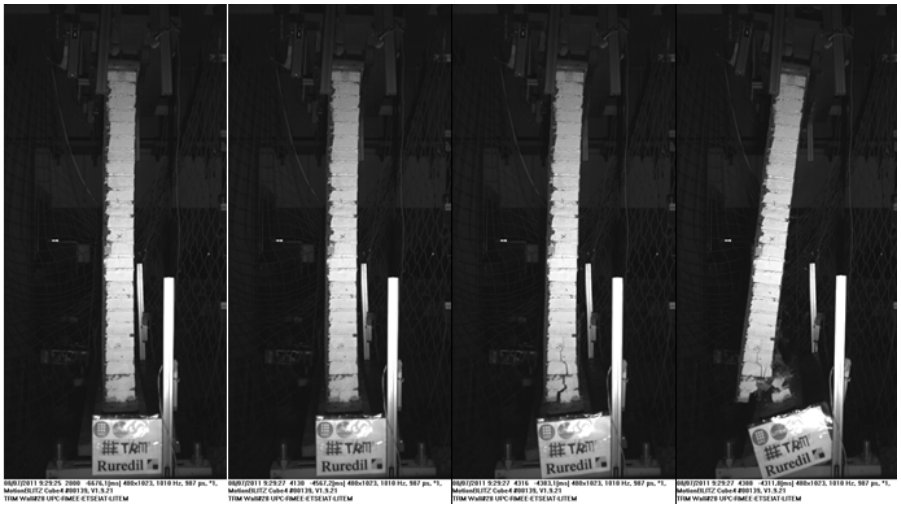

Figure A1. 235 Failure of the wall W#28. Masonry failure at wall's bottom.

As can be seen in Figure A1. 235, the wall broke by crushing the masonry at the bottom part. In this case, the crack that appeared in most of the strengthened walls was shorter and crossed the wall's section with a littler angle. It reached the compression side approximately at the height the first row of connectors were placed. In the second picture of Figure A1. 235, the almost straight shape of wall W#28 just before the collapse is observed.

Wall W#29

Wall W#29 is equivalent to wall W#27 and W#28 but nine connectors were placed in this case. Three rows of three connectors at bottom, top and mid-height sections were placed to assure the bonding of the TRM with the masonry. Although the lower and upper hinges were rotated (both in the opposite direction to the expected movement during the test) the hinges' alignment was worse than in previous cases (see Table A1. 54). This, together with the major eccentricity at mid-height than at the extremes prove the poor geometric quality of this wall. The TRM thickness was the maximum of the three walls strengthened with carbon fibre and Rurcem XMesh M25 mortar.

Wall W#29 geometry	
Masonry rows	27
Width	0.868m
TRM thickness	11mm
Grid position	6mm
Height between hinges	1.827m
Theoretical eccentricity	30mm
Initial rotation lower hinge	-0.14°
Initial rotation upper hinge	-1.00°
Hinges alignment	8.5mm
Real mid-height eccentricity	31.37mm

Table A1. 54 Geometry of wall W#29

In relation with the in-plane response of wall W#29 (Figure A1. 236), it was like the previous walls except for the last stage with a great load applied. At this moment, the wall deformed more for little load increases but soon it changed its behaviour to a stiffer response that changed again relaxing the system. Thus, for wall W#29 two softening processes were observed in contrast with previous walls. The descending displacement of the distribution beam for the maximum load (330.2kN) was 7.7mm.

The out-of-plane behaviour might be observed in the graph in Figure A1. 237. An anomalous response is noticed. To begin with, the maximum out-of-plane deformation was recorded at ¾ of the buckling height during the first half of the test although near the collapse this measure was similar to the one done at mid-height. The sensor placed at ¼ of the effective height was always de littler. A clear asymmetric behaviour was observed. The out-of-plane displacement at maximum load was 13.9mm.

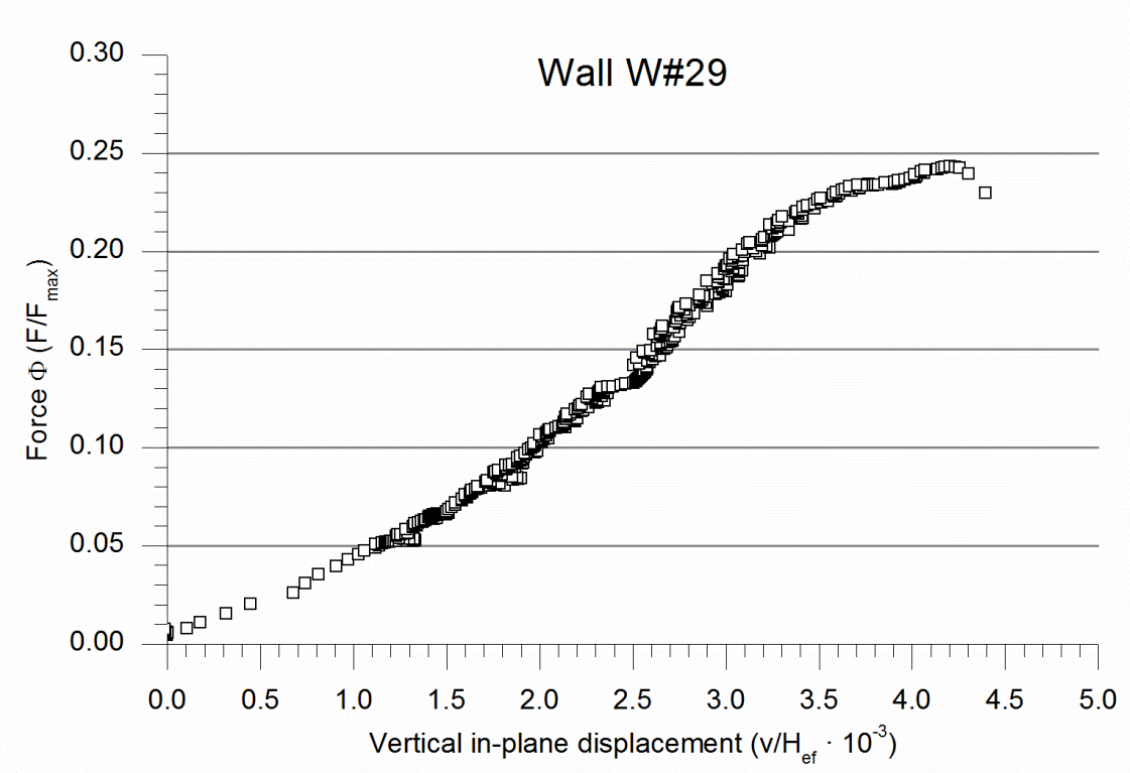

Figure A1. 236 Vertical in-plane response of wall W#29

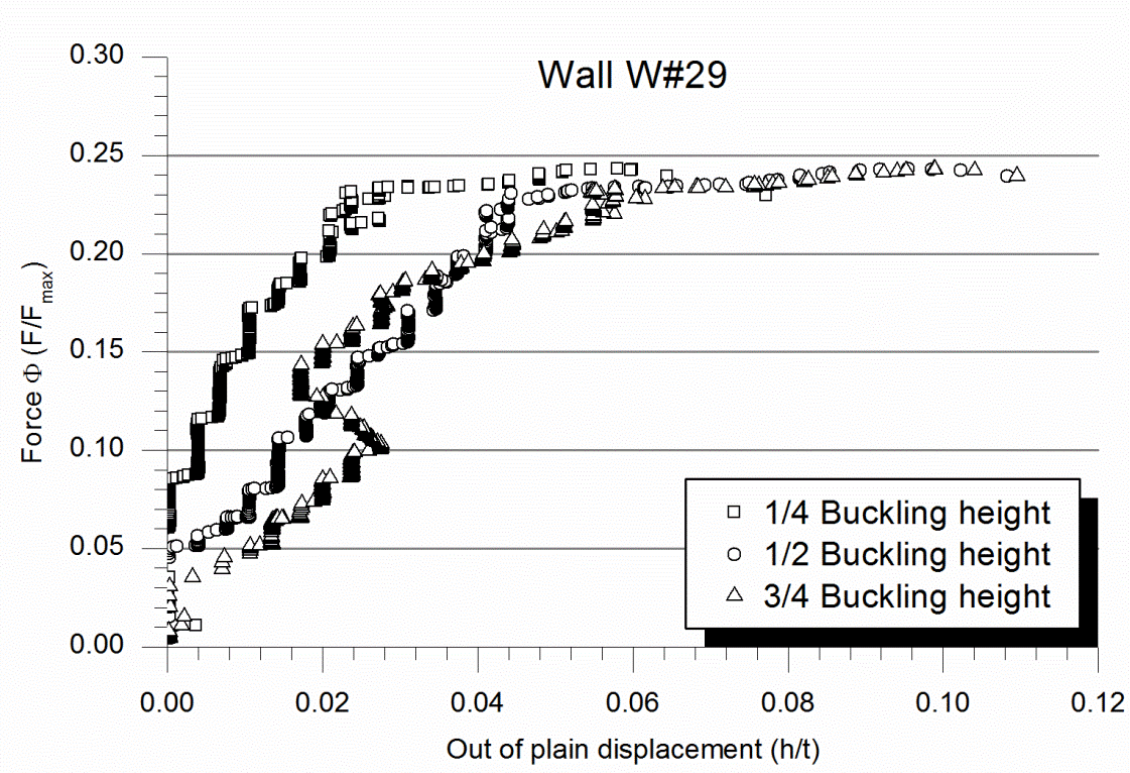

Figure A1. 237 Out-of-plane response of wall W#29

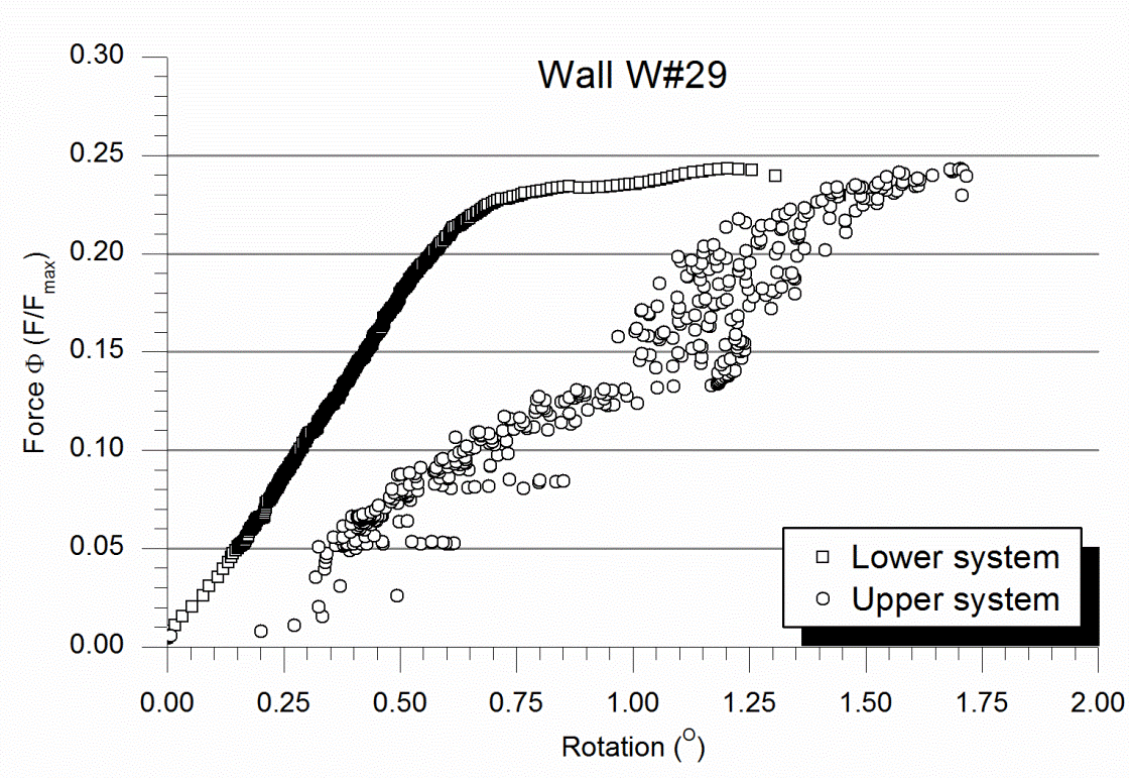

Figure A1. 238 Rotation at wall's endings for wall W#29

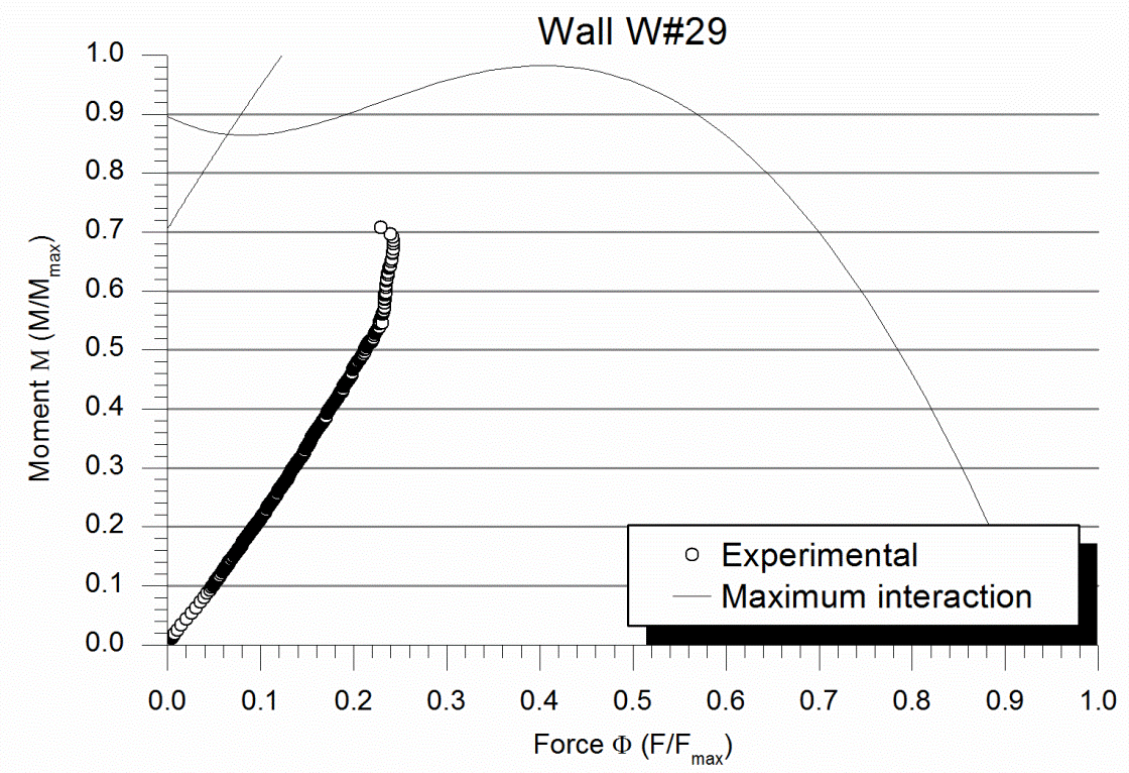

Figure A1. 239 Bending moment vs. Force response and interaction curve for wall W#29

In relation with the rotation of the supports, a constant speed rotation is observed for the lower hinge which only accelerated near the collapse. In contrast, the upper system showed a constant speed movement but very instable (see Figure A1. 238) due to the control of the horizontal movement of the distribution beam.

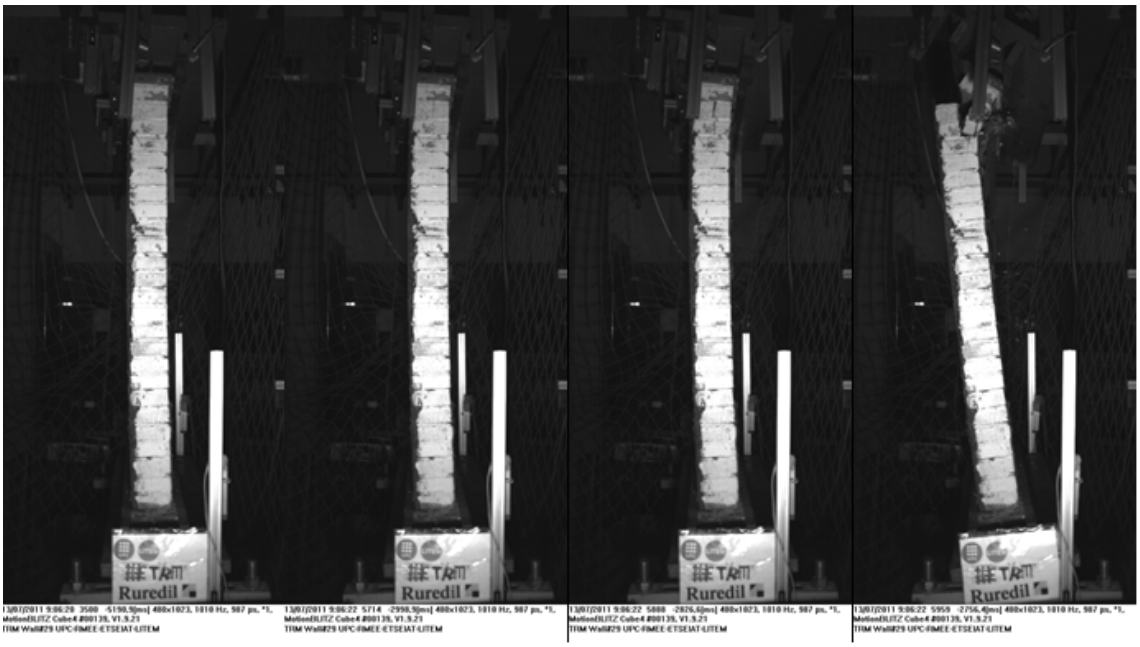

Figure A1. 240 Failure of the wall W#28. Masonry failure at wall's top.

Observing Figure A1. 239, it might be noticed that the second order effect is less important than in previous strengthened walls except for wall W#28 which showed a similar response. In fact, the axial load-bending moment relation is proportional up to values close to the collapse ones. Like in previous tests, the flexural effort is more important (in relation with its possible maximum) than the compressive force.

The failure mode (Figure A1. 240) was cracking the masonry at the top of the wall. In this case, as in the previous one (wall W#28), only three masonry rows were affected by the crack that finished at the height corresponding with the upper connectors row. The collapse was sudden and the crack divided the wall in two parts that allowed it to fall.